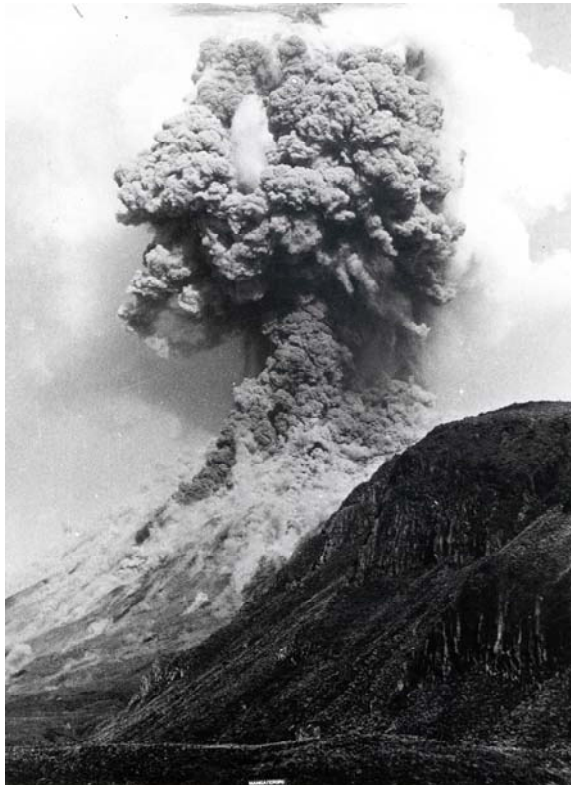**The flow and depositional mechanisms of granular matter:**

Experimental and field studies with implications for pyroclastic flows.

Dissertation

zur Erlangung des Doktorgrades der

Mathematisch-Naturwissenschaftlichen Fakultät

der Christian-Albrechts-Universität zu Kiel

vorgelegt von

Gert Lube

Kiel

2006

Referent:...Dr. PD A. Freundt

Korreferenten:...Prof. Dr. C. Devey

Prof. Dr. FRS R.S.J. Sparks

Tag der mündlichen Prüfung:..14.07.2006

Zum Druck genehmigt: Kiel, den...

Prof. Dr. rer. nat. Jürgen Grotemeyer   Der Dekan

Hiermit erkläre ich, dass die vorliegende Abhandlung, abgesehen von der Beratung durch meine akademischen Lehrer, nach Inhalt und Form meine eigene Arbeit darstellt. Ferner habe ich weder diese noch eine ähnliche Arbeit an einer anderen Abteilung oder Hochschule im Rahmen eines Prüfungsverfahrens vorgelegt.

Gert Lube

Abstract

The physical behaviour of granular material has ubiquitous application in industrial processes, the agriculture, engineering problems and comes across everyone of us in form of granular segregation while opening the breakfast muesli box. In the Earth Sciences the tendency of granular matter to behave as either static piles or form mobile flows is encountered in a broad range of research disciplines studying the subaerial and subaqueous environment. Of particular concern for assessing the hazard potential of geophysical mass flows are the complex processes of flow and deposition of granular media that occur in debris avalanches, snow avalanches and pyroclastic flows.

This Doctorial Thesis investigates the fundamental problem of flow and deposition processes of unsteady, inertial flows of granular media and elucidates its implications for the behaviour of pyroclastic flows formed in explosive volcanic eruptions. A three-fold approach is followed including laboratory experiments, their theoretical analysis, and field work on the pristine pyroclastic flow deposits of the 1975 eruption of Mt. Ngauruhoe (New Zealand).

The experiments are based upon the physical problem of the sudden collapse of vertical columns of granular media onto a base and their subsequent spreading behaviour. Three different geometries are used: the axisymmetric collapse of vertical cylinders of particles onto horizontal planes; the quasi two-dimensional collapse of rectangular columns into horizontal channels; and the collapse of rectangular columns of granular material into inclined channels. These flows are characterised by their unsteady motion, the occurrence of different flow regimes, a time-dependent form of the upper free surface of the flow, and deposition processes governed by the upward propagation of an internal interface between static and moving particles. Granular collapse flows differ significantly from the well-investigated situations of steady-state granular flow on chutes at inclinations close to the static angle of repose, in rotating drums and heap flow geometries.

The major results from the experimental investigations are:

- The major part of flow behaviour is characterised by the dominance of inertial forces over frictional forces. Only at the end of flow, when there is an abrupt halt, is internal friction important.

- According to this inertial nature, the motion is largely independent of the grain type. Thus, the final geometry of the collapsed columns can be mathematically described in terms of scaling laws entirely based upon the external geometry of the initial columns. These scaling laws take different forms for two flow regimes based upon the value of the initial aspect ratio, a, of the column (the ratio of vertical height and radius (in axisymmetric geometry) or basal length (in two-dimensional geometry).

- Most of the flow takes place on a layer of static (already deposited) particles, which is separated from the overriding flow by a moving internal interface. Therefore, column collapses are also independent of the nature of the basal surface.

- In the two-dimensional geometry for the flow regime at $a > 2.8$, an initial free-fall phase of the column is followed by a lateral spreading phase. In the lateral spreading phase, the deposition rate is a constant dependent on a, but it is independent of flow depth and velocity. In addition, there is a time-invariant form of the vertical velocity profile across the flowing layer, which again is dependent on a but independent of flow depth and surface speed.

- The mathematical form of the scaling laws obtained for the two-dimensional collapses into horizontal channels are valid up to basal inclinations of 20° to the horizontal. The effect of the basal inclination can be included by separate mathematical terms for the initial geometry of the columns and the inclination of the channel. These laws include mathematical descriptions for the length, height and shape of the final deposit and the duration of flow.

Through investigations of the pyroclastic flow deposits of the 1975 eruption of Mt. Ngauruhoe, first complete data sets of the internal structure and grain-size distribution and the morphology of the upper free surface of small-volume pyroclastic flow deposits as a function of travel distance, underlying slope and topographic confinement are presented. This detailed data set is interpreted using the experimental findings on the propagation of an internal interface, and a qualitative time- and space-dependent model on transport, segregation and deposition is developed for pyroclastic flows.

Kurzfassung

Das physikalische Verhalten von granularen Medien findet allgegenwärtig Anwendung in der Industrie, in der Landwirtschaft, in Ingenieur-wissenschaftlichen Fragestellungen, und begegnet uns schliesslich allmorgentlich in der Form von granularer Segregation beim Öffnen der Müslidose. In den Erdwissenschaften spielt das Verhalten von Granulaten eine vielfältige Rolle in subaerischen und subaquatischen Milieus. Die komplexen Fliess- und Ablagerungsprozesse granularer Medien sind von besonderer Bedeutung für die Gefahrenforschung an geophysikalischen Masseströmen (wie z.B. an Schutt- und Schneelawinen, aber auch an Pyroklastischen Strömen).

Diese Doktorarbeit untersucht das Problem der Fliess- und Ablagerungsprozesse in unstetigen, Trägheits-dominierten granularen Strömen und deren Implikation für Pyroklastische Ströme. Ein dreiteiliger Ansatz zu dieser Problemstellung beinhaltet Laborexperimente, deren theoretische Analyse und Feldarbeit an den jungen Pyroklastischen Stromablagerungen der 1975 Eruption des Mt. Ngauruhoe in Neuseeland.

Die Experimente widmen sich der fundamentellen physikalischen Situation des Kollaps- und Fliessverhaltens vertikaler Granulatsäulen auf dem Boden. Die so generierten Ströme zeichnen sich durch unstetiges Fliessen, eine zeitlich veränderliche Geometrie der freien Stromoberfläche und durch Ablagerung verursacht durch die Bewegung einer internen Grenzfläche zwischen statischen und bewegten Partikeln aus. Die durch den Kollaps granularer Säulen erzeugte Ströme unterscheiden sich signifikant von der bereits gut untersuchten Situation stetigen, granularen Fliessens.

Die Experimente wurden in drei verschiedenen Geometrien untersucht: als radialsymmetrische Ströme auf horizontaler Ebene, als zwei-dimensionale, horizontale Kanalströmungen und als zwei-dimensionale Ströme in geneigten Tanks.

Die wichtigsten Resultate der experimentellen Studie lassen sich wie folgt zusammenfassen:
- Das Fliessverhalten ist fast ausschliesslich durch die Dominanz von Trägheitskräften gegenüber Reibungskräften geprägt. Erst zum Ende des Fliessens, wenn es zu einem abrupten Anhalten kommt, werden Reibungskräfte zwischen den einzelnen Partikeln massgebend.

- Durch die Trägheits-dominierte Art des Fliessens ist die Bewegung weitestgehend unabhängig von der Art des Granulats. Daher kann die Geometrie der Ablagerungen in mathematischen Gesetzmäßigkeiten ausgedrückt werden, die nur auf den externen geometrischen Parametern der Säule beruhen. Diese mathematischen Terme weisen eine unterschiedliche Form in zwei Fliessregimen auf, die wiederum auf dem Wert des Verhältnisses vertikaler Höhe zu horizontaler Weite, a, beruhen.

- Die Ströme bewegen sich fast auf ihrer gesamten Länge auf einer Lage bereits abgelagerter Partikel. Diese ist durch eine interne, unstetige Grenzschicht von dem sich darüber bewegenden Material getrennt. Daher ist das Fliessverhalten auch unabhängig von der Beschaffenheit des festen Untergrunds.

- In zwei-dimensionaler Geometrie im zweiten Fliessregime ($a > 2.8$), existieren zwei aufeinanderfolgende Fliessphasen: eine erste Phase, die durch den freien Fall der Säule geprägt ist, gefolgt von einer sogenannten lateralen Ausbreitungsphase. In der letzteren Phase ist die Ablagerungsrate der Ströme konstant und eine Funktion von a, jedoch unabhängig von der Stromhöhe und –geschwindigkeit. Des weiteren zeichnen sich vertikale Geschwindigkeitsprofile durch eine Zeit-unabhängige Form aus. Sie sind Funktionen von a aber unabhängig von Stromtiefe und Geschwindkeit.

- Die mathematische Form der Gesetzmäßigkeiten, die das zwei-dimensionale Strömen in horizontalen Kanälen beschreiben, sind auch für Ströme in Kanälen mit Neigungen bis zu 20° gültig. Der Einfluss der basalen Neigung kann durch separate mathematische Terme für die Geometrie der initialen Säule und für die Neigung ausgedrückt werden. Mathematische Beschreibungen ergeben sich für die Länge, Höhe und Form der Ablagerung, sowie für die Fliessdauer.

Durch Felduntersuchungen an den Pyroklastischen Stromablagerungen der Eruption des Mt. Ngauruhoe von 1975, konnten erstmalig komplette Datensätze der internen Textur, Korngrößenerteilung, sowie der Oberflächenmorphologie klein-volumiger Pyroklastischer Ströme als Funktion der Fliessdistanz, der Reliefneigung und der lateralen Begrenzung durch die Topographie gewonnen werden. Mit Hilfe dieser Daten und der experimentellen Untersuchung der internen Grenzschicht wurde ein qualitatives Fliess- und Ablagerungsmodell für Transport-, Segregations- und Ablagerungsprozesse Pyroklastischer Ströme erarbeitet.

Acknowledgements

I would like to thank all the people that aided this Doctorial thesis to come where it stands.

Over the last years, I was in the fortunate situation to discover most fascinating research subjects together with three of the world's best experts in the fields of Volcanology and Fluid Dynamics. I am strongly indebted to Dr. Armin Freundt, Prof. Herbert E. Huppert FRS, and Prof. R. Stephen J. Sparks FRS who supervised this work. I would like to thank them the most for sharing their knowledge, for their patience in revising and discussing the manuscripts and in particular for creating an amicable and open working atmosphere. A number of the presented results would not have been gained without the numerous discussions with Armin Freundt, his engagement in organising the research funds needed for the study, and his ability to discover science in a particular sense of ease and depth. This ambience, in a number of situations, helped me significantly to circumvent frustration and to keep the curiosity needed for protruding into such an interdisciplinary field of science. I am most thankful to Steve Sparks and Herbert Huppert for giving me, as a foreigner in algebra and fluid dynamics, a cautious lift into this field. I would like to thank both of them for their personal and scientific support, their tremendous patience in teaching me scientific writing and for their exceptional gift to treat young scholars as equal scientists. Working in a most fascinating environment as a volcanologist on Montserrat and observing pyroclastic flows on a daily base would not have been possible without the help and trust of Steve Sparks. My largest step forward in understanding granular flows definitely succeeded while over at the Department of Applied Mathematics and Theoretical Geophysics in Cambridge among the care and hospitality of Herbert Huppert.

Sincere thanks go to Dr. Shane Cronin for organising and (partially) funding field work in New Zealand, for his spirit of adventure while excavating the ring at Mt. Doom and roaming the jungle at Taranaki. A thankful "whatsupwhatsupwhatsup" to the "bubble" at the Montserrat Volcano Observatory for their hospitality, for protecting me from the island traffic police and of course for training me as a volcanologist. Without the work of the student helpers experimental and field data would not have been gained in this detail. Many thanks to Sebastian Münn, Carla Wiegers and Carlos Cabezas Banda. I am particularly indebted to Sebastian for many fruitful discussions of the experimental results, his creativity and improvisation skills in the laboratory and his careful work.

Contents

Chapter II   Axisymmetric collapses of granular columns

Chapter V   **Flow and deposition of pyroclastic granular flows:**
                   A type example from the 1975 Ngauruhoe eruption, New Zealand

Chapter VI   Static and flowing regions in granular collapses down channels

Chapter VII Granular column collapses down rough, inclined channels

Curriculum Vitae

Chapter I

Introduction

CHAPTER I

1. Why does the granular matter?

The physics of granular matter has long been a focus of research in a broad range of scientific disciplines as diverse as chemical engineering, fundamental physics, pharmacy, biology, agriculture, and the Earth Sciences. Granular flow is widely encountered in the industrial handling of grains and powders, while the mechanical stability of static piles of granular material is of central concern in civil engineering. In nature, accumulations of particles occur in both subaerial and subaqueous environments over scales ranging from millimetres to several tens of kilometres. The dynamical behaviour of granular matter is fundamental to phenomena ranging from the incessant processes of erosion and deposition to the sudden disastrous failures of landslides and generation of snow avalanches in mountainous areas and pyroclastic flows in explosive volcanic eruptions. However, the physics of granular flows are still poorly understood.

2. Understanding granular matter

A distinctive characteristic of granular matter is their complex transitional behaviour between solids, liquids and gases (Kadanoff, 1999). Despite a large number of studies and ubiquitous applications, there are no general constitutive laws to describe granular media. This is in marked contrast to the understanding of the solid, liquid and gaseous states, where the equations of statics, the theory of linear elasticity, the Navier-Stokes equations and the kinetic theory of gases have a long time of investigation. A key approach to the understanding of granular media is experimental studies. Over the last three decades, a large number of laboratory experiments, grain-following computations and numerical continuum simulations have been undertaken. A number of insightful reviews on granular flow research have appeared, including those by Campbell (1990), Savage (1995) and Jaeger, Nagel & Behringer (1996).

The largest progress in understanding free-surface granular flows driven by gravity has been reached for flow of mono-disperse particles in steady-state situations. There are three main experimental geometries which have been studied extensively over the last 15 years: flow of granular material down rough chutes with inclination close to the (static) angle of repose; flow in rotating drums; and heap flows. A review of the rheological models obtained in these steady flow situations was recently presented in the collective paper by G.D.R. Midi (2004).

The general approach has been to derive depth-averaged equations for steady flow conditions and introduce empirical friction laws to try to obtain agreement between data and experiments (see, for example Savage & Hutter 1989; Anderson & Jackson 1992; Savage 1998; Pouliquen 1999; Iverson & Denlinger 2001, and some of the references therein).

However, dense geophysical flows and most industrial particulate flows involve unsteady motion. This is evident for the case of pyroclastic flows and debris avalanches which are initiated on the steep flanks of a volcano and then run out and deposit on shallow terrain. Their motion involves stages of acceleration and deceleration. Particles can enter the flow by erosion of loose bed material, and particularly fine particles can leave the flow via elutriation. Deposition from these currents involves poorly understood processes that vary in space and time.

3. Understanding of pyroclastic flows

Pyroclastic flows are ground-hugging, gravity driven mixtures of hot poly-disperse pyroclastic particles and gas (Druitt 1998, Freundt & Bursik 1998, Freundt et al. 2000). They are among the most spectacular and fascinating flow phenomena occurring in nature. Their devastating behaviour and poor predictability constitute an enormous hazard to human life and valuables. Our ability to predict flow behaviour is steadily gaining in importance, particularly in the face of an increasing world population, demanding further occupation of volcanic areas. Pyroclastic flows can be produced by: (1) explosive and/or gravitational disruption or collapse of lava domes or flows, (2) the collapse of eruption columns; or (3) the collapse of still hot pyroclastic deposits. Physical models of flow vary from dense, granular flows, where motion is dominated by particle interactions, through gas-fluidised flows, where gas plays a significant role, to highly diluted systems where gas is the dominant phase and transports particles in turbulent suspensions.

The difficulty to describe physically pyroclastic flows consists of two major problems. First, measurements on moving pyroclastic flows are sparse and a detailed characterisation of flow regimes and deposition mechanisms are still awaited. The scarcity of quantified dynamic variables in these currents mostly inhibits the design of usefully scaled analogue experiments. Second, most of our current knowledge stems from interpretations made upon their final deposits. Interpretations of all such geological observations, however, remain qualitative as

long as the physical relations between deposit characteristics and flow and deposition mechanism cannot be quantified.

Pyroclastic flows that occurred in historic times and particularly during recent volcanic crises are envisaged as high-concentration, avalanche-like flows; they are typically hidden from observation by an overriding ash cloud. The challenge to physically describe these currents has resulted in a plethora of rheological models. These mainly differ in the description of energy dissipation. Early models were inspired by observations, suggesting bulk fluid-like rheologies, although the essential nature of the flowing material is granular. Various hypotheses to explain a reduction of internal friction were proposed. Some volcanologists suggested that certain depositional features, such as lobate fronts, levees, reverse grading of large lithics within massive matrix-supported beds were consistent with flows as high yield-strength, non-Newtonian, density-driven currents. Resulting models comprised resistant terms to some power of velocity (Rodriguez-Elizarraras et al. 1991; Wilson & Head, 1981). Uncertainties in the choice of the stress tensor gave large variations in flow behaviour, especially flow velocity. A different line of reasoning that has let to much the same result was taken by those who used the rapid granular flow tensor of Bagnold (1954), which is based on the kinetic theory, to develop models with resistance terms dependent on the squared velocity gradient (Takahashi & Tsujimoto 2000, Yamamoto et al. 1993). Using the pioneering work of Bagnold on sand dunes (Bagnold, 1954), volcanologists derived the hypothesis that pyroclastic flows moved as density-modified grain-flows, in which grains were separated by intergranular dispersive pressure (Denlinger 1987, Boudon et al. 1993, Fujii & Nakada 1999). Where dispersive pressure was low, flows would be in the frictional regime and shear stress at failure was proportional to normal stress (Mohr-Coulomb friction). A different approach was suggested that assumes constant resisting shear stress to flow spread (Dade & Huppert 1998). This approach leads to a useful mobility parameter with which different kinds of geophysical mass flows can be compared, particularly as it includes flow volume as a factor favouring mobility that was ignored by the Mohr-Coulomb-models. This model, however, does not consider the mechanisms of granular stress. Recently, continuum descriptions of particulate flows in the shallow-water theory framework have been applied to all different kinds of geophysical mass flows (Denlinger & Iverson 2001). This approach stems from initial works of Eglit and Sveshnikova (1980) and Savage and Hutter (1989) and introduces a Coulomb frictional resistance term into a consistent set of equations of motion.

All present models for high-concentration flows have deficits in their application to pyroclastic flows. Constant yield strength and viscosity are non-realistic assumptions for pyroclastic flows; Mohr-Coulomb models do not explain increasing mobility with flow volume. Numerical models, that simulate the propagation of pyroclastic flows over natural terrain (Denlinger & Iverson 2001), remain unsatisfactory as long as they are based upon poorly validated physical assumptions. Moreover, disregarding deposition mechanisms in all these models inhibits the much demanded comparison between field data and physical models.

4. Objectives of this study

This thesis addresses two prevailing subjects interdisciplinary between volcanology and physics:

> (a) The physical behaviour of inertial flows of granular media driven by gravity.
> (b) The transport and deposition mechanisms of small-volume pyroclastic flows.

Problem (a) was investigated by laboratory experiments and theoretical analysis. The experiments considered the fundamental physical situation of the sudden collapse of a vertical column of particles and their subsequent flow behaviour. Whereas this experimental situation is a common approach for the investigation of fluid dynamical problems (and there referred to as the *dam-break problem*), it has never been studied before for the case of dry granular matter. The resulting flows are characterised by their time-dependent unsteady form of motion, large changes of the free upper surface with time and the creation of final deposits. These situations differ significantly from the well-investigated problems of frictional flows on inclined planes, heap-flows and rotating drums which all consider thin flows in steady, uniform motion. The main objectives of subject (a) were:

> (1) To investigate the mobility of collapse flows and to obtain the physical relationships between the initial geometry of the particulate columns and their resulting deposits;
> (2) To characterise the time-dependent dynamics of the free upper surface and in particular the flow front propagation; and

(3) To examine internal deformation and deposition processes in granular collapse flows - in particular the dynamics of a moving, internal interface separating static (already deposited) from flowing particles.

These problems were studied for three major flow geometries: axisymmetric collapses of granular columns onto horizontal planes (Chapters II, III); two-dimensional collapses of granular columns into horizontal channels (Chapter IV) which were also used to investigate the interface between static and flowing grains (Chapters VI); and two-dimensional collapses of granular columns into inclined channels (Chapter VII). Different experimental set-ups, explicitly explained in the following chapters, were built that allowed detailed investigations with laser measurements and digital image analysis of high-speed cinematography and involved a variety of grain types and basal surfaces.

The experimental part of this thesis was done in close collaboration with Prof. R. Stephen J. Sparks FRS from the University of Bristol (U.K.), Prof. Herbert E. Huppert FRS and Dr. Mark A. Hallworth from the University of Cambridge.

Problem (b) was investigated through field work on the pristine pyroclastic flow deposits of the 1975 eruption of Mt. Ngauruhoe in New Zealand (Chapter V). The major aims of this study were:

(1) To obtain a first complete data set of the sedimentology of small-volume pyroclastic flows from most proximal to distal reaches.

(2) To characterise the deposit morphology through high-resolution GPS surveys to determine its dependence on travel distance, underlying slope and topographic confinement.

(3) The use of these unique data sets to develop a detailed qualitative model on flow and deposition that can be later tested against analogue and numerical experiments.

The 1975 eruption of Ngauruhoe suited such a detailed analysis as: it constitutes one of the world's geometrically simplest examples of pyroclastic flows, it was witnessed and closely documented, deposits are fully exposed, nowhere eroded, altered or modified by secondary motion, and because of the relatively small runout length and deposit width which allowed complete excavation. This study involved two periods of field work during 2004 and 2005. It

involved the excavation of 30 m^3 of pyroclastic material and the analysis of large masses of samples (~250 kg per location). The sedimentological analysis was partially done in New Zealand and partially at IFM-GEOMAR in Kiel. Beside the GPS measurements and sedimentological analysis, discussions with the original observers (Dr. Ian Nairn and Herb Spannagl) helped correlate individual flow units with timed pyroclastic flow events.

The field work was done in close collaboration with Dr. J. Shane Cronin, Thomas Platz and Jonathan Procter from Massey University in Palmerston North, and with Prof. Michael E. Sheridan from the State University of Buffalo (U.S.).

5. Thesis outline

The aims and topics of this Doctorial Thesis as outlined above are presented in six separate articles:

CHAPTER II – **Axisymmetric collapses of granular columns**

Authors	Gert Lube, Herbert E. Huppert, R. Stephen J. Sparks, Mark A. Hallworth
Status	published in Journal of Fluid Mechanics **508** (2004)

CHAPTER III – **Granular column collapse**

Authors	Gert Lube, Herbert E. Huppert, R. Stephen J. Sparks, Mark A. Hallworth
Status	published in XXI ICTAM Proceedings, Kluwer Academic Publishers

Chapters II and III comprise the first analysis of the fundamental problem of axisymmetric collapses of granular column onto a horizontal plane. It investigates the relationship between the initial column geometry and the geometry of the final deposit as a function of grain type and basal roughness. Data of the instantaneous position of the flow front as a function of time is used to compare inertial granular collapse flows with gravity currents of Newtonian fluids.

CHAPTER IV – **Collapses of two-dimensional granular columns**

Authors	Gert Lube, Herbert E. Huppert, R. Stephen J. Sparks, Armin Freundt
Status	published in Physical Review E **72** (2005)

Chapter IV investigates granular collapses into two-dimensional, horizontal channels. The paper focuses on the mathematical description of the deposit as a function of external parameters, and explains in detail the deformation and deposition processes that characterise the time-dependent inertial flow behaviour.

CHAPTER V – **Flow and deposition of pyroclastic granular flows:**

A type example from the 1975 Ngauruhoe eruption, New Zealand

Authors   Gert Lube, Shane J. Cronin, Thomas Platz, Armin Freundt, Jonathan N. Procter, Cargill Henderson and Michael F. Sheridan

Status   sub judice at Journal of Volcanology and Geothermal Research

Chapter V investigates the transport and deposition processes of pyroclastic granular flows exemplified by the 1975 eruption of Mt. Ngauruhoe. A first complete data set on the sedimentology and morphology of the upper free surface of small-volume pyroclastic flows from most proximal to distal reaches is established. This unique data are used to develop a detailed qualitative flow and deposition model for granular-type pyroclastic flows.

CHAPTER VI – **Static and flowing regions in granular collapses down channels**

Authors   Gert Lube, Herbert E. Huppert, R. Stephen J. Sparks, Armin Freundt

Status   sub judice at Physics of Fluids

Chapter VI is dedicated to the dynamical behaviour of static and moving regions in two-dimensional collapse flows. Detailed data of the time-dependent shape of the free upper surface and the internal interface, as well as vertical velocity profiles are being used to elucidate the flow and deposition mechanism by which inertial granular collapse flows can propagate over inclination well below the (static) angle of repose.

CHAPTER VII – **Granular collapses down rough, inclined channels**

Authors   Gert Lube, Herbert E. Huppert, R. Stephen J. Sparks, Armin Freundt

Status   to be submitted to Journal of Fluid Mechanics

Chapter VII constitutes an unpublished article on granular collapses into rough, inclined channels. The study carries further the ideas established in Chapters II-IV and VI and investigates the influence of the basal inclination on flow and deposition behaviour.

Beside these main articles particular aspects of this study were presented at several conferences and workshops:

EGS-AGU-EUG Joint Assembly, Nice (2003):

Lube G., Sparks R.S.J., Huppert H.E. and Hallworth M.A., Granular column collapses, EGS – AGU – EUG Joint Assembly, Geophysical Research Abstracts, Vol. 5, 03357 (2003).

Isaac-Newton Conference on Geophysical Granular & Particle-Laden Flows, Bristol (2003):

Lube G., Huppert H.E., Sparks R.S.J. and Hallworth M.A., Scaling behaviour of granular flows, Isaac Newton Institute – Abstracts, Geophysical Granular & Particle-Laden Flows Workshop (2003).

Isaac-Newton Conference on Geophysical Granular & Particle-Laden Flows, Bristol (2003):

Huppert H.E., Lube G., Sparks R.S.J. and Hallworth M.A., Axisymmetric Granular Collapses, Isaac Newton Institute – Abstracts, Geophysical Granular & Particle-Laden Flows Workshop (2003).

APS Annual Meeting, Rutherford, New Jersey (2003):

Huppert H.E., Hallworth, M. A., Lube G. and Sparks R.S.J., Granular column collapses, DJ002, The American Physical Society 56th Annual Meeting of the Division of Fluid Dynamics (2003).

European Geosciences Union General Assembly, Vienna 2005:

Lube G., Huppert H.E., Platz T., Sparks R.S.J., Freundt A., Cronin S.J. and Procter J., Transport and sedimentation processes of small-volume pyroclastic flows, Geophysical Research Abstracts, Vol.7, 01102 (2005). (Support by Young Scientist's Travel Award)

European Geosciences Union General Assembly, Vienna 2006:

Lube G., Cronin S.J., Platz T., Freundt A., Procter J., Henderson C. and Sheridan M.F., Flow and deposition of pyroclastic granular flows of the 1975 Ngauruhoe eruption, New Zealand, Geophysical Research Abstracts, Vol. 8, 03628 (2006).

The following study:

Lube G., Huppert, H.E., Sparks R.S.J and Freundt A., Static and flowing regions in granular collapses down channels, Gordon Research Conference Granular and Granular-Fluid-Flow, Oxford July 23-28 2006.

has been nominated as one of four Gordon-Research Young Scholar's Awards of the Queen's College Oxford 2006.

6. Future prospects

Based on the herein presented research results, three major lines of future investigations emerge.

- In order to understand better complex flow and deposition behaviour in pyroclastic flows (or more generally geophysical mass flows), experiments on granular flows involving multiple particle sizes and a (hot) interstitial gas-phase need to be investigated. An important question to address is also the effect of variable lateral flow confinement and its mathematical description. The problem to define a three-dimensional stress tensor and realistic boundary conditions in numerical models is well known. However, it is generally circumvented by non-validated mathematical assumptions and/or the limitation to two-dimensional simulations.

- The implementation of the presented physical relationships (in particular the description of a moving internal interface) into numerical models will improve the computational hazard assessment for geophysical mass flows. The successful numerical simulation of time-dependent flow and deposition processes for geophysical flows over natural terrain could enable the much demanded comparison between field data and numerical models.

- As demonstrated in chapter V, detailed sedimentological data-sets of pyroclastic flow deposits from proximal to distal reaches allow identifying variations in flow, erosion and deposition that occur with distance downstream, and the calculation of reliable approximations of the bulk (or initial) grain-size distribution. It is shown how these bulk distributions in turn can be used to quantify time- and space-dependent segregation, erosion, deposition mechanisms. Currently no comparably detailed data sets exist for other pyroclastic flow deposits. It is suggested to augment the data-set for flows of different volumes and granulometric compositions through GPS surveys and detailed grain-size analysis for multiple fresh and young flow deposits. A comparison of these different data sets will allow understanding better flow and deposition mechanisms as a function of initial flow volume, granulomery, travel distance and topography.

REFERENCES

Anderson, K. G. & Jackson, R. 1992 A comparison of the solutions of some proposed equations of motion of granular materials for fully developed flow down inclined planes. J. Fluid Mech. **92**, 145–168.

Bagnold, R. A. 1954 Experiments on a gravity-free dispersion of large solid spheres in a Newtonian fluid under shear. Proc. R. Soc. Lond. A. **225**: 49–63.

Boudon, G., Camus, G., Gourgaud, A. & Lajoie, J. 1993 The 1984 nuee ardente deposits of Merapi volcano, Central Java, Indonesia: stratigraphy, textural characteristics, and transport mechanisms. Bull. Volcanol. **55**: 327–42.

Campbell, C. S. 1990 Rapid granular flows. Annu. Rev. Fluid Mech. **22**, 57–92.

Dade, B. & Huppert. H.E. 1998 Long-runout rockfalls. Geology **26**: 803–6.

Denlinger, R. P. 1987 A model for generation of ash clouds by pyroclastic flows, with application to the 1980 eruptions at Mount St Helens. J. Geophys. Res. **92**: 10284–98.

Denlinger, R. P. & Iverson, R. M. 2001 Flow of variably fluidized granular masses across three-dimensional terrain; 2, numerical predictions and experimental tests. J. Geophys. Res. B **106**: 553–66.

Druitt, T. H. 1998 The eruption, transport and sedimentation of pyroclastic flows. In: Gilbert, J. & Sparks, R.S.J. (Ed.), The Physics of Volcanic Eruptions, Geol. Soc. London Spec. Publ. **145**: 147–200.

Eglit, M. E. & Sveshnikova, Y. I. 1980 Matematicheskoye modelirovaniye snezhnykh lavin; mathematical modeling of snowavalanches Materialy Glyatsiologicheskikh Issledovaniy, Khronika Obsuzhdeniya **38**: 79–84.

Freundt, A. & Bursik, M. I. 1998 Pyroclastic flows transport mechanisms. In: Freundt A. and Rosi M. (Ed.), From Magma to Tephra: Modelling Physical Processes of Explosive Volcanic Eruptions, Developments in Volcanology 4: 173–245. Elsevier.

Freundt, A., Wilson, C.J.N. & Carey, S.N. 2000 Ignimbrites and block-and-ash flows. In: Sigurdson, H. et al. (Ed.) Encyclopedia of volcanoes. Academic Press: 581-599.

Fujii, T. & Nakada, S. 1999 The 15 September 1991 pyroclastic flows at Unzen volcano (Japan): a flow model for associated ash-cloud surge. J. Volcanol. Geotherm. Res. **89**: 159–72.

G.D.R. Midi 2004 On dense granular flows. Eur. Phys. J. E **14**, 341.

Iverson, R. M. & Denlinger, R. P. 2001 Flow of variably fluidized granular masses across three-dimensional terrain. Part I: Coulomb mixture theory. J. Geophys. Res. **106**, 537–552

Jaeger, H. M., Nagel, S. R. & Behringer, R. P. 1996 Granular solids, liquids, and gases. Rev. Mod. Phys. **68**, 1259–1273.

Kadanoff, L. P. 1999 Built on sand: Theoretical ideas inspired by granular flows. Rev. Mod. Phys. **71**, 435–444.

Pouliquen, O. 1999 Scaling laws in granular flows down rough inclined planes. Phys. Fluids **11**, 542–548.

Rodriguez-Elizarraras, S. R., Siebe, C., Komorowski, J. C., Espindola, J. M. & Saucedo, R. 1991 Field observation of pristine block-and-ash-flowdeposits emplaced on 16–17 April 1991 at Volcan de Colima,Mexico J. Volcanol. Geotherm. Res. **48**: 399–412.

Savage, S. B. 1995 Flows of granular materials. Proc. CANCAM '95 (ed. B. Tabarrok & S. Dost), pp. 62–73. University of Victoria, BC, Fleming Express Press Ltd, Victoria, BC.

Savage, S. B. 1998 Analyses for slow quasi-static, high concentration flows of granular materials. J. Fluid Mech. **377**, 1–26.

Savage, S. B. & Hutter, K. 1989 The motion of a finite mass of granular material down a rough incline. J. Fluid Mech. **199**, 177–215.

Takahashi, T. & Tsujimoto, H. 2000 A mechanical model for Merapi-type pyroclastic flows J. Volcanol. Geotherm. Res. **98**: 91–115.

Wilson, L. & Head, J. W. 1981 Morphology and rheology of pyroclastic flows and their deposits, and guideline for future observations. vol 1250, In: Lipman; P.W. and Mullineaux, D.R. (Ed.), USGS pp 1259: 513–24.

Yamamoto, T., Takarada, S. & Suto, S. 1993 Pyroclastic flows from the 1991 eruption of Unzen Volcano Japan. Bull. Volcanol. **55**: 166–75.

Chapter II

Axisymmetric collapses of granular columns

Abstract

Experimental observations of the collapse of initially vertical columns of small grains are presented. The experiments were performed mainly with dry grains of salt or sand, with some additional experiments using couscous, sugar or rice. Some of the experimental flows were analysed using high-speed video. There are three different flow regimes, dependent on the value of the aspect ratio $a = h_i/r_i$, where h_i and r_i are the initial height and radius of the granular column respectively. The differing forms of flow behaviour are described for each regime. In all cases a central, conically sided region of angle approximately $59°$, corresponding to an aspect ratio of 1.7, remains undisturbed throughout the motion. The main experimental results for the final extent of the deposit and the time for emplacement are systematically collapsed in a quantitative way independent of any friction coefficients. Along with the kinematic data for the rate of spread of the front of the collapsing column, this is interpreted as indicating that frictional effects between individual grains in the bulk of the moving flow only play a role in the last instant of the flow, as it comes to an abrupt halt. For $a<1.7$, the measured final runout radius, r_∞, is related to the initial radius by $r_\infty = r_i(1+1.24a)$; while for $1.7<a$ the corresponding relationship is $r_\infty = r_i(1+1.6a^{1/2})$. The time, t_∞, taken for the grains to reach r_∞ is given by $t_\infty = 3(h_i/g)^{1/2} = 3(r_i/g)^{1/2}a^{1/2}$, where g is the gravitational acceleration. The insights and conclusions gained from these experiments can be applied to a wide range of industrial and natural flows of concentrated particles. For example, the observation of the rapid deposition of the grains can help explain details of the emplacement of pyroclastic flows resulting from the explosive eruption of volcanoes.

CHAPTER II

1. Introduction

Granular media have been the focus of an increasing amount of research in recent years, because their properties and behaviour as either static piles or highly mobile flows are fundamental to the understanding of many man-made processes and natural phenomena. The deliberate flow of particulate matter is widely encountered in the industrial handling of grains and powders, while the mechanical stability of static piles of granular material is of central concern to many civil engineering projects. In nature, accumulations of non-cemented grains occur in both subaerial and subaqueous environments over scales ranging from millimetres to several tens of kilometres. Their tendency to remain statically packed or move is fundamental to phenomena ranging from the inexorable processes of erosion and sedimentation to the sudden catastrophic failures of landslides and generation of snow avalanches on mountains and pyroclastic flows in explosive volcanic eruptions.

In spite of these ubiquitous applications, even static problems involving granular media, such as the central issue of determining the pressure at the base of a stationary sand pile, are still controversial – see, for example, the reviews by Cates et al. (1999) or de Gennes (1999). Part of the difficulty stems from trying to describe quantitatively the forces set up between individual grains. In addition, the static friction against confining walls, if present, leads to a pressure with depth dependence that can be far from the hydrostatic relationship valid in a fluid.

Flowing granular media present further problems of great richness and complexity. While there are a variety of theories, and related governing equations, to describe particular aspects of granular motion, these (generally) continuum theories and equations are still deficient and much debated. Some progress has been made in considering the flow of granular material down chutes whose initial steepness is greater than the (static) angle of repose of the granular media, thus assuring its initial motion. The approach generally used by a variety of researchers has been to derive depth-averaged equations for flow down a rough inclined plane and introduce empirical friction factors to try to obtain agreement with data from experiments (see, for example Savage & Hutter 1989; Anderson & Jackson 1992; Savage 1998; Pouliquen 1999; Iverson & Denlinger 2001, and some of the references therein). However, to quote Pouliquen (1999) "despite this apparent simplicity and the numerous experimental, numerical and theoretical works devoted to

granular chute flows, their description and prediction are still a challenge". Some of the reasons why the challenge remains are described by Kadanoff (1999).

Many insightful reviews of the exciting and diverse areas of research into granular flows have appeared, including those by Campbell (1990), Savage (1995) and Jaeger, Nagel & Behringer (1996).

The aim of the current work is to present experimental results for the fundamental problem of the collapse of initially vertical cylinders of granular material. The study focuses on the subsequent axisymmetric spreading of the dense granular flows. Aside from intellectual curiosity and the central nature of the problem, the study is primarily motivated by a need to understand the flow mechanics of granular material in the environment, such as occur in pyroclastic flows and debris avalanches. The study may also be relevant to understanding industrial granular flows generated either by accident or design. Pyroclastic flows and debris avalanches are some of the most destructive phenomena in nature. In order to assess their hazard potential, an understanding of their underlying physics is essential. Geophysical particulate flows are understood as multi-phase flows where volume, mass flux, grain size, particle concentration and bulk density can vary over several orders of magnitude (Druitt 1998). Thus, physical models describing the state of flow range from dense, granular flows, where the gas phase plays a subsidiary role (Dade & Huppert 1998) and motion is dominated by particle interactions, through gas-fluidized flows, where gas plays a significant role (Roche et al. 2002), to highly diluted, turbulent systems where gas is the dominant phase and transports particles in turbulent suspension (Druitt 1998; Freundt & Bursik 1998; Huppert 1998). Direct observations of such geophysical flows are rare and the study is often limited to making inferences from the characteristics of their resulting deposits. Interpretations of all such geological observations depend on a good understanding of the underlying fluid mechanics.

In contrast to classical fluid mechanics, general constitutive laws for granular flows are largely unknown and experimental studies in these circumstances provide a key approach to the investigation of their dynamical behaviour. Recent experimental studies on chute flows of granular matter (e.g. Savage & Hutter 1989; Daerr & Douady 1999; Pouliquen 1999; Pouliquen & Forterre 2002) reveal interesting scaling laws on granular dynamics, but many of these

experiments are performed under steady flow conditions. However, most of the dynamics in dense, geophysical flows are likely to involve unsteady motions. For example, many pyroclastic flows and debris avalanches are initiated on the steep flanks of a volcano and then run out and deposit on shallow slopes. The flows involve acceleration and deceleration and also stages of erosion and deposition.

In this paper we present the results of a series of experiments on axisymmetric granular flows in a simple set-up that (to our knowledge) has not been studied before. The experiments consist of suddenly releasing cylindrical columns of rough granular material over a flat surface, by rapidly raising the containing cylinder. The material then collapses radially and forms a symmetrical pile. The simplicity of this approach enables us to vary the initial parameters of the system (height and radius or volume of the column) systematically. Our aim in this study is twofold. First we are interested in the scaling behaviour for the flow motion and how the geometry of the resulting deposit varies with the initial parameters. To this end we have run experiments which change the initial geometry over at least 2 orders of magnitude. Once the simplest scenario of axisymmetric spreading of dense, well-sorted grains on a flat surface is understood, the set-up can be varied in the future to simulate situations closer to natural flows (e.g. by considering multiple grain sizes and densities, inclination of the ground, temperature etc.). Secondly, our experiments consider processes of flow deformation and sedimentation in dense granular flows. Experimental observations may help to understand the formation of sedimentary features in deposits of pyroclastic flows and debris avalanches that are still controversial. We note, by contrast, that if instead of rough grains we used smooth, frictionless spheres, the collapse would continue indefinitely. Alternatively, an ordered stack of regular shapes, such as a pile of bricks will not collapse at all.

The duration of each experiment was typically less than 2 s and detailed investigations of the flow process required the use of a high-speed video camera. This technique was employed in experiments conducted in Bristol University using sand as the granular material. A complementary set of experiments, aimed mainly at analysing the final geometries of axisymmetric collapses, was performed in Cambridge University, using predominantly sand and salt. Some additional experiments were conducted with couscous, rice, or sugar in order to investigate variations in grain shape and roughness.

The detailed descriptions of the experimental procedure, measurement methods and variations of experimental parameters are given in § 2. Experimental observations are presented in § 3. Results on the geometry of the final deposits of axisymmetric spreading flows are given in § 4. In that section we also show how the geometry of the final deposits scales with the initial parameters and that the presented scaling laws change significantly within the large range of experimental parameters but little between the different grains. The dynamics of laboratory flows with sand are analysed using data on the motion of the flow front in § 4. We present a scaling that describes the radial displacement of the flow front as a function of time for a range of initial parameters and compare this with the spreading of a fluid gravity current released instantaneously from a lock. Expressions for the total collapse time of the column are also obtained. A summary of our results and further discussion are presented in § 5. Aside from our quantitative results describing the motion, the study points to the abrupt transition undergone between the flowing grains and the final static state, the only time during in which intergranular friction appears to be important in controlling the motion of the flowing material.
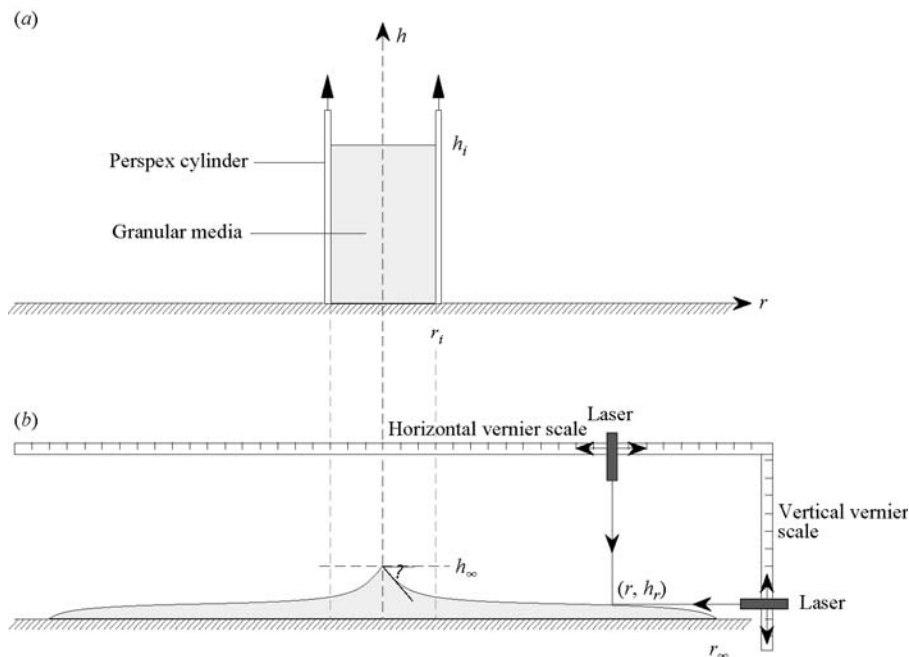

Figure 1. (a) Initial set up for the experiments and (b) rough sketch of the geometry of the final deposit and how it was measured.

2. The experiments

2.1. Experimental set-up

The experiments were performed by rapidly releasing granular materials, initially contained in a partially filled cylinder, on to a flat surface and allowing them to spread out unhindered, as sketched in figure 1. Both dry sand with a narrow grain size distribution and vacuum-dried salt were primarily used as the particulate matter, and their density, mean grain size and angle of repose are given in table 1. Granular flows with salt were carried out on a smooth surface of baize. The sand flows were studied on three different surfaces: a smooth wooden plane, a smooth transparent Perspex plane and a rough plane made of sandpaper. The granular roughness of the sandpaper was of the order of the mean particle size of the granular flows. Additional experiments with couscous, rice and sugar were performed on both a smooth wooden plane and a smooth baize surface to further investigate interparticle friction for different grains. A photo of the different sets of grains, clearly showing their different geometrical shapes, makes up figure 2. All the results were independent of the different grains and the surface over which the grains flowed.

The initial aspect ratio a, given by the ratio of initial height, h_i, to radius r_i was varied systematically by using different initial masses of material, m_i, and different diameter cylinders. The radii of the cylinders and the range of the initial aspect ratios used with each material are given in table 2. The initial columns were prepared by quickly pouring a measured mass of particles from above the centre of the cylinder. In order to produce a cylindrical shape the upper surface of the granular column was then flattened. A number of different ways of filling the cylinder were tested and they all lead to the same results. At the start of each experiment, the cylinder was quickly raised at velocities of around 2 ms^{-1} and the column collapsed and spread out to form a symmetrical pile, as sketched in figure 1(*b*).

Particle	Mean density (g/cm³)	Mean grain size (mm)	Angle of repose (deg.)
Sand	2.6	0.32	30
Salt	2.16	0.30	30
Couscous	1.39	2	34
Rice	1.46	7×2	31
Sugar	1.58	1	35

TABLE 1. Properties of particles used in the experiment

2.2. Measurement methods

In order to investigate the dynamic behaviour of the granular motion, a digital high-speed video camera was used for all the experiments conducted in Bristol using sand. To preserve the images at reasonable sharpness, the experiments were recorded digitally at rates of 500 frames per second. Distance versus time data of the flow front were obtained from the footage by measuring the elapsed time at radial markings 1 cm apart. To study the flow and sedimentation processes at the base of the granular body, experiments were performed on a transparent Perspex plane and filmed from below. In order to help visualize the deformation and sedimentation processes during flow, two experimental columns were prepared with zones of differently coloured particles. In the first experiment, three concentric zones were established, consisting of an inner cylinder of non-dyed particles, a middle ring of dyed particles and an outer ring of non-dyed particles. In the second experiment, the cylinder was filled with eight alternating horizontal layers of non-dyed and dyed particles. Both these experiments were carried out on a Perspex plane to study the base of the final deposit. For visualization of the internal deformation, some of the final deposits were cut by a thin transparent vertical Perspex plane.
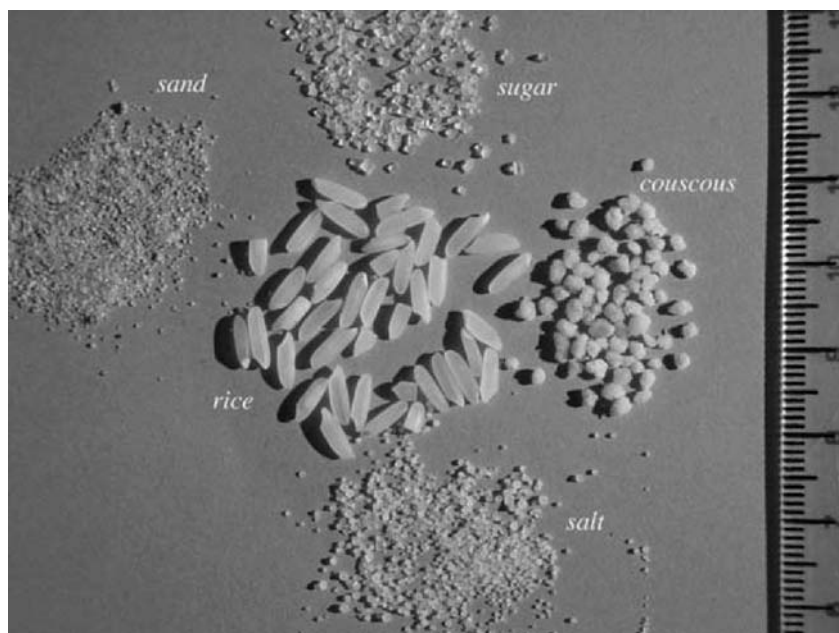

Figure 2. Photo of five different grains used in the experiments.

After flow, measurements of the final runout r_∞, the final cone height h_∞, the steepest inclination of the pile α and a radial height profile through the pile were measured from the deposit using a point laser focusing technique, as shown in figure 1(*b*). In some cases, radial height profiles

across the pile were also obtained using a penetrometer. This tool consists of thin wires 2 cm apart from each other and covered by a thin film of silicon grease. The wires are inserted vertically into the deposit down to its base, and then withdrawn. Heights were obtained by measuring the distance along which particles stuck to the wire. This method resulted in some destructive disturbance of the granular pile, and could not be used in areas where the angle of rest of the grains approached unstable values, particularly around the steep central cone. Heights obtained in this manner were accurate to ± 1 mm, whereas heights and radii obtained by the laser point technique had errors estimated as ± 0.1 mm. Repeatability of measurements for the final radius between experiments was of order ± 5 mm.

Particle	Initial radius (cm)	Range in h_i/r_i
Sand	9.7	0.19–4.8
	7.45	0.44–4.62
	2.92	1.5–13.8
Salt	5.75	0.25–5.22
	3.19	1.09–17.7
	2.6	2.7–31.4
	2.25	2.0–35.0
	1.69	4.8–42.9
Couscous	7.3	0.31–1.89
	5.75	1.91–4.76
	2.55	9.10–25.1
Rice	7.3	0.44–1.99
	5.75	0.49–8.45
	2.55	5.22–25.3
Sugar	7.3	0.37–1.84
	5.75	1.86–3.69
	2.55	4.23–25.0

TABLE 2. Radius of cylinder and range of initial aspect ratio for each material.

3. Flow description

Our observations of axisymmetric granular flows from high-speed movies reveal the subdivision into three regimes of flow behaviour dependent on the initial aspect ratio.

3.1. Flows with aspect ratios less than 1.7

For the situations with aspect ratios less than 1.7 (the reason for this limit is explained below), the free upper surface of the column divides into an inner, static axisymmetric region and an outer
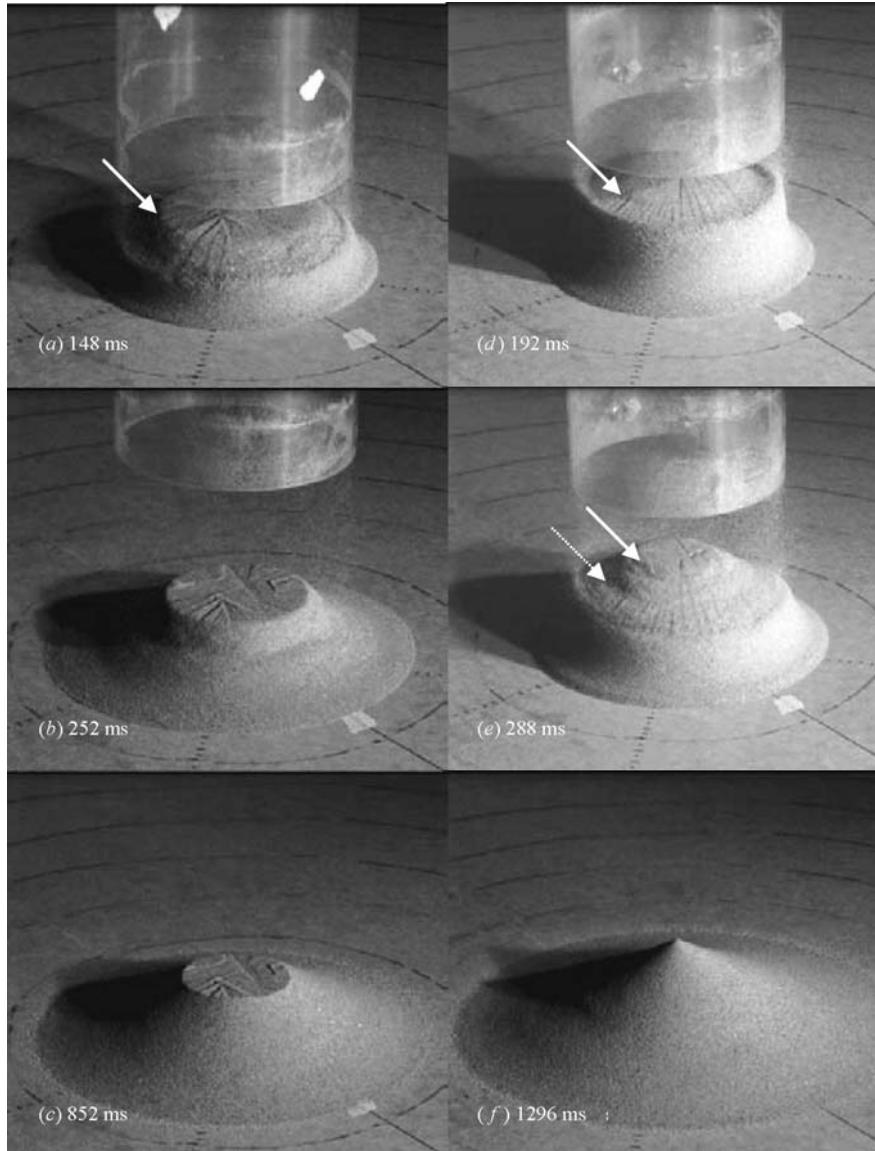
Figure 3. Two experiments, at three different times, with a < 1.7. The photographs for the first experiment, with a = 0.55, were taken at (a) 148 ms, (b) 252 ms and (c) 852 ms, and are typical results for a < 0.74. The photographs of the second experiment, with a =0.9, are at (d) 192 ms, (e) 288 ms and (f) 1296 ms and show the flow evolution for a typical experiment with $0.74 < h_i/r_i <1.7$. The arrows mark discontinuities in the slope of the free surface.

flowing region. Figure 3 depicts typical photographs for this situation. For flows with $a<0.74$ a single circular discontinuity on the surface of the column separates an outer, slumping region from a non-deformed inner region (figure 3*a–c*). For flows with $0.74<a<1.7$ the flow is more complex. Two circular discontinuities develop on the upper surface of the column, one rapidly

after the other (figure 3*d*). Material beyond the first discontinuity starts flowing before material between the two discontinuities (figure 3*e*). The slope of the free surface gradually steepens from the flow front to the flat top, attaining the angle of repose there.

From photographs taken during the flow from below, three different regions were observed at the base: a static circular region, with the same radius r_i as the initial container; a ring of previously deposited particles; and an outer ring of still flowing material. The last two regions are divided by a moving interface, which propagates outwards until the flow comes to rest. After the flow front stops, another moving interface, separating an outer static zone from an inner zone of flowing grains, was seen to propagate along the upper free surface from the stationary front towards the centre. The motion in the inner zone is in response to avalanching of the margins of the static circular region observed at the upper surface. This avalanching gradually reduces the radius of the inner zone. The extent of erosion of the circular region at the surface increases with increasing aspect ratio.

After all motion has ceased, for flows with $a<1$ a circular undisturbed area at the upper surface of the column, which remains at h_i, is preserved (figure 3*c*), connected to a slope with maximum inclination approximately at the static angle of repose ($\alpha = 32°–32.5°$ for sand). In contrast, late-stage avalanching for $1<a<1.7$ erodes the entire initial column surface leaving a conical pile at the peak (figure 3*f*). The maximum inclinations for flows with $1<a<1.7$ were between 3° and 5° less than the static angle of repose.

3.2. Flows with intermediate initial aspect ratios

For columns of $a>1.7$ (figure 4*a*), the entire upper surface starts to flow immediately. At the base of the column a flow front develops and axisymmetrically propagates outwards (figure 4*b*). In the first stage of flow the upper free surface of the column remains undeformed and horizontal (figure 4*b*). After the column has lost some height, deformation of the top occurs to form a dome whose radius of curvature decreases with time (figure 4*c, d*). Just before the central body relaxes towards its final cone-like shape, two concentric stationary bulges appear on the surface around its steep slope (white arrows in figure 4*e*). Additionally, as the flow front decelerates, two outwardly propagating concentric surface waves develop across the free surface (black arrows in figure 4*e*). Their amplitude of a few millimetres is relatively small compared to their wavelength
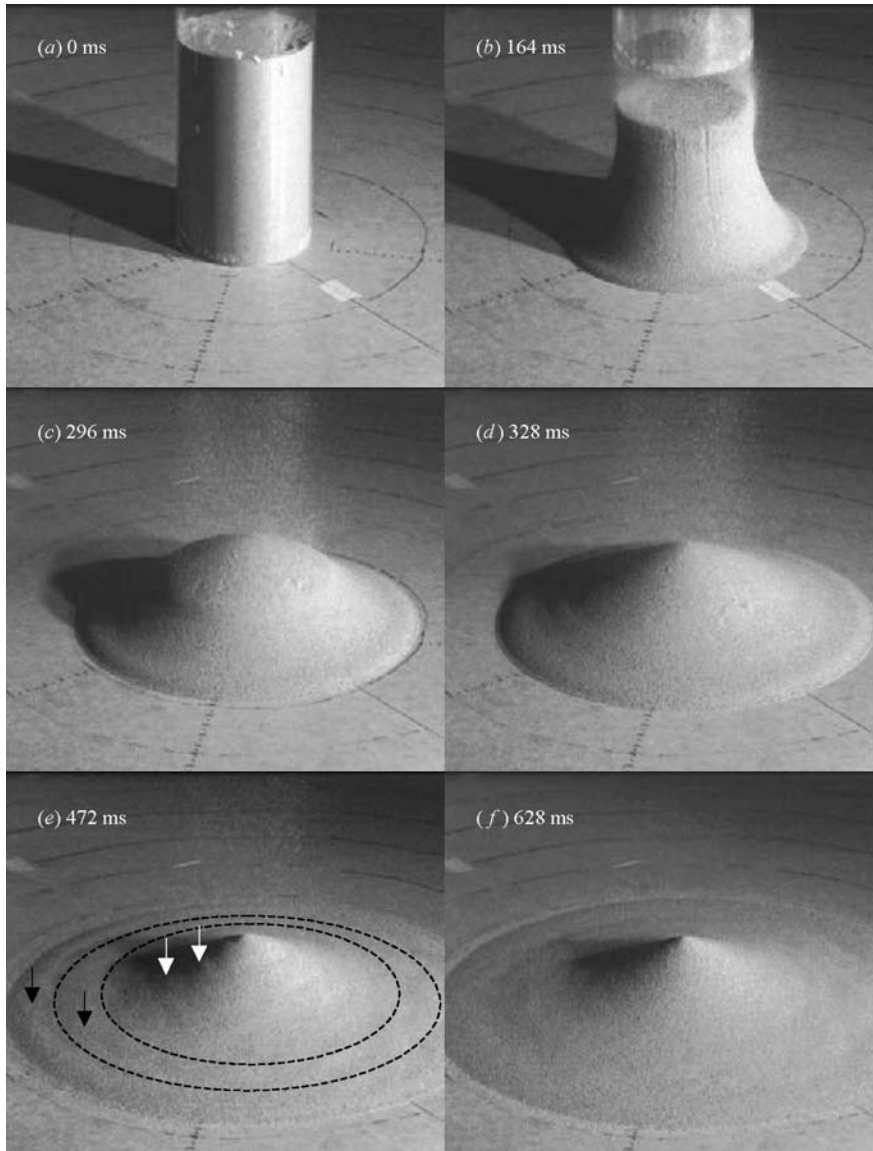
Figure 4. Flow evolution at various times for an experiment for which a =2.75.

of 2–3 cm. From the time the flow front stops, a moving interface between deposited and flowing grains propagates inwards across the free surface from the flow front to the central cone (figure 4*f*). This surface phenomenon eliminates the waves and they are not preserved in the final deposit. As with flows for *a*<1.7, there are three regions at the base of the flowing granular body: an originally static circular region with radius r_i; a ring of previously deposited particles; and an outer ring of still moving particles. In this outer ring, particle velocities increase with radial distance. For most of the experiment the basal interface between deposited and moving particles continuously propagates outwards. As the flow front decelerates, the interface between deposited and moving grains abruptly jumps to a position further out. After the jump, the new interface
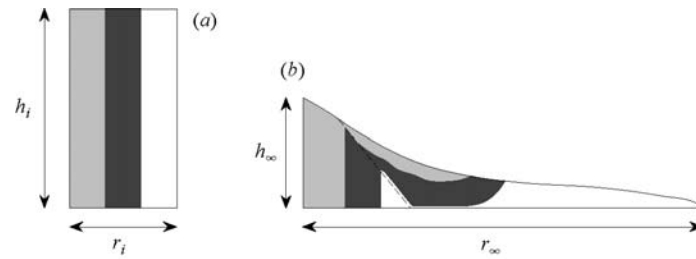
Figure 5. A vertical section of the deposit (b) of a column with three initially concentric zones (a).
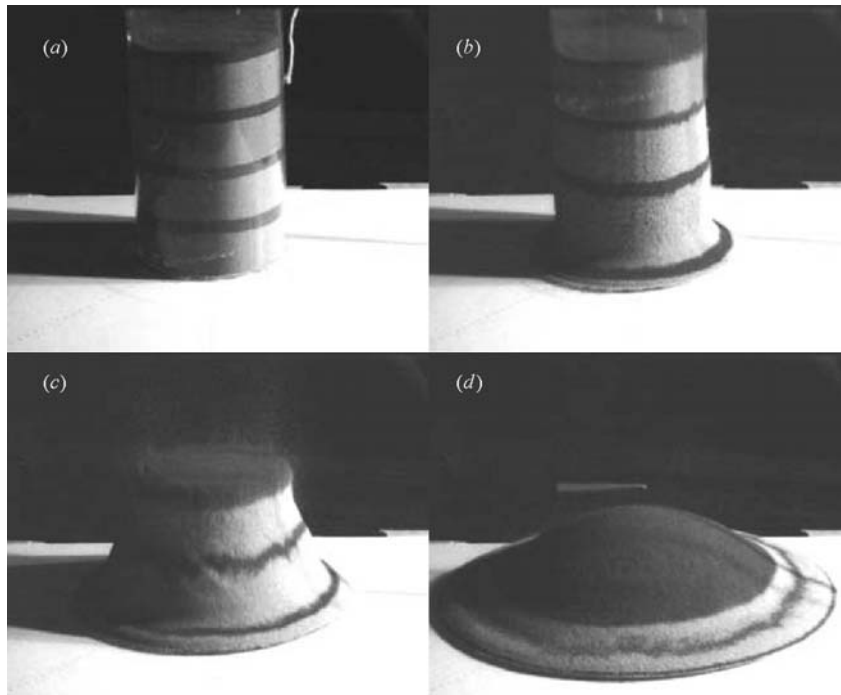
Figure 6. Sequence of photographs from an experiment with four marked horizontal layers and a = 3.0.

between deposited and moving particles becomes wavy. A second jump of the interface between deposited and moving particles occurs just before the flow front stops. The radial distances of the regions before and after the jumps were measured in the high-speed movies. They coincide with the radial distances of the troughs of the concentric waves at the free surface.

The final deposit had a steep central cone and an axisymmetric tapering frontal region. The maximum inclination α of the deposit was slightly smaller than the static angle of repose. Flows with $1.7 < a \leq 4.6$ show similar inclinations ($\alpha = 25.5° - 27°$ for sand).

When the experiment with three marked concentric zones was vertically sectioned (figure 5) an originally static, central cone-like body can be observed. The most distal parts of the deposit originate from the outermost initial concentric zone. The middle zone has slumped closer to the original position, but is always separated from the ground by a thin zone (a few grain diameters) with particles from the outer zone. This implies that the interface between deposited and moving particles evolves into the flowing body as a shallow plane.

Qualitative observations of grain motion along the free upper surface can be deduced from experiments with a column of initially marked horizontal layers. From the top of the column towards the flow front, the free surfaces of these layers are first increasingly stretched in the flow direction at the steep inclined part of the failing column and then increasingly compressed at the outer, flat tapering region (figure 6). The stretching and compression of the free surfaces of these layers is due to different particle velocities at different positions along the free surface. Thus, as observed for the flow front motion, the velocity of particles along the upper free surface change with time. Additional experiments with specially placed marker grains indicated that grains initially in the uppermost region ended up blanketing most of the final pile. Also, of those grains initially on the vertical margins of the cylinder, all but those in a small region near the top ended up at the base of the deposit. This parallels the fluid mechanical concept that in free flow a fluid parcel which starts on a surface remains on a surface. The experiments with marker beds also indicated that these granular flows do not involve much mixing between initially horizontal, different layers, which become deformed and distorted but not mixed during their displacement.

3.3. Flow with large initial aspect ratios

The flow behaviour of the collapse changes as the initial aspect ratio increases; and our data suggest that another transition occurs at around an aspect ratio of roughly ten. After lifting the container, the entire free surface starts to flow immediately. A flow front develops at the basal margin of the column and propagates radially as a thin sheet (figure 7*b*). In contrast to low-aspect-ratio flows, the upper surface of the column remains undeformed until its height is reduced to that of the neighbouring flat frontal region (figure 7*c, d*). From that time a concentric wave originates from the margin of the falling column and propagates outwards (figure 7*d* and *e*). Since the wave moves at greater velocity than the flow front it eventually reaches the front, whereupon a thickening of the flow front is observed. Before the flow front has stopped, a

moving interface between an inner zone of static grains and surrounding flowing grains propagates along the free surface from the cone towards the front (figure 7*f*).
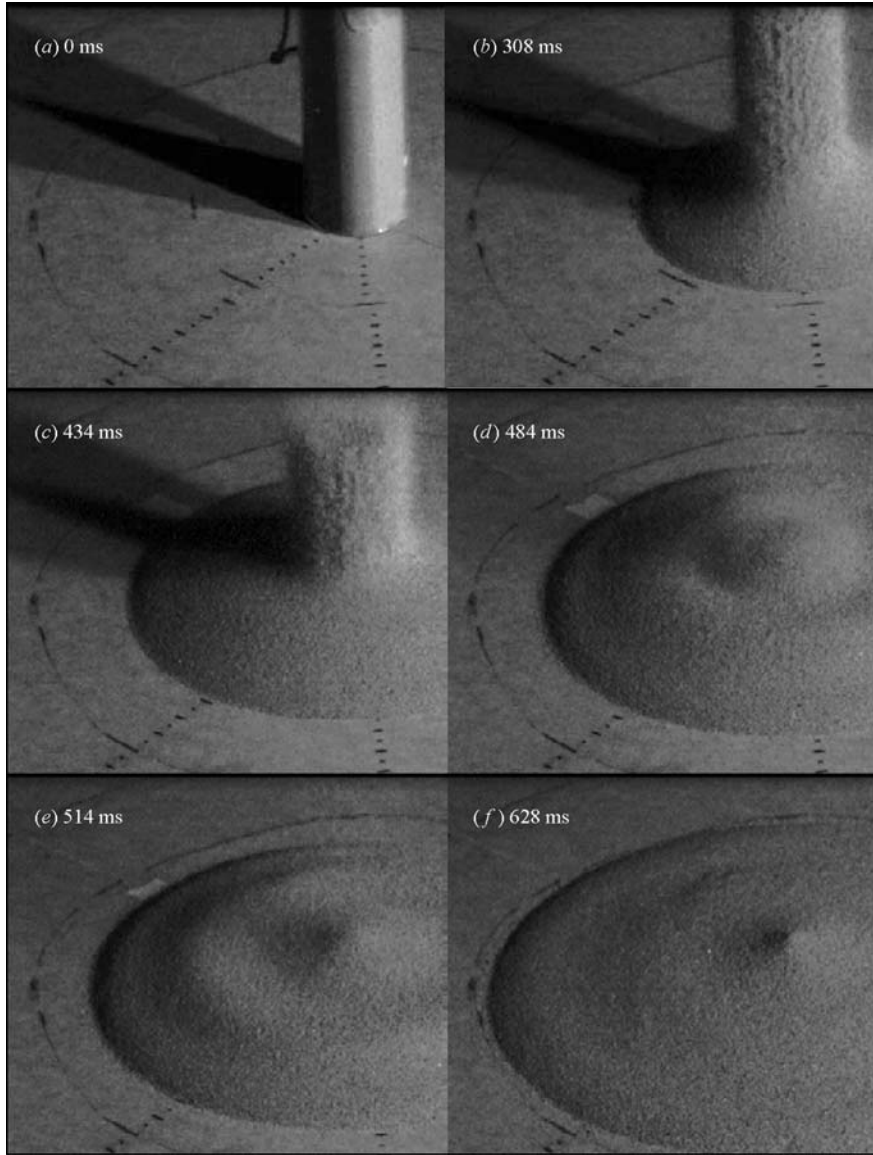
Figure 7. Flow evolution at various times from an experiment with a = 13.8.

As with flows of lower initial aspect ratios, three different regions were observed at the base of the flow: an originally static circular area with radius r_i; a ring of previously deposited particles; and an outer ring of moving particles. In the first phase of the experiment the interface between deposited and flowing grains continuously propagates outwards. Approximately from the time the wave develops at the free surface, this interface propagates backwards. Thus, already deposited particles are remobilized. A few tens of milliseconds later the direction changes again

and the interface between deposited and moving particles propagates outwards. As with flows of intermediate initial aspect ratios, the interface can then jump abruptly outwards. After the jump the interface continuously propagates outwards until a second jump appears a few centimetres behind the flow front.

The final deposit shows a small central cone and a tapering frontal region. The maximum inclination α at the cone is much smaller than the static angle of repose. Our data suggest that α decreases with increasing initial aspect ratio. Much of the remainder of the deposit is of almost uniform thickness. Two concentric bulges were preserved, one near the flow front and the other approximately at half of the runout distance. The bulges were centred above the radial positions where the jumps of the interface between deposited and moving grains were observed at the flow base near the end of emplacement.

4. Results

4.1. Geometry of the inner, static body

When viewed from below, a static region with radius r_i was observed in all sand experiments carried out in Bristol. For flows with $a<1.7$ a circular discontinuity between a static and a surrounding flowing region was observed at the upper surface of the column. The size of this static region was measured in the high-speed movies after its first appearance at the radial distance r_a. There is a good linear relationship between r_a and h_i, the height of the static region at the upper surface of the column, for cylinders with radii r_i =9.7cm (figure 8). The regression line through the data indicates a zero height at a radial distance of 9.64 cm, satisfyingly close to r_i =9.7 cm. This result is consistent with an inner, static body with a cone geometry. The outer inclination of that cone, calculated from the regression line, corresponds to an angle of 59.4°, which can be interpreted as an internal friction angle for the sand. The aspect ratio of this cone is $\tan^{-1} 59.4°$=1.7.

For flows with $a>1.7$ no discontinuity was observed at the upper surface of the column. However, the relaxation of the central region towards a cone-like shape suggests a static interior in the centre. Cutting a deposit of a column with marked layers shows the geometry of this inner, static body to be a steep inclined cone with a slightly flattened top (figure 5), which is consistent with the partial erosion of the primary inner, static body by the flow.
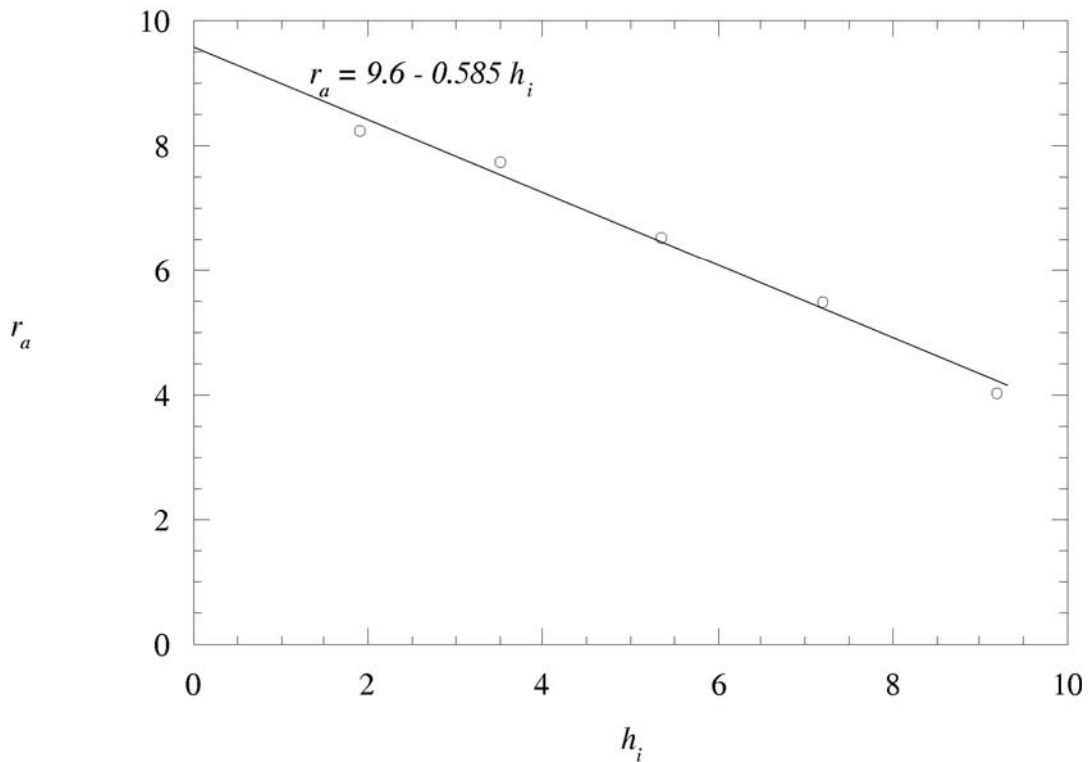
Figure 8. The radius of the undisturbed free surface, r_a, as a function of the initial height, h_i, from experiments on sand with $a < 1.7$. The best-fit straight line through the data is also presented.

4.2. Scaling laws for the final runout

The initial experimental set-up is uniquely expressible in terms of any two of the variables r_i, h_i and $V = \pi r^2_i h_i$. Thus, under the assumption that no internal parameters, such as the value of the Coulomb friction between grains, are relevant during the flow, the final runout radius, r_∞, and height, h_∞, can also be written in terms of any two of these three variables. Put another way, the success with which we can quantitatively describe all our experimental data, for different grains, in terms of two of these variables only supports the validity of the assumption that no other parameter plays an essential role. Further confirmation of this result comes from the kinematic data discussed in § 4.6.

Our observations that the form of the collapses differs with different aspect ratios $a = h_i/r_i$ suggests using a as a fundamental parameter, to which we add, for convenience, r_i. (Either h_i or V_i could also be used to lead to the same results.) Then, by dimensional analysis, we can write

$$r_\infty = r_i \tilde{f}(a),$$ (1)

where $\tilde{f}(a)$ is a (non-dimensional) function of the aspect ratio, to be determined from our experiments (or theory). It turns out in what follows that it is more convenient to express (1) in the slightly different, but equivalent, form

$$\frac{r_\infty - r_i}{r_i} = f(a),$$ (2)

where it is now the unknown (non-dimensional) function $f(a)$ which is sought (and related to $\tilde{f}(a)$ by $f(a) = \tilde{f}(a) - 1$). Part of the reason to prefer the use of $f(a)$ is that for a very low column $r_\infty - r_i \to 0$ and so $f(a) = 0$, i.e. the function sought goes through the origin.
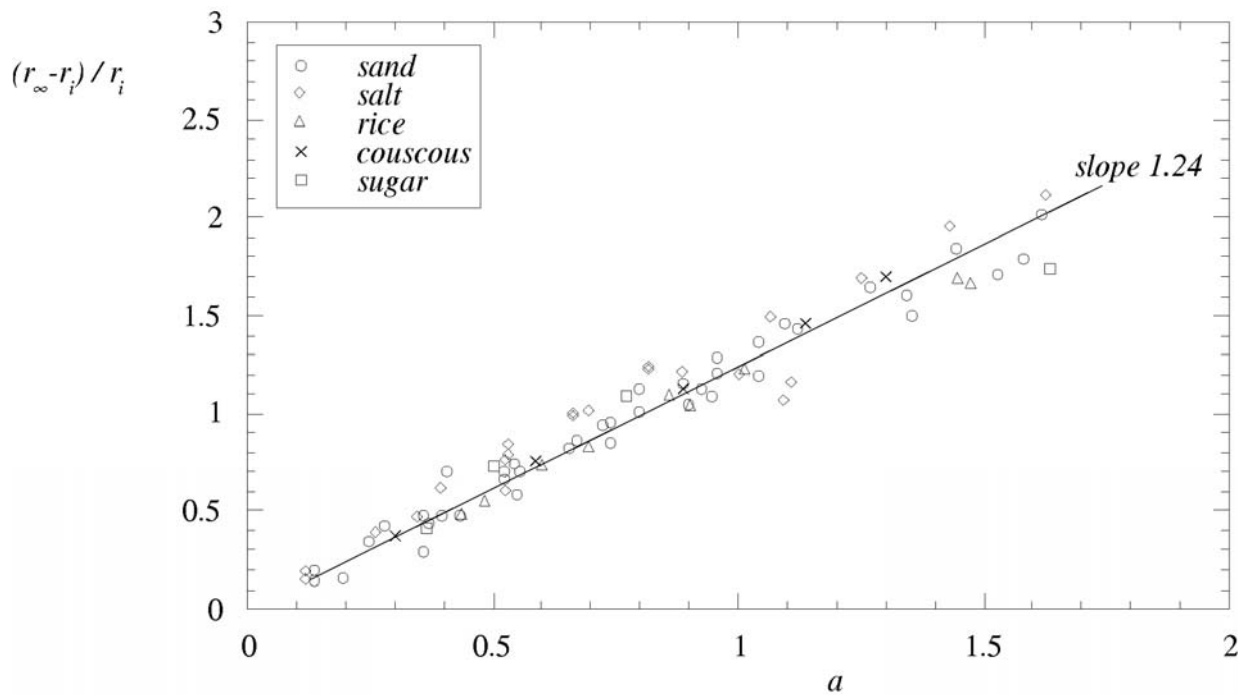
Figure 9. The non-dimensional radial excursion, $(r_\infty - r_i)/r_i$, as a function of the aspect ratio a with a < 1.7 for sand, salt, rice, couscous and sugar. A straight line through the origin at slope 1.24 has a regression coefficient of 0.975.

In the flow regime with $a<1.7$, the functional form of $f(a)$ can be determined by either physical or mathematical reasoning. Both arguments depend on the fact that, in this range, since only
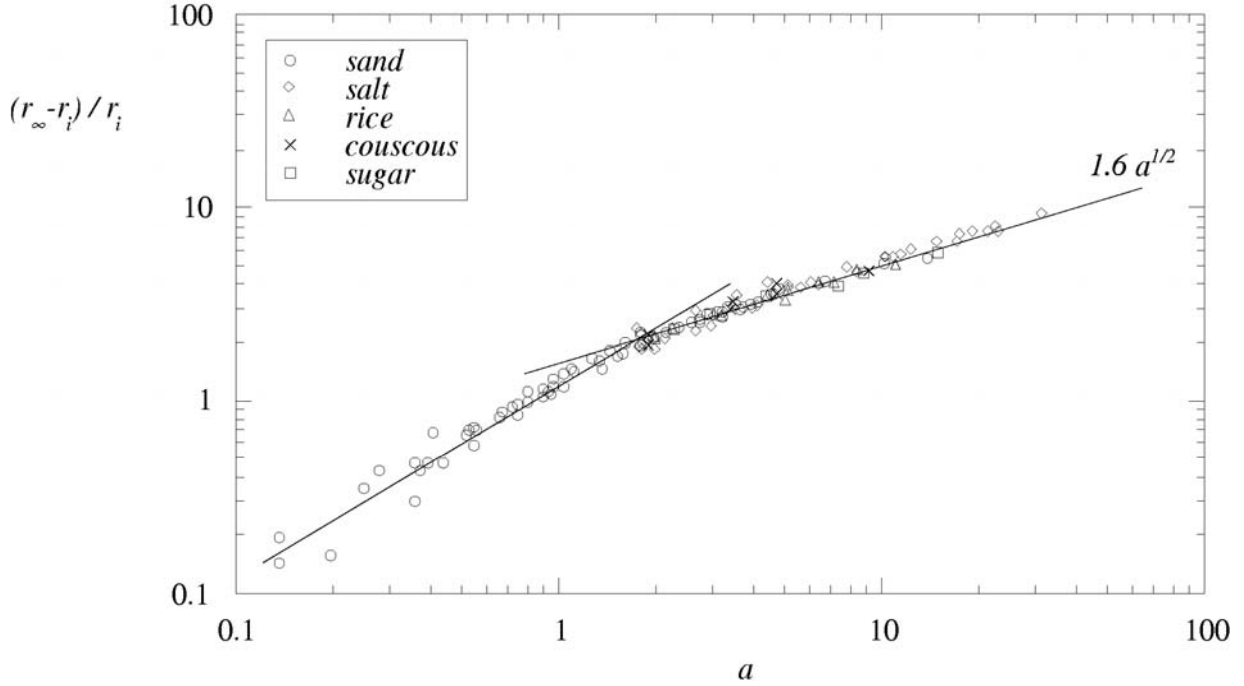
Figure 10. The non-dimensional radial excursion, $(r_\infty - r_i)/r_i$ as a function of the aspect ratio a (on logarithmic axes). The curve $1.6a^{1/2}$ is the best-fit half-power law through the data for a > 1.7 with a regression coefficient of 0.988.

grains initially beyond a specific radius, r_a, take part in the motion, the value of r_i itself must be irrelevant except in relation to the displacement of the cylindrical edge, $\delta r \equiv r_\infty - r_i$. This displacement is a length and the only length to which it can be related is h_i, and by dimensional analysis the relationship must be linear. Thus $\delta r = ch_i$, for some constant c. Or in terms of (2)

$$f(a) = ca \ (0 \leq a < 1.7). \tag{3}$$

The complementary, mathematical argument is that the only way (2), expressed as $\delta r/r_i = f(a = h_i/r_i)$, can be independent of r_i is if $f(a) = ca$.

In figure 9 we plot all our data for all the different grains for $\delta r/r_i$ as a function of a. We see that they are represented well by a straight line, with $c = 1.24$ (for all materials).

We plot all our data for $\delta r/r_i$ in figure 10 on logarithmic axes. For the range of collapses with $1.7 < a$, a good power-law representation of the data is given by
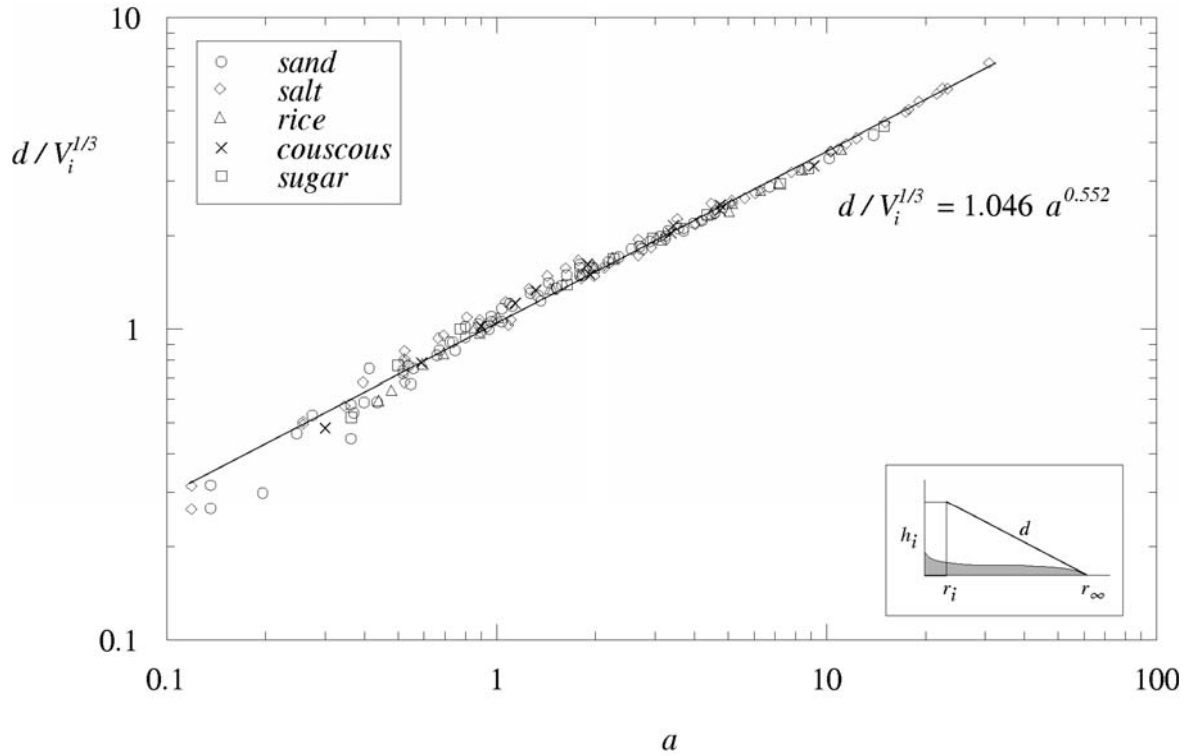
Figure 11. Data for $d/V_i^{1/3} = [(r_\infty - r_i)^2 + h_i^2]^{1/2}/V_i^{1/3}$ as a function of the aspect ratio a with the best curve fit $d/V_i^{1/3} = 1.05a^{0.55}$ and an inset to define d.

$$f(a) = 1.6a^{1/2} \tag{4}$$

(for all materials).

Equation (4) is the major quantitative result of our investigation, and can be written as

$$r_\infty = r_i + 0.90(V/r_i)^{1/2}. \tag{5}$$

A theoretical determination of (5), which indicates that the radial spread increase with the square root of the volume, remains a challenge for the future.

Note that the data plotted in figure 10 include those taken from flows on sandpaper. The similarity of the results with rough and smooth surfaces confirms that the interaction of the flow with the ground suface makes little difference to the runout. This is consistent with the interpretation, based on the formation of the broad layer in figure 6, that a dynamic interface

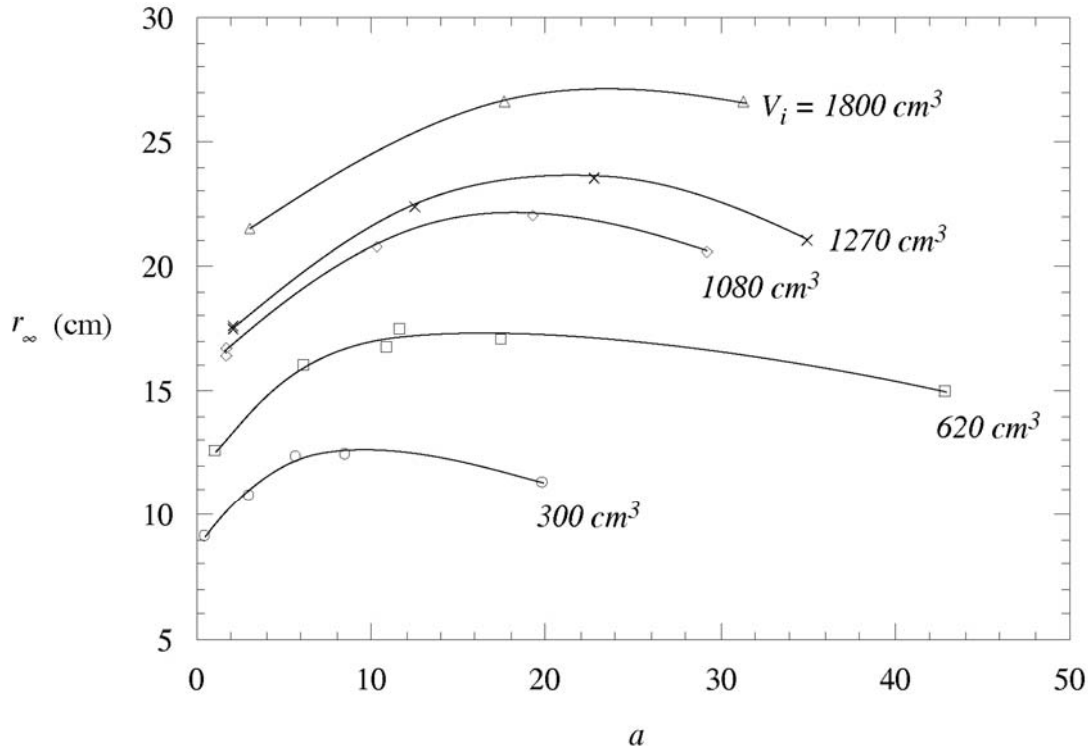*Figure 12. The (dimensional) final runout, r_∞, as a function of the initial aspect ratio, a, for various experiments with constant volumes. There is a tendency for r_∞ to slightly decrease for large a.*

develops within a few particles of the base and separates the flow between deposited and flowing material.

While analysing the salt and sand data for the final runout length, we noticed that the length of the straight line from a point on the top perimeter of the initial cylinder of granular material to the furthest point on the base (see inset of figure 11) $d = [(r_\infty - r_i)^2 + h_i^2]^{1/2}$ was accurately represented by $1.05 V_i^{1/3} a^{0.55}$, which is expressible (with a little algebra) as

$$r_\infty = r_i [1 + (2.36a^{1.77} - a^2)^{1/2}]. \qquad (6)$$

The result is displayed in figure 11. Even though (6) gives a simple continuous representation of the data, it cannot be appropriate for large a, because while the right-hand side of (6) is a monotonically increasing function of a until $a = 27$, thereafter it begins to decrease until at $a = 46$ it is zero. However, we notice that plotting r_∞ as a function of a for constant volumes (figure 12)

tentatively suggests an increase for smaller values of a and a tendency to decrease beyond that, at a value of a which increases with V_i, but our data are sparse in this region.

4.3. Final cone height

The final cone height is dependent on the initial height and aspect ratio and is a consquence of both the collapsing and subsequent avalanching. The relationship for the final cone height on the basis of dimensional analysis is of the form

$$h_\infty = r_i \varphi(a), \tag{7}$$

where $\varphi(a)$ is a non-dimensional function of a.

For $0 \leq a < 1.7$, $h_\infty = h_i$, which indicates that

$$\varphi(a) = a \qquad (0 \leq a < 1), \tag{8}$$

which is consistent with the argument that in this range of a, h_∞ is independent of r_i.

For $1.7 \leq a < 10$, all our data, plotted on figure 13, are represented well by

$$\varphi(a) = 0.88 a^{1/6} \qquad (1.7 < a < 10) \tag{9}$$

or alternatively,

$$h_\infty = 0.73 (V\, r_i^3)^{1/6} \qquad (1.7 < a \leq 10). \tag{10}$$

These coefficients are mean values, with some slight systematic deviations of approximately 10% for salt and sand. This variation is thought to reflect the different influences of intergranular friction on late-stage avalanching.

For $a>10$ there is an indication that $h\infty$ decreases with increasing a, as shown on the graph. This is probably an effect of the wave that originates from the centre and with increasing a increasingly transports material from the centre.
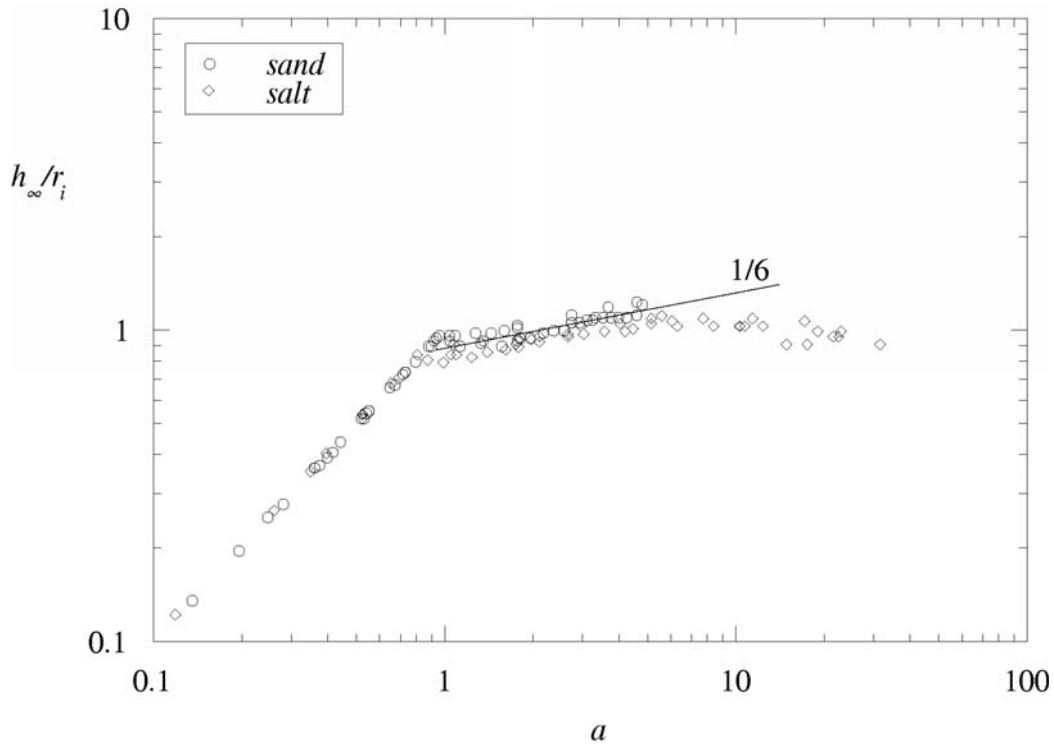
Figure 13. The non-dimensional final height at the centre of the granular pile, h∞, as a function of the aspect ratio a. The data between a = 1.7 and a = 10 have a slope of 1/6.

4.4. Height profiles

The shape or height profiles of the deposit are dependent on the value of a. Using dimensional arguments, the contour of the final deposit must be expressible as

$$h(r)/h_\infty = \eta(r/r_\infty, a), \tag{11}$$

where η is a dimensionless function of its two dimensionless variables with, by definition,

$$\eta(0, a) = 1 \text{ and } \eta(1, a) = 0. \tag{12}$$

Figure 14 plots $h(r)/h_\infty$ as a function of r/r_∞ for several values of a. A test of any theoretical model to describe column collapse would be its agreement with the data of this figure.

Determining the appropriate integrals using the data displayed in figure 14, we confirm that the final volume of the granular pile equals its initial volume, so that there is no net volume inflation. Determining the final surface area of the free surface S_∞, non-dimensionalized with respect to πr_i^2, we obtain a graph which approximates 1 for small a ($r_\infty \approx r_i$ and so $S_\infty \approx \pi r_i^2$) and increases linearly with a for large a ($S_\infty \approx \pi r_\infty^2$).
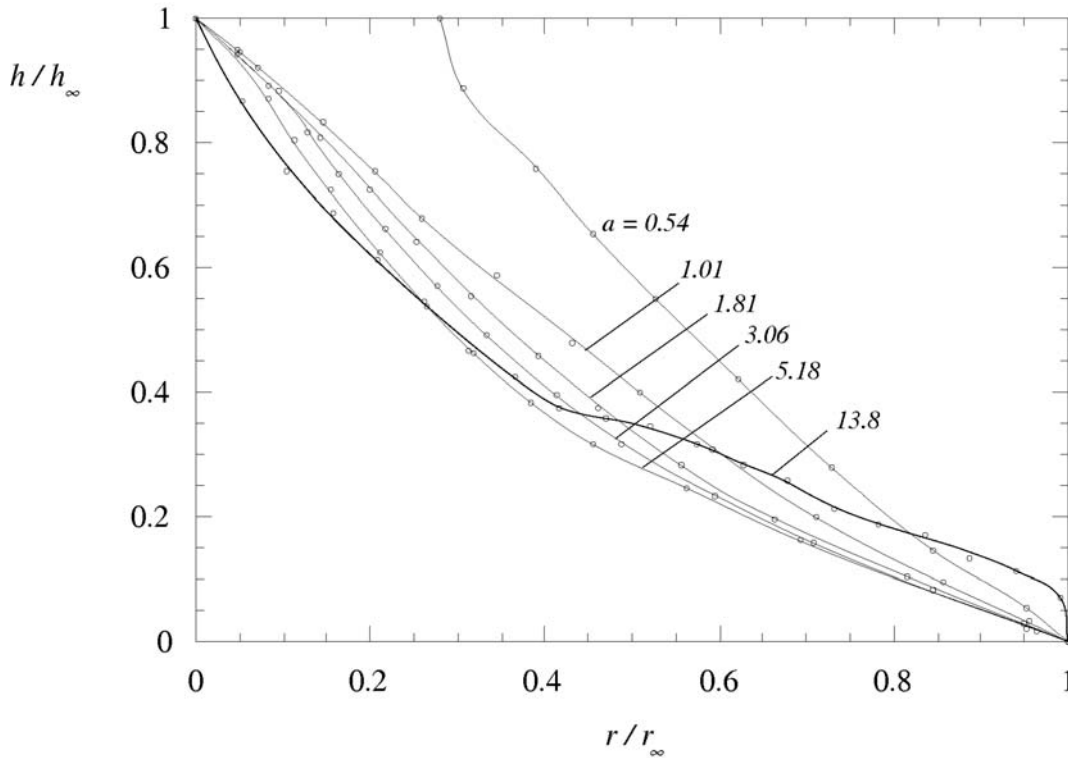
Figure 14. The non-dimensional height of the final profile as a function of non-dimensional radius for different aspect ratios.

4.5. Further experiments

We have also conducted some preliminary 'drop' experiments for which the cylinder of granular material was raised by a height H off the base and then dropped, to fall to the base and then spread axisymmetrically. All the material dropped a height H under gravity, whereafter the bottom of the pile hit the base and radial spreading commenced. Preliminary results of the non-dimensionalized radial displacement $(r_\infty - r_i)/r_i$ and the final central height h_∞/h_0 are plotted as functions of an extended aspect ratio $a_H \equiv (H + h_i)/r_i$ in figure 15 which includes all the previous data with $H = 0$. The majority of the new values of a_H are large, in the third aspect-ratio regime. Rather surprisingly, the results for $r\infty$ and $h\infty$ dovetail well with the results for $H = 0$, although

the shape of the deposits must be quite different. This suggests that allowing the granular material to drop before it hits the ground introduces no new phenomena (other than the initial downward acceleration under gravity) and allows an effective aspect ratio a_H, which is much larger than the aspect ratio of the initial cylinder, to be investigated. The result is also consistent with the idea that the final extent of the deposit is reached by grains in the uppermost region of the initial cylindrical pile. We plan to present further results of this case in a subsequent publication.

$$a_H = (H + h_i)/r_i$$
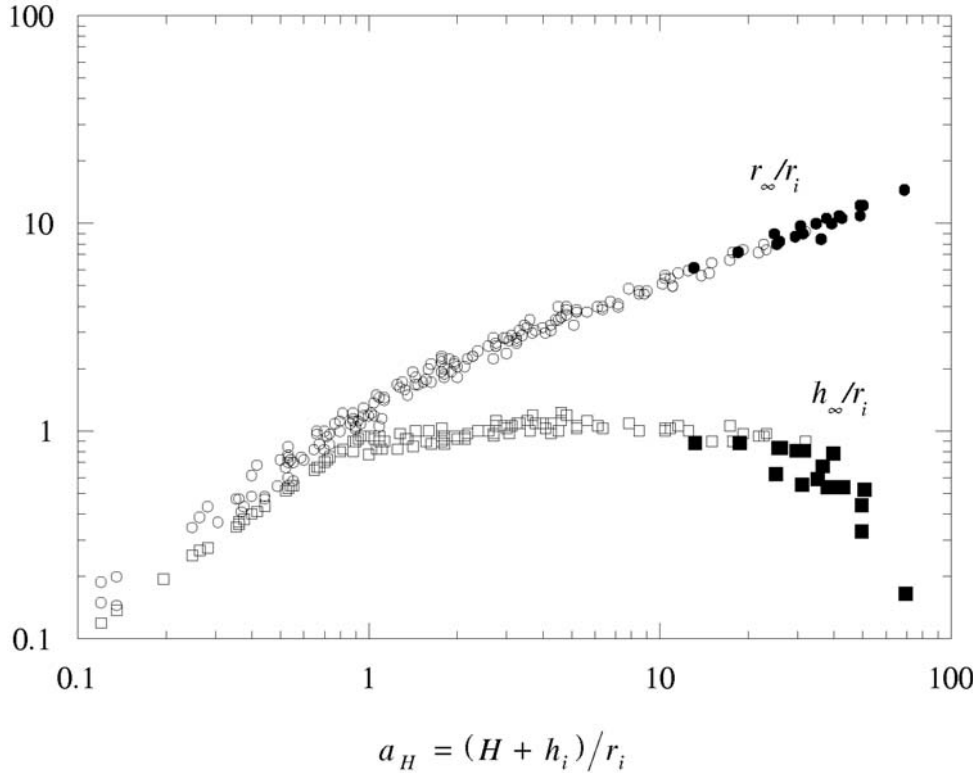
Figure 15. The non-dimensional final runout, r_∞/r_i, and central height, h_∞/r_i, as functions of the extended aspect ratio a_H for our 'drop' experiments. The open symbols represent $H = 0$ while the solid symbols represent $H \ne 0$.

4.6. Kinematic data

In order to understand the dynamic behaviour better we analysed the data collected of the radius r of the flow front as a funtion of time t. Three different patterns were observed, dependent on the initial aspect ratio (figure 16a–c). For flows with aspect ratios less than 1.7 there was a primary acceleration phase followed by a deceleration phase (figure 16a). Flows with $1.7<a<10$ had an acceleration phase, followed by an intermediate phase of constant velocity and finally a deceleration phase (figure 16b). Our data suggest that the change from the acceleration phase to

the phase of constant velocity coincides with the beginning of deformation of the upper surface of the column. The pattern for higher-aspect-ratio flows (figure 16c) slightly deviates from that observed for flows with intermediate aspect ratios. Before the final deceleration phase the flow front gently accelerates. Comparison of these curves with the high-speed movies suggests that the slight acceleration seems to coincide with the arrival of the wave that travels through the flow at the front.

For all flow regimes, the initial horizontal acceleration was approximately constant at between 0.25 and 0.3 g. Further analysis is constrained due to the non-uniformities in lifting the cylinder.
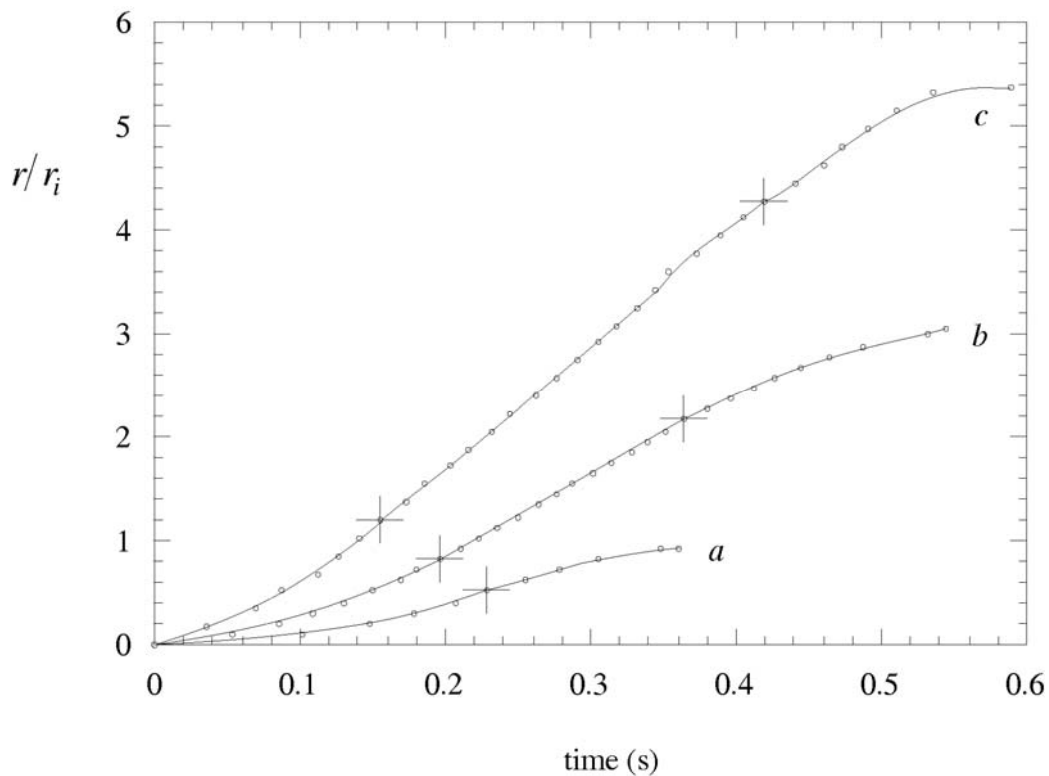
Figure 16. Typical radial displacements as functions of time. (a) Flows with small aspect ratio have a primary acceleration phase followed by a deceleration phase. (b) Flows with intermediate aspect ratios incorporate also a constant velocity phase. (c) Flows with large aspect ratios additionally incorporate a very small deceleration phase before the constant velocity phase and a very small acceleration phase after it. The large crosses mark the ends of the acceleration phase at (τ_f, r_f) and the constant velocity phase.

It is interesting to compare the remainder of the flow to the evolution of an initially cylindrical volume of radius r_i, height h_i (and volume $V_i = \pi r_i^2 h_i$) of fluid of density ρ propagating below a large body of fluid of small density ρ_1 (Simpson 1997; Huppert 2000). For an instantaneous release (like that considered above) there is a brief acceleration phase (which to our knowledge has not been quantitatively addressed), followed by a phase during which the front of the flow propagates at a constant velocity, while the free surface bore initiated by the removal of the confining gate propagates inward towards the centre, from where it is reflected and catches up with the propagating front (Rottman & Simpson 1983). This constant velocity is proportional to $(gh)^{1/2}$, where g is the acceleration due to gravity. Thereafter a similarity form of solution develops with the radial coordinate at the front r proportional to $(gV_i)^{1/4}t^{1/2}$ (Hoult 1972). The transition between these two phases occurs on a timescale

$$\tau_i = (gV_i)^{1/2}/(gh_i) = \pi r_i^2 /(gV_i)^{1/2}. \qquad (13)$$

Figure 17. The radial displacement from r_f, non-dimensionalized by r_i, as a function of the time since τ_f, non-dimensionalized by $\tau_i = \pi r_i^2 /(gV_i)^{1/2}$, for experiments for various a with a constant-velocity phase. A clear linear phase is followed by a phase of slope 1/2.

This timescale suggests analysing the motion after the acceleration phase, which is defined to end at t_f, r_f, by using the lengthscale r_i and the timescale τ_f to graph the non-dimensional runout

distance $(r - r_f)/r_i$ as a function of the non-dimensional time $(t - t_f)/\tau_i$. This is done, using logarithmic scales, in figure 17. We see that there is a clear first phase of unit slope, followed by a brief second phase of slope 1/2 – before the quite sudden cessation of motion. A better collapse of the data can be obtained by instead plotting $(r - r_f)/r_i$ against $(t - t_f)/\tau_i$ where $\tau_f = \pi r_f^2 /(gV_i)^{1/2}$, as shown on figure 18. The close analogy between the forms of motion identified here and with a frictionless fluid gravity current strengthens further our argument that intergranular frictional forces play a negligible role in the spreading of granular columns (except just at the end, during the stopping phase).
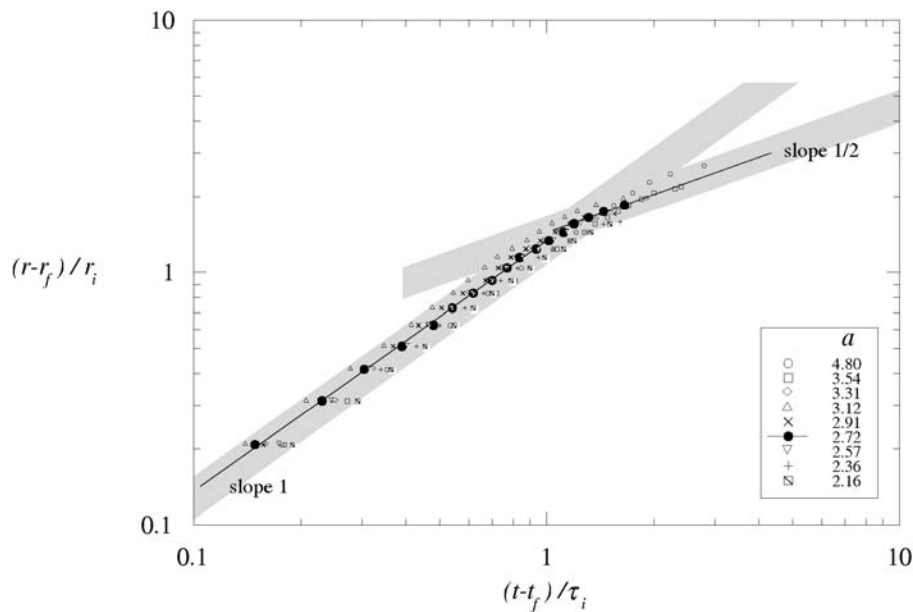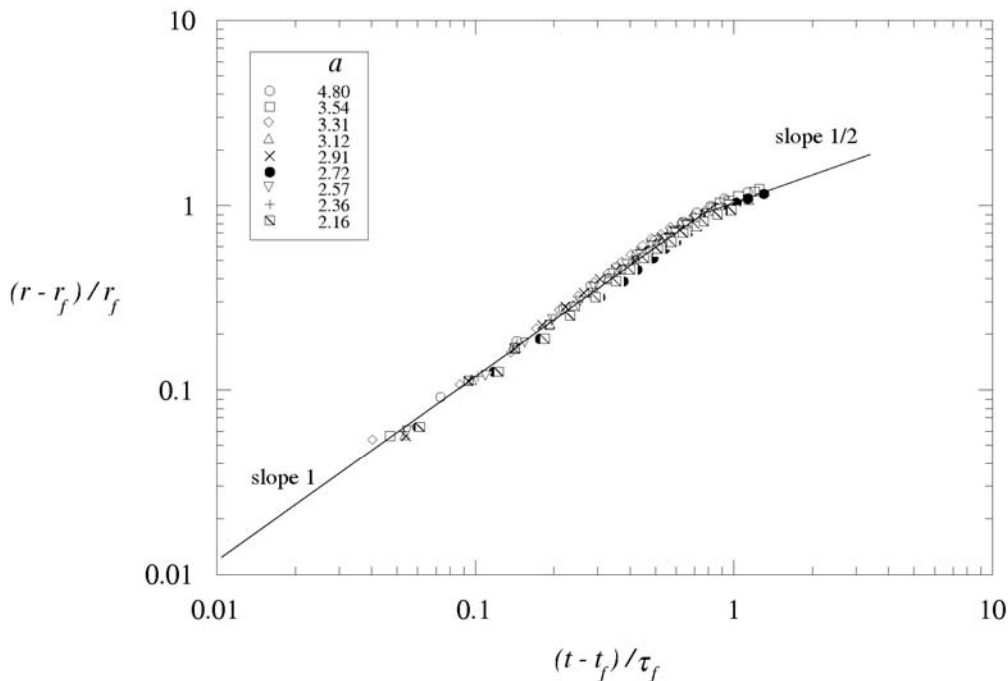

Figure 18. The radial displacement from r_f, non-dimensionalized by r_f, as a function of the time since τ_f, non-dimensionalized by $\tau_f = \pi r_f^2 /(gV_i)^{1/2}$. This non-dimensionalization collapses all the data.

From our high-speed cinematography we determined the time, t_∞, at which the motion of the flow front ceased. By dimensional arguments t_∞ must be of the form

$$t_\infty = (r_i/g)^{1/2}G(a), \qquad (14)$$

for some functional form of $G(a)$. For $a<1.7$, the expression for t_∞ must be independent of r_i and so

$$G(a) = Ka^{1/2}, \tag{15}$$

for some constant K. In figure 19 we plot the data for sand, from which it is seen that there is good agreement with the functional form (15) if $K = 3.0$. Somewhat surprisingly, for $a > 1.7$ the data are still well represented by

$$G(a) = 3.0a^{1/2}, \tag{16}$$

or $t_\infty = 3.0(h_i/g)^{1/2}$. Note that the time of free-fall of a particle from a height h_i is given by $(2h_i/g)^{1/2} \approx 1.41(h_i/g)^{1/2}$ which indicates that the total spreading time is approximately twice the free-fall time.
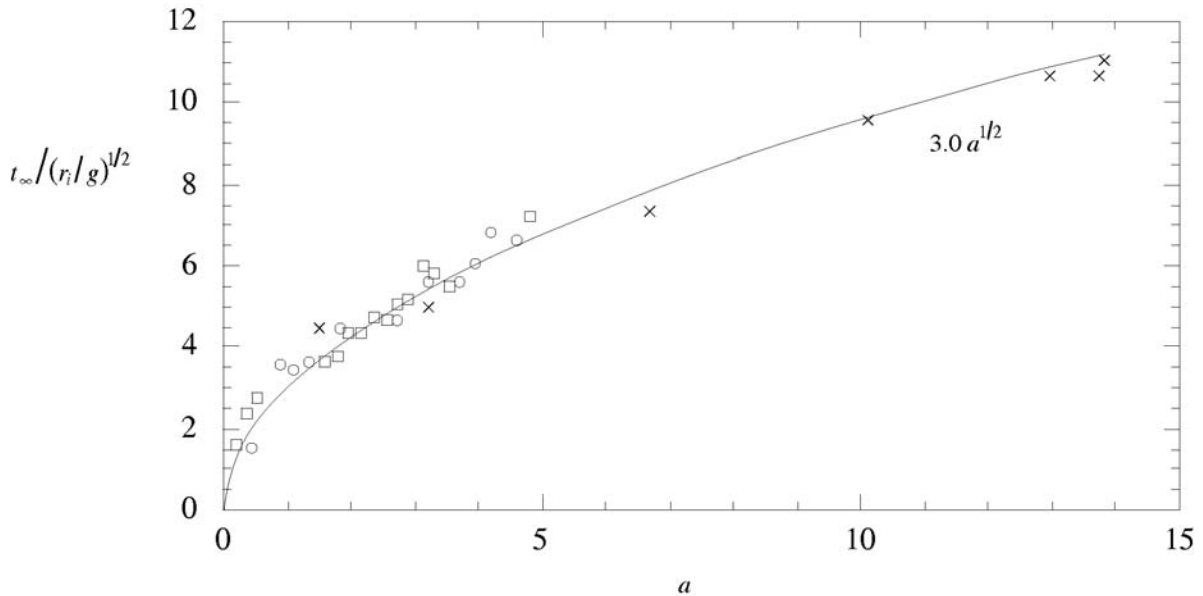
Figure 19. The non-dimensional time for the flow front to cease motion as a function of the aspect ratio, a. Initial radius r_i = 2.9, 7.5 and 9.7 cm are represented by ×, ○ and □ respectively.

We note that all the experimental flows come to an abrupt halt. Typical times between the flow front and the adjacent particles in the frontal region ceasing motion was in the order of 100 milliseconds, which represents approximately 5% of the total emplacement time. The process of freezing the flow involves rapid and sometimes jump-like propagation of interfaces between flowing and static particles which are observed at the base and free surfaces of the flow. This behaviour contrasts with the motion of density currents of simple Newtonian fluids which flow continuously, with a transition from the inertial regime to a viscous regime of slow creeping flow

(Huppert 1982). We interpret this difference as a consequence of intergranular friction becoming dominant as the flows lose energy and freely flowing granular material is converted into a static 'solid-like' granular pile.

5. Discussion

A common approach to understanding fluid flow phenomena is to develop fundamental theoretical analyses of the fluid forces, usually using the continuum approach. Results of model calculations using such theories can then be verified by experiments. In the case of granular materials this approach has proved difficult. The continuum approach may not be strictly valid and it has proved hard theoretically to develop models of the small-scale particle interactions and relate these to the larger-scale motion of granular materials except for extremely simplified systems. Experimental work is also complicated by the problem that steady flows of granular materials can only be established under rather special circumstances, for example down slopes where the slope is between the dynamic and static angles of friction. However, in nature and probably in most industrial situations granular flows occur in circumstances where steady flow conditions are unlikely.

These difficulties suggest that an alternative approach might help advance understanding. Here we have investigated experimentally a simple flow configuration in which a cylinder of granular material is allowed to relax to a stable configuration by slumping on a horizontal surface. Observation of the motions, flow phenomena and final configuration of the system combined with scaling arguments then provide clues to the mechanisms of granular flow. The flows can also be compared with other kinds of fluids flowing in similar configurations to give insight into the dynamics.

In the present experiments we observe that the flows are in general unsteady with three main phases being recognized: an initial acceleration; a constant-velocity phase (which may be absent); and a gentle deceleration followed by an abrupt halt of the flow front in typically less than 5% of the overall time for the experiment. The observation of a significant period of constant-velocity flow is particularly interesting, because this kind of behaviour is also observed for slumps of Newtonian fluids where the flow is dominated by inertia. The granular materials are effectively

behaving as if they were simply dense fluids with internal friction playing no role. For a Newtonian fluid the internal friction is viscosity and for granular flows it is the frictional interactions between particles. Thus the gross behaviour of the currents in the constant-velocity phase can be described in a very similar way to a simple gravity current in the initial slumping phase. The experimental observations also indicate that during this constant-velocity stage there is very little particle deposition except for the formation of a very thin layer of particles at the base derived from the leading edge of the flow. It is clear from observations of the final position of different concentric zones in the flow that almost all of the slumped material is in motion until very close to the end.

The flows are finally emplaced in a rather short decelerating phase. The observations of the kinematics can be usefully compared to simple gravity currents of Newtonian fluids. We observe that in the decelerating phase the flows follow a power law, which is similar to that observed for inertial gravity currents of Newtonian fluids. Thus even in the third phase, shortly before they come to a halt, the flows seem to behave as inertial currents where internal friction due to particle interactions is not important. It is only at the very end that the flows depart significantly and fundamentally from behaviour consistent with a simple balance of buoyancy and inertia. In a Newtonian fluid the system would have a final transition to a viscous regime where buoyancy and viscosity are balanced. The granular flows instead come to an abrupt halt which is associated with transmission of very rapidly moving interfaces between static and moving material. These observations can be interpreted as the consequence of the flow losing energy and the rather abrupt onset of strong frictional interactions between the particles. The flow ceases motion in all places over a very short period of time ($\approx 5\%$ of the total) and can be viewed as close to en masse freezing. A competing view of the decelerating phase is that it represents the period when frictional forces start to become important and that the similarity of the power law of distance versus time to an inertial gravity current is merely a coincidence.

The final configuration of the flow deposits is not strictly self-similar and depends on the initial geometry of the cylinder of sand. Flows with more potential energy (generally higher cylinders) can produce deposits with a conical geometry that are well below the angle of static or even dynamic friction.

These results and the ideas that derive from our observations may serve to elucidate many different features of granular flows. For example, there has been a long-running controversy about the mechanism of emplacement of pyroclastic flows. Two schools of thought have emerged as follows.

In one concept, pyroclastic flows are envisaged as dilute and turbulent particulate currents from which a deposit is formed by progressive aggradation (Branney & Kokelaar 1992). In this model the deposit is built up layer by layer over a significant period of time, perhaps comparable to the time it takes the current to move from its source to its maximum distance or longer. In another concept, pyroclastic flows are envisaged as concentrated flows, which come to an abrupt halt by en masse freezing (Sparks 1976). The cause of freezing was originally attributed to the flow having non-Newtonian rheology, with the flow stopping abruptly when the basal shear stress falls below the yield strength. The non-Newtonian model is no longer thought to represent a helpful way of describing concentrated pyroclastic flow behaviour. Instead it is increasingly recognized, on the basis of observations, experiment and theory, that pyroclastic flows are better envisaged as granular flows, which may also be partially fluidized (e.g. Sparks 1976; Wilson 1980; Drake 1990; Grunewald et al. 2000; Roche et al. 2002).

Our experiments show that an alternative mechanism exists to bring granular flows to an abrupt halt. The flow stops abruptly when the particle frictional forces start to dominate. In this case it is not strictly en masse freezing as it takes a finite (but small) time for the interface between moving and deposited material to sweep through the deposit. However, this depositional time is much shorter than the emplacement time of the current and material can only move rather short lateral distances. If particles of different size and density have been sorted within the flow during transport then these arrangements might be expected to be preserved with rather limited modification within the final deposit. This is in contrast to the model of Branney & Kokelaar (1992) where vertical variations in the final deposit reflect the fluctuations in the current properties passing a local point of deposition. This mechanism thus provides a model for pyroclastic emplacement from concentrated currents, which is rather closer to that envisaged by Sparks (1976) and Wilson (1985).

CHAPTER II

Our novel investigation immediately suggests further studies which we have already begun to consider. First, we plan to explore further the effects of raising the material to a height H before it drops initially to the base, as discussed briefly in § 4.5. Second, how are the various phenomena categorized and what are the quantitative results for a wide rectangular box of granular material – essentially a Cartesian, two-dimensional situation? Third, what new phenomena are introduced when the base is inclined – below or above the angle of response? Fourth, how do these results differ if the spreading is into water, not air, or into a very viscous fluid, like oil? Fifth, how is the transition between a flowing granular material and a static deposit best described quantitatively? We intend to provide answers to each of these queries in subsequent publications.

REFERENCES

Anderson, K. G. & Jackson, R. 1992 A comparison of the solutions of some proposed equations of motion of granular materials for fully developed flow down inclined planes. J. Fluid Mech. **92**, 145–168.

Branney, M. J. & Kokelaar, B. P. 1992 A reappraisal of ignimbrite emplacement: changes from particulate to non-particulate during progressive aggradation of high grade ignimbrite. Bull. Volcanol. **54**, 504–520.

Campbell, C. S. 1990 Rapid granular flows. Annu. Rev. Fluid Mech. **22**, 57–92.

Cates, M. E., Wittmer, J. P., Bouchaud, J.-P. & Claudin, P. 1999 Jamming and static stress transmission in granular materials. Chaos **9**, 511–522.

Dade, W. B. & Huppert, H. E. 1998 Long runout rockfalls, Geology **26**, 803–806.

Daerr, A. & Douady, S. 1999 Two types of avalanche behaviour in granular media. Nature **399**, 241–243.

Drake, T. G. 1990 Structural features in granular flows. J. Geophys. Res. **95**, 8681–8696.

Druitt, T. H. 1998 The eruption, transport and sedimentation of pyroclastic flows. In The Physics of Volcanic Eruptions (ed. J. Gilbert & R. S. J. Sparks). Geol. Soc. London Spec. Publ. **145**, 147–200.

Freundt, A. & Bursik, M. I. 1998 Pyroclastic flows transport mechanisms. In From Magma to Tephra: Modelling Physical Processes of Explosive Volcanic Eruptions (ed. A. Freundt & M. Rosi). Developments in Volcanology, vol. 4, pp. 173–245. Elsevier.

de Gennes, P. G. 1999 Granular matter: a tentative view. Rev. Mod. Phys. **71**, 5374–5382.

Grunewald, U., Sparks, R. S. J., Kearns, S. & Komorowski, J. C. 2000 Friction marks on blocks from pyroclastic flows at the Soufriere Hills volcano, Montserrat: Implications for flow mechanisms. Geology **28**, 827–830.

Hoult, D. P. 1972 Oil spreading on the sea. Annu. Rev. Fluid Mech. **4**, 341–368.

Huppert, H. E. 1982 The propagation of two-dimensional and axisymmetric viscous gravity currents over a rigid horizontal surface. J. Fluid Mech. **121**, 43–58.

Huppert, H. E. 1998 Quantitative modelling of granular suspension flows. Phil. Trans. R. Soc. Lond. **356**, 2471–2496.

Huppert, H. E. 2000 Geological Fluid Mechanics. In Perspectives in Fluid Dynamics: A Collective Introduction to Current Research (ed. G. K. Batchelor, H. K. Moffatt & M. G. Worster), pp. 447–506. Cambridge University Press.

Iverson, R. M. & Denlinger, R. P. 2001 Flow of variably fluidized granular masses across three-dimensional terrain. Part I: Coulomb mixture theory. J. Geophys. Res. **106**, 537–552.

Jaeger, H. M., Nagel, S. R. & Behringer, R. P. 1996 Granular solids, liquids, and gases. Rev. Mod. Phys. **68**, 1259–1273.

Kadanoff, L. P. 1999 Built on sand: Theoretical ideas inspired by granular flows. Rev. Mod. Phys. **71**, 435–444.

Pouliquen, O. 1999 Scaling laws in granular flows down rough inclined planes. Phys. Fluids **11**, 542–548.

Pouliquen, O. & Forterre, Y. O. 2002 Friction law for dense granular flows: application to the motion of a mass down a rough inclined plane. J. Fluid Mech. **453**, 133–151.

Roche, O., Gilbertson, M., Phillips, J. & Sparks, R. S. J. 2002 Experiments on gas-fluidized granular flows and implications for pyroclastic flow mobility. Geophys. Res. Lett. **29**, 40–44.

Rottman, J. W. & Simpson, J. E. 1983 Gravity currents produced by instantaneous releases of a heavy fluid in a rectangular channel. J. Fluid Mech. **135**, 95–110.

Savage, S. B. 1995 Flows of granular materials. Proc. CANCAM '95 (ed. B. Tabarrok & S. Dost), pp. 62–73. University of Victoria, BC, Fleming Express Press Ltd, Victoria, BC.

Savage, S. B. 1998 Analyses for slow quasi-static, high concentration flows of granular materials. J. Fluid Mech. **377**, 1–26.

Savage, S. B. & Hutter, K. 1989 The motion of a finite mass of granular material down a rough incline. J. Fluid Mech. **199**, 177–215.

Simpson, J. E. 1997 Gravity Currents in the Environment and the Laboratory, 2nd Edn. Cambridge University Press.

Sparks, R. S. J. 1976 Grain size variations in ignimbrites and implications for the transport of pyroclastic flows. Sedimentology **23**, 147–188.

Wilson, C. J. N. 1980 The role of fluidisation in the emplacement of pyroclastic flows: an experimental approach. J. Volcanol. Geoth. Res. **8**, 231–249.

Wilson, C. J. N. 1985 The Taupo eruption, New Zealand II. The Taupo ignimbrite. Phil. Trans. R. Soc. Lond. A **314**, 229–310.

Chapter III

Granular column collapse

Abstract

We present a study of initially vertical cylinders of granular material collapsing onto a horizontal base. We describe the spreading in terms of three regimes dependent on the aspect ratio $a = h_i/r_i$, where the initial cylinder of material has radius r_i and height h_i. The motion is described by the same scaling relationships for all the materials, independent of internal friction due to interactions between grains. Only at the end of flow, when there is an abrupt halt, is internal friction important.

We conducted a series of experiments in which various granular materials, initially contained in a vertical cylinder, were rapidly released onto a horizontal surface to spread out unhindered over it. The main materials were dry sand and salt, but, for comparison purposes, we also conducted experiments with couscous, rice and sugar, all of which have a quite different size and shape. Nevertheless there was no difference in the resulting spreading relationships. The horizontal plane used was either wood, a smooth surface of baize lying on wood, a smooth transparent Plexiglas plane or a rough plane of sandpaper. The detailed spread of the granular material was also independent of these surfaces. Eight different cylinders, ranging in radius, r_i, from 1.7 to 9.7 cm, were used. The volume of granular material varied from 125 to 13,000 cm^3. Some experiments were recorded and later analysed on a digital high-speed video at 500 frames per second. After all motion had ceased, the profile of the resultant deposit was measured, to find the final runout radius, r_∞, central cone height, h_∞, and the steepest incline, α, of the upper surface.

For all values of a there was a central undisturbed cone of material which did not partake in the motion, whose angle was close to 60°, corresponding to an aspect ratio of 1.7. This can be interpreted as an internal friction angle for the material. At the base, three different regions were captured by video during the collapse: a stationary circular region, of radius r_i; a ring of previously deposited particles; and an outer ring of material which was still flowing. These last two regions were divided by a moving interface that propagated outwards until the flow front came to rest.

Observations from the high-speed photography indicate that other aspects of the motion naturally divide themselves into three different regimes dependent of the initial aspect ratio $a = h_i/r_i$. For initial aspect ratios $a < 1.7$, the upper surface of the released material was divided into an inner stationary circle (which remained at the initial height, h_i) outside of which was flowing material. After the flow front had ceased propagating, a moving interface on the upper free surface appeared which separated static from flowing particles and which propagated inward from the stationary front. For $a < 1$ the final deposit consisted of an inner, undisturbed central region beyond which there was an axisymmetric, tapering frontal region with α in the range of the angle of repose. For $1 < a < 1.7$ the avalanching which occurred after the flow front had stopped moving removed the undisturbed central region.

For $a > 1.7$ the entire upper surface flowed from the beginning of each experiment. Initially, the upper free surface remained undeformed and horizontal. After the column had lost some height, deformation of the top occurred, to form a dome whose radius of curvature decreased with time. The final deposit had a steep central zone and an axisymmetric tapering frontal region with α less than the angle of repose.

A transition in behaviour of collapse was evident from the video analyses to occur when a exceeds about ten. Immediately upon lifting the container the entire free surface began to flow. A flow front developed at the base of the column and propagated outwards while removing material from the centre. In contrast to lower initial aspect ratios, the upper surface of the column remained undeformed until its height sank to that of the neighbouring flat frontal region. Also, once the flow at the base had ceased, an interface between moving and stationary material appeared on the upper free surface but propagated outward from the centre to the flow front. The value of α decreased monotonically with increasing a.

The quality of the observational data and the similarity of the results for the different materials suggest that, with the use of dimensional analysis, the data can be collapsed in a systematic way. The initial experimental set up is uniquely determined by r_i, a and g, the acceleration due to gravity. Our ability to collapse all the data using only this input, and not any material properties, is a robust test for the assumption that no additional material property, such as the friction between individual grains, is needed to describe the motion. This is because, as described in more detail below, the motion stops rapidly at the end, in a very small fraction of the total time of the runout.

The difference between the initial and final radius, $\delta r = r_\infty - r_i$, must be expressible as $\delta r = r_i f(a)$. A plot of $\delta r / r_i$ makes up figure 1. For $a < 1.7$, because there is no motion of the inner region, the resultant expression must be independent of r_i, which requires that $f(a) \propto a$. From figure 1 we determine that the constant of proportionality which best fits the data is 1.3. For $a > 1.7$ the best fit power law to the data for all grains is given by $f(a) = 1.6a^{1/2}$.

The final height at the centre is similarly expressible as $h_\infty = r_i \eta(a)$. Figure 1 also presents all the data for h_∞ / r_i as a function of a. For $a < 1.7$, $h_\infty = h_i$, and so $\eta(a) = a$, as indicated by the data. For $1.7 < a < \text{c.}10$ the best fit power law to the data is given by $\eta(a) = 0.88a^{1/6}$. For $a > \text{c.}10$ there is a clear indication that h_∞ decreases with increasing a. This is in response to the
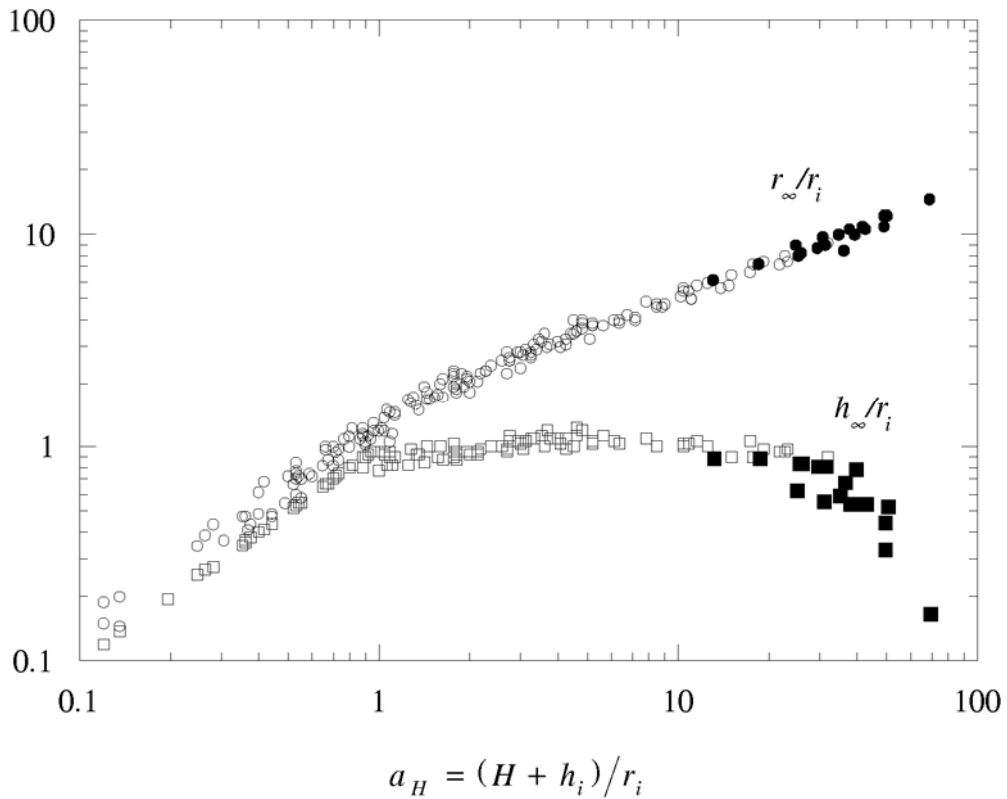
Figure 1. Non-dimensional radial displacement and height at centre of pile. Points marked with a solid dot are for experiments in which the cylinder was raised height H from the base before releasing grains, and aspect ratio is defined as $(H+h_i)/r_i$. This shows that in the final runout distance only maximum initial height is relevant (and initial radius).
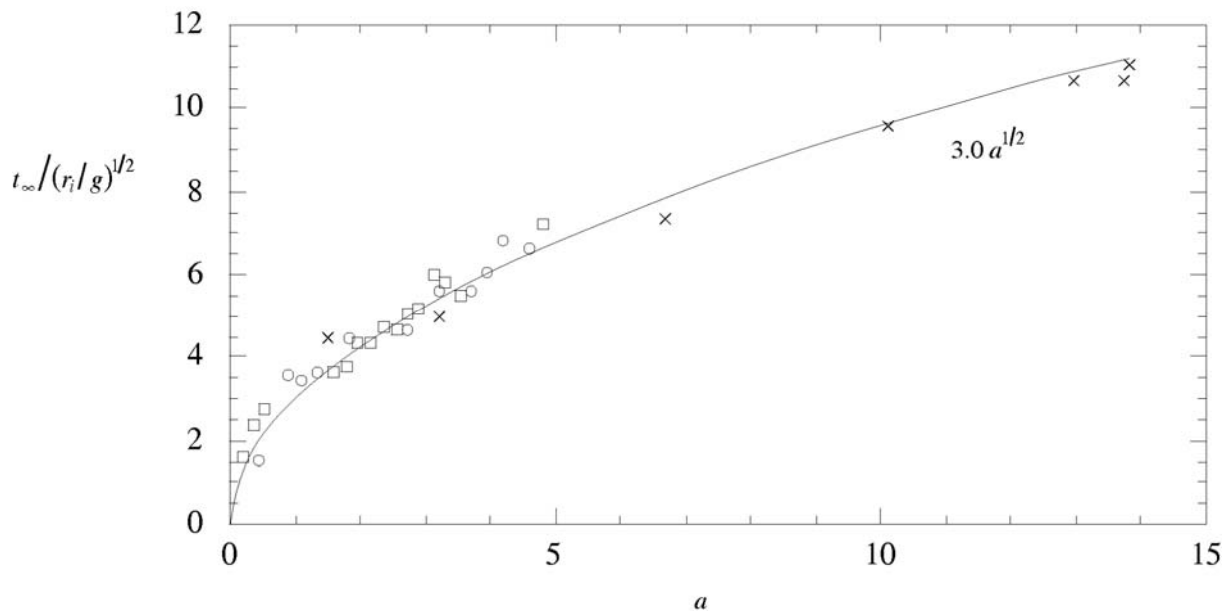

Figure 2. Non-dimensional time until the grain front ceased motion as a function of a. The initial radii of the columns $r_i = 2.9$, 7.5 and 9.7 cm are represented by $\times$, $\circ$ and $\square$ respectively.

50

wave that originates from the centre and removes material outwards. Unfortunately, the data are a little too scattered to be quantitatively analysed with confidence.

So far the parameter g has not entered our expressions because it is the only input parameter for which time is involved in its dimensions, and δr, h_∞/ r_i are both independent of time. The value of g will affect the total time for collapse, t_∞, which is defined as the time between the initiation of the experiment and that at which the flow front stops propagating. The high speed video, used on all the experiments with sand, allowed us to determine t_∞ reasonably accurately. By dimensions, it must be of the form $t_\infty = (r_i /g)^{1/2}\psi(a)$, for some function $\psi(a)$. A plot of $t_\infty/(r_i/g)^{1/2}$ as a function of a is presented in figure 2. As before, for $a < 1.7$, an expression independent of r_i requires $\psi(a) \propto a^{1/2}$, which is consistent with the data for a constant of proportionality of 3.8. For $a > 1.7$ the best fit power law through the data yields $\psi(a) = 3a^{1/2}$, which indicates that $t_\infty = 3(h_i/g)^{1/2}$. Note that the time taken for a particle to fall a height h_i under gravity is $(2h_i/g)^{1/2}$, which is just less than a half of t_∞.

Further insight on the flow characteristics is obtained by an analysis of our kinematic data on the radius of the flow front as a function of time, $r(t)$. For all flows there was a primary acceleration phase during which the acceleration was approximately constant between 0.25 g and 0.3 g. For $a < 1.7$ this acceleration phase was followed by a phase of deceleration which came quite abruptly to a halt. For $a > 1.7$ these two phases were separated by a phase of constant velocity of the flow front whose duration increased with increasing a. This phase of constant velocity has an analogue with the evolution of a fluid axisymmetric gravity current spreading at high Reynolds number, which also goes through a stage of constant velocity (Huppert & Simpson 1980). A fluid current then adjusts under a balance between buoyancy and inertial forces, spreading like $t^{1/2}$ (Hoult 1972) – the same result as obtained for the granular collapse described here. This analogy, which uses quantitative relationships to describe the motion of the granular medium that are closely analogous to those used to describe the motion of density currents of Newtonian liquids, further strengthens our argument that intergranular frictional effects play a negligible role until the abrupt halt commences.

Obtaining the spreading relationships that our experiments have indicated remains a challenge for the future. In the meantime a clue to understanding the emplacement we have observed may come from an interpretation of the final stages, when the spreading pile comes to a rapid

halt. It has been suggested that granular materials can be considered in two states (Jaeger *et al.* 1996): a static solid state, where intergranular forces at particle faces give the material strength; and a liquid state, exemplified by granular flows and fluidised beds, where the particles are in an agitated state and the system has negligible strength. The abrupt cessation of the motion of the granular flows that we observed can be likened to a phase change between two states (Huppert 1990). In accord with the characterisation put forward in (Jaeger *et al.* 1996), the change of state can be envisaged as a kinetic process analogous to solidification of a true liquid. In the case of a granular medium, we suggest that as the flow decelerates, the granular temperature falls below a threshold value and frictional interactions between particles become dominant and the granular material converts to a static solid (or deposit).

REFERENCES

Hoult, D. P. 1972 Oil spreading on the sea. Annu. Rev. Fluid Mech. **4**, 341–368.

Huppert, H.E. & Simpson, J.E. 1980 The slumping of gravity currents. J. Fluid Mech. **99**: 785, 1980.

Huppert, H. E. 1990 The fluid mechanics of solidification. J. Fluid Mech. **212**, 209–240.

Jaeger, H. M., Nagel, S. R. & Behringer, R. P. 1996 Granular solids, liquids, and gases. Rev. Mod. Phys. **68**, 1259–1273.

Chapter IV

Collapses of Two-dimensional Granular Columns

Abstract

The first detailed quantitative observations of the two-dimensional collapse of a granular column along a horizontal channel are presented for a variety of materials. Together with the complementary study for the axisymmetric situation, we conclude that for granular collapses the generally accepted approaches, that are highly dependent on frictional parameters, do not describe the main flow phenomena. The motion divides in two main flow regimes at $a \sim 1.8$, where the aspect ratio $a = h_i / d_i$ and h_i and d_i are the initial height and width of the column. We describe the details of collapse by emphasising the sequential occurrence of a main spreading followed by a final avalanching phase. For the low a regime, $a < 1.8$, we derive descriptions of the final geometry by direct physical arguments. For the large a regime, $a > 1.8$, we determine that nearly all details of the collapse, including the position of the flow front as a function of time, the emplacement time, the self-similar final profiles, and especially their maximum vertical and horizontal extension, are established during the spreading phase and can be expressed in terms of the initial geometrical parameters but are independent of basal and internal friction parameters.

CHAPTER IV

1. Introduction

The flow of granular media plays an important role in many different areas, including agriculture, chemical engineering, the Earth Sciences, fundamental physics, hazard management and the pharmaceutical industry. Partly because of this multidisciplinary nature there has been considerable research interest in this area recently. In differing circumstances a granular medium can behave like a solid, a liquid or a gas. Three inspiring reviews use these analogies as the foundation (Jaeger et al. 1996, Kadanoff 1999, de Gennes 1999) and have discussed the change from one form to another, somewhat akin to a phase transition. However, the major obstacle in all this work and the aim of many recent studies has been the absence of general governing equations to describe the motion and behaviour of granular media. This is in marked contrast to the understanding of solids, liquids and gases, where the equations of statics have been known for centuries and the theory of linear elasticity, the Navier-Stokes equations and the kinetic theory of gases have almost a century of investigation.

Some progress has been made to develop an understanding of granular media. For flowing granular media, equations akin to the shallow water equations of fluid mechanics (Whitham 1974, Pedlovsky 1979) have been developed for a mono-dispersed granular medium flowing in steady state down an inclined plane at an angle to the horizontal greater than the static angle of repose (Savage & Hutter 1989, Anderson & Jackson 1992, Savage 1998, Pouliquen & Forterre 2002, Iverson & Denlinger 2001 and references therein). These equations emphasize frictional effects between the grains and along the bottom boundary, and also assume that variations in the slope of the free surface are small. It is not yet clear how well these equations will apply to large-scale flows, as are commonly observed in the gigantic rockfalls which occur on the Earth, the Moon and Mars, involving up to $10^4 km^3$, in contrast to the $10^3 cm^3$ in laboratory experiments (Hsü 1975, Voigt 1978, Hutter et al. 1995, Iverson 1997, Huppert & Dade 1998, Dade & Huppert 1998). As in many areas of science, experimental data help to develop the intuition needed for the derivation of the fundamental equations; and indeed many experiments with granular flows have been conducted. However, one difficulty is that, unlike other fluid-mechanical systems, sometimes the flow behaviour can depend on the distance between bounding walls, even when the distance is much larger than the size of the granular material itself (G.D.R. Midi 2004, Jop et al. 2004).

Recently, we initiated a fundamental experimental investigation on the collapse of an initially cylindrical volume of granular material released instantaneously onto a rough horizontal bed (Lube et al. 2004). Unknown to the present authors, a similar study was undertaken by a French group (Lajeunesse et al. 2004). These axisymmetric studies show that the major governing parameter is the aspect ratio a, defined as the ratio of the initial height, h_i, to the initial radius, r_i, of the cylinder of granular material. Almost all of the details of the collapse, such as the time, t_∞, taken to reach the final runout distance, r_∞, and the final height at the centre of the resultant deposit, h_∞, were found to be independent of the different grains used – couscous, rice, salt, sand and sugar – and the roughness of the lower boundary. Basal frictional effects are minimal because a thin layer of particles is lain down over which the main flow rides. Intergranular frictional effects are dominated by inertial forces, until very near the end of the collapse, where the flows come to a quite abrupt halt (except for some thin, small scale avalanching which occurs on the upper free surface of the deposit).

The aim of the present paper is to investigate the details of the collapse in a two-dimensional geometry. The paper is not just a presentation of results in a different geometry, but builds on and extends the intuition and techniques developed for the axisymmetric investigation utilizing the advantage to observe the flows in cross-section. The plan of the paper is as follows. We explain the two experimental set-ups and techniques in section 2 and describe the observations in section 3. Section 4 presents quantitative representations of the shape of the final deposit, including the final runout distance and maximum central height, and the time for collapse, which are represented by simple powerlaw functions of the initial aspect ratio. A collapse of all the data for the non-dimensional position of the front as a function of non-dimensional time is also documented. The final section summarises our study, compares the results with the previous axisymmetric studies and draws some conclusions. The two-dimensional results presented here were first announced in the conference proceedings (Huppert et al. 2003).

2. The experiments

2.1. Experimental set-ups

The experiments investigate two-dimensional granular flows created by rapidly releasing particulate columns, initially contained in a rectangular box, into a wide channel. Two main experimental series were studied using different set-ups.
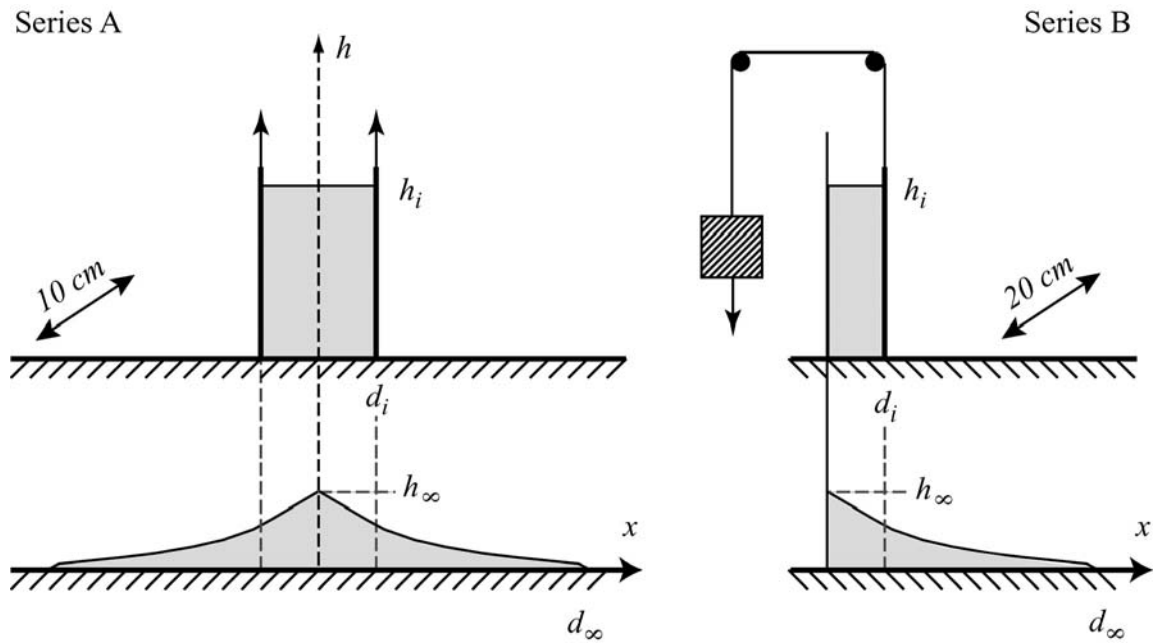
Figure 1. Initial set-ups for the experiments of series A and B with a rough sketch of the final deposit beneath.
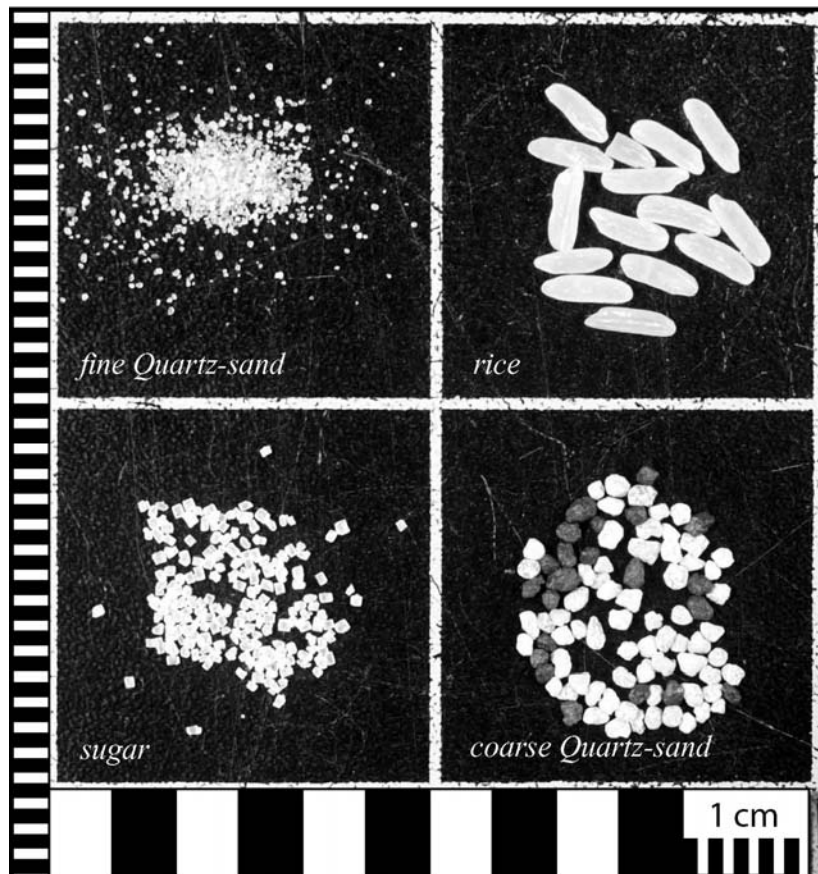

Figure 2. Photo of the four different types of grain used in the experiments with millimetre markings on the side and half centimetre markings at the bottom.

Series A involved symmetric spreading along a channel that had a constant width of 10 cm (Fig. 1a). The rear panel and the base of the tank, constructed of wood, were covered with a thin sheet of paper, whereas the frontal panel was transparent Plexiglas. Lube et al. (2004) showed that the roughness of the floor made no difference to the results, because, irrespective of the roughness of the surface, a thin layer of grains was deposited and the main flow took place over these stationary grains. Moreover, the general validity of this result was confirmed here by some additional experiments performed using a rough surface made of sandpaper with roughness of the same order as the flowing sand. The container in which the initial columns were prepared consisted of two parallel, vertically movable gates. Symmetrical column collapses resulted from the fast manual lifting of the gates (Fig. 1a). The geometry of the initial columns was varied by using different horizontal spacing of the gates and different masses of material. We carried out experiments with two different quartz-sands, rice and sugar, thus covering a wide range of grain sizes and shapes. Grain sizes were chosen so that cohesion effects would be negligible. A photo of the different sets of grains, clearly showing their different geometrical shapes, is given in Fig. 2. Density, mean grain size and angle of repose for each set of material are given in table 1.

Particle	Mean density (g/cm^3)	Mean grain size (mm)	Angle of repose (deg.)
Fine Quartz-sand	2.6	0.15	29.5
Coarse Quartz-sand	2.6	1.5	31
Sugar	1.58	1	35
Rice	1.46	7×2*	32

(* long axis $\times$ short axis)

TABLE 1. Properties of particles used in the experiments.

Experiments of series B involved uni-directional spreading and were performed in a tank of 20 cm width. A different type of container to accommodate the initial particulate columns was connected to one end of the tank. The rectangular box of the same width as the channel and variable initial basal length d_i comprised only one frontal gate to release the granular material (Fig. 1b). A release mechanism was constructed to allow for very fast and reproducible lifting velocities of the gate. It consisted of releasing a large weight connected to the gate via a pulley construction at the ceiling. The weight fell free for the first 0.75 m to reach a high

velocity before it lifted the gate nearly instantaneously. The time for the gate release in any experiment was very much less than the typical time scale of the resulting motion.

In both series the initial aspect ratio a, defined by the ratio of initial height, h_i, to initial basal distance, d_i, was varied systematically over two orders of magnitude. The initial basal lengths and range of aspect ratios for each set of grains and experimental series are presented in table 2.

Experiment	Particle	Initial basal length (cm)	Range of $a = h_i / d_i$
Series A	Fine Quartz-sand	1.95	0.7 - 7.6
	Coarse Quartz-sand	1.95	0.5 - 17
		4.8	0.6 - 8.6
	Sugar	1.95	1 - 21
	Rice	1.95	1 - 18
Series B	Coarse Quartz-sand	4.5	0.7 - 18
		8.3	0.5 - 11
		12.5	2 - 4.7

TABLE 2. Initial basal length and range of aspect ratio for each material.

2.2. Measurement methods

Both sets of experiments were recorded by video to investigate the behaviour of the collapses through the vertical Plexiglas plane. A normal 25 frames per second (fps) camera was used for series A, whereas a fast industrial camera at 240 fps was employed in series B. Data for distance against time of the flow front were obtained from the movie sequences by measuring the elapsed time at horizontal markings in spacings of 3 mm. We used three different approaches to study flow and sedimentation processes in detail. In order to measure the geometry and the continuously reducing volume of the flowing layer as a function of time, we mapped the free surface and the interface between deposited and static material by manually cross-correlating between neighbouring frames of a high-speed sequence. For some experiments, we also observed the deformation of the flowing layer by calculating the intensity difference between consecutive images. Velocity profiles with depth in the flowing

layer were obtained using the Particle Image Velocimetry (PIV) algorithm written by Dalziel (2005).

After each run, the contour of the final deposit was measured to determine d_∞, the maximum runout distance and h_∞, the maximum deposit height at *x=0*. The measuring system consisted of the combination of a grid printed on the vertical transparent plane and a point laser projected horizontally at variable heights onto the pile. The accuracy in determining the granular surface height is limited by grain size. However, the optical resolution was higher than the mean grain size of all tested grains except for fine quartz-sand.

3. Experimental observations

Qualitative observations of granular collapses within a channel reveal a strong dependence of the flow behaviour on the value of the initial aspect ratio *a*, as found for axisymmetric collapses by Lube et al. (2004) and Lajeunesse et al. (2004). To help emphase the similarities and differences between the two-dimensional and axisymmetric collapses, we will first explain the two major flow regimes in the quasi two-dimensional situation and the general modes of granular flow observed. We then give a detailed description of the internal deformation and sedimentational processes as seen in the high-speed movies filmed through the Plexiglas plane.

3.1. Flow regimes and form of final deposits

In Fig. 3 we depict images from experiments with aspect ratios of 0.5, 1.5 and 7 to illustrate the two flow regimes, namely that of *low* (Fig. 3a-h) and *high* aspect ratios (Fig. 3i-l), and two modes of granular flow behaviour which are found to determine the shape of the final deposits. The most apparent difference between the two regimes is that for low values of *a* only the edges of the initial column are in motion (Fig. 3a,e), whereas for large *a* the entire free surface flows from the beginning (Fig. 3i). In a similar manner to axisymmetric collapses, the different behaviour dependent on *a* stems from the development of an initial failure plane along which material flows down, and below which particles remain static (Fig. 3a,e,i).

The geometrical position of this initial discontinuity, which has a conical geometry in the axisymmetric case, was observed in two ways. In cross-sectional view through the Plexiglas

plane, the discontinuity has the same initial position independent of the value of the aspect ratio and the grain type. It appears as a straight line intercepting at a zero height at $x = d_i$,
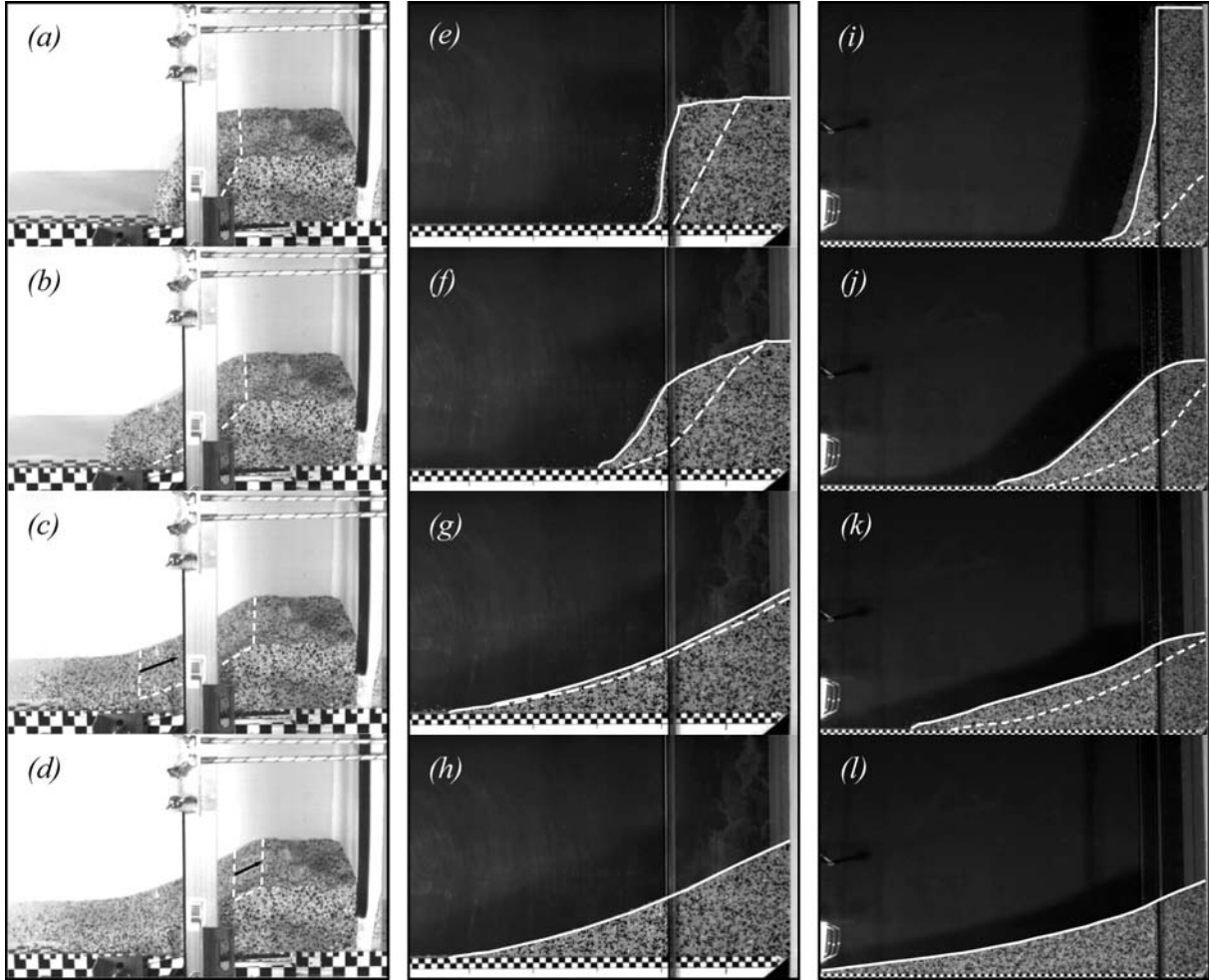

Figure 3. Flow evolution at different times for experiments with a=0.5 (a-d), a=1.5 (e-h) and a=7 (i-l). The dashed curves mark the position of the interface between static and moving particles, whereas the solid curve highlights the upper free surface.

where x is the distance from the origin, which is inclined at 61° to the horizontal. For experiments with aspect ratios less than 1.8, the discontinuity can also be initially observed as a straight line on the upper free surface of the column (Fig. 3a). We measured the horizontal distance, d_a, between that line and $x=0$ for several experiments. When normalised by d_i and plotted against the aspect ratio (Fig. 4) the data are accurately represented by the best-fit linear form

$$d_a / d_i = 0.99 - 0.54a. \tag{1}$$

This reveals that d_a becomes satisfyingly close to d_i as $a \to 0$. The difference between 0.99 and the expected value of 1 gives an indication of the magnitude of error in our experiments. The slope of 0.54 corresponds to an inclination to the horizontal of $\beta = 61.6°$. Both these
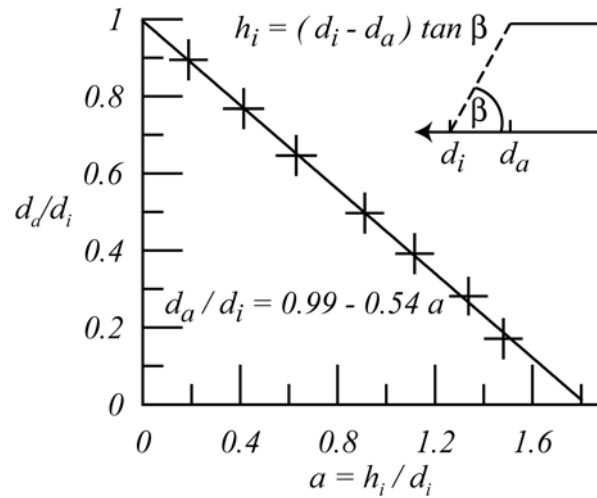

Figure 4. The non-dimensional horizontal distance of the undisturbed free surface, d_a / d_i, as a function of the aspect ratio from experiments of series A for a<1.8 with the best straight line fit through the data.

observations suggest that the inner, static body of material initially takes the form of a two-dimensional wedge with a corresponding aspect ratio of about 1.8.

For all aspect ratios, the flowing material passes through two characteristic phases of granular flow before the material arrests in its final configuration. In the first *spreading phase*, the flowing layer moves as a largely deforming, deep bulk flow. Particles originally at the free surface remain at the upper free surface or become incorporated into a thin basal layer when overrun by the flow front. In this phase of the collapse, the interface between moving and static grains propagates towards the upper free surface (Fig. 3) and continuously reduces the volume of the flowing layer. The flat frontal region quite abruptly ceases motion when the interface has reached the free surface and thereby determines the maximum runout at the end of the spreading phase. In analogy to our axisymmetric study, we define the time t_∞ as the duration of the spreading phase ending with the flow front coming to rest. At the steeper central slope, granular flow is observed to continue considerably longer than t_∞, in a phase that we refer to as the *final avalanching phase*. It consists of the backward propagation, along the free surface of the steep central slope, of the interface between already deposited and still moving grains (Fig. 3c,d & g,h). The relatively slow granular motion takes the form of thin

avalanches (a few grain diameters in depth) and modifies the free surface further. In Fig. 5 we show a plot of $(t_e - t_\infty)/t_e$ against the aspect ratio for fine and coarse sand, where t_e is the duration of the entire experiment. We observe that the non-dimensionalised time of avalanching is a decreasing function of the aspect ratio for $a < 4$ and remains rather constant (less than 0.2) for larger values of a. In addition, the duration of final avalanching strongly depends on the type of grain. This, as we will discuss later, is in contrast to t_∞, which appears to be independent of the grain type. For $a < 1.8$, the final avalanches progressively erode the initially static part of the upper surface. Whereas for $a < 1.15$ a static region on top of the initial column remains in the final deposit (Fig. 3d), the avalanches consume its entire area for $1.15 < a < 1.8$ (Fig. 3h). For $a > 1.8$, erosion by final avalanching appears to play a negligible role. Here the strongest alteration of the free surface by final avalanching at $x = 0$ accounts to less than 2 mm for fine sand and not more than 1.5 mm for the other materials. Two major forms of final deposits can thus be distinguished: truncated wedges for a < 1.15; and wedge-like deposits with a flatter frontal region and a steeper central region for a > 1.15. A third more or less flat form, as observed for the axisymmetric collapses [19], was not observed in the range of aspect ratios tested.
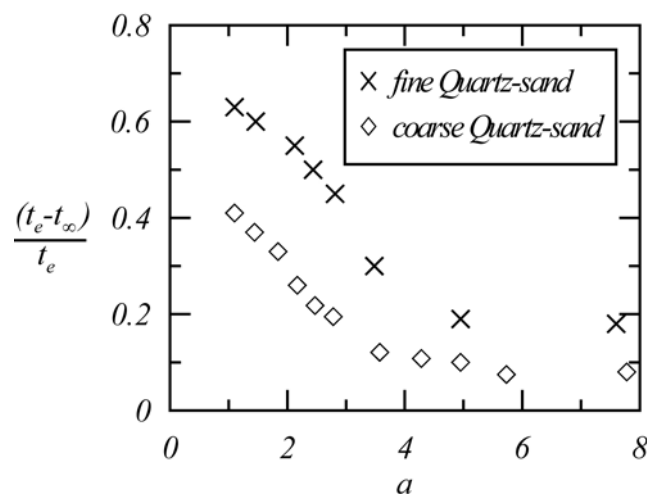

Figure 5. The non-dimensional duration of final avalanching, shown as the ratio $(t_e - t_\infty)/t_e$, as a function of the aspect ratio for fine and coarse Quartz-sand.

3.2. Internal deformation and sedimentation

Granular collapses within a channel allow the observation of internal deformation directly through the Plexiglas wall, which is an advantage to the previously studied axisymmetric experiments (Lube et al. 2004). A major reason to conduct these experiments in a wide channel was to reduce the effects of frictional interaction with the walls which will certainly become important in the case of very narrow flumes. We analysed the evolution of the

velocity profiles at the free surface to constrain the influence of the walls on experimental results. Velocity profiles across the surface of the channels (Fig. 6) show contrasted features between the spreading and avalanching phases. The velocity profiles indicate plug flow for the
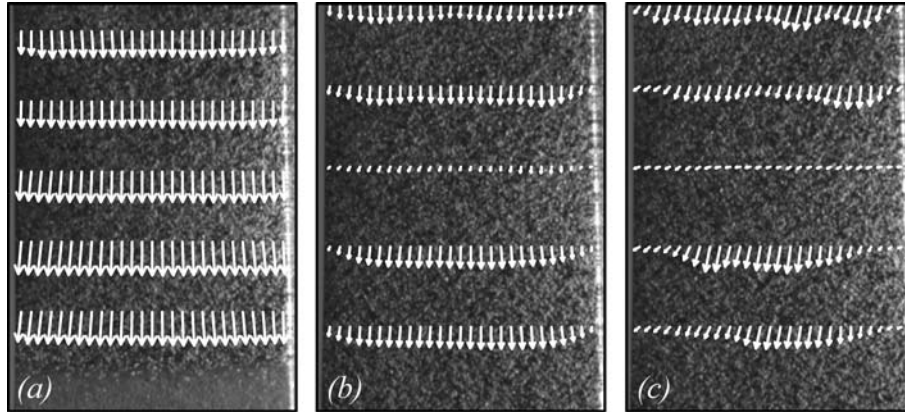

Figure 6. Velocity profiles across the free surface during (a) the spreading phase, (b) the commencement and (c) the end of the avalanching phase. To enhance visibility the length of velocity vectors are scaled by factors in (a) of 2, in (b) of 10 and in (c) of 30.
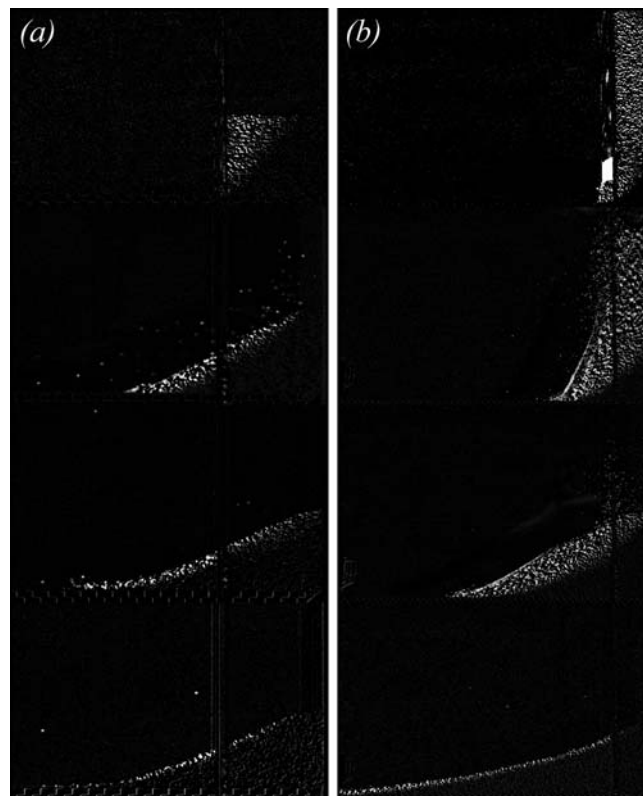

Figure 7. Difference calculations between consecutive images of a high-speed sequence for (a) a=1.5 and (b) a=5 to visualise the evolution of the flowing layer with time.
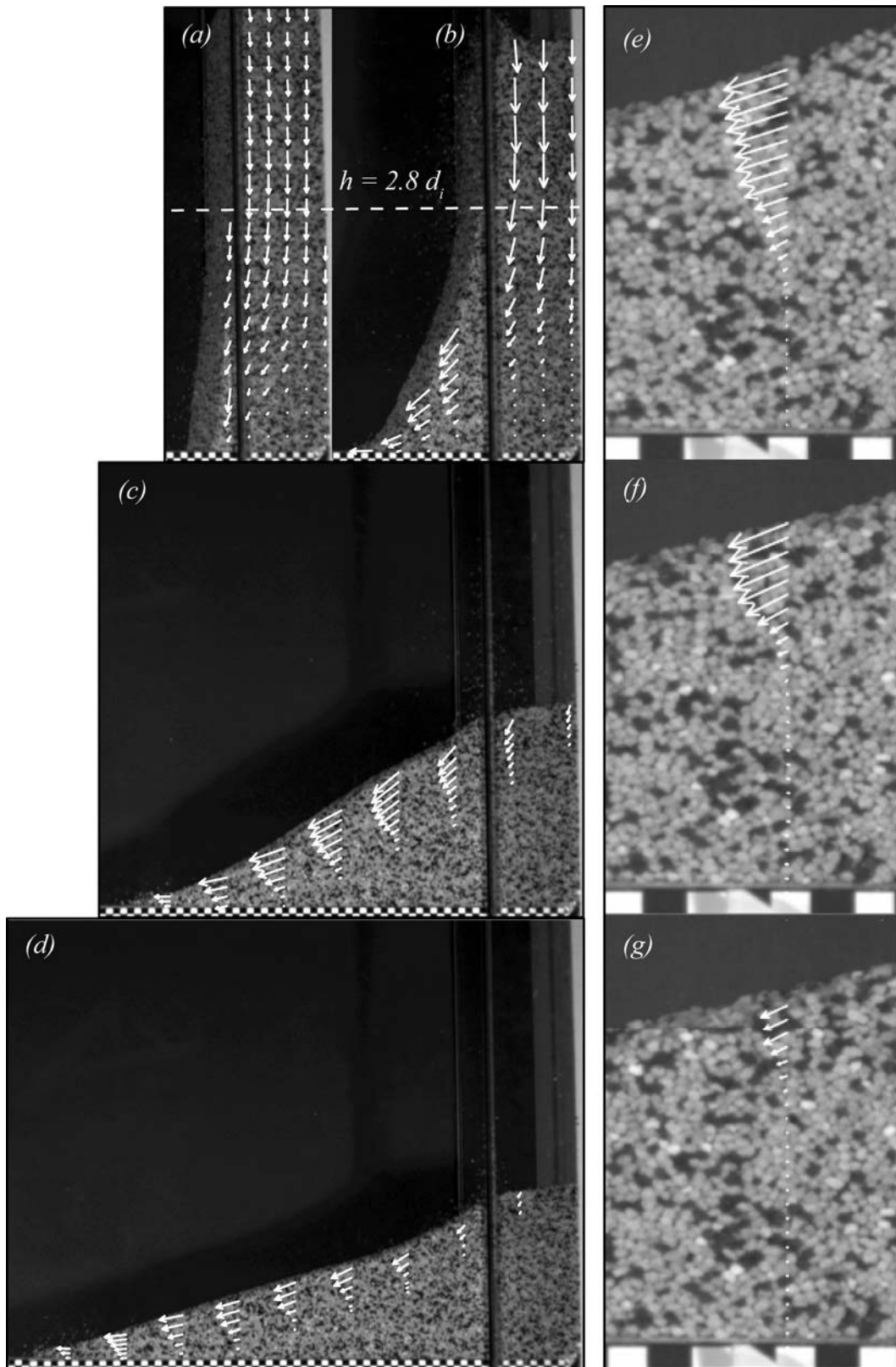
Figure 8. Velocity profiles with depth at different times during the spreading phase for an experiment where a=7 (a-d), and close-ups of the evolution of the velocity profile with time for the same experiment at a distance $d_\infty / 3$ (e-g).

spreading phase with minor shear at the walls and strong slip. The avalanching phase shows much stronger shear towards the walls and unsteadiness with simultaneous zones of no movement and actively flowing zones.

One way to illustrate the deformation of the flowing layer with time is to calculate the intensity differences between consecutive frames of a high-speed sequence. Typical results of such calculations for low and high aspect ratio flows are shown in Fig. 7. Similar to axisymmetric collapses, only the frontal part of the flowing layer is in contact with the basal surface, whereas the major flow takes place over deposited material. In both flow regimes, the interface between moving and static particles first develops a strong concave upwards profile with the degree of concavity decreasing with time. Thus the lower and upper surfaces of the flowing layer become increasingly parallel until the two merge at the end of the spreading phase.

Velocity profiles with depth have been measured for large aspect ratio flows. Based on PIV measurements two transient stages of collapse become evident. The first stage is related to the constant acceleration of the flow front (see section IV D), and the falling column can be divided into two zones of different behaviour. The upper part of the column falls vertically as shown by the vertical vectors of similar length and the non-deforming top (Fig. 8a, b). Deformation is restricted to the lower part of the column. Systematic measurements for different values of a indicate that the non-deforming upper part of the column develops above a height of about $2.8\ d_i$ independent of h_i. Deformation of the top occurs when it becomes less than this critical height. Also, in this second stage of deformation, when the flow front moves at an approximately constant velocity, velocity profiles with depth are not linear and vary with the position in the flowing layer and time (Fig. 8c, d). Figure 8e-g show close-ups of the form of the velocity profile above the flowing / static interface with time. These may be subdivided into three transient vertical regions with an upper low-shear, plug-like zone, a middle region with an approximately linear gradient and a lower exponential tail towards the interface. Velocity profiles in the frontal region with direct contact to the basal surface reveal a basal slip velocity and an approximately linear form above that.

4. Quantitative results

4.1. Scaling arguments for the final runout distance

Our observations that the form of collapses differ with different values of the aspect ratio $a = h_i / d_i$ immediately suggest using a as a fundamental parameter for the analysis of the final runout distances, d_∞. Arguments that a is the only parameter were presented in Lube et al. (2004). With the use of dimensional analysis we can then express d_∞ as
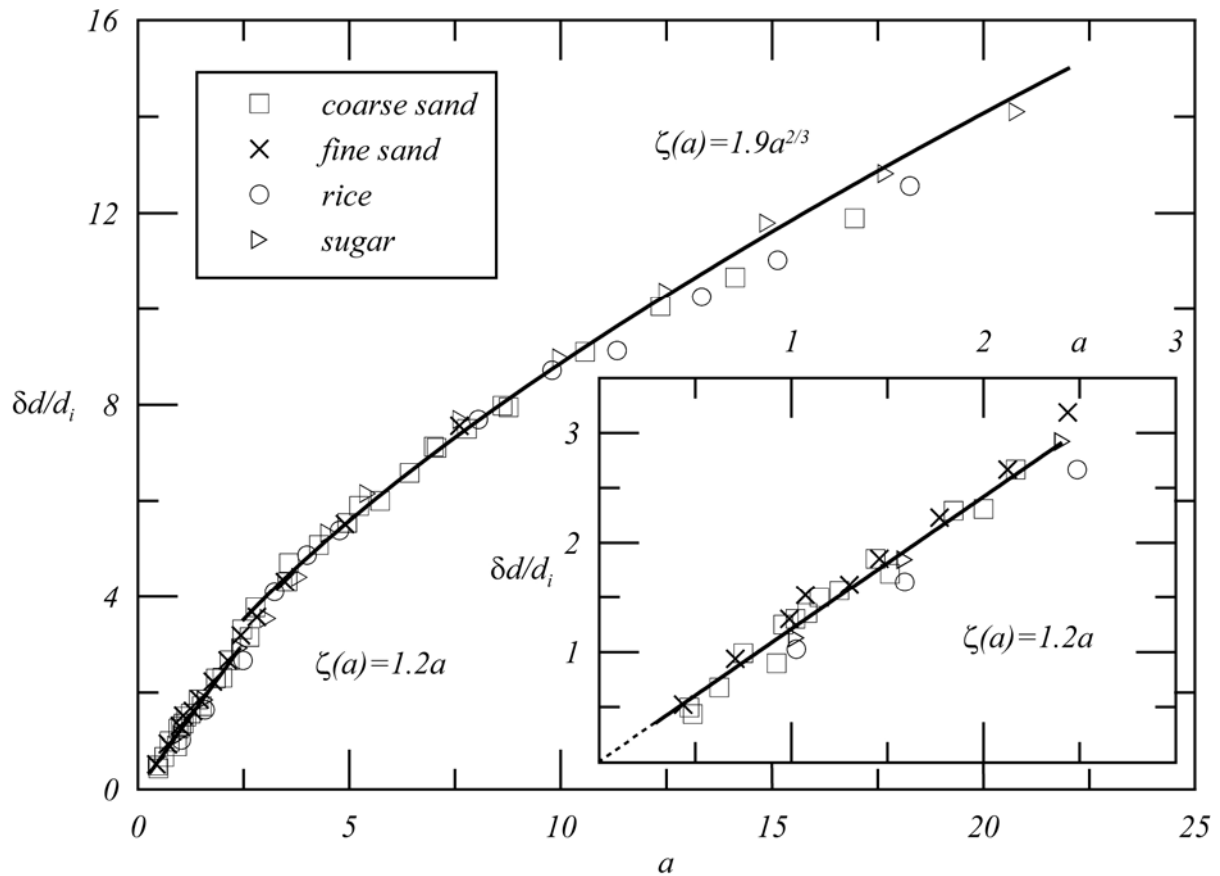

Figure 9. The non-dimensional incremental runout distance, $\delta d / d_i$, as a function of the aspect ratio for all our grains of series A. The inset highlights the data for small aspect ratios.

$$\delta d \equiv d_\infty - d_i = d_i \zeta(a), \qquad (2)$$

where $\zeta(a)$ is a non-dimensional function of the aspect ratio. In Fig. 9 we plot the incremental runout distance, δd, normalised by the initial basal length d_i, against the aspect ratio for all our different grains from series A. All the runout data collapses onto a single curve, suggesting that no further external parameters, such as the inter-granular or basal friction, are needed for their mathematical description.

The function $\zeta(a)$ could theoretically take any form. However, for the low aspect ratio regime the function can be determined by simple physical arguments. Collapses for aspect ratios in this range display granular motion only beyond a specific distance d_a. The function $\zeta(a)$ must consequently be independent of the value of d_i. Thus in terms of equation (2) the initial height is the only length the incremental runout distance can be related to, and thus $\delta d = c_1 h_i$, and the functional form $\zeta(a)$ is given by
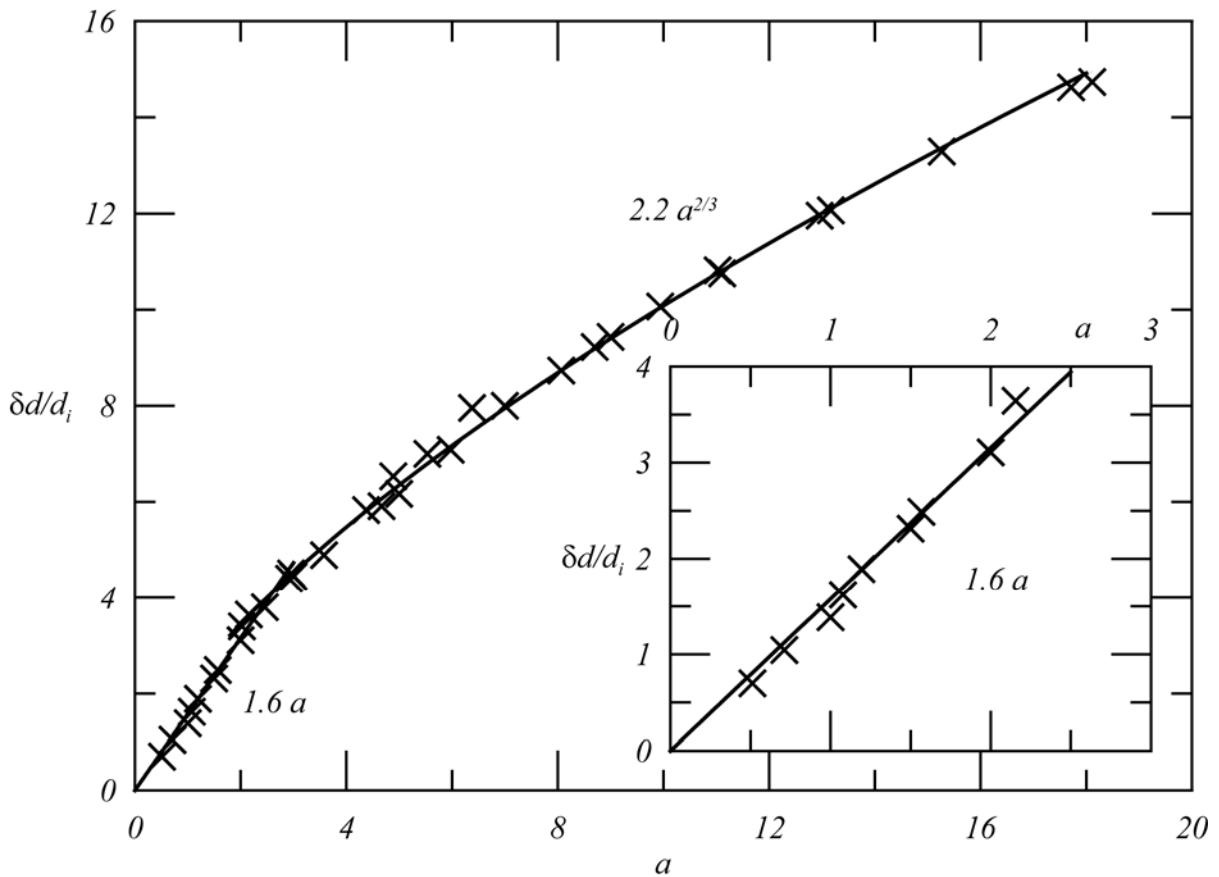

Figure 10. The non-dimensional incremental runout distance, $\delta d / d_i$, as a function of the aspect ratio for experiments of series B.

$$\zeta(a) = c_1 a . \qquad (a < 1.8) \qquad (3)$$

The coefficient c_1 remains to be determined experimentally. For series A at low a the data are well represented by a $\zeta(a) = 1.2a$ (inset of Fig. 9).

For larger aspect ratios we cannot obtain a formulation for $\zeta(a)$ *a priori* by simple physical or dimensional arguments. A good representation of the experimental data, however, is given by the powerlaw form

$$\delta d / d_i = c_2 a^{2/3} \quad \text{with } c_2 = 1.9. \quad (a > 2.8) \tag{4}$$

Together with the analysis of the final height profiles, we give a geometrical explanation for this result in (4C). There is not an abrupt break in the curve $\zeta(a)$, but a small transitional region for 1.8<a<2.8 exists between the linear and the powerlaw descriptions.

For the experiments of series B the same analysis can be applied. Again, the collapse of the data for three different values of d_i is obtained when the runout is plotted as a function of the aspect ratio (Fig. 10). Note that the data plotted in Fig. 10 include those taken from flows on sandpaper. The curve coincides in mathematical form with that given for experiments of series A with a linear section at low aspect ratios and a 2/3 powerlaw for the large aspect ratio regime. The experimentally determined coefficients in (3) and (4), however, are larger than those of series A with $c_1 = 1.6$ and $c_2 = 2.2$. Since all other experimental parameters are kept the same, these differences must reflect the different nature of collapse when the column supports itself during the experiment, as in series A, or flows between a static wall as in series B.

4.2. Scaling arguments for the maximum deposit height

The maximum deposit height at *x=0* is dependent on the initial height and the aspect ratio and is a consequence of both the initial spreading phase and the late stage avalanching along the free surface. By dimensional analysis the final maximum height can be expressed as

$$h_\infty = d_i \varphi(a), \tag{5}$$

where $\varphi(a)$ is a non-dimensional function of *a*. The function can be specified for small aspect ratio collapses where $h_\infty = h_i$ and thus

$$\varphi(a) = a, \tag{6}$$

as indicated by the data for $a \leq 1.15$ (Fig. 11). The expression for h_∞ is only linear, and independent of d_i, for $a \leq 1.15$, whereas the function for the maximum runout remains linear up to $a \sim 1.8$, the aspect ratio of static wedge. At $1.15 < a < 1.8$ an inner part of the upper surface of the column initially remains static but is then eroded by late stage avalanching.

For $a > 1.15$ the data suggest the functional form
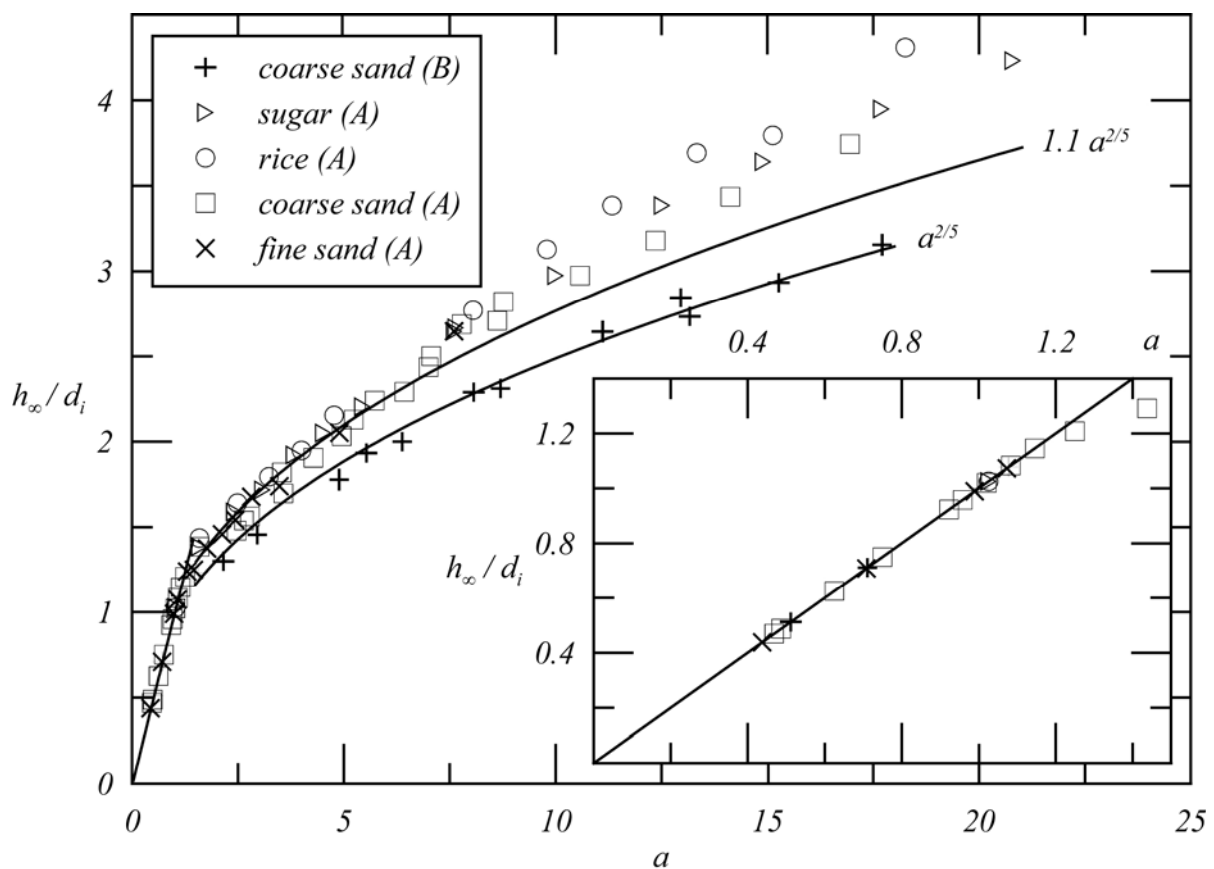
$$\varphi(a) = ka^{2/5}, \tag{7}$$

Figure 11. The non-dimensional maximum deposit height, h_∞ / d_i, as a function of the aspect ratio. Functions of the form $\varphi(a) = ka^{2/5}$ are shown for experiments of series A and B. There is the tendency of series A data to increasingly deviate from the curve at large aspect ratios.

with the constant k differing just slightly for experiments of series A ($k=1.1$) and B ($k=1$) (Fig. 11). Series A data further show a deviation from the functional form (7) for $a > 8$. We assume that this deviation is caused by frictional effects due to the vertical walls of the channel that become important during low-velocity grain motion during the final avalanche

stage. This interpretation is supported by the fact that such a deviation is not observed for experiments in a wider channel (series B).

4.3. Final height profiles

The contour of the final deposits can be written in non-dimensional form as

$$h(x)/h_\infty = \eta(x/d_\infty, a) \tag{8}$$

with η being a dimensionless function of x/d_∞ and a. In addition we know by definition that

$$\eta\,(0,a) = 1 \quad \text{and} \quad \eta\,(1,a) = 0. \tag{9}$$

The normalised final height profiles at low aspect ratios (Fig. 12) reveal the large variation of form with the aspect ratio. However, the normalisation of our final height profile data for all large aspect ratio flows results in a collapse of all data points onto a universal curve (inset of Fig. 12). The minor scatter might be entirely explained by the modification of the deposit shape during the final avalanching stage. The important result from this analysis is that this normalised universal curve is independent of the value of the aspect ratio

$$h(x)/h_\infty = \eta(x/d_\infty) \qquad (a>2.8). \tag{10}$$

The integral of this curve gives A_n, defined by

$$A_n = \int_0^1 \eta(y)dy\,. \tag{11}$$

The integral was evaluated for series A and B data and gives nearly identical values for both curves with $A_n \approx 0.37$ (for $a>2.8$).

We will use this result to discuss now the final runout data for large a. On a macroscopic scale, volume conservation must be valid for granular column collapses. For the two-dimensional spread we can thus assume that the initial and final cross-sectional areas in the flow direction are equal
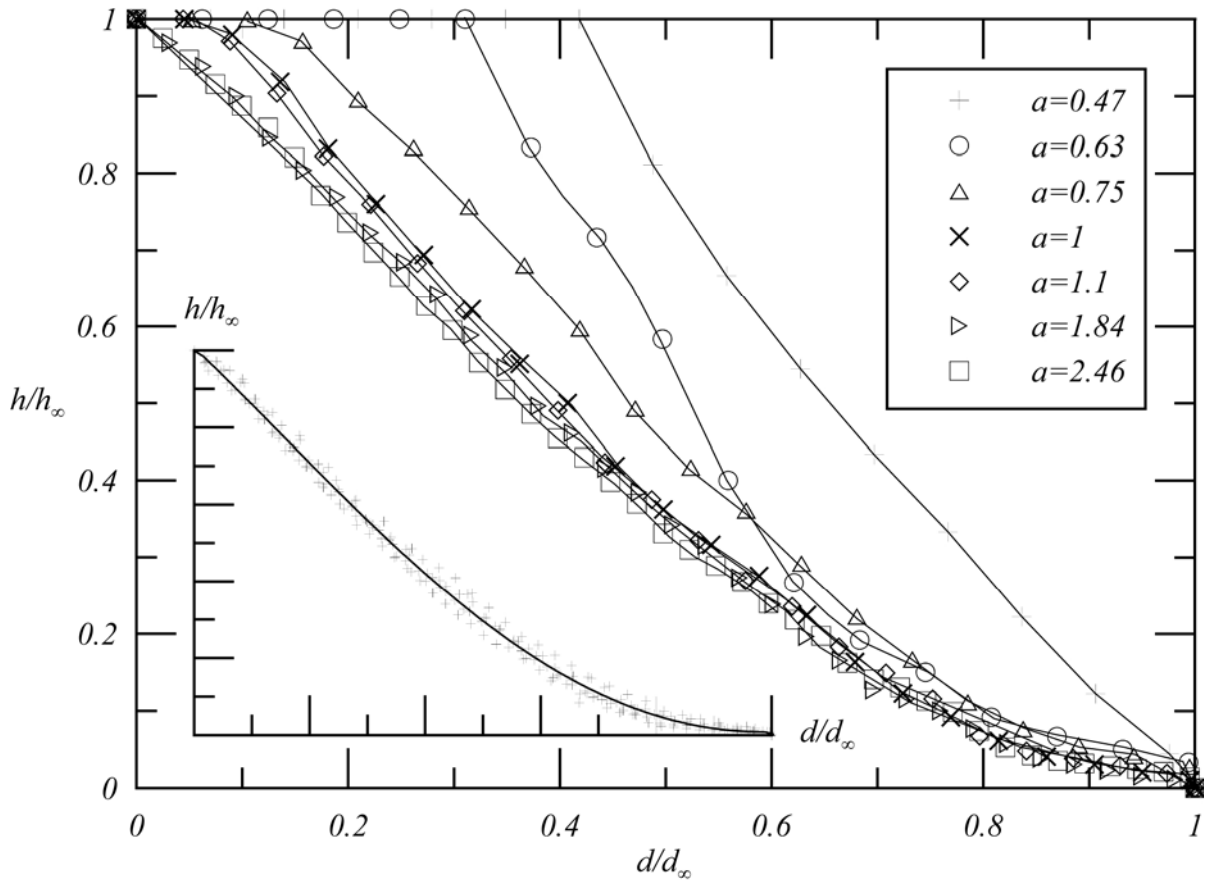
Figure 12. The non-dimensional height of the final deposits as a function of non-dimensional distance for a<2.5 for some series A experiments. The inset shows the same plot for a>2.8.

$$\int_0^{d_\infty} h(x)dx = h_\infty d_\infty \int_0^1 \eta(y)dy = h_i d_i \,. \tag{12}$$

Thus

$$\int_0^1 \eta(x)dx = \frac{h_i d_i}{h_\infty d_\infty} \,. \tag{13}$$

Substituting (5) and (2), rewritten as $d_\infty = d_i f(a)$, into (12), we can write

$$\int_0^1 \eta(x)dx = a\frac{1}{\varphi(a)f(a)} \approx 0.37 \qquad \text{(independent of } a\text{)}. \tag{14}$$

71

The expression (14) can only be independent of a if the product $\varphi(a)f(a)$ is directly proportional to a. We can use this relationship to calculate the final runout distance by using (7), the experimentally determined expression for h_∞, to determine that

$$d_\infty / d_i = a^{3/5} / (0.37k) \tag{15}$$

or

$$\delta d / d_i = a^{3/5} / (0.37k) - 1. \tag{16}$$

Using the experimentally determined coefficients k for series A and B we obtain a good fit to the runout data at $a>2.8$ (Fig. 13). Although (16) reveals a geometrical relationship for the final runout distance at large aspect ratios a physical explanation remains a challenge for further studies.
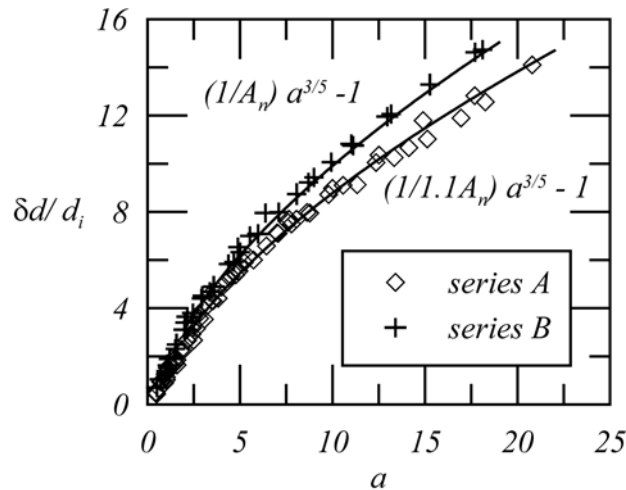

Figure 13. The non-dimensional incremental runout distance, $\delta d / d_i$, as a function of the aspect ratio for experiments of series A and B. The functions drawn through the data for the large a regime are of the form $\delta d / d_i = a^{3/5} / (A_n k) - 1$, where k is an experimentally determined coefficient from the analysis of h_∞ and A_n is the normalised cross-sectional area of the final deposits, calculated as $A_n \approx 0.37$.

4.4. Kinematic data

Data of the position of the flow front as a function of time were collected for aspect ratios in the range *0.5<a<18* for different values of d_i. The typical form of the distance-time path is shown for $d_i = 8.3$ cm in Fig. 14. We clearly distinguish three transient stages, with an initial acceleration, a phase of approximately constant velocity and a final deceleration. The initial

horizontal acceleration is constant at *0.75 g* for all values of d_i. The duration of constant velocity motion decreases with lower values of *a* and does not develop for *a<1.5*.

From the high-speed movies we also determined the time, t_∞, at which the motion of the flow front ceases. By dimensional arguments it must be of the form
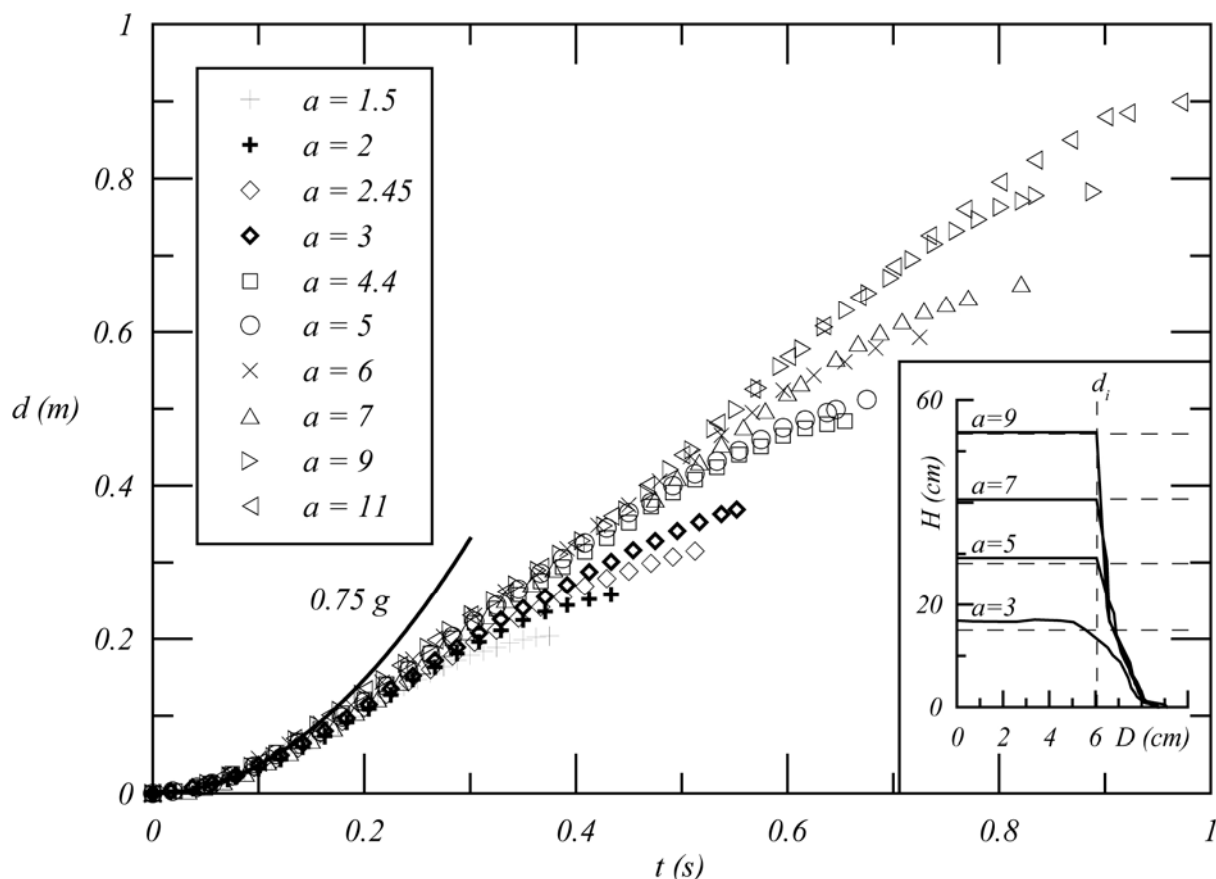
$$t_\infty = (d_i/g)^{1/2}\psi(a),\qquad(17)$$

Figure 14. The horizontal excursion of the flow front as a function of time for d_i =8.3 cm. The inset compares profiles of the free surface for four experiments with d_i =6.05 cm 83 ms after initial motion. Horizontal dashed lines mark the calculated free-fall heights of the top of the columns at this time.

for some functional form of $\psi(a)$. For small values of the aspect ratio t_∞ must be independent of d_i and $\psi(a) = ca^{1/2}$. From Fig. 15 it is seen that the data for large aspect ratios are also well represented by $\psi(a) = 3.3a^{1/2}$, suggesting that the time for the columns to spread only depends on the value of h_i. Series A data shows a larger scatter around (17) which is due

to the low frame rate of the CCD footage from which it was measured. Note that a grain in free fall from height h_i would hit the ground in a time

$$t_0 = \left(2h_i / g\right)^{1/2} = \left(2ad_i / g\right)^{1/2} \approx 0.43 t_\infty . \qquad (18)$$

The initial collapse is driven by vertical free-fall behaviour. This is confirmed by the experimental observation that the upper part of the column, above a height $\sim 2.8 d_i$, undergoes
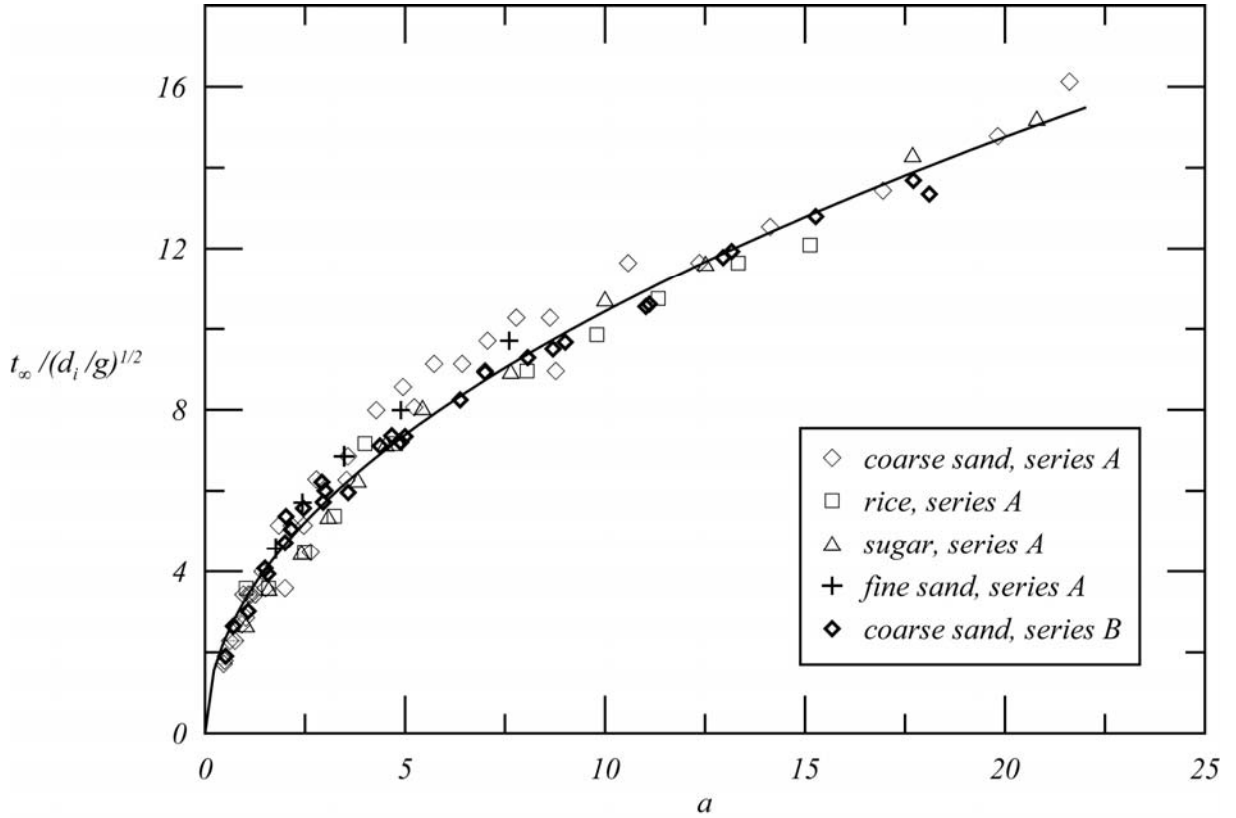

Figure 15. The non-dimensional time for the flow front to cease motion as a function of the aspect ratio with the curve $\psi(a) = 3.3 a^{1/2}$.

undisturbed vertical motion. To further analyse this, we compared the free surface profiles of flows with aspect ratios 3, 5, 7 and 9 at a time *83 ms* after initial motion (inset of Fig. 14). At this time the flow fronts for *a=9* and *a=7* still move at constant horizontal acceleration *0.75 g*, while for *a=5* the acceleration is smaller than *0.75 g*, and for *a=3* the motion of the flow front is already at constant velocity. The horizontal dashed lines correspond to the theoretical free-fall heights $h_f = h_i - 0.5 g t^2$ at *t=83 ms*. For *a=7* and *a=9* the tops of the columns match this relationship, but remain higher than h_f for *a=5* and *a=3*. Hence, the phase where the upper part of the column is in vertical free-fall corresponds to the stage of constant horizontal

acceleration of the flow front. As long as the column height remains greater than $2.8 d_i$ ($a \geq 5$ in Fig. 14) flow cross-sectional profiles remain self-similar as the flow front accelerates at 0.75g. Lateral flowage during this stage is thus independent of h_i. The cross-sectional profile changes notably when the height falls below $2.8 d_i$ ($a=3$ in Fig.14) and the flow front assumes a constant velocity, indicating that the dominant control by the column's free-fall has terminated.
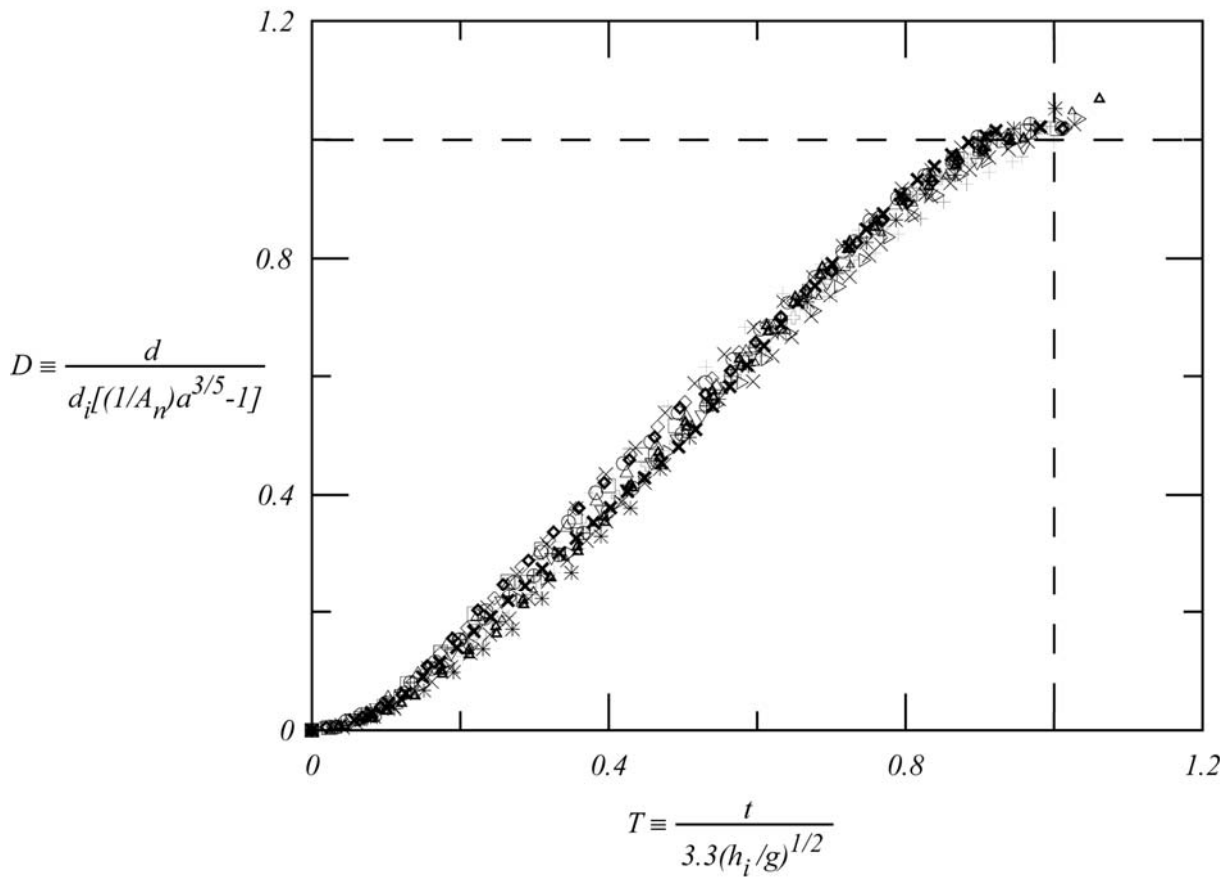

Figure 16. The normalised distance-time data of the flow front for a>2.8 of series B.

The distance and time data of flow front propagation can be expressed in non-dimensional form as fractions of their terminal values (16, 17) such that

$$D \equiv d / d_\infty = d / \left[d_i \left(a^{3/5} / A_n \right) - 1 \right] \tag{19}$$

and

$$T \equiv t / t_\infty = t / 3.3 \left(h_i / g \right)^{1/2}. \tag{20}$$

Figure 16 shows that this approach results in the collapse of all distance-time data onto a universal curve that preserves the three stages of initial acceleration, constant velocity and terminal deceleration.

5. SUMMARY AND CONCLUSIONS

This paper presents the first detailed, quantitative observations of the collapse of a granular column in a two-dimensional manner down a horizontal channel. The experimental work complements two previous studies on axisymmetric granular column collapses on a horizontal base (Lube et al. 2004, Lajeunesse et al. 2004). We carried out two different series of experiments: A) symmetrical spreading, for which the two gates across the channel holding the column were lifted simultaneously and the column spread in a symmetrical manner up and down the channel; and B) uni-directional spreading, for which only one retaining gate was lifted and the grains spread down the channel, constrained by the fixed backwall. The differences in flow behaviour between these two situations were small. The main experimental results are as follows:

- In each case there was a triangular wedge (or trapezoidal wedge for low aspect ratio columns) having the basal width of the column and making an angle of $61 \pm 2°$ with the horizontal, within which the grains never moved. Two forms of collapse were recorded, corresponding to a low aspect ratio regime, for $a<1.8$ (=tan 61º), and a large aspect ratio regime, for $a>1.8$.

- In both flow regimes the volume of flowing material reduced continuously by the propagation towards the upper free surface of the interface between static and flowing grains. The vertical velocity profiles between the interfaces varied both downstream and with time. The flow front propagated in a manner that varied with time. The flowing grains never contact the floor except for a small region just behind the flow front.

- We distinguish two subsequent flow phases. In the initial spreading phase, most details of the final form of the deposit are established in time t_∞, independent of the type of grain, and effects of the limiting channel walls are minimal. The final avalanching phase includes the stabilisation of the steep inner part of the pile via thin avalanches. Here strong velocity gradients across the free surface develop and the motion shows a clear temporal dependence on the grain type.

- All data of the rescaled maximum horizontal and vertical excursion of the final deposit collapse onto single curves, as a function of the initial aspect ratio only, and independent of internal and basal friction. For low aspect ratios, these functions are linear, while they take a powerlaw form for high aspect ratios.

- The time for collapse, t_∞, varies as the square root of the initial column height and is independent of its width. For $a > 2.8$, the collapse is mainly controlled by the initial free-fall behaviour of the column.

- All collapses for $a > 2.8$ generated self-similar deposit shapes that can be functionally described using volume conservation. As a consequence, non-dimensional distance-time paths are also self-similar.

These results are not compatible with earlier continuum representations of granular flows that used the shallow water approximation and invoked roughly uniform vertical velocity profiles, small surface slopes, and heavily depend upon friction coefficients (Savage & Hutter 1989, Iverson & Denlinger 2001, Hutter et al. 1995). In our experiments the velocity profiles were not linear, the slopes were large and friction was not important until the end. This last statement is in itself surprising and the explanation is that frictional effects are relatively small, just like a fluid flowing at high Reynolds number, until the velocity falls sufficiently that friction can dominate, and does so in this granular case quite rapidly. There is an interesting analogy, which can be pursued analytically, with a cooled and solidified liquid at low values of the Stefan number,

$$S = L/(c_p \Delta T), \tag{32}$$

where L is the latent heat, c_p the specific heat and ΔT the temperature fall needed for the fluid to solidify. Latent heat effects are essential for the fluid to solidify, just as frictional effects are essential for the flow to cease. However, in the limit of low Stefan number, the time for solidification is independent of the explicit value of the latent heat. An alternative numerical approach would be to employ individual grain-following computations, which involve as many as 10^8 grains. However, these have generally produced results, which are heavily dependent upon intergranular friction and the exact shape of the grains (Campbell 1990, Shinbrot et al. 1999, Cleary & Sawley 1999, Zenit 2005). Nevertheless, it might be interesting to pursue such an approach.

The results for two-dimensional collapses are all similar in spirit to those found for the axisymmetric case (Lube et al. 2004). In both cases the dimensions of the final deposit and the collapse time are represented by similar functions, but the values of limiting aspect ratios and empirical constants differ.

We plan to present further insights regarding the dynamics of the interface between moving and deposited grains in subsequent papers.

Note added

We have recently become aware of two papers which appeared after the submission of our work. In (Siavoshi & Kudrolli 2005) the authors detail the collapse of an essentially semi-infinite granular step of non-cohesive steel beads (a ~ 0 in our notation) and propose a simple theoretical model which yields reasonable results, even though, in the authors' words "some of the assumptions in the model ... are not met in the experiments". In (Kerswell 2005) a shallow water model, based on small slopes of a spreading layer of grains, is presented. The agreement between the theoretical results and experiments by the author to be published in the future is not good. This is not surprising given that, as we explain herein, considerably less than half the time of the collapse is spent as a thin layer; and in that time the velocity profile is far from uniform, with much of the lower part of the layer stationery.

REFERENCES

Anderson, K.G. & Jackson, R. 1992 A comparison of the solutions of some proposed equations of motion of granular materials for fully developed flow down inclined planes, J. Fluid Mech. **92**, 145.

Campbell, G.S. 1990 Rapid granular flows. Ann. Rev. Fluid Mech., **22**, 57.

Cleary, P.W. & Sawley, M. L. 1999 Three dimensional modelling of industrial granular flows. Proc. 2nd Int. Conf. On CFD in the Minerals and Processing Industries, CSIRO, Melbourne, Australia.

Dade, W.B. & Huppert, H.E. 1998 Long runout rockfalls. Geology **26**, 803.

Dalziel, S.B. 2005 DigiFlow User Guide, http://www.damtp.cam.ac.uk/lab/digiflow/.

de Gennes, P. G. 1999 Granular matter: a tentative view. Rev. Mod. Phys. **71**, 5374.

G.D.R. Midi 2004 On dense granular flows. Eur. Phys. J. E **14**, 341.

Hsü, K.J. 1975 Catastrophic debris streams (Struzstroms) generated by rockfalls Geol. Soc. Am. Bull. **86**, 129.

Huppert, H.E. & Dade, W.B. 1998 Natural disasters: Explosive volcanic eruptions and gigantic landslides. Theo. and Comp. Fluid Dynamics **10**, 201-212.

Huppert, H.E., Hallworth, M.A., Lube, G. & Sparks, R.S.J. 2003 Granular column collapses Bull. Am. Phys. Soc. **48**, 68.

Hutter, K., Koch, T., Plüss, C. & Savage, S.B. 1995 The dynamics of avalanches of granular materials from initiation to runout. Part II. Experiments. Acta Mech. **109**, 127.

Iverson, R.M. 1997 The physics of debris flows. Rev. Geophys. **35**, 245.

Iverson, R. M. & Denlinger, R. P. 2001 Flow of variably fluidized granular masses across three-dimensional terrain. Part I: Coulomb mixture theory. J. Geophys. Res. **106**, 537–552.

Jaeger, H. M., Nagel, S. R. & Behringer, R. P. 1996 Granular solids, liquids, and gases. Rev. Mod. Phys. **68**, 1259–1273.

Jop, P., Forterre, Y. & Pouliquen, O. 2004 Crucial role of sidewalls in granular surface flows: consequences for the rheology. J. Fluid Mech. **541** , 167 - 192.

Kadanoff, L. P. 1999 Built on sand: Theoretical ideas inspired by granular flows. Rev. Mod. Phys. **71**, 435–444.

Kerswell, R. R. 2005 Dam break with Coulomb friction: A model for granular slumping? Phys. Fluids **17**, 057101, 1–16.

Lajeunesse, E., Mangeney-Castelnau, A. & Vilotte, J. P. 2004 Spreading of a granular mass on a horizontal plane. Phys. Fluids **16**, 2371–2381.

Lube, G., Huppert, H. E., Sparks, R. S. J & Hallworth, M. A. 2004 Axisymmetric collapses of granular columns. J. Fluid Mech. **508**, 175–199.

Pedlosky, J. 1979 Geophysical Fluid Dynamics. (Springer-Verlag, New York).

Pouliquen, O. & Forterre, Y. O. 2002 Friction law for dense granular flows: application to the motion of a mass down a rough inclined plane. J. Fluid Mech. **453**, 133–151.

Savage, S. B. & Hutter, K. 1989 The motion of a finite mass of granular material down a rough incline. J. Fluid Mech. **199**, 177–215.

Savage, S. B. 1998 Analyses for slow quasi-static, high concentration flows of granular materials. J. Fluid Mech. **377**, 1–26.

Siavoshi, S. & Kudrolli, A. 2005 Failure of a granular step. Phys. Rev. E., **71**, 051302,1-6.

Shinbrot, T., Alexander, A., Moakher, M. &Muzzio, F.J. 1999 Chaotic granular mixing. Chaos **9(3)**, 611.

Voigt, B. 1978 Rockslides and Avalanches, *Vol. 1*, (Elsevier, New York).

Whitham, G.B. 1974 Linear and Nonlinear Waves. (Wiley).

Zenit, R. 2005 Computer simulations of the collapse of a granular column. Phys. Fluids **17**, 031703, 1–4.

Chapter V

Flow and deposition of pyroclastic granular flows:

A type example from the 1975 Ngauruhoe eruption, New Zealand

Abstract

Small-volume pyroclastic flows are generated frequently during explosive eruptions with little warning and are thus one of the most hazardous volcanic phenomena. Assessing this hazard requires a physical understanding of their high mobility, transport and sedimentation processes. Experimental and numerical models of geophysical mass flows need to be tested against natural flows and/or deposits, but suitable complete data sets are still scarce. We therefore studied a series a pristine small volume deposits from the 1975 eruption of Ngauruhoe volcano which are one of the world's best examples of low-energy, coarse-grained pyroclastic flows, which were also witnessed during eruption. Through a high-resolution GPS survey of flow morphology, excavations across the flow deposits along the entire flow length, and sedimentological analysis we acquired a unique data set. This includes the geomorphology, internal structure and texture with respect to laterally varying modes of deposition. The detailed data is used to elucidate transport, segregation and deposition mechanisms of low-energy pyroclastic flows as a function of flow volume, travel distance, granulometry, generation mechanisms and local slope. In particular, the field data allows us to define a type-unit for pyroclastic granular flows comprising three characteristic zones. It is shown how the sedimentology and geometry of this unit varies systematically as a function of travel distance, local slope and topographic confinement. On a base of this data, we derive a new model for pyroclastic granular flows explaining the spatially and temporally varying mechanisms of flow and deposition.

1. Introduction

Small-volume pyroclastic flows are one of the most hazardous volcanic phenomena known. They form frequently during explosive eruptions as well as by repeated lava-dome collapse, are initiated with little warning and can spread at high velocities. A physical understanding of their high mobility, their transport and sedimentation processes is a prerequisite to assess their hazard potential. Similarly, the validation of any experimental analogue or numerical model of geophysical mass flows requires testing against natural flows and/or deposits.

Currently, pyroclastic flows are understood to be multi-phase flows where volume, mass flux, grain size, particle concentration and bulk density can vary over several orders of magnitude (Druitt, 1998). Thus, physical models describing the state of flow vary from dense, granular flows, where gas plays a subsidiary role (Dade & Huppert, 1998) and motion is dominated by particle interactions, through gas-fluidised flows, where gas plays a significant role (Roche *et al.*, 2002), to highly diluted, turbulent systems where gas is the dominant phase and transports particles in turbulent suspensions (Druitt, 1998; Freundt & Bursik, 1998; Huppert, 1998). Ngauruhoe flows are believed to represent the low-energy, dense, granular flow end-member pyroclastic flows, typically generated by gravitationally driven collapses from: active lava domes (e.g. Saucedo *et al.*, 2004), dense vulcanian eruption columns (Nairn & Self, 1978), unstable agglutinate and lava autobreccias (Rodriguez-Elizarraras *et al.*, 1991). These phenomena are the most frequently occurring type of pyroclastic flow, particularly in subduction-related andesitic settings. In addition, these granular flow properties are not only restricted to pyroclastic flows, but also play an important role in many other industrial processes in the agricultural, chemical engineering and pharmaceutical industries. Despite this, and in contrast to classical fluid mechanical physics, general constitutive laws for granular flows are largely unknown, particularly when composed of a polydisperse grain mixture (G.D.R. MIDI, 2004).

Measurements of moving small volume pyroclastic flows are restricted to approximations of their flow front velocities. The internal structure and qualitative physical models of transport and deposition are generally inferred from interpreting resulting deposits. Hindrances to this approach include the complex flow paths, the absence of complete profiles from proximal to distal reaches, and partial erosion or alteration of deposits. As yet, few ideal field locations

have been described that allow a detailed quantitative comparison of flow and depositional models and natural deposits.

A series of pristine small volume deposits from the 1975 eruption of Ngauruhoe volcano, New Zealand, make one of the world's best examples of low-energy, coarse-grained pyroclastic flows, which were also witnessed during eruption (Nairn & Self, 1978). In 2004/2005 we carried out detailed mapping campaigns with the following aims in mind:

- Obtaining a complete data set of the morphology, internal structure and texture of pyroclastic flow deposits with respect to laterally varying modes of deposition.
- Acquiring detailed sedimentological data to elucidate transport, segregation and deposition mechanisms of low-energy pyroclastic flows in relation to flow volume, travel distance, granulometry, generation mechanism and local slope variation.
- Developing a transport and depositional model from these deposits that can be later tested against analogue or numerical experiments.

2. The 1975 eruption history of Mt. Ngauruhoe

The 1975 eruption of Ngauruhoe volcano was one of the first well-documented vulcanian eruptions. The frequently cited papers of Nairn (1976) and Nairn & Self (1978) have served as important guidelines for the interpretation of other pyroclastic flow deposits (e.g. Wilson & Head, 1981) and for the discussion of more recent pyroclastic-flow-forming eruptions (e.g. Cole *et al.*, 2005). In the following, we will briefly summarise the volcanological observations based on the paper by Nairn & Self (1978) and the original interim reports of the eruption. Ian Nairn kindly provided us with the latter documents, along with a photographic record of the eruption.

The 1975 eruption commenced with a series of intermittent ash eruptions, accompanied by volcanic tremor from February 12 to 17. Aerial inspections made in the morning of February 19 revealed no significant changes to the crater region during this pre-climactic phase. About three hours after the aerial observation, the climactic phase of volcanic activity commenced at 1300 hrs (local time 19/2/75) with a volcanic earthquake of $M_L = 2.7$. From this point onward, c. 2.4×10^6 m^3 pyroclastic fall and c. 1-1.5×10^6 m^3 pyroclastic flow deposit was produced before the eruption ceased on the same day at 2328 hrs. Two contrasting phases of eruption style were recognised.
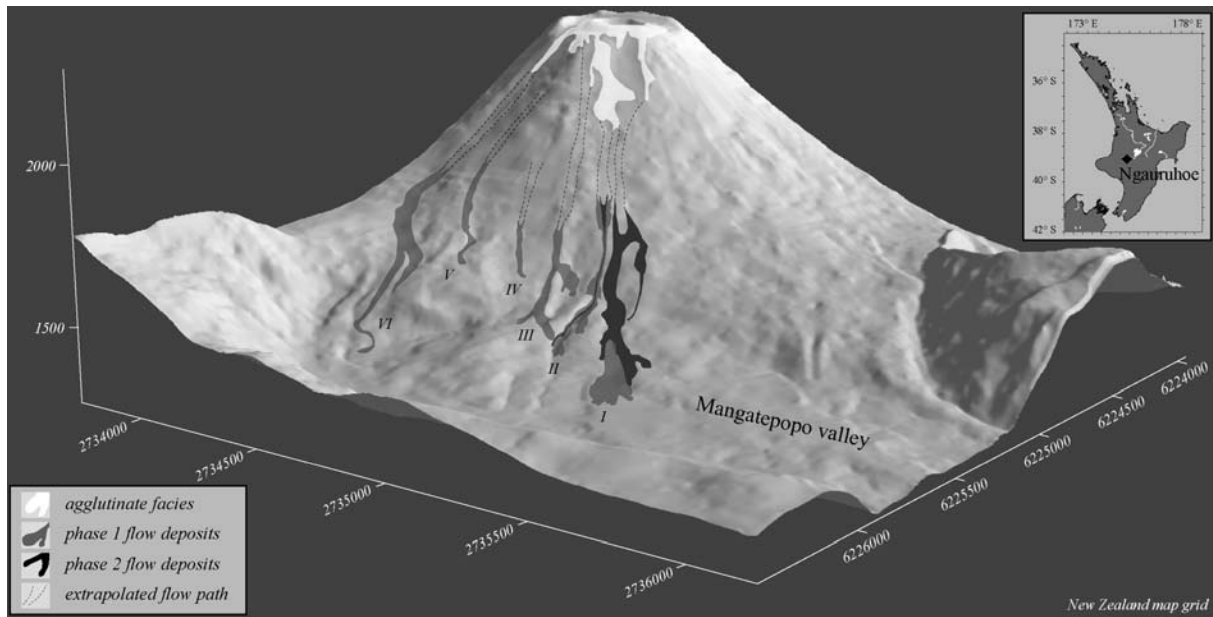
Figure 1. DEM of the NW-N flank of Ngauruhoe showing the distribution of pyroclastic flow deposits of eruption phases 1 and 2 in six major sectors I-VI.

Phase 1: An initial subplinian phase occurred between 1300-1430 hrs and was accompanied by high amplitude tremor (titled the "gas-streaming" phase by Nairn & Self (1978)). This phase produced the majority of pyroclastic fall and flow deposits. During these 1.5 hours, a sustained eruption column rose to 8 km above the crater. Within the lower part of the column, partly incandescent blocks were ejected in fountains reaching heights of 150 – 200 m before accumulating in a region from within the somma crater and around the upper outer flanks of the cone. Pyroclastic flows were reported to have formed in part from the remobilisation of this rapidly-accumulated proximal fallout and in part from an ongoing feeding from a dense eruption column. Our re-analysis of eye-witness descriptions and discussions with some of the observers suggests that the role of ongoing collapse from rapidly accumulating piles of poorly welded agglutinate was potentially the dominant pyroclastic flow generation process. More or less continuous avalanching occurred from the steep upper NW-N flanks of the volcano from 1300 to 1420 hrs. The earliest and largest flows, reaching down into the Mangatepopo valley, represent distinct events and accumulated in six major sectors (Fig. 1).

Phase 2: At the end of the high-tremor period, a second, vulcanian phase of eruption commenced at 1507 hrs with the first of nine individual explosions, each accompanied by distinct large volcanic earthquakes. Each cannon-like explosion generated a visible atmospheric shock wave, followed by the ejection of a pyroclastic slug. The dense eruption clouds initially expanded sub-spherically before large dense blocks of the solidified cap of the

magma column and of disrupted conduit and crater wall rocks followed ballistic trajectories to mainly land on the upper slopes of the cone. Pyroclastic flows were generated from the collapse of the dense central part of the eruption cloud, preceding further ascent of an ash-dominated plume. The largest pyroclastic flows of phase 2 occurred at 1810 and 1906 hrs and reached the valley floor of sectors I, II and VI (Fig. 1). The vast majority of flows had volumes of <5000 m^3 and stopped on slopes of 30°-35° in a region 400 – 900 m travel distance from the crater rim.

3. 1975 Pyroclastic flows and deposit geometry

Pyroclastic flows of both eruption phases followed shallow (<2 m) pre-existing channels on the steep upper NW slopes (30° - 35°; Fig. 2), which they successively eroded. Averaged flow front velocities on the upper slopes to c. 1600 m elevation were about 30 ms^{-1}. When reaching the flatter lower slope and valley floor (20° to 4° slopes; Fig 2) beyond a break in slope, the flows decelerated and propagated at an average of c. 10 ms^{-1} from flow-front propagation time estimates. Fine ash elutriated from the moving flows formed turbulent ash clouds up to 500 m above the ground-hugging basal avalanches. The ash clouds left very little fallout, which was found closely confined around the overlapping, lobate flow deposits.
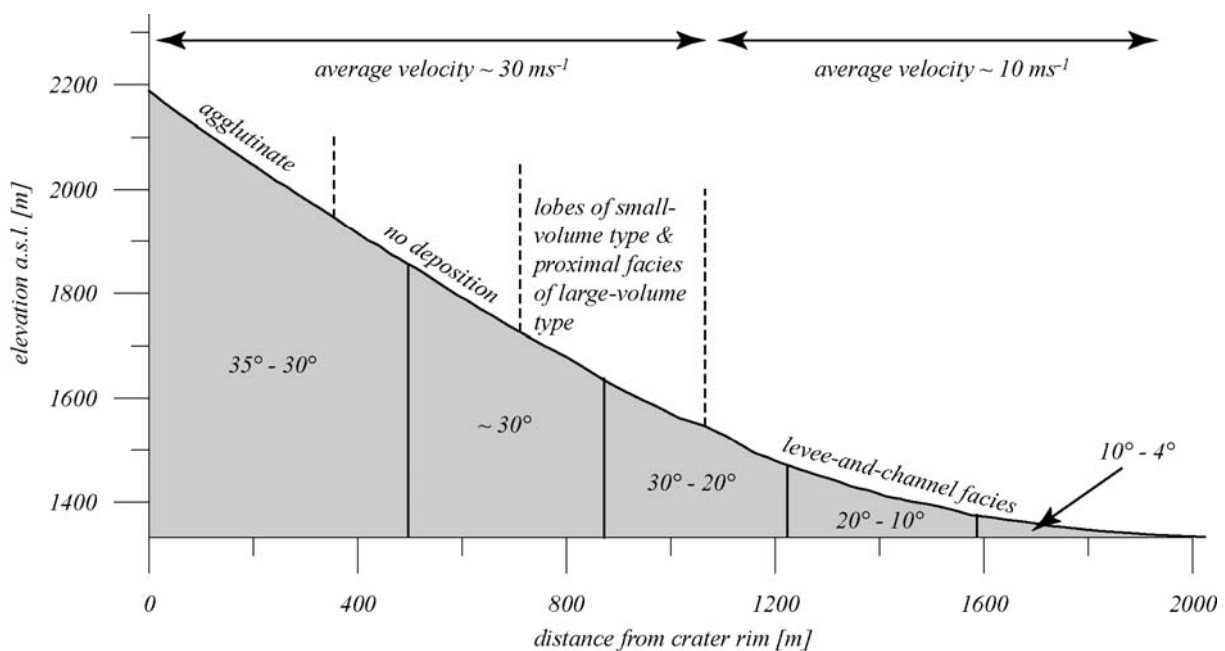

Figure 2. Typical longitudinal profile of the NW flank of Ngauruhoe (taken through sector I) with the distribution of individual deposit facies and average velocities from flow front propagation time estimates.
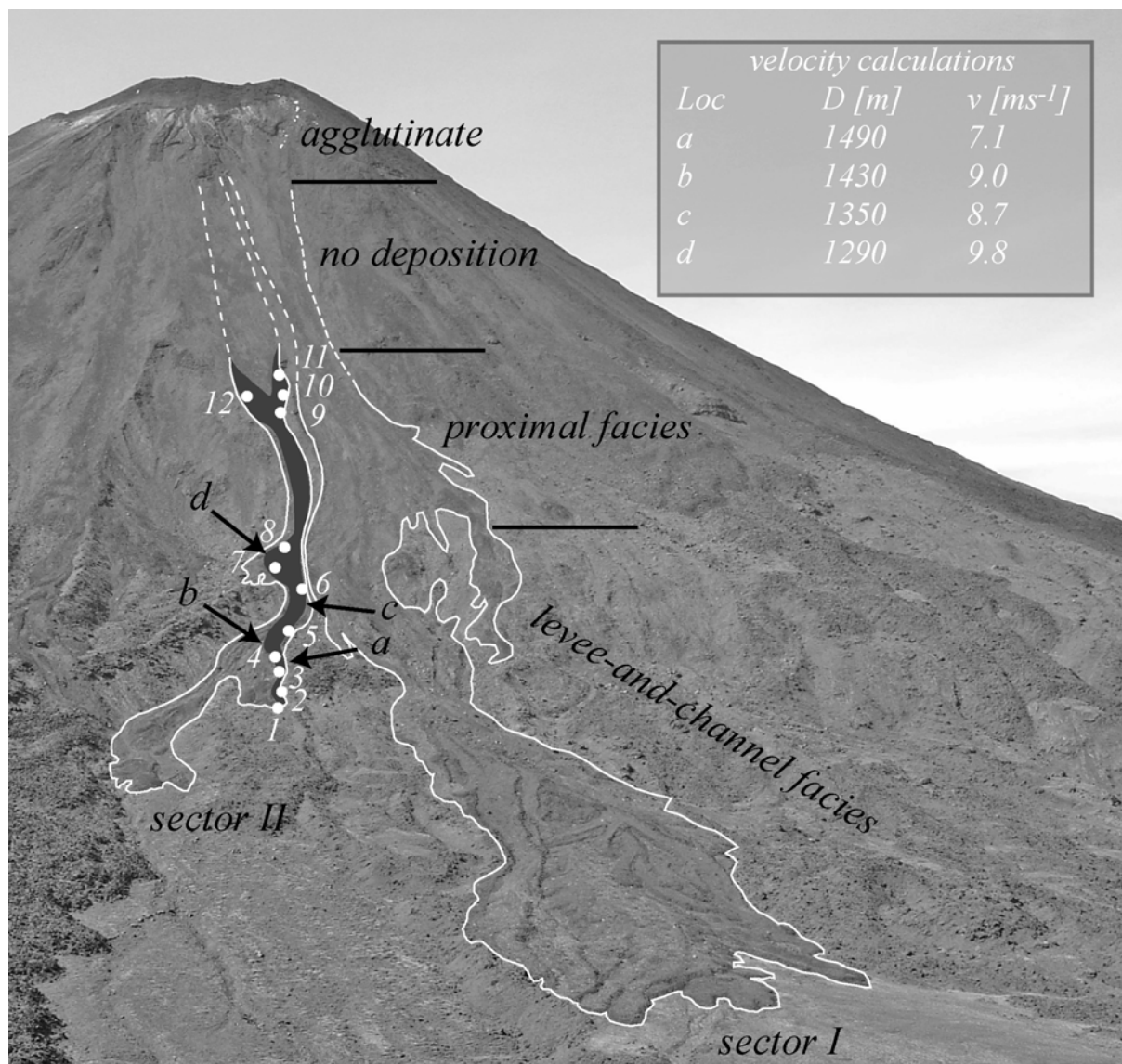
Figure 3. Oblique view onto sector I and II at the NW flank of Ngauruhoe. Deposit of type unit II-S2 in dark grey with the locations of the excavation trenches (white circles) and the positions of flow bends with superelevations (a-d) used for flow velocity calculations. Inset shows results of these calculations along with the local travel distance, D, measured from the crater rim.

Two major types of deposit define a stratigraphy that directly relates to the two eruptive phases described above (Fig. 1). The earliest, most widely distributed and most voluminous deposits have outer surfaces that are monolithologically composed of scoria with common agglutinate fragments. Later deposits of the vulcanian phase 2 have lower volumes and runouts. These units are easily distinguished by their surface clasts comprising a mix of blocky, high to medium density clasts of varying lithology with minor juvenile scoria.

The overall deposit consists of a complex of partially overlapping and anatomising lobes (Fig. 3). Individual flow deposits, where they can be followed, show distinctive and consistent changes in morphology with distance from source. Near their terminations, the deposits are 1-2 m thick and consistently show a droplet-like morphology with a convex upper surface, steep fronts and sides, which are covered by coarse scoria-dominated blocks. The scoria fragments are highly angular, very fragile and commonly include flattened fragments of partly welded agglutinate. Closer to source and for a major part of the exposed units, the deposits have a concave upper surface profile. Here we describe this profile as being composed of high

lateral "levees" of dominantly coarse- scoria, and a 0.5-1.5 m lower central "channel" fill of more poorly sorted breccia. In areas above the levee-channel form deposits, thinner sheet-like deposits occur on the progressively steeper slopes before pinching out into areas of non-deposition.

4. Methods

4.1. GPS mapping and measurements of morphology

Each individual flow unit was first mapped by hand-held GPS, along with documentation of the underlying topography, major stratigraphic/lithological differences, general forms of deposit morphology and local slope. If present, superelevations in deposit heights between the inside and outside of flow bends were measured for velocity estimates. Pyroclastic flow deposits in sectors I, II and V were chosen for detailed survey, using both Differential-corrected GPS with Laser-Distance-Meter (LDM; 1 m x,y,z precision) and Real-Time-Kinetic (RTK) GPS techniques (10 cm x,y,z precision). Flow-perpendicular traverses over deposit surfaces were measured in 5-10 m intervals to characterise downstream changes in height and width of levees and channel fill. In addition, longitudinal traverses of deposit margins, levee crests and deposit centrelines were carried out with waypoints measured at 2 m intervals.

4.2. Detailed sedimentology of a type-unit

Unit II-S2 (Fig. 3) with a ground-travel runout length of 1542 m and a volume of approx. 2600 m³ was chosen for a detailed sedimentological analysis. This deposit occurs in sector II at the NW flank of Ngauruhoe which was best observed by eyewitnesses. It is also fully exposed from proximal to distal reaches, unmodified by erosion, and of moderate size (c. 8.5 m wide on average), which allowed excavation. A total of about 30 m³ of pyroclastic material was removed to cut 12 trenches perpendicular to flow direction from the deposit margin to the

centreline. The 0.5 m wide trenches allowed the detailed documentation of the vertical and lateral deposit structure. At seven locations, continuous samples were taken at the centreline from top to base. Depending on the local thickness and the internal structure, the unit was subdivided into 2 to 5 zones which were carefully sub-sampled in squares of 30 x 30 cm horizontal area. Large particles at the margin of the sampled area were collected with the sample when protruding more than 50% into the 900 cm² sample box. Box height of each sample was measured to approximate a bulk density. Each sample, having an average mass of ~ 50 kg, was first weighed with a field scale. The grain-size distribution for the fractions coarser than -4 phi fraction was determined by dry sieving in full phi intervals in the field. Particles of each phi fraction were further subdivided into two broad classes of density and three classes of angularity and counted. Low-density clasts ranging from 0.9 to 1.4 g/cm³ were juvenile scoria, rare accessory scoria and highly altered crater-facies clasts. Poorly vesicular accessory clasts and dense lava made up the high-density lithologies at 1.65 to 2.4 g/cm³. Approximately three kilograms of the remaining fractions smaller than -4 phi were sieved in the laboratory at 1 phi intervals, down to 4 phi. The 1-2 phi fraction was split by density at 2.45 g/cm³ for further characterisation of the ash. In addition, the largest (and often very fragile) clasts at the outer levee flanks were characterised measuring the long-axis of the 20 largest low-density scoria and the 20 largest dense lithics within a 2 m² surface area.

5. Deposit morphology variations with distance

The mapped volumes of individual pyroclastic flows of the 1975 eruption range over two orders of magnitude from <1000 m³, up to c. 16000 m³. Their runout lengths range between 0.85 and 1.9 km, measured along their flow paths starting at the crater rim. The H/L ratios of these flows lie at the extreme low-energy end of the spectrum of mass flows, including pyroclastic flows (c.f. Sheridan 1979). Deposit architecture varies with slope on the NW flank of the volcano. The uppermost part of the flank is inclined at >30°. At c. 1850 m a.s.l., slope-break I changes inclination to 30° on the middle flank. Slope-break II, at c. 1600 m a.s.l., leads to a slope gradually decreasing from 30° on the lower flank to 4° on the Mangatepopo valley floor. The flows were strongly topographically controlled and funnelled at high points of the cone into shallow (<2 m) gullies. On the upper flanks over slopes >30°, the successive passage of individual flows gradually deepened these gullies by 1-2 m by erosion. There is no evidence for deposition on these upper flanks where the surface material was loose ash and

gravel. Emplacement started at c. 700-800 m distance on the middle flank, following slope-break I where gradients drop to around 30° (Fig. 2).

Flow volume appears to be the major controlling parameter on the subdivision of two major deposit morphologies. The low-volume type (<1000 m³) rests below and near slope-break I, often in local depressions at inclinations from 20° to 30°. They form 30 to 100 m long, 5 to 15 m wide and up to 4 m high lobes that increase in width and thickness with distance. When followed upstream, the lobes gradually pinch out.

Larger-volume flows, ranging from approx. 1500 m³ to 16000 m³, reached the 5° to 20° slopes at the base of the volcano. We distinguish two deposit facies: (A) a proximal facies, which, similar to the distribution of the low-volume type, rests on the middle flank below slope-break I; and (B) a levee-and-channel facies on slopes below 20° of the lower flank. The proximal facies forms 15 to 100 cm thick sheets each side of the central gullies (Fig. 4a). In contrast to the low-volume morphology, these sheets do not have steep margins, but gradually thin towards the central gully and towards their outer margins. Their width is strongly affected by small changes in local slope, generating a meandering outer margin that migrates outwards in local depressions and towards the central gully in steeper regions. There is a positive correlation between the local width and the local maximum thickness.

In sectors I, III, V and VI, the proximal sheet-like facies continuously grades downwards into the lower levee-and-channel facies. At inclinations of approx. 20° to 25° the deposit margins begin to form coarse-grained, nearly fines-free levees. Between the levees is a fill of comparatively ash-rich, clast- to matrix-supported breccia. In sector II, a local, 80 m long cliff interrupted deposition downstream of the proximal facies. At the apron of the cliff, only isolated, coarse-grained levee bars were deposited and the channel in-between remained empty. Further downstream at 1250 m travel distance, where the slope decreases to less than 20°, the levee-and-channel morphology is fully developed.

The general characteristics of the levee-and-channel morphology are similar to that reported from other unconfined deposits of small-volume pyroclastic flows (Wilson & Head, 1981; Rodriguez-Elizarraras *et al.*, 1991) and have been described in detail by Nairn & Self (1978). The morphology and thickness of lobate levee-and-channel deposits have been used in earlier models to evidence the non-Newtonian rheology of such currents (Wilson & Head, 1981), and

(a)

(b)

(c)
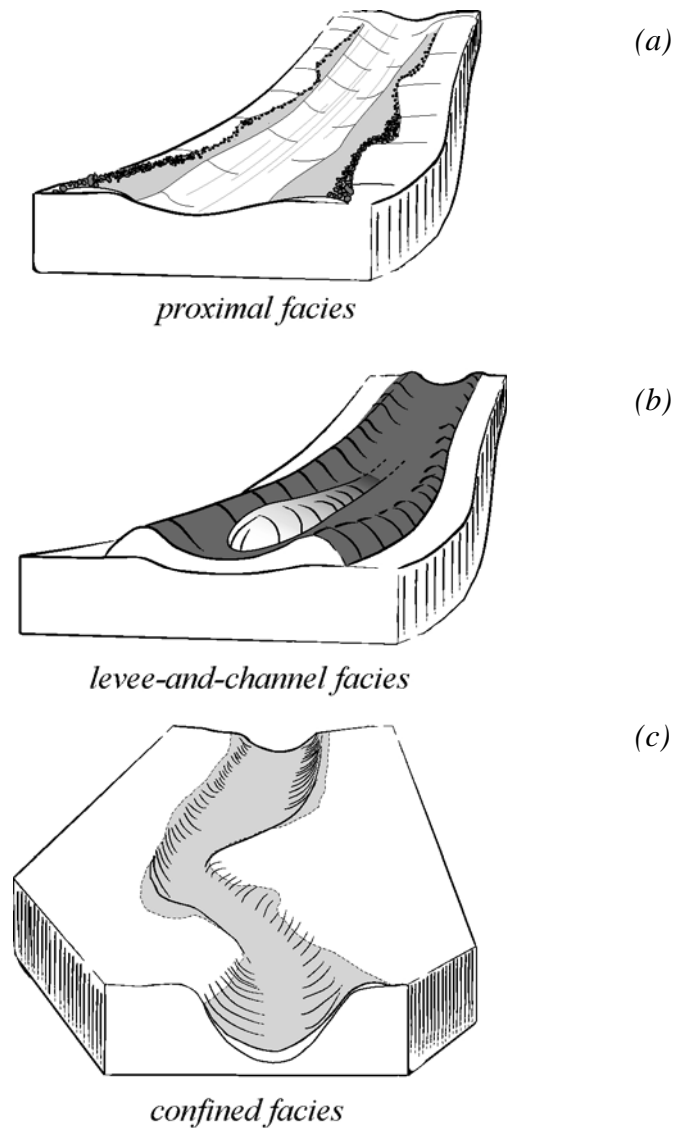
Figure 4. The deposit morphology of (a) large-volume type flows in the proximal facies; (b) internal lobes occurring within the levee-and-channel facies in a locally flat region, immediately below a long and steep incline; and (c) flows in the middle slope region of sector VI funnelled within an old lava channel.

in recent experimental studies on unconfined, quasi-steady granular flows to relate to the flow front height and velocity (Felix & Thomas, 2004). However, no detailed data has yet been gathered in field studies to quantify the variation of the flow morphology with travel distance and local slope.

For the type unit II-S2 the levee-and-channel facies is c. 600 m long. Over this stretch, the slope varies from 4° to 16°. In the intervals from 955 to 1135 m and from 1380 to 1510 m from the crater, the local slope and the deposit width show a pronounced negative correlation (Fig. 5a). In contrast, for the interval in-between, where the deposit reaches its maximum
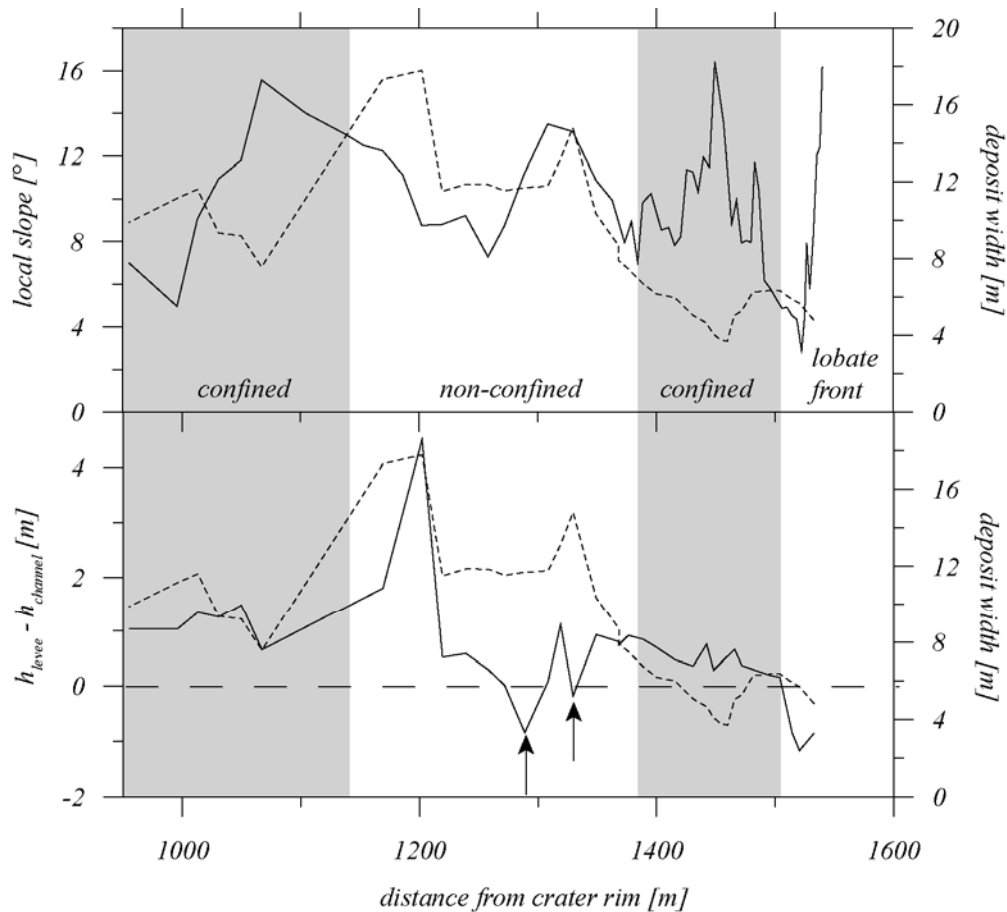
Figure 5. Measurements of the deposit morphology in the levee-and-channel facies of unit II-S2. (a) Variation of the local slope (solid line) and deposit width (dashed line) with travel distance. (b) Variation of deposit width (dashed line) and (h_{levee} - $h_{channel}$) (solid line) with travel distance. Arrows mark regions where internal lobes occur. Local slope was measured at the centreline of the deposit's free surface.

width, there is a positive correlation. The two different types of relationship appear to be related to a lateral confinement by topography. Positive correlation between slope and width occurs in relatively open and unconfined regions, whereas the negative trends can be related to sections where the flow passed steeper-sided channels. The height difference between levees and the channel surface ($h_{levee} – h_{channel}$; Fig. 5b) is positively correlated to the local deposit width, illustrating the field observation that the morphology becomes enhanced when the flow widens. There are three regions, characterised by negative values of $h_{levee} – h_{channel}$, where no obvious correlation exists. This occurs in the frontal region where the levee-and-channel morphology vanishes and grades into a convex lobe. In the other two regions (marked by arrows in Fig. 5b), droplet-shaped lobes occur as fills within the channel. These internal lobes are 5 to 20 m long, wedge-formed and show a gradual coarsening towards their steep-sided, up to 1.5 m high fronts. These structures are commonly observed in a locally flat

region, immediately below a long and relatively steep incline (Fig. 4b). Trains of up to four drop-shaped lobes can occur, producing an undulating free surface within the channel.

The presented data suggests that the levee-and-channel morphology depends on both the local slope and confinement, although there are examples where one of these external parameters dominates the other. In the medial to distal reaches of sector VI, the pyroclastic flows were funnelled within an old lava channel with lateral walls sloping up to 20°. This strong lateral confinement inhibited levees to develop. The deposit simply fills the lava channel and overflows its margins at the luff side of channel bends (Fig. 4c). In contrast, the earliest and largest pyroclastic flows of sector I passed onto the flat, unconfined valley base of Mangatepopo valley. The deposits spread out to form sheet-like fans with steep-sided margins but no levees. Other regions were observed where the flow cascaded over >25° steep cliffs, resulting in the deposition of isolated bars of blocks in local depressions of the cliff.

Where levee-channel facies are well developed, velocities can be calculated for the flows based on superelevation measurements of the h_{levee} difference on the inside versus outside of channel bends. This can be expressed as the function (Evans *et al.*, 2001):

$v = [ghr/b]^{1/2}$

Where, v = flow velocity (ms^{-1})

$\quad$ g = acceleration due to gravity (ms^{-2})

$\quad$ h = superelevation height, or $h_{levee(out)} - h_{levee(in)}$ (m)

$\quad$ r = radius of curve measured to the centre of the flow (m)

$\quad$ b = channel width (m)

This equation has been tested on debris flows and volcanic debris avalanches, and found to underestimate flow velocity by around 15% (Pierson, 1985). For unit II-S2, velocity calculations could be obtained at four superelevations distributed over a 200 m long stretch within the levee-and-channel facies (inset Fig. 3). The obtained values, ranging from 7.1 to 9.8 ms^{-1}, compare well with the eyewitness estimate of 10 ms^{-1}.

6. Sedimentology

6.1. Flow path and deposit distribution

The flow path of Unit II-S2 in sector II can be subdivided into three major depositional regions and two intervening sections, where the current did not deposit (Fig. 6). The agglutinate deposit on the uppermost flank may represent the source area for some of the
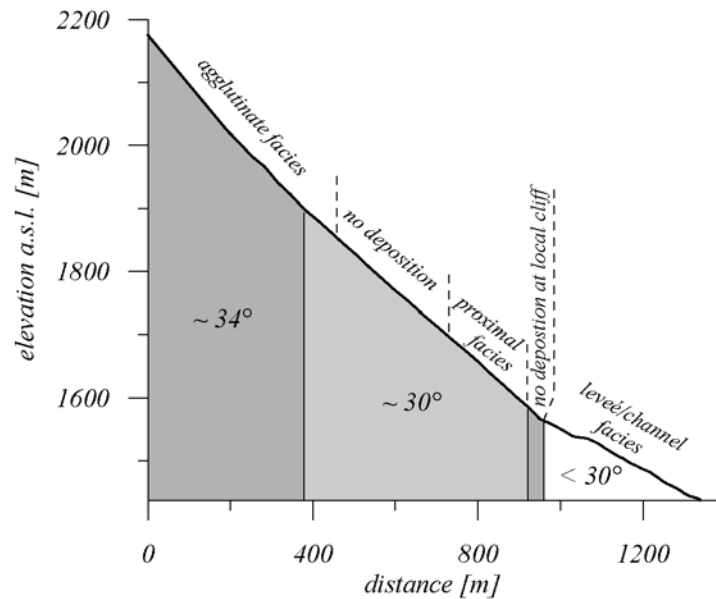
Figure 6. The flow path of unit II-S2 in an elevation vs. distance plot.

pyroclastic flows. It extends for about 450 m distance from the crater rim reaching 1825 m elevation. This agglutinate deposit terminates in ca. 1.5 m high cliffs that form a 40 m wide amphitheatre above a gully that funnelled sector II flows. The most proximal facies of the Unit II-S2 flow occurs at the margins of the gully, over a section from 760 m to 950 m from the crater rim, on slopes of $30° ± 2°$. Its structural variation was documented in four trenches (Locations 9 - 12; Fig. 3). Further downstream, deposition is interrupted again over a ca. 80 m long, 33° sloping cliff section. The main proportion of the deposit has accumulated from the apron of this cliff downwards over slopes between 22° and 4° and has a typical levee-and-channel morphology (Loc. 1-8; Fig. 3).

6.2. Typical structure of the levee-and-channel facies

Based on our detailed excavation, we describe the typical deposit structure of the levee-and-channel facies at Loc. 4 as a reference to better illustrate the downstream facies variation (Figs. 7 and 8). Based on sedimentological and compositional characteristics we distinguish three structurally and compositionally different zones:

Zone I is a coarse-grained, nearly fines-free unit (fines = ash finer than -1 phi) that makes up the thick levees and extends as a layer along the base to the centreline. It comprises mainly juvenile scoria clasts within an open-framework structure. Individual clasts in *zone I* are highly irregular in shape, very brittle and fragile, but despite this, surprisingly intact. Some are broken, but obviously only in the last instant of emplacement or during compaction as
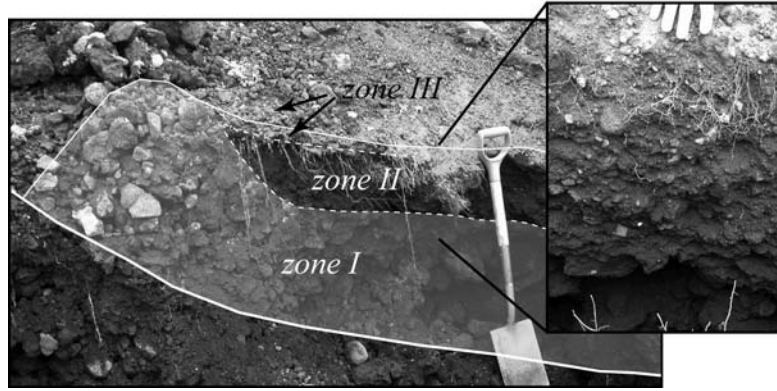
Figure 7. Vertical section through the levee-and-channel facies illustrating zones I-III.

evidenced by their jig-saw character. The lower contact of *Zone I* is non-erosive, and the upper contact to the middle *Zone II* is gradational.

Zone II is a clast- to matrix-supported breccia that predominantly forms a channel fill between the levees. There is a weak normal coarse-tail grading and a continuous upward increase in the ash content.

Zone III consists of an open-framework, coarse-grained, 1-2 grain-thick plaster of mostly juvenile scoria blocks and lapilli that rest on *Zone II* breccia.
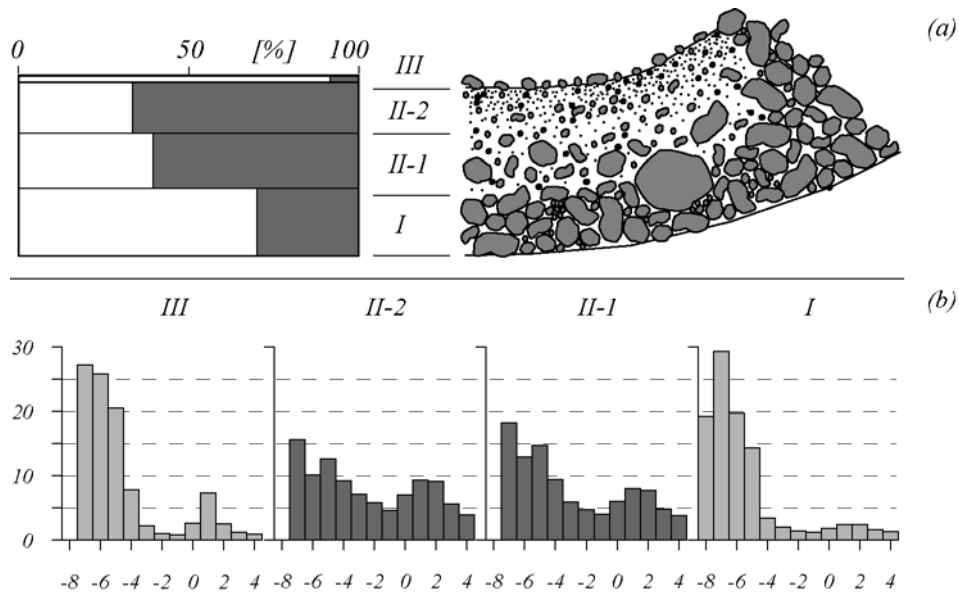
Figure 8. (a) Internal structure of the levee-and-channel facies at location 4 and LDC% for four continuous samples at the centreline. (b) The corresponding histograms for the centreline samples.

The threefold zoning of the levee-and-channel structure is also reflected in a contrasting coarse-tail particle-size distribution (Fig. 8). The grain-size distributions of all samples at the centreline show a bimodal form with peaks at -7 and 1.5 phi and a trough at -1 phi. In all three zones, neither the coarse- nor fine-tail follow a Gaussian or Rosin-Rammler distribution. The histograms for *Zones I* and *III* are very similar with a pronounced coarse-tail and low ash content. The two samples of *Zone II* show clearly higher ash contents and a slight increase in ash content upwards. A further characteristic of all centreline samples is the strong positive skewness of their coarse-tail fraction. There is also a vertical variation in the percentage of low-density clasts (LDC%), coarser than -5 phi at the centreline (Fig. 8). *Zones I* and *III* are distinctly richer in low-density scoria with 92% and 70% LDC, respectively, compared to 33 to 40% for the middle *Zone II*.

6.3 Whole-deposit grain-size distribution and coarse-tail componentry

By combining in volumetric proportion all of the grain-size estimates made for Unit II-S2, an overall grain-size distribution was obtained, a calculation rarely possible for pyroclastic flow deposits (Fig. 9). The overall distribution is clearly bimodal, with modes at -6 and 1.5 phi and a trough at -1 phi, the latter two points in common with the standard unit above. The distribution is dominated by the coarse mode (coarser than -1 phi) which comprises c. 65% of the whole deposit. Similarly the overall coarse-tail componentry has been calculated, with ca. 58% of particles coarser than -5 phi being of low-density scoria.
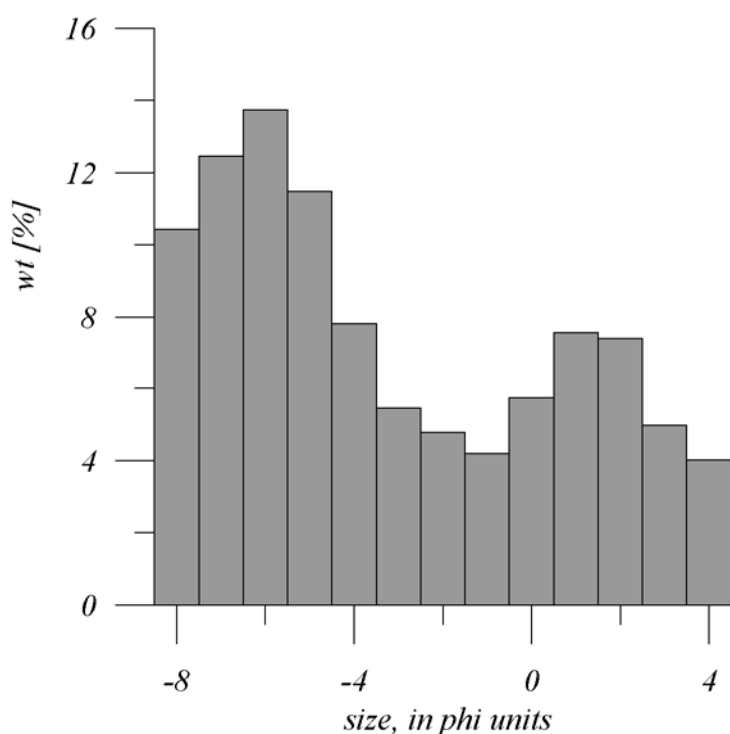

Figure 9. Bulk grain-size distribution resulting from combining in volumetric proportion of all grain-size analysis made for Unit II-S2.

6.4. Variation with distance

Internal structure and composition

In addition to changes in the surface morphology with distance, the internal structure of the proximal facies (Loc 10; Fig 10) differs from that of the lower levee-and-channel facies (Loc 1 – 8: Fig. 10). The flat veneering sheet-like deposit of the proximal facies on both sides of a central gully comprises nearly fines-free, clast-supported outer margins. A large amount of broken scoria fragments at the margins is attributed to collisional to saltational motion just prior to halt. The marginal fines-free material grades laterally inward into a 15-50 cm thick, clast- to matrix-supported breccia forming the basal part of the deposit in central areas. There is a distinct upper contact to a central, ca. 10 cm thick, ash-rich, weakly layered, normally graded and matrix-supported layer. As for the levee-and-channel facies, the top is composed of a 5-10 cm (~2-3 grain diameter) plaster of juvenile scoria blocks and lapilli similar to *zone III*.

Downstream of a local cliff, at a travel distance of 1030 m from the crater rim, the first discontinuous levees occur. The channel remains empty until a levee-and-channel morphology is fully developed at 1250 m (Loc. 8). Here, the open-framework *Zone I* is only developed in the levees. It has a 70° steep lateral contact to the channel-filling, clast- to matrix-supported *Zone II*. Thus, within the channel, *Zone II* forms the basal layer. Approximately 40 m further downstream (Loc. 7), *Zone I* extends farther along the base towards the centreline. Another 70 m downstream (Loc. 6), *Zone I* is developed along the entire base of the flow unit. From Loc. 6 downward, the internal structure is similar to that described in 6.2. *Zone I* increases in thickness towards a maximum at Loc 4 and 3 before decreasing thereafter. At the two most distal locations, 1524 to 1537 m travel distance from the crater rim, the levee-and-channel morphology has graded into a convex lobe form. Here *Zones I* and *III* form a thin continuous shell encasing the central *Zone II*.

Zones I and *III* are much richer in low-density clasts than *Zone II* (Fig. 10). The pronounced lateral density differences suggest that a process of density segregation has occurred that was important for the entire flow duration. The LDC% of the basal *Zone I*, or basal zone II where it rests on the ground, increases continuously with distance from the crater rim (Fig. 11). No
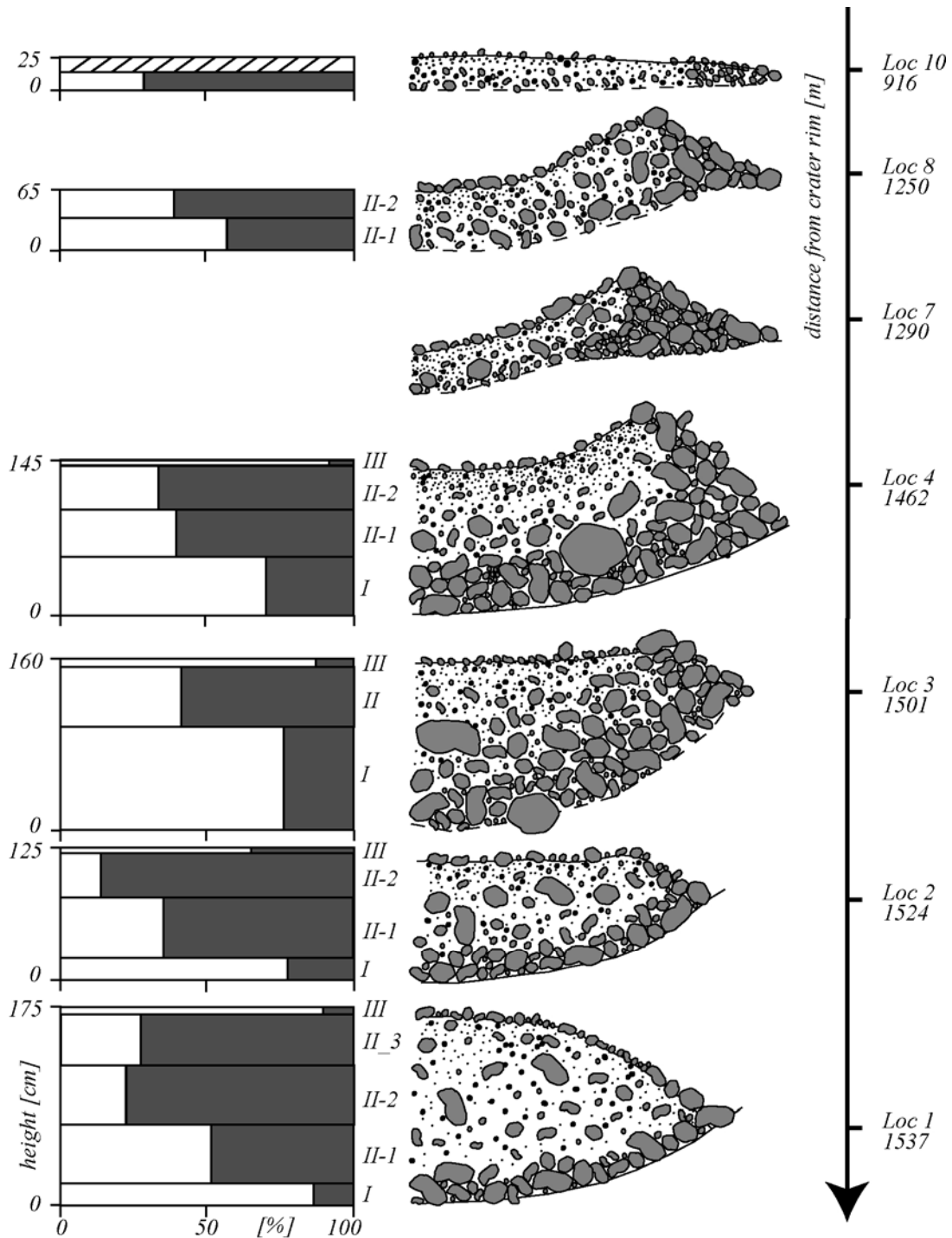
Figure 10. At the right-hand side: variation of the internal structure with distance. At the left-hand side: LDC% for continuous samples at the centreline.

such downstream tendency exists for the *Zone II* samples, which actually vary more strongly in the vertical profile. Considering that the overall deposit has 58% LDC, the proximal deposit at Loc. 10 is highly overrepresented in dense clasts. By comparison, Locs. 5-1 show progressively stronger enrichment in low-density clasts.
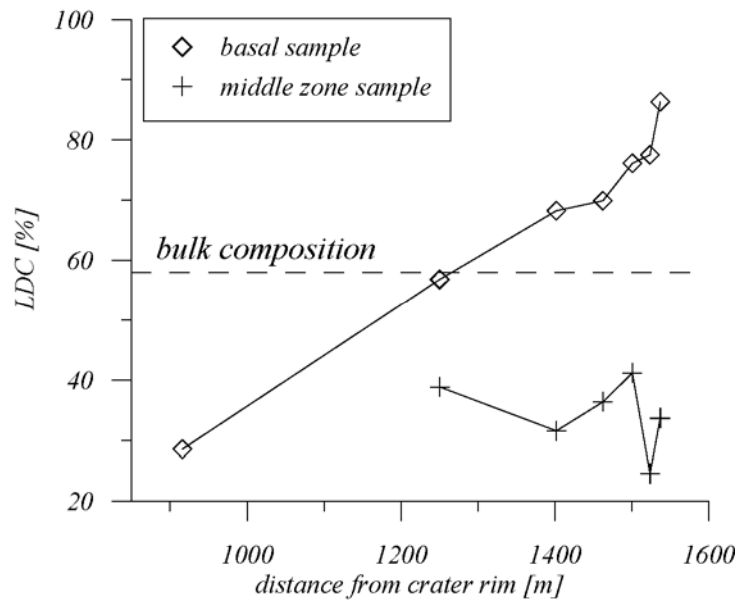
Figure 11. LDC% as a function of travel distance starting at the crater rim.

Grain-size distribution

The data set of Unit II-S2 allows quantification of the downstream variation of the grain-size distribution at the centreline of basal samples (*Zone I* or basal deposit sample at Loc. 8 and 10) and averaged *Zone II* samples (Fig 12). All samples show a bimodal distribution with a common fine mode at 1 to 2 phi. Generally, the basal (mostly *Zone I*) samples become coarser, ash-poorer and better sorted with distance; whereas the distributions of the middle zone samples vary little with a coarse mode around - 5.5 phi. Contrasting with all other samples, the weakly layered central portion of the deposit at Loc. 10 comprises a significantly larger content of fine ash. These trends can be quantified in a ternary diagram comparing the relative proportions of the fractions A=-7 to -6 phi, B=-3 to -1 phi, and C=2 to 4 phi (Fig. 13). For all samples of the levee-and-channel facies, the ratio B/C is constant while A/(B+C) varies greatly, reflecting downstream improving coarse-tail grading. The bulk distribution plots close to this trend line, between the proximal and levee-channel facies groups. This shows that the initial composition was efficiently segregated into compositionally distinct *zone I* and *II* deposit batches.

The maximum clast size of the levees does not continually increase with distance in parallel with the increasing coarse-tail fraction of the centreline samples (Fig. 14). There is an increase in maximum clast size of both high and low-density blocks towards a maximum at Loc5 and thereafter a decrease. While analysing our geometrical data, we noticed that this trend is positively correlated to the local cross-sectional area of the deposit.
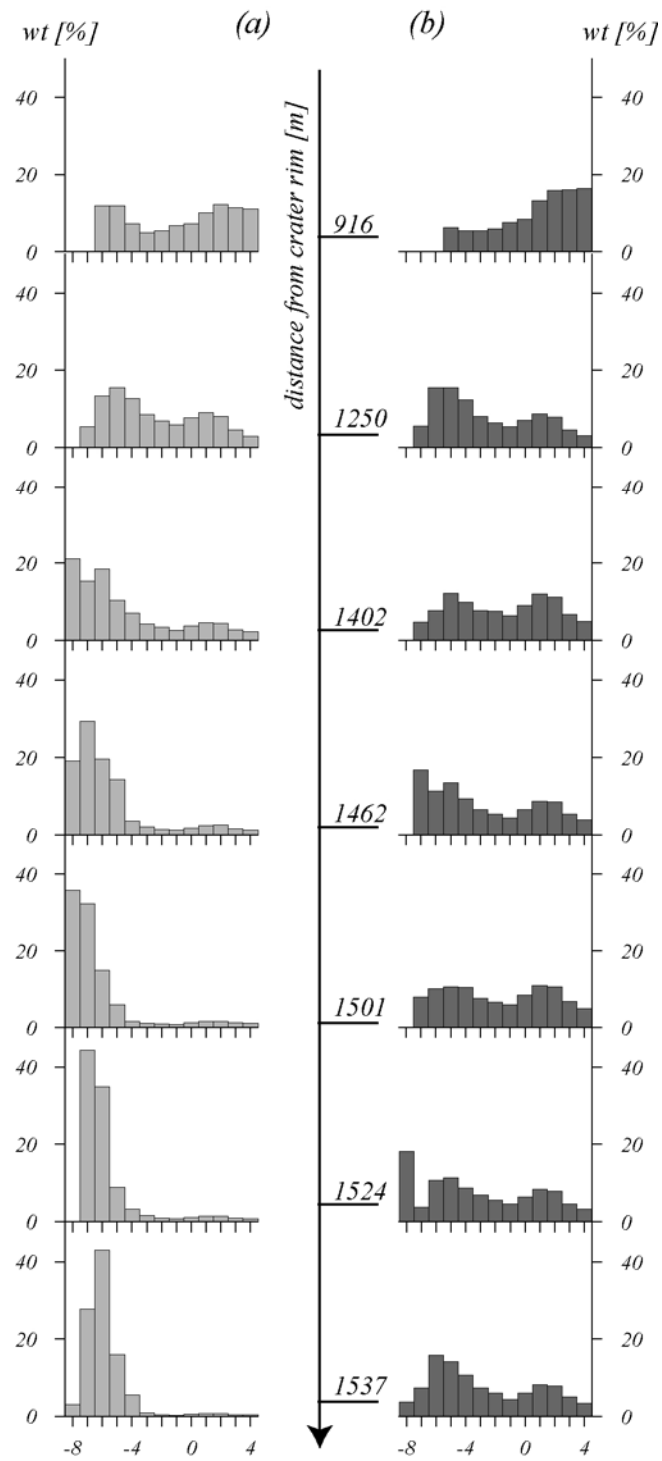
Figure 12. Histograms of (a) basal samples and (b) middle zone samples with travel distance.
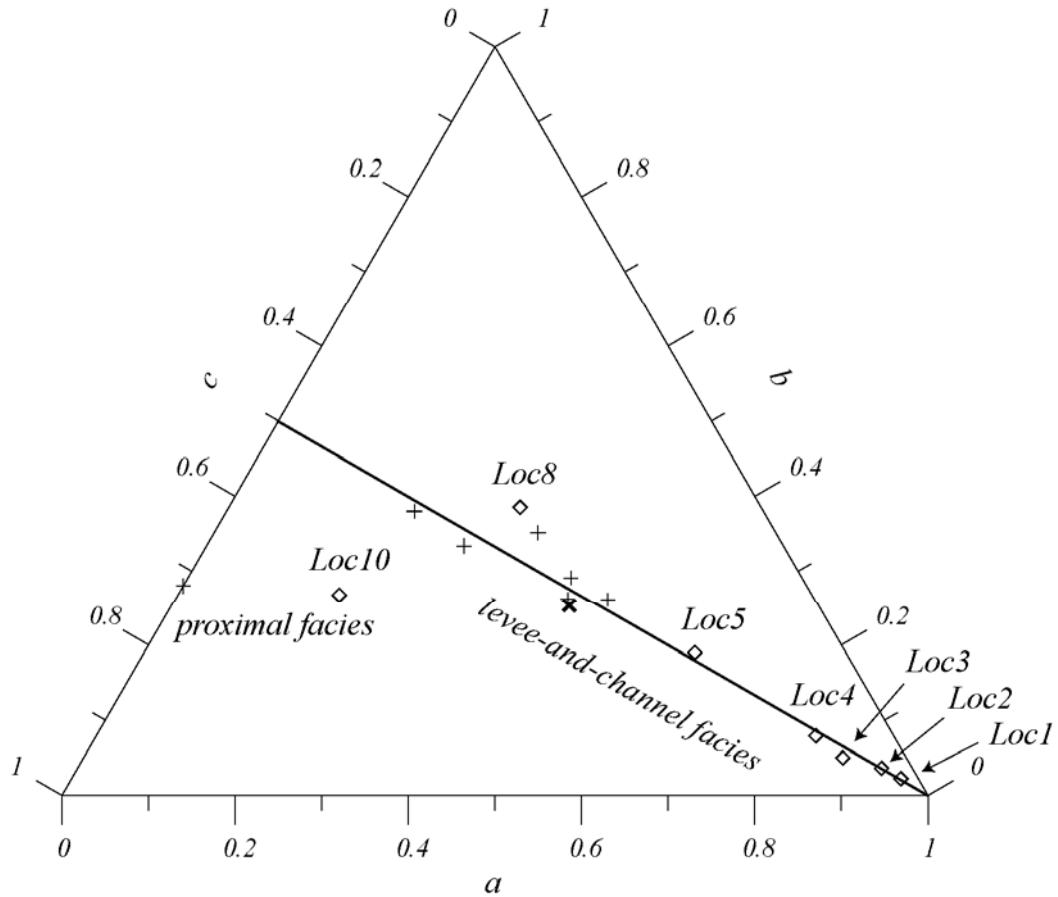
Figure 13. Comparison of the relative proportions of the fractions a=-7 to -6 phi, b=-3 to -1 phi, and c=2 to 4 phi for the basal (◊) and middle zone samples (+) and for the calculated bulk composition (×).
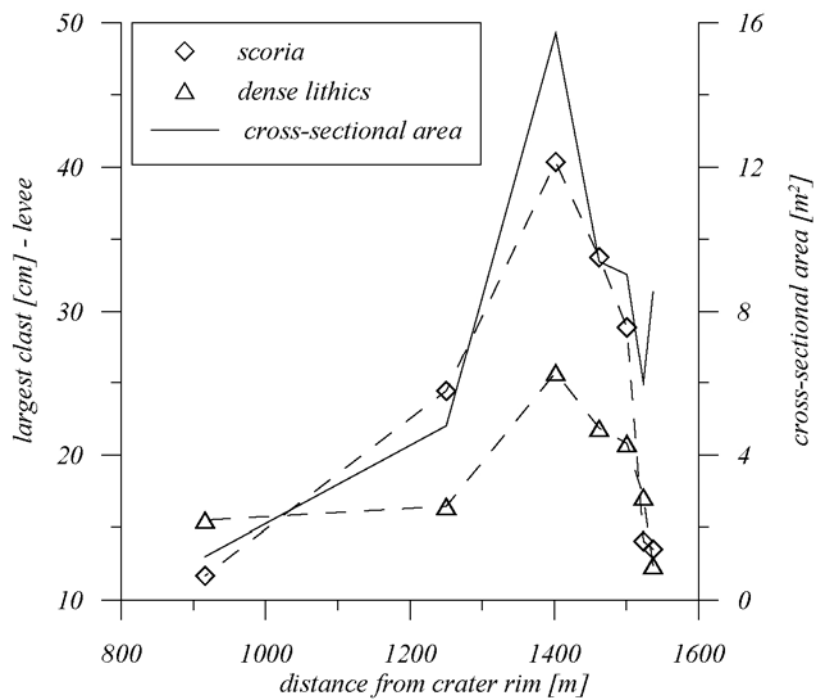

Figure 14. Maximum clast size at the outer levee flanks and local cross-sectional area of the deposit against distance from crater rim.

Density separation of the 1-2 phi fraction

So far, we have only described apparent segregation features and downstream variations of the coarse-tail fraction, because larger clasts are expected to be more easily segregated than smaller ones (Vallance & Savage, 2000). To check for segregation in the fine fraction, we have separated the 1-2 phi fraction of each sample at 2.45 g/cm³. This gives a good separation of vesiculated glass shards from dense glass, lithic fragments and crystals in the Ngauruhoe samples. The weight percent ratio of low-density ash to high-density ash is nearly invariable with distance (Fig. 15). Only the upper zone III is distinctly enriched in low-density shards. The composition of the ash fraction can be modified by three processes: (1) segregation by the same processes that affected the coarse mode, (2) abrasion and breakage of coarser clasts, leading to downstream enrichment of components according to the clasts' modal composition, and (3) elutriation of preferentially vitric ash, leading to downstream depletion in this component. The absence of downstream variations in the Ngauruhoe deposits suggests these processes remained inefficient, unless they operated in perfect balance which seems unlikely. The enrichment in low-density shards in top-layer III probably reflects fallout from elutriated ash clouds.
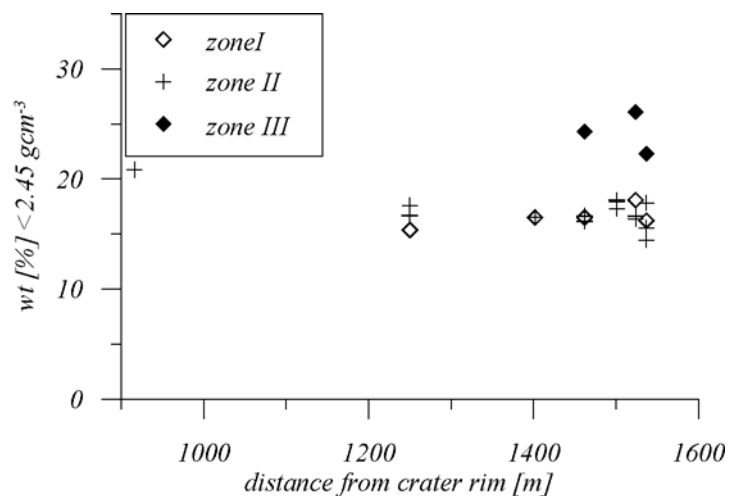

Figure 15. Weight percentage of the 250-500 μm fraction with a density smaller than 2.45 gcm^{-3} against distance from crater rim.

7. Discussion

7.1. Evidence for granular flow mechanisms

The close observation of the 1975 eruption led Nairn & Self (1978) to conclude that the pyroclastic flow transport had "been by inertial grain flow mechanisms; erosion of chutes and short runout distances indicate that the avalanches were neither highly fluidised nor of air-layer lubricated type". Beside their low mobility, the strong topographic control of their flow

paths and erosion in the upper slope region, additional arguments promote the granularity of the Ngauruhoe flows and distinguish them from slightly more energetic pumice and block-and-ash flows (Calder *et al.*, 2002; Cole *et al.*, 2002). The 1975 flow deposits are also unusually coarse-grained, with a very low fines-content that does not appear to be altered during transport by particle breakage. These features together with the low thickness of the flow units, absence of gas-escape and compaction structures count against gas-fluidisation acting during transport and deposition. Further, observation of the flows during eruption and first visits of the deposits suggest that there was small influence of the ash cloud on pyroclastic flow motion. Individual flow units, which, owing to the pristine nature of the deposits, can be traced from most proximal to termination reaches, consistently show well-defined unit boundaries. The detailed observation reports and timed photography allows relating several column collapse flows of eruption phase II to distinct deposit units of sector II. Thus, each of these well-defined units constitutes the deposit from a short-lived single pulse flow. This is in contrast with even small-volume eruptions producing block-and-ash flows, which typically build up stacked flow unit deposits.

7.2. Processes operating during flow

One major result from our sedimentological analysis is the pronounced coarse-tail grading in vertical and longitudinal profiles. The three characteristic *zones I* to *III* in vertical profiles, and each zone in downstream direction, vary almost exclusively in the coarse sub-population. The data further suggests that this spatial variation of the grain-size distribution can be understood by a continuous un-mixing of coarse particles from the bulk (or initial) composition. We infer that un-mixing occurs by granular segregation which preferentially drives large particles to the upper free surface of the flow. As a consequence the flow develops distinct regions of enrichment and depletion of segregated large particles. Due to the vertical velocity gradient (figure 16, cross-sectional view) the segregated particles successively propagate along the upper free surface towards the flow front to concentrate there. When deposited at the front and overrun by trailing portions of the flow, such particles form the basal *zone I*. Moreover, the velocity gradient across the upper free surface forces a typical pattern of flow lines deflected towards the margins, as sketched schematically in figure 16 (top-view). This causes successive migration of segregated clasts towards the flow margins where they concentrate and come to rest as *zone I* levees. Thus, the flow forms a frontal to marginal region enriched in coarse, low-density particles and a central region with a corresponding depletion.
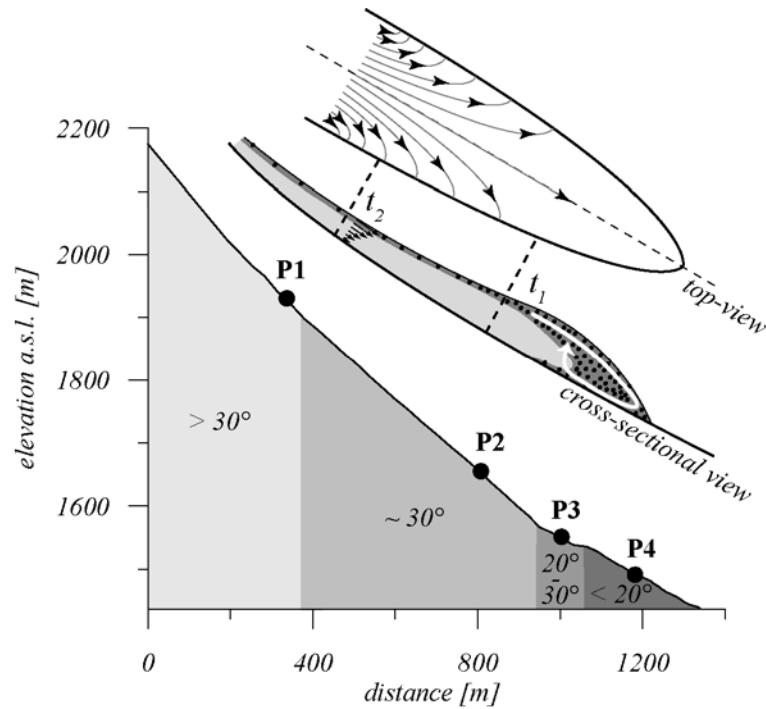
Figure 16. Position of "observation points" P1-P4 along the flow path of a pyroclastic granular flow. Top view: typical pattern of flow lines across the free surface. Cross-sectional view: flow segregation into zone I (dotted dark grey) and zone II (light grey) material batches. Indices t_1 correspond to the time, when the coarse-rich flow front has just past by the observation point, and t_2 marks a later time when the ash-richer tail passes.

For the interpretation of transport and deposition processes of pyroclastic granular flows we introduce the concept of an internal interface separating already deposited, static material from still moving material. Recent laboratory experiments have shown that the dynamics of such an interface plays a major role in the physical behaviour of inertial granular flows (Lajeunesse *et al.*, 2005; Lube *et al.*, 2005). In contrast to the widely studied situation of quasi-steady granular flows on inclines slightly above the static angle of repose, these studies focus on unsteady free-surface flows propagating on slopes well below the angle of repose. In this situation, the thick, transient flow consists of a basal layer of already deposited particles and an upper flowing layer. The separating internal interface propagates with time towards the free surface. Flow occurs until the interface reaches the free surface and the flow runs out of material.

7.3. Qualitative model of flow and deposition

We now discuss a model to explain the changes in the deposit's internal structure and composition with travel distance and the pre-existing slope. We illustrate the model by

following flow and deposition of a pyroclastic granular flow at four characteristic "observation points" along its flow path (positions P1 to P4 in figure 16). In order to capture the time-dependence of these processes, we consider the instantaneous flow structure at each position at a time t_1, when the coarse-rich frontal region has just passed by, and at a later time t_2, when the coarse-depleted tail-region passes (figure 16 and 17).
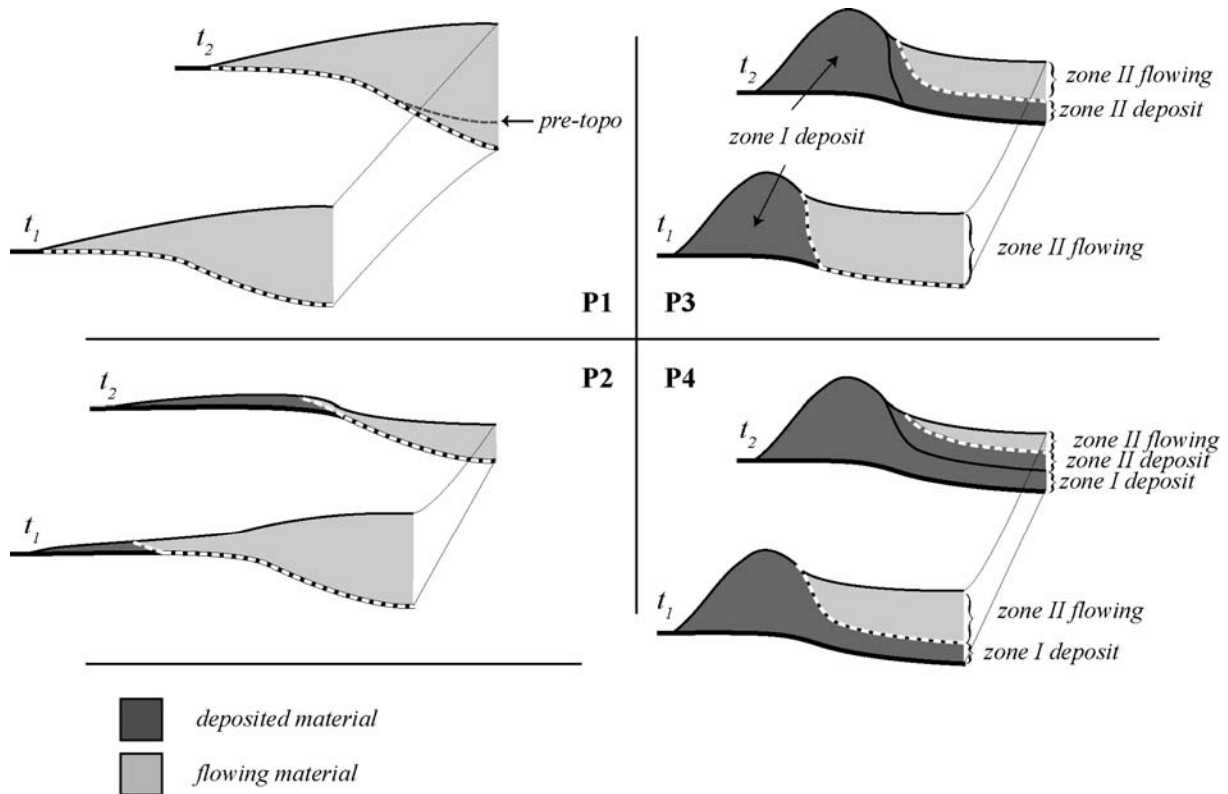

Figure 17. Qualitative model on flow and deposition of a pyroclastic granular flow. Half cross-sections at t_1 and t_2 at the positions P1-P4. The white dashed line marks the internal interface between static and moving pyroclastic material. For further explanation see text.

Position P1 is characteristic for accelerating flow on the >30° steep flanks (figure 17, P1). No deposition occurs, suggesting that the flow propagates on slopes larger than the static angle of repose for the pyroclastic material. The interface either coincides with the flow base or, in particular at the centreline, propagates downwards into the loose surface material resulting in the erosion of longitudinal gullies.

Position P2 captures the flow below the first break in slope at c. 30° where the most proximal deposits occur (figure 17, P2). An averaged flow front velocity of c. 30 ms^{-1} is sufficiently high to inhibit deposition from the central part of flow at any time. Here the interface remains at the flow base. In comparison to P1, erosion is attenuated, probably due to the lower sloping bed. The segregation process described above is already fully developed. Thus, the coarse-

rich, ash-free margins of the frontal region deposit the material of *zone I* (figure 17, P2 t_1). Successively finer grained, ash-richer material from the flow tail laterally accretes with time as *zone II* material, while the interface propagates slightly upwards and towards the centreline (figure 17, P2 t_2).

Position P3 is characteristic for flow below the static angle of repose at c. 20° to 30° where the earliest levee-and-channel forms occur (figure 17, P3). In this region, the flow front decelerates to c. 10 ms^{-1}. At time t_1, the coarse margins of the frontal region have deposited levees (*zone I* material) that confine the central, still moving flow region. The velocity of the flow front at the centreline is still too high for deposition of a basal *zone I*. Thus, the internal interface runs sub-vertically at the inner sides of the levees and sub-horizontally along the flow base at the centreline. With time, the interface propagates up- and inwards, consecutively depositing *zone II* material (figure 17, P3 t_2). This requires a decrease upstream of the basal centreline velocity below a certain threshold. The levee height provides a maximum estimate for the instantaneous thickness of the flow region while passing P3. Since the channel filling *zone II* material never overflows the levees, the flow thickness behind the front must be smaller than within the frontal region. Ongoing segregation of coarse clasts within the still moving tail region produces the coarse plaster of *zone III*. The flow behaviour suggested here shows similarities with results from monitored coarse-grained debris flows in the Illbach valley in the Swiss Alps (Swartz & McArdell, 2005). In the distal flow regions of the Swiss flows, the local maximum in flow height occurs at passage of the bouldery debris flow front and gradually decreases with the flow tail passing. Particle-image-velocimetry performed on large blocks at the flow free surfaces, reveal an increase of velocity to a maximum during passage of the frontal flow region and a continuous decrease thereafter.

Position P4 shows the flow at <20° slopes, the region over which the volumetrically largest proportion of the deposit is distributed. Flow front velocities drop below 10 ms^{-1}. This is sufficiently low to allow for deposition of *zone I* from the frontal region along the entire wetted perimeter (figure 17, P4 t_1). Thus, at time t_1, particles of the bouldery frontal region are deposited by two interrelated processes. Similar to P3, particles at the flow front slow down and arrest in form of levees, dominantly owing to the lateral velocity gradient across the free surface. Close to the centreline, particles at the surface overflow the snout and slow down after incorporation into the flow base. Similar to P3, the internal interface propagates up- and inward with time (figure 17, P4 t_2) depositing the ash-rich, channel-filling *zone II* from the overriding flow tail.

It is notable that the migration and consecutive concentration of large scoria clasts in the frontal region did not result in their excessive breakage or abrasion. The bread-crusted surface textures and flattened forms of the scoria point towards their transport in a relatively hot, plastic state, which would affect the elasticity of particle collisions and attenuate breakage. Much of the current brittle nature of the clasts is probably due to cooling after emplacement forming tension cracks. Second, the maintenance of a particle in the bouldery front was probably short-lived. The propagation on slopes below the angle of repose and the interlocking of the irregularly shaped scoria, favour an almost immediate arresting of particles after overflowing the snout. Furthermore, at the convex deposit front, *zones I* and *III* form an encasing shell of up to 0.5 m thickness around the middle zone II. This suggests that the bouldery, frontal region, in general, was relatively short, but was maintained by permanent supply of segregated coarse clasts as described in 7.1.

7.4. Segregation mechanisms

The mechanisms by which poorly sorted mixtures of granular material can segregate and desegregate has been the focus of numerous experimental, computational and theoretical studies (refer to Duran, 2000; Rosato & Blackmore (Ed.), 2000). Currently, it is thought that segregation is not solely caused by a single mechanism, rather a number of mechanisms can operate at the same time (e.g. Johanson, 2005). For the case of steady granular free-surface flows driven by gravity, these include percolation and expulsion of particles into adjacent layers, gravitational settling in solid-liquid mixtures and diffusion (Vallance & Savage, 2000). We thus might expect that the segregation by size and density observed in the Ngauruhoe deposits is also the result of more than one mechanism.

Percolation, the process by which particles move downwards into void spaces beneath them, is size-dependent and gravity-driven. Small particles percolate downwards more frequently than larger particles resulting in inverse segregation. The process becomes enhanced with increasing shear rate, the diameter ratio of percolating to bulk particle and with increasing solids fraction (Cooke *et al.*, 1978; Bridgwater *et al.*, 1985). Whereas, for relatively slow, frictional granular flows, percolation can result in 100% un-mixing of initially bimodal mixtures, the process is attenuated in fast, collisional flows where particle collision cause diffusive mixing (Savage & Lun, 1988; Vallance & Savage, 2000). Thus, the interplay of diffusion (probably dominant during acceleration in upper and middle slope regions) and percolation (probably more efficient during slow, frictional flow at the lower slope) could

explain the better sorting, coarse-enrichment and relative fines-depletion with travel distance. Percolation, however, does not show a great dependence on particle density (Savage, 1987) and would thus not explain increasing LDC% with distance. While percolation moves particles downwards, the process of squeeze-expulsion of particles into adjacent layers (commonly, in combination with percolation called kinetic sieving) is thought to maintain zero net mass flux in the bed-perpendicular direction. The squeeze-out of particles requires imbalances in the contact forces (Savage & Lun, 1988) which can occur when particles of similar size but different density encounter one another. Denser particles have a greater tendency to push downwards than lighter particles of the same size. As squeeze-expulsion is not gravity-driven, we speculate that this process might even explain the nearly linear increase in LDC% with travel distance over the gradually flattening slope of Ngauruhoe. We note, however, that the current understanding of particle segregation is mainly based on studies of steady granular flows comprising not more than 2 or 3 particle species. In order to understand better or even quantify segregation processes in ill-sorted natural flows, further investigations of flowing mixtures comprising multiple particle sizes are needed (see e.g. the discussion by Thomas (2000)).

7.5. Comparison with other deposits

Proximal to distal facies variation in small-volume pyroclastic flows

For large, pumiceous pyroclastic flows, a broad database of stratigraphic sections and descriptions of abundant facies variations have led to detailed interpretations of their transport and deposition mechanisms (e.g. Druitt, 1998; Branney & Kokelaar, 2002). Despite their frequent occurrence and observations during flow, the construction of a similarly well-constrained knowledge about small-volume pumice and block-and-ash flows remains difficult. Part of the reason lies in the paucity of exposures from proximal to distal reaches and the difficulty in obtaining statistically reasonable grain-size distributions.

Distinct facies transitions could be characterised in the deposits of the 1991 Merapi-type block-and-ash flows from Volcan de Colima (Saucedo *et al.*, 2004). Similar to the Ngauruhoe deposits, proximal and distal facies regions exist and are separated by a break-in-slope from >30° to < 20°. Massive, clast-supported breccias devoid of segregation features characterise the c. 1 m thick proximal facies, whereas the gradually ash-richer, clast- to matrix-supported distal facies displays weak segregation and forms up to 8 m thick stacks of individual flow pulses. The increasing ash-content and a gradual decrease in size and fraction of large clasts

with travel distance in the Colima flows contrasts with the trends for the Ngauruhoe units described here. Saucedo *et al.* (2004) interpret the Colima trends as a combination of particle breakage, erosion of ash-rich surface material, partial deposition of dominantly coarse material near the slope-break and a resulting flow transformation from granular avalanches to relatively more dilute, mobile density currents. They also describe, however, shorter runout flow units comprising a lower ash-content, which did not undergo this flow transformation and produced lobate levee-and-channel deposits below and close to the slope-break. A generalisation of the proximal-distal trends described by Saucedo *et al.* (2004) to other Merapi-type block-and-ash flow deposits appears difficult. Largest-clast measurements in the 1984, 1994 and 1998 Merapi flows (Boudon *et al.*, 1993; Schwarzkopf *et al.*, 2005) reveal a first increase and final decrease with travel distance - trends that are in common with all 1975 Ngauruhoe flows and are quantified in Fig. 14.

Levee-and-channel morphology

The levee-and-channel morphology is a common deposit feature of small-volume pyroclastic flows in their medial to distal reaches (e.g. Wilson & Head, 1981, Cole *et al.*, 2002). It is, thus, not restricted to similarly coarse-grained and ash-poor deposits as formed in the 1975 eruption of Ngauruhoe. The analysis of the July 22 and August 7 1980 pumice flows of Mount St. Helens (Wilson & Head, 1981) also reveals nearly ash-free levees with a coarse, pumiceous open-framework structure. The lateral extension of the levees as a basal *Zone I* has not been reported before. In the Mount St. Helens deposits, the relatively ash-rich channel-filling breccia showed evidence for partial fluidisation. Previously, various hypotheses have been proposed explaining the genesis of levee-and-channel structures with a non-Newtonian rheology of pyroclastic flows (Davies *et al.*, 1978; Wilson & Head, 1981; Rowley *et al.*, 1981; Yamamoto *et al.*, 1993). A similar explanation for the generation of levee-and-channel forms as suggested above (section 7.3) has been found by Felix & Thomas (2004) in analogue experiments on laterally unconfined granular flows near the static angle of repose (a.o.r.). These flows can develop marginal static zones that dam central, still-flowing material. Final deposits resemble natural levee-and-channel forms. Experimental results critically depended on bed slope and initial flux: different flow behaviour and corresponding deposits resulted at inclinations strongly departing from the a.o.r. or at very low or high initial mass fluxes. Unfortunately, spatial limitations in the laboratory restricted these studies to relatively slow and thin flows. It might be interesting to also consider fast, inertial flows that can propagate a

certain distance at inclinations below the angle of repose along with an analysis of lateral and longitudinal velocity profiles across the unconfined, free surface.

8. Summary and conclusions

This paper presents a detailed morphological and sedimentological data set for the deposits of the 1975 pyroclastic flows of Ngauruhoe. Their low volume and pristine preservation along with the documentation of the eruption by Nairn & Self (1978) allowed us to study the variation of the free surface morphology, internal structure, granulometry and componentry from most proximal to distal reaches. In addition, through complete excavations of cross-sectional trenches and continuous sampling from top to base at the centreline we are able to determine first realistic estimates of the bulk componentry of the coarse-tail and the bulk grain-size distribution for such coarse-grained small-volume pyroclastic flows.

The main conclusions reached by this study are that:
- The 1975 deposits can be subdivided into three transitional regions downslope whose distribution is controlled by two slope-breaks: a non-depositional region on upper slopes where erosion occurred; a proximal facies in middle slope regions; and a levee-and-channel facies towards the base of the volcano.
- Whereas the maximum runout is dominantly controlled by initial volume, the local morphology of the resulting deposit is affected by both, the underlying slope and the degree of lateral confinement.
- Each single-pulse flow laid down a well-confined depositional unit comprising three characteristic vertically and longitudinally distinctive parts, Zones *I-III*. Lateral and longitudinal coarse-tail grading can be well explained by segregation of coarse-enriched and coarse-depleted material batches from the initial composition.
- The facies distribution and clear trends of their granulometry and componentry developing with travel distance can be explained by granular-type flow and deposition mechanisms. The flow envisaged was an unsteady inertial granular flow, involving a temporally and spatially varying propagating internal interface, separating static (already deposited) pyroclastic material from that which was still moving.

A test and/or quantification of the qualitative transport and deposition model suggested here requires further investigations of the rheology of unsteady, inertial free-surface flows of

granular material with polydisperse grain-size distributions and also multiple clast-densities. These could be acquired in analogue experiments or computational particle simulations. We also hope that these data can contribute some new aspects for the further development of continuum models on granular mass flows.

REFERENCES

Boudon, G., Camus, G., Gourgaud, A., Lajoie, J., 1993. The 1984 nuee-ardente deposits of Merapi volcano, Central Java, Indonesia: stratigraphy, textural characteristics, and transport mechanism. Bull. Volcanol 55, 327-342.

Bridgwater, J., Cooke, H.H., Drahun, J.A., 1985. Shear induced percolation, Institute of Chemical Engineers Symposium Series *number* 69, 171-191.

Calder, E.S., Luckett, R., Sparks, R.S.J., Voight, B., 2002. Mechanisms of lava dome instability and generation of rockfalls and pyroclastic flows at Soufriere Hills Volcano, Montserrat. In: Druitt, T.H., Kokelaar, B.P. (Ed.), The eruption of Soufriere Hills Volcano, Montserrat, from 1995 to 1999. Geol Soc Lond Mem 21:173–190.

Cole, P.D., Calder, E.S., Sparks, R.S.J., Clarke, A.B., Druitt, T.H., Young, S.R., Herd, R.A., Harford, C.L., Norton, G.E., 2002. Deposits from domecollapse and fountain-collapse pyroclastic flows at Soufriere Hills Volcano, Montserrat. In: Druitt, T.H., Kokelaar, B.P. (Ed.), The eruption of Soufriere Hills Volcano, Montserrat, from 1995 to 1999. Geol Soc Lond Mem 21:231–262.

Cole, P.D., Fernandez, E., Duarte, E., Duncan, A.M., 2005. Explosive activity and generation mechanisms of pyroclastic flows at Arenal volcano, Costa Rica between 1987 and 2001. Bull. Volcanol. 67, 695-716.

Cooke, M.H., Bridgwater, J., Scott, A.M., 1978. Interparticle percolation: lateral and axial diffusion coefficient. Powder Technology 21, 183-193.

Davies, D.K., Quaerry, M.W., Bonis, S.B., 1978. Glowing avalanches from the 1974 eruption of the volcano Fuego, Guatemala. Geol. Soc. Am. Bull. 89, 369-384.

Druitt, T. H. 1998 The eruption, transport and sedimentation of pyroclastic flows. In: Gilbert, J. & Sparks, R.S.J. (Ed.), The Physics of Volcanic Eruptions, Geol. Soc. London Spec. Publ. 145, 147–200.

Duran, J., 2000. Sands, powders, and grains: An introduction to the physics of granular material. Springer, New York.

Evans, S.G., Hungr, O., Clague, J.J., 2001. Dynamics of the 1984 rock avalanche and associated distal debris flow on Mount Cayley, British Colombia, Canada; implications for landslide hazard assessment on dissected volcanoes. Engineering Geology 61, 29-51.

Felix, G., Thomas, N., 2004. Relation between dry granular flow regimes and morphology of deposits: formation of levees in pyroclastic deposits. Earth Planet. Sc. Lett. 221, 197-213.

Freundt, A. & Bursik, M. I. 1998 Pyroclastic flows transport mechanisms. In: Freundt, A. & Rosi, M. (Ed.), From Magma to Tephra: Modelling Physical Processes of Explosive Volcanic Eruptions, Developments in Volcanology, vol. 4, pp. 173–245. Elsevier.

GDR MIDI, 2004. On dense granular flow. Eur. Phys. J. E 14, 341.

Huppert, H. E. 1998 Quantitative modelling of granular suspension flows. Phil. Trans. R. Soc. Lond. 356, 2471–2496.

Johanson, K., Eckert, C., Ghose, D, Djomlija, M., Hubert, M., 2005. Quantitative measurements of particle segregation mechanisms. Powder Technology 159, 1-12.

Lajeunesse E., Monnier J.B. and Homsy G.M., 2005. Granular slumping on a horizontal surface. Phys. of Fluids 17, 103302.

Lube, G., Huppert, H.E., Sparks R.S.J., Freundt, A., 2005. Collapses of two-dimensional granular columns. Phys. Rev. E 72, 1-10.

Nairn, I.A., 1976. Atmospheric shock waves and condensation clouds from Ngauruhoe explosive eruptions. Nature 259, 190-192.

Nairn, I.A., Self, S.,1978. Explosive eruptions and pyroclastic avalanches from Ngauruhoe in February 1975. J. Volc. Geotherm. Res. 3, 39-60.

Pierson, T. C., 1985. Initiation and flow behaviour of the 1980 Pine Creek and Muddy River lahars, Mount St. Helens, Washington. Geol. Soc. Am. Bull. 96, 1056-1069.

Thomas, N., 2000. Reverse and intermediate segregation of large beads in dry granular media. J. Volcanol. Geotherm. Res. 2, 961-974.

Roche, O., Gilbertson, M., Phillips, J. & Sparks, R. S. J., 2002. Experiments on gas-fluidized granular flows and implications for pyroclastic flow mobility. Geophys. Res. Lett. 29, 40–44.

Rodriguez-Elizarraras, S., Siebe, C., Komorowski, J.-C., Expindola, J.-M., Saucedo, R., 1991. Field observations of pristine block and ash flow deposits emplaced April 16-17, 1991 at volcan de Colima, Mexico. J. Volc. Geotherm. Res. 48, 399-412.

Rosato, A.D., Blackmore, D.L. (Ed.), 2000. IUTAM Symposium on Segregation in Granular flows.

Rowley, P.D., Kuntz, M.A., McLeod, N.S., 1981. Pyroclastic flow deposit, in: Lipman, P.W., Mullineaux, D.R. (Ed.), The 1980 Eruption of Mount St. Helens, Washington. US Geol. Prof. Paper 1250, 489-512.

Savage, S.B., 1987. Interparticle percolation and segregation in granular flows: A review, Developments in Engineering Mechanics, Elsevier, 347-363.

Savage, S.B., Lun, C.K.K., 1988. Particle size segregation in inclined chute flow of dry cohesionless granular solids. J. Fluid Mech. 189, 311-335.

Saucedo, R., Macias, J.L., Bursik, M., 2004. Pyroclastic flow deposits of the 1991 eruption of Volcan de Colima, Mexico. Bull. Volcanol. 66, 291-306.

Sheridan, M.F., 1979. Emplacement of pyroclastic flows: A review. In: Chapin, C.E., Elston, W.E. (Ed.), Ash flow tuffs. Geol. Soc. Am. Spec. Pap. 180, 125-136.

Swartz, M., McArdell, B.W., 2005. Motion of large particles in debris flows. Geophysical Research Abstracts Vol. 7, 05943.

Schwarzkopf, L.M., Schmincke, H.-U., Cronin, S.J., 2005. A conceptual model for block-and-ash flow basal avalanche transport and deposition, based on deposit architecture of 1998 and 1994 Merapi flows. J. Volc. Geotherm. Res. 139, 117-134.

Thomas, N., 2000. Reverse and intermediate segregation of large beads in dry granular media. Phys. Rev. E, 1, 62, 961-974.

Vallance, J.W., Savage, S.B., 2000. Particle segregation in granular flows down chutes. In: Rosato, A.D., Blackmore, D.L. (Ed.), IUTAM Symposium on Segregation in Granular flows.

Wilson, L., Head, J.W., 1981. Morphology and rheology of pyroclastic flows and their deposits, and guidelines for future observations. In: Lipman, P.W., Mullineaux, D.R.

(Ed.), The 1980 Eruption of Mount St. Helens, Washington. US Geol. Prof. Paper 1250, 513-524.

Yamamoto, T., Takarada, S., Suto, S., 1993. Pyroclastic flows from the 1991 eruption of Unzen volcano, Japan. Bull. Volc. 55, 166-175.

Chapter VI

Static and flowing regions in granular collapses down channels

Abstract

Through laboratory experiments we investigate inertial granular flows created by the instantaneous release of particulate columns into wide, rectangular channels. These flows are characterised by their unsteady motion, large changes of the free surface with time, and the propagation towards the free surface of an internal interface separating static and flowing regions. We present data for the time-dependent geometry of the internal interface and the upper, free surface for aspect ratios, a, in the range from 3 to 9.5 (where $a = h_i/d_i$ is the ratio of the initial height to basal width of the column). The data were analysed by two different approaches. First, by integrating under the entire internal interface we obtained data for the static area, A_D, as a function of time for different a. Second, in order to characterise vertical deposition rates, we measured the thicknesses of the flowing region, $h_F(x, t)$, and the static region, $h_D(x, t)$, at fixed horizontal positions, x, and time, t, since the initiation of the experiment. We also determined detailed velocity profiles with depth at distances scaled to the final maximum runout distance to analyse the kinematic behaviour of the flowing layer. In the initial free-fall phase, the temporal variation of the static area is independent of h_i and scales as $gd_i t$. During the subsequent lateral spreading phase, $A_D(t)$ varies linearly with time and the deposition rate dA_D/dt scales as $f(a)(gd_i^3)^{1/2}$, where $f(a)$ is a linear function. The thickness of the interface $h_D(x, t)$ at constant x depends on a and varies linearly with time. The local deposition rate $\partial h_D / \partial t$ is not constant along the flow length. Data show that for the major part of the flow length $\partial^2 h_D / \partial t \partial x$ is constant. In the lateral spreading phase, the velocity profiles are characteristically linear with a basal exponential region, a few grains in thickness, which separates static from moving regions. The shear rate is a constant dependent on a modified initial height $\tilde{h}_i$ as $\left(g / \tilde{h}_i\right)^{1/2}$, where $\tilde{h}_i$ is a characteristic length scale in the system describing the fraction of the granular column actually involved in the flowing region.

1. INTRODUCTION

The complex physical behaviour of granular media is of great interest in diverse areas including agriculture, chemical engineering, fundamental physics, the pharmaceutical industry and the Earth sciences. Understanding the physics of dense, granular flows is of particular importance in understanding the propagation of geophysical mass flows and how to predict their runout. Examples of such flows include highly destructive pyroclastic flows formed in explosive volcanic eruptions and avalanches of debris or snow. Numerical simulations of geophysical mass flows over natural terrain are being used more frequently by geologists and geophysicists to produce hazard maps for volcanic (Sparks & Aspinall 2004) and mountainous areas (Margreth et al. 2003). Despite many fundamental studies dedicated to the dynamics of dense granular flows, these simulations have to circumvent the problem that the underlying constitutive equations are still unknown. The general approach has been to derive depth-averaged equations for steady flow conditions and introduce empirical friction laws to try to obtain agreement between data and experiments (Savage & Hutter 1989, Anderson & Jackson 1992, Savage 1998, Pouliquen 1999, Iverson & Denlinger 2001). For the case of free-surface flows driven by gravity, three major flow geometries have been studied extensively: chute flows on rough inclines at angles slightly above the static angle of repose, rotating drums and heap flows. A review of the rheological models obtained in these steady flow situations was recently presented in the collective paper by G.D.R. Midi (2004).

Recently, free-surface flows of granular media have been investigated in a fourth type of flow geometry by laboratory experiments (Huppert et al. 2003, Balmforth & Kerswell 2005, Lajeunesse et al. 2004, Lube et al. 2004, Lajeunesse et al. 2005, Lube et al. 2005) and by computer simulations (Kerswell 2005, Staron & Hinch 2005, Zenit 2005). These studies all consider the fundamental problem of the collapse of an initially static granular column released instantaneously onto a rough horizontal bed. Granular collapse flows differ considerably from thin, quasi-steady granular chute flows at inclines slightly above the static angle of repose referenced above. The main differences are that they are unsteady and involve large changes of the free surface with time as well as the propagation towards the free surface of an internal interface separating static and flowing particles.

Here we present detailed experimental results on the dynamics of the internal interface and the dynamic and kinematic behaviour of the overlying particle flow. This work develops

further our studies of column collapses in axisymmetric (Huppert et al. 2003, Lube et al. 2004) and two-dimensional geometries (Lube et al. 2005), which we now briefly summarise. In axisymmetric geometry, we considered the unhindered spreading of initially cylindrical columns of heights h_i and radii r_i. In the two-dimensional geometry, the granular regions had initial height, h_i, basal length, d_i, and were released into long channels of different but large width. In both geometries, we employed a wide range of particle sizes, shapes and densities and varied the floor roughness systematically from smooth to rough. The major governing parameter is the initial aspect ratio, a, in axisymmetric geometry defined as the ratio h_i/r_i and in two-dimensional geometry as h_i/d_i. Maximum runout distances, r_∞ and d_∞, in axisymmetric and two-dimensional geometries respectively, the maximum deposit height at the origin, h_∞, and the time, t_∞, to reach the final runout, were found to be independent of the different grain types and the roughness of the base. The axisymmetric experiments focussed on the final geometry and propagation of the flow front with time. Our study of two-dimensional granular collapses included the observation of the internal deformation, the dynamics of the free surface and the interface between the static and the flowing layer.

These experiments allowed investigation of the three major stages describing the collapse. In the first stage, the collapse is controlled by the free-fall behaviour of the column. The upper part of the column, above a critical height of approximately 2.8 d_i, is in purely vertical motion (in two dimensions). Once the top of the column has reached this critical height, the second phase of collapse is dominated by lateral motion, which ceases abruptly at t_∞, when the interface between static and flowing particles has reached the free upper surface. In these first two phases, the influence of the bounding walls is very small, as indicated by (horizontal) plug flow velocity profiles across the free surface with minor shear at the walls and strong slip. There is a (quite different) third phase of motion, which involves thin and slow avalanching across the free surface to stabilise the steep central part of the pile. In this phase, frictional effects of individual particles between each other and with the bounding walls become strong. The form of collapse, its duration and the shape of the final deposit are effectively controlled by the physics of the flowing layer and the propagation of the separating interface towards the free surface.

The plan of the paper is as follows. In section 2, we explain the experimental set-up and the techniques that were used to determine the velocity profiles in the flowing layer and the geometry of the free surface and the interface. An analysis of the spatial and temporal

evolution of the free surface and the interface is presented in section 3. Data of the velocity profiles in the flowing layer is presented in section 4. A summary of our results and further discussion are presented in section 5.

2. METHODS

The experiments investigate two-dimensional granular flows formed by the collapse of rectangular columns of sand into a wide horizontal channel. We employed the same experimental set-up described in Lube et al. (2005) (Figure 1). A container accommodated the granular material at one end of the tank. A rectangular box of the same width, 20 cm, as the channel and variable initial basal length d_i comprised a frontal gate to release the granular material. A release mechanism was constructed to allow for very fast and reproducible lifting velocities of the gate. It consisted of releasing a large weight connected to the gate via a pulley construction at the ceiling. The weight fell freely for the first 0.75 m to reach a high velocity (approximately 4 m s^{-1}) before it lifted the gate extremely rapidly. The time for the gate release in any experiment was very much less than the typical time scale of the resulting motion. We employed a mixture of industrial black and light grey coloured Quartz sands of grain-size 1.4 ± 0.4 mm. This was found to give the best contrast results for the digital image analysis described below. In this study, the initial aspect ratio a was varied systematically from 3 to 9.5 by using two different values of d_i (6 cm and 9 cm) and different masses of sand.

Each experiment was conducted twice. In the first run, the entire flow was filmed through the transparent frontal pane. Before preparing the initial columns of sand, a 5 mm grid was tied to the inner side of the frontal pane to give a reference frame and a fast camera at 120 frames/sec then recorded the experiment. The flows were captured and analyzed digitally. At every fifth frame (at intervals of ~0.04 s), we mapped the free surface to obtain $h_F(x, t)$ (figure 1). To obtain curves of the interface between static and flowing particles, $h_D(x, t)$, we first analyzed every fifth and sixth frame using the Pattern Match algorithm of Dalziel (2005). Finally, we carefully corrected, were necessary, these curves to match exactly the interface between the uppermost static and the lowermost flowing particle. In the second run, we positioned the camera as close as possible and perpendicular to the frontal pane at a distance $\delta d/3 + d_i$, where δd is the difference between the maximum runout distance, d_∞, and the initial width d_i
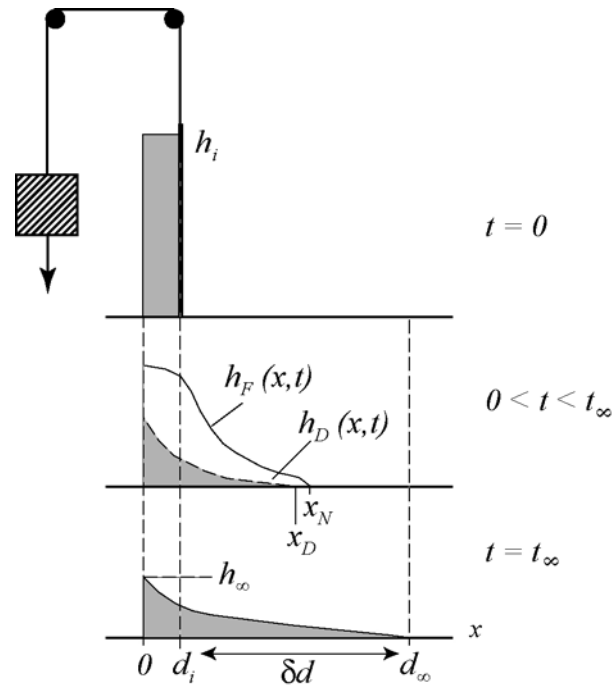
Figure 1. Experimental setup with a sketch of the initial column, the interface between a lower static layer (grey) and an upper flowing layer (white); and the final deposit.

(figure 1). We could thus obtain very detailed high-speed movies for the analysis of the velocity profile with depth, again using the 5 mm grid as a reference.

3. EVOLUTION OF THE INTERFACE AND FREE SURFACE

3.1. The spatial evolution: qualitative observations

We first contrast the temporal evolution of the free surface, the interface and the depth of the flowing layer for a typical experiment (Figure 2a-c). The inset in figure 2b shows the length of the interface, L_D, determined from appropriately integrating $h_D(x, t)$ as a function of time. A detailed description of the evolution of the free surface as a function of the aspect ratio is given in Lube et al. (2005). Figure 2a illustrates the two subsequent phases of collapse. The first phase is dominated by the free fall of the column, and the top of the column remains nearly undisturbed. In this free fall phase, the point of maximum height of the flowing layer remains at an approximately constant distance d_i from the y-axis (Figure 2c). In the second, lateral spreading phase, deformation occurs along the entire free surface (Figure 2a). The point of maximum height of the flow propagates outwards with time (Figure 2c). As the flowing layer increases in length, its maximum thickness reduces until the flowing layer has reached an approximately constant thickness (except for the origin and at the front where it
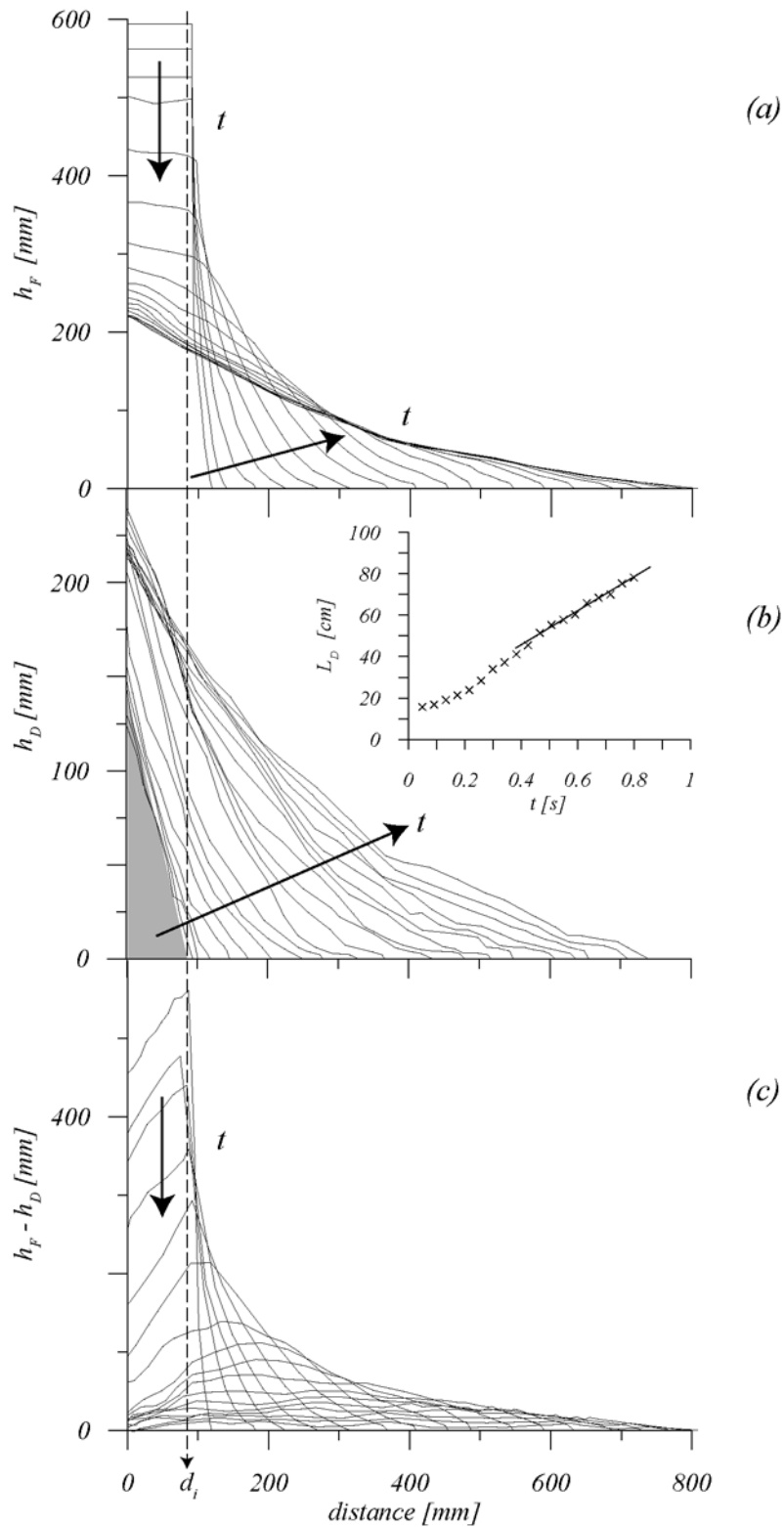
Figure 2. An example of the evolution of: (a) the free surface; (b) the internal interface; and (c) the thickness of the flowing layer with time at constant time intervals of 0.416 sec for an experiment where a = 7. Note the different scale of the y-axis in 2b chosen for a clearer illustration. Inset shows the temporal variation of the length of the interface, L_D. The grey triangle drawn in 2b marks the static wedge formed in the beginning of the experiment.

goes to zero). As shown previously in (Lajeunesse et al. 2005, Lube et al. 2005), at the beginning of the experiment the internal interface appears as a straight line intersecting at a zero height at $x = d_i$, where x is the distance from the origin. This initial line is inclined at approximately 60° to the horizontal. Throughout the entire experiment, the internal interface propagates upwards towards the free surface (Figure 2b), and the static area increases with time. In the lateral spreading phase, L_D also varies approximately linearly with time (inset figure 2b). Results similar to those presented in figure 2 for $a = 7$ were obtained for all tested values of the aspect ratio.

3.2. Static vs. flowing material

Column collapses can be geometrically described by the two time-dependent functions $h_F(x, t)$ and $h_D(x, t)$. Plots similar to figure 2b can be used to determine the area of static material, A_D, defined by

$$A_D(t) = \int_{x=0}^{x=x_D(t)} h_D(x,t)dx,\tag{1}$$

where $x_D(t)$ is the horizontal coordinate of the front of the deposited layer. The data so obtained are plotted as A_D - A_W against time in figure 3a, where $A_W = 0.5d_i^2 tan60°$ is the area of the initial static wedge, and hence the initial value of A_D. Two different phases can be recognised. Without any normalisation, the curves of A_D - A_W against time for different values of a collapse onto a universal curve in the first phase of collapse, where $A_D - A_W$ is proportional to $gd_i t^2$. There is a departure from this universal curve at a time dependent on a. In the lateral spreading phase, the static area increases linearly with time. Deposition rates dA_D/dt vary from 390 to 940 cm²/s for $d_i = 9.05$ cm and $a = 3.4$ to $a = 9$, respectively. By dimensional analysis we can express the deposition rate as

$$dA_D / dt = (gd_i^3)^{1/2} f(a),\tag{2}$$

for some dimensionless function f of the aspect ratio. The inset in figure 3a, where the deposition rate is plotted against $a(gd_i^3)^{1/2}$, shows that $f(a)$ is linear.

In figure 3b the same data is shown in non-dimensional form where $(A_D$ - $A_W)$ is normalised by $(A_i$ - $A_W)$ and time by the final emplacement time t_∞, and $A_i = h_i d_i$ is the initial cross-sectional area. Using this scaling collapses the data in the lateral spreading phase. The notable point about this scaling relationship is that the final emplacement time, t_∞, appears to be a critical time-scale for the propagation of the interface, which as shown in Lube et al. (2005) can be expressed in terms of the external parameters as $t_\infty = 3.3 (h_i/g)^{1/2}$.
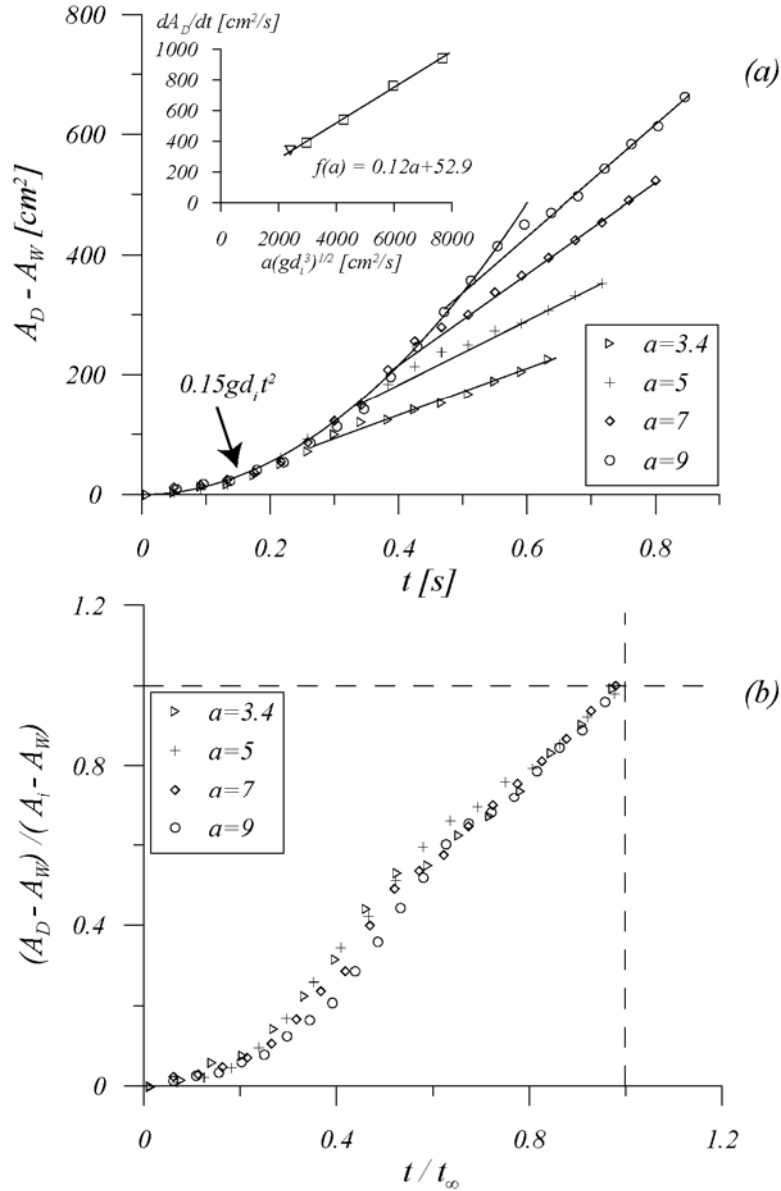
FIG. 3. *The area of the static layer against time in (a) non-normalised and (b) normalised form for different values of the aspect ratio and d_i = 9.05 cm. There is a collapse of the data in the first phase to the function A_D - A_W = 0.15 gd_i t^2. Linear functions and corresponding slopes drawn to data points in the lateral spreading phase illustrate the constant global deposition rates dA_D/dt for different aspect ratios. Inset in 3a shows data of the deposition rate (dA_D/dt) against $a(gd_i^3)^{1/2}$ for d_i = 9.05 cm (□) and d_i = 6.05 cm (∇), and a linear best-fit through the data.*

3.3. Vertical motion of boundaries

Figure 4 shows the temporal evolution of the thickness of the static layer, h_D (x, t), at different horizontal distances x for a representative experiment where a = 5 and d_i = 9.05 cm. At x = 12 cm and x = 22 cm, the data h_D against time are well-represented by two linear segments and a short, nonlinear, transitional region in between. The initial linear part is observed during the

free-fall phase, whereas the final linear segment occurs during the lateral spreading phase. At the outer
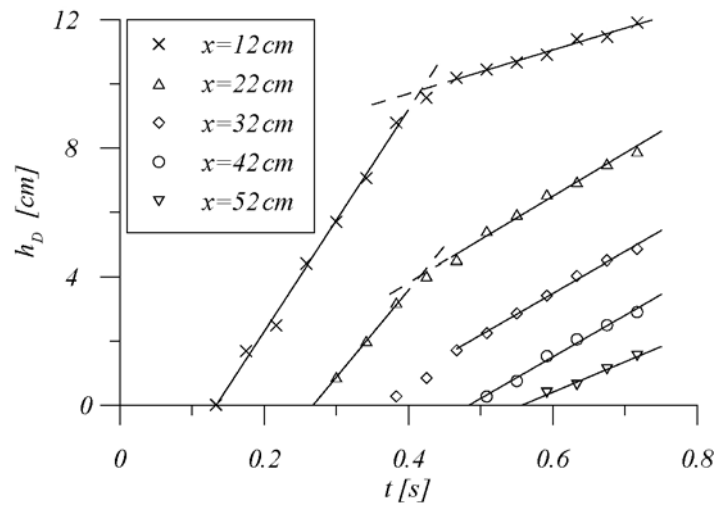
Figure 4. The temporal variation of the thickness of the static layer, h_D, at different horizontal distances, x, for an experiment where a = 5 and d_i = 9.05 cm. There are two linear regions, representing the free-fall and lateral spreading phase, respectively, and a short transitional region in between.
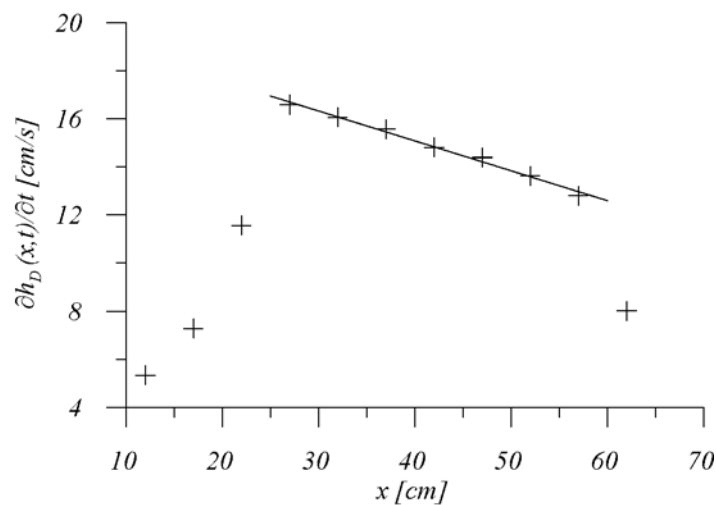
Figure 5. The variation of the local deposition rate, $\partial h_D (x, t)/ \partial t$ in the lateral spreading phase as a function of the horizontal distance, x, for an experiment where a = 7. Deposition rates were determined as the slope from best-fit linear regressions to the data $\partial h_D(x)$ against time in the lateral spreading phase.

horizontal positions (x = 32, 42, and 52 cm), there is only one behaviour corresponding to linear growth of the layer during the lateral spreading phase. The data show that during the lateral spreading phase there is a linear growth with time of the static layer along the flow length. However, $\partial h_D /\partial t$ is not constant along the flowing layer, but varies slightly with the horizontal distance, x. For the lateral spreading phase, where the variation of h_D with time is

linear, we can calculate local horizontal deposition rates $\partial h_D (x, t)/ \partial t$ by linear best-fits. Figure 5 shows a graph of the local deposition rate as a function of x for an experiment where $a = 7$. It is seen that, except close to $x = 0$ and $x = d_\infty$, the deposition rate declines slightly in linear fashion during the spreading phase.
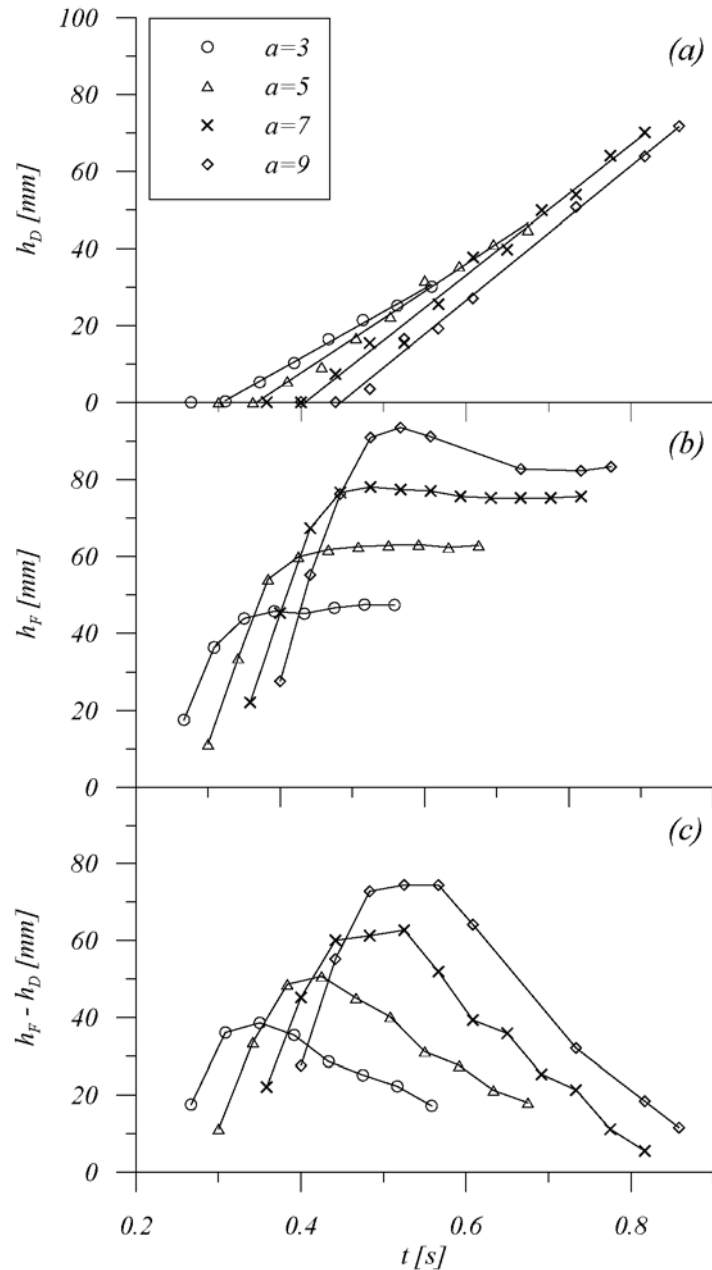
Figure 6. Variation of: (a) the thickness of the static layer; (b) the free surface height and (c) the thickness of the flowing layer with time at a fixed position δd/3 + d_i for different values of a.

Without a general dynamical model for the internal interface and the free surface, we investigate the vertical variation of h_F and h_D at scaled horizontal distances only. We derive the scaling relationships for $h_D(t)$, $h_F(t)$ and $h_F(t) - h_D(t)$ at a fixed horizontal distance

$\delta d/3 + d_i$. We choose this representative distance to be far from both $x = 0$ and $x = d_\infty$, where either vertical or horizontal motions dominate, respectively. The flow front reaches this distance at constant fractions of the final time, t_∞ for different values of a (Lube et al. 2005). Figure 6 shows the temporal evolution of h_D, h_F and $h_F - h_D$ for different values of a and $d_i = 9.05$ cm. After the flow front reaches the observation point, the thickness of the static layer, h_D, increases approximately linearly with time. The (near constant) local deposition rate, dh_D/dt, at $\delta d/3 + d_i$ increases with increasing aspect ratio. The local flow height, h_F, first increases before equilibrating at a final height, dependent on a. The thickness of the flowing layer, $h_F - h_D$, increases with time towards a maximum before decreasing to zero.
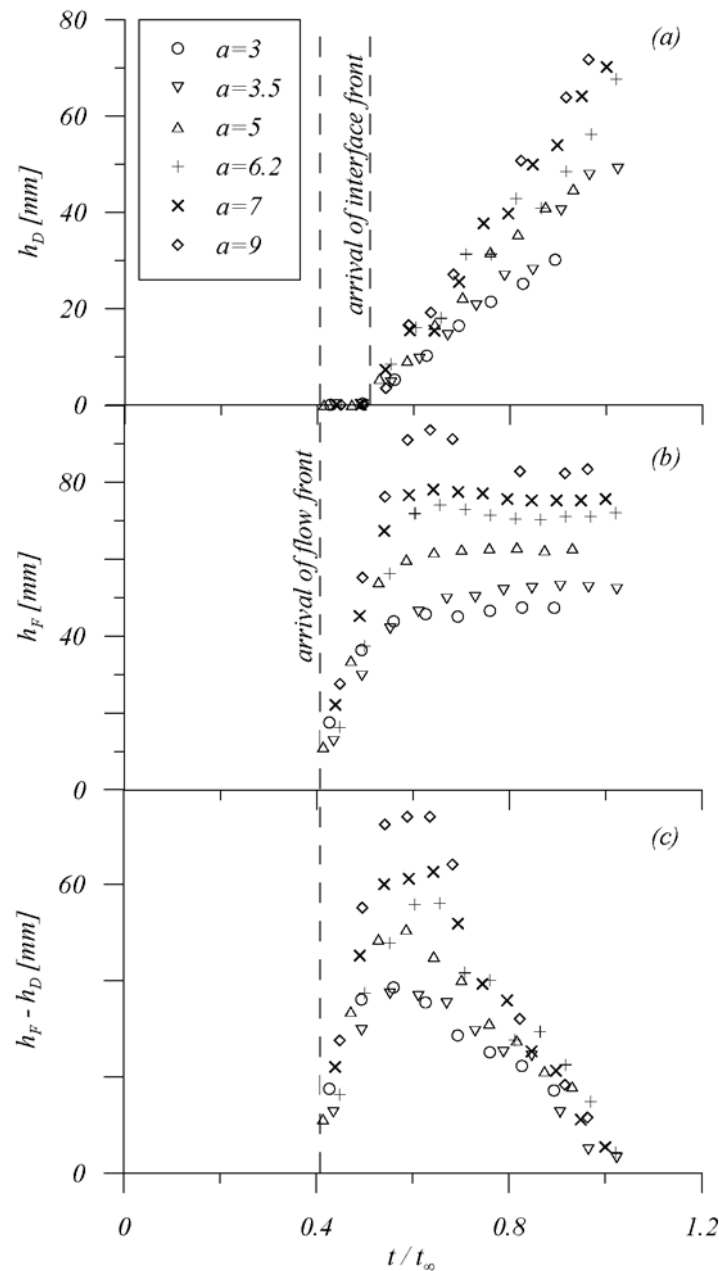
Figure 7. The thickness of the static layer, h_D, the free surface height, h_F, and the thickness of the flowing layer, $h_F - h_D$, against non-dimensional time at the fixed position $\delta d/3 + d_i$.

125
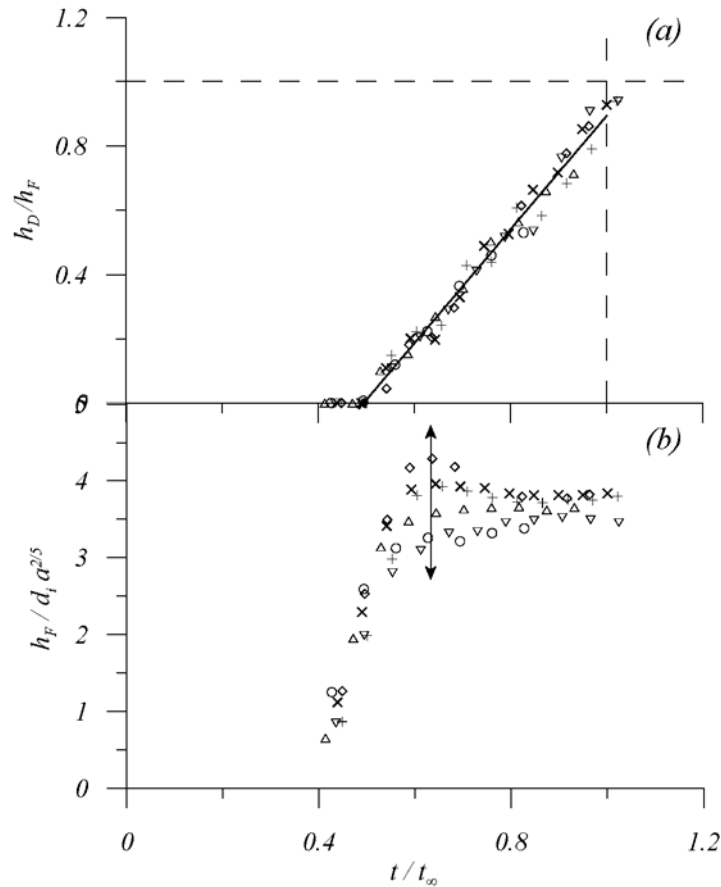
Figure 8. (a) Collapse of $h_D(t)/h_F(t)$ in non-dimensional form. (b) collapse of the data for h_F $(t)/(d_i\,a^{2/5})$ in non-dimensional form. Same symbols as in fig. 6 and 7.

Figures 7 presents the same thickness data plotted against the non-dimensional time, t/t_∞. The flow front and the internal interface arrive subsequently at constant fractions of the non-dimensional time at the scaled horizontal distance $\delta d/3 + d_i$ ($\sim 0.4\ t_\infty$ and $\sim 0.5\ t_\infty$, respectively). Growth of the static layer thus starts a little time after the flow front has passed the location. The initial height, h_i, might be a relevant length to scale all the curves $h_D(t)$, $h_F(t)$ and $h_F(t)-h_D(t)$ in order to obtain universal curves for the data. However, using this scaling neither the time nor length scale would depend on the initial width of the column, d_i. Indeed, no collapses are obtained for non-dimensional groupings of h_D/h_i, h_F/h_i or $(h_F(t)-h_D)/h_i$ against non-dimensional time. Figure 8a demonstrates that a very good collapse of the data for the ratio h_D/h_F and for both values of d_i (9.05 cm and 6.05 cm) as a function of t occurs in the form

$$h_D/h_F = H(t/t_\infty),\qquad(3)$$

where *H* is linear. Note that this normalisation applied to the data of the thickness of the flowing layer, (h_F - h_D), results in a similar collapse. By purely dimensional arguments, this result might seem somewhat unsatisfactory, as h_F is not an external parameter. In figure 8b we see that only a partial collapse of the data for h_F against *t* data can be obtained in terms of external parameters as

$$h_F / (d_i a^{2/5}) = K(t / t_\infty),$$ (4)

where $d_i a^{2/5} \propto h_\infty$ (Lube et al. 2005). Recall that h_∞ is the maximum final height of the deposit at the origin, thus the point of the pile which is least affected by lateral motion. The initial and final parts of the data points collapse rather well, but a major deviation occurs in between. This deviation is attributed to a wave propagating through the flowing layer whose amplitude increases with the aspect ratio.
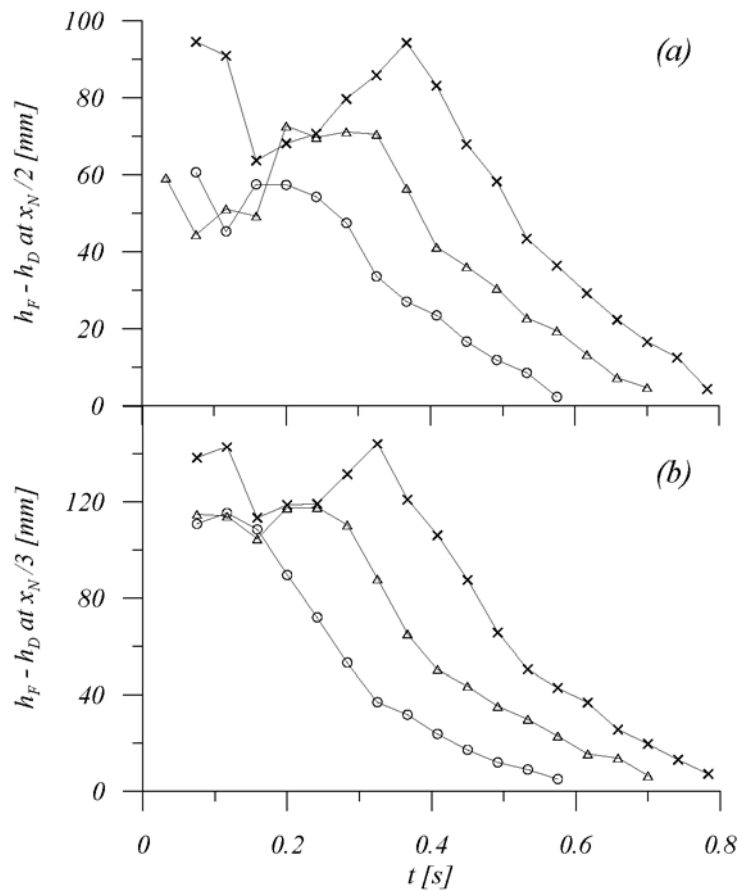
Figure 9. The depth of the flowing layer at a scaled distance x_N (t)/n with (a) n = 2 and (b) n = 3 for a = 3.4, 5 and 7. Same symbols as in fig. 6 and 7.

We now develop a Lagrangian view of this problem. As shown in Lube et al. (2005), the propagation of the flow front with time in two dimensions is self-similar; and all columns for *a* > 2.8 relax towards self-similar profiles. Therefore, self-similarity of the curves $h_F(x, t)$ and $h_D(x, t)$ might be expected. From our experimental data we obtained $h_F(x, t)$ and $h_D(x, t)$ at

constant fractions of the instantaneous flow front position $x_N(t)$. Figure 9 shows the temporal evolution of the depth of the flowing layer for three values of a at the time-dependent distance $x_N(t)/n$ (with $n = 2$ in Fig. 9a and $n = 3$ in Fig. 9b). The first part of the curves, which relates to the initial free-fall phase, shows a decreasing region followed by an increasing region. There is a final continuously decreasing part constituting the lateral spreading phase. In Fig. 10 we plot the same data in non-dimensional form, using the length-scale h_i and the time-scale t_∞, to determine the function M defined by

$$(h_F - h_D)/h_i = M(t/t_\infty) \tag{5}$$

A very good collapse is obtained for all tested values of h_i after approximately 0.4 to 0.5 t_∞ in the spreading phase. We have also tested other values of n $(2/3 \leq n \leq 10)$, which also results in a collapse of the data $(h_F - h_D)/h_i$ against non-dimensional time during the lateral spreading phase. The different curves $M(t/t_\infty, n)$ merge as $t/t_\infty \rightarrow 1$, illustrating the experimental observation that, towards the end, the thickness of the flowing layer is approximately constant along the flow length.
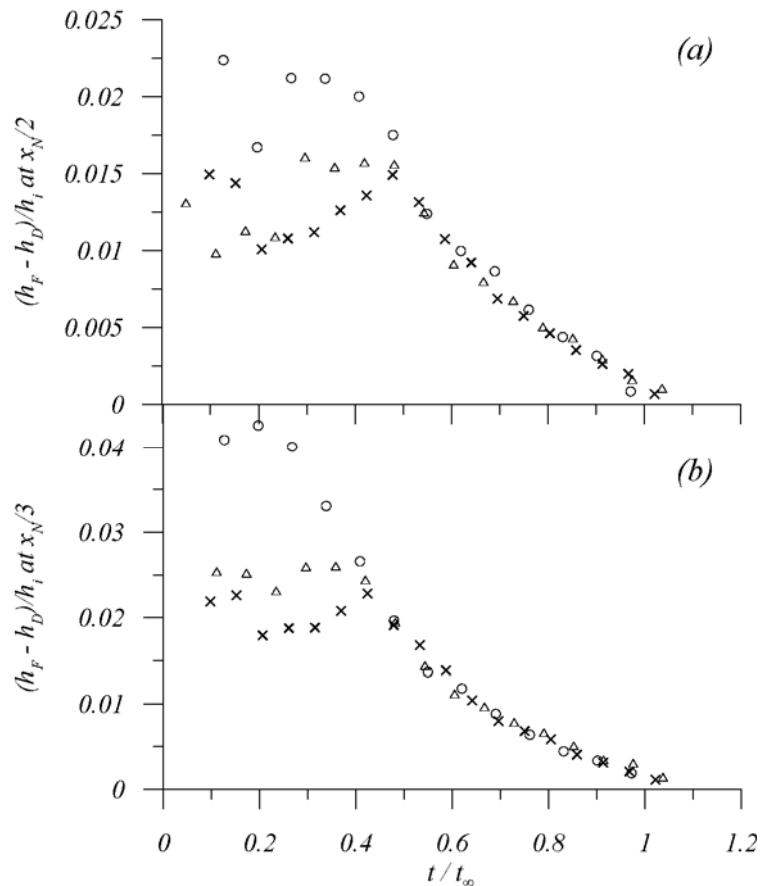
Figure 10. The non-dimensional depth of the flowing layer at a scaled distance $x_N(t)/n$ with (a) $n = 2$ and (b) $n = 3$. Same symbols as in fig. 6 and 7.

4. VELOCITY PROFILES IN THE FLOWING LAYER

The velocity profiles in the flowing layer vary in both space and time. In the initial free-fall phase, all particles above a critical height, $h_c \sim 2.8\ d_i$, are in purely vertical motion. In the flow front region in direct contact with the base, a strong parabolic profile with a plug-like top and a high slip velocity at the base exists. During the entire experiment, close to $x = 0$ or $x = x_N$, the profiles tend to purely vertical or horizontal motion, respectively.

In the second, lateral spreading phase, except close to the origin and the flow front, the velocity profiles show the typical form illustrated in Figure 11. From the internal interface upwards, we distinguish two transient regions: a lower exponential part and an upper linear part. At the very top of the flowing layer, there is a thin region of roughly constant thickness (approximately 3 particle diameters) deviating from the major, linear part. The region with the largest change in velocity and depth with time is the linear part of the profile. The typical form of velocity profiles during the lateral spreading phase has been previously reported in (Lajeunesse et al. 2005, Lube et al. 2005). Velocity profiles similar to that described here are also typical for heap flow and rotating drum geometries under steady flow conditions (Bonamy et al. 2002, G.D.R. Midi 2004). A common characteristic of all three geometries is the existence of an internal interface separating static and flowing regions of granular material.
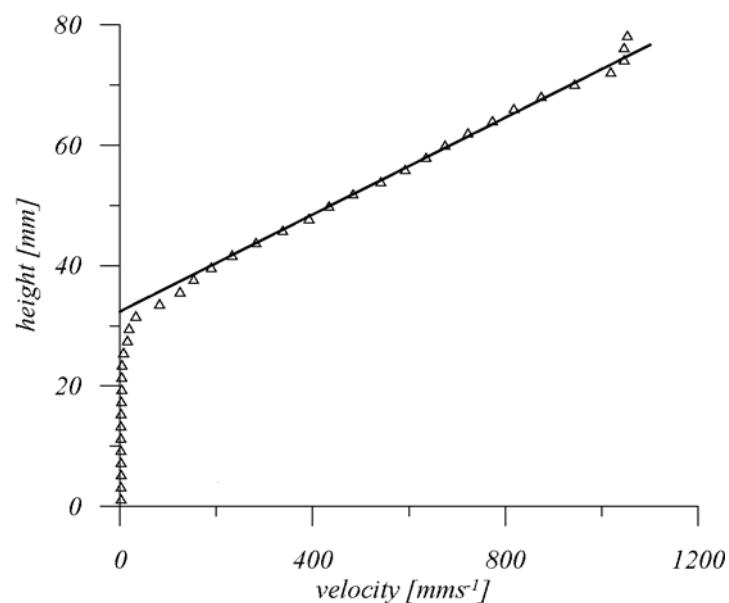
Figure 11. Example of the typical form of velocity profile in the lateral spreading phase, including the static layer, a lower exponential region, an upper linear section and an upper plug-like region restricted to a few grains.

PIV analysis on high-speed movies of our second experimental series allows us to obtain detailed velocity profiles with depth at scaled distances $\delta d/3 + d_i$. For each aspect ratio, a universal curve $h - h_D$ against velocity exists that collapses all profiles obtained after the arrival of the interface front at times $t > 0.5\ t_\infty$. Figure 12 illustrates the collapse for an
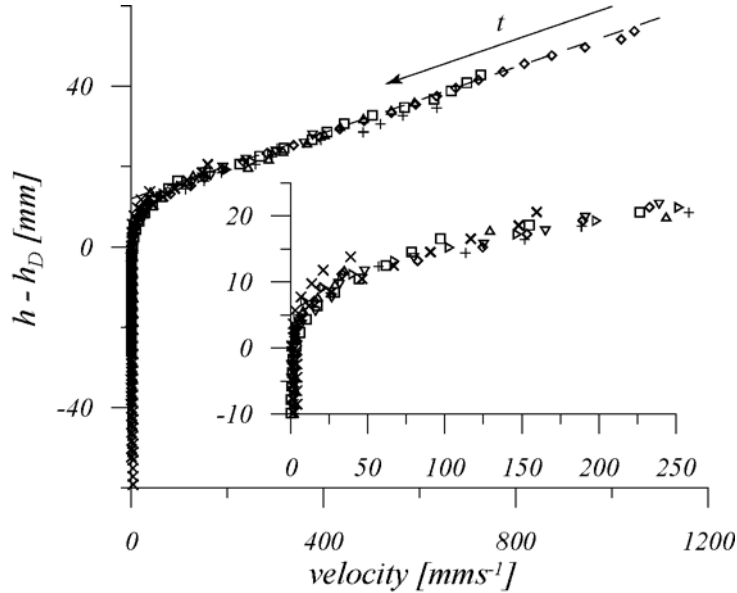

Figure. 12. Collapse of all velocity profiles for an experiment where a = 7 after the development of the interface at $\delta d/3 + d_i$. Different symbols represent the velocity profiles at different times in the interval $0.5\ t_\infty < t < t_\infty$. Inset highlights the region close to the interface.
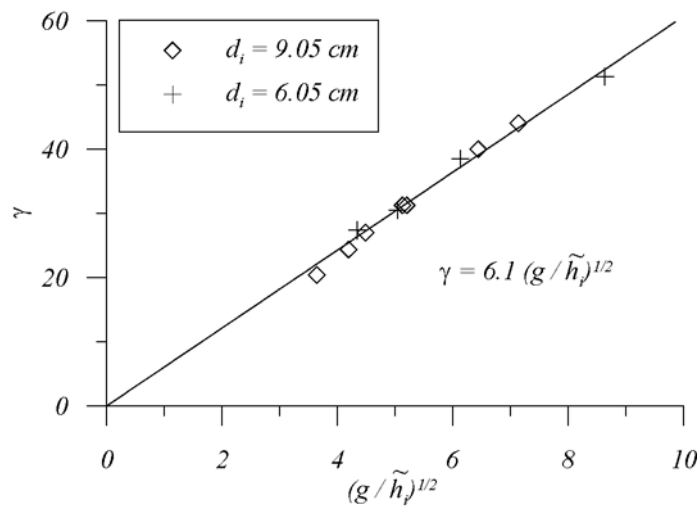
Figure 13. The shear rate obtained from best linear fits of the linear part of the velocity profiles plotted against $\left(g/\tilde{h}_i\right)^{1/2}$, where $\tilde{h}_i$ is the modified initial height (see text for details).

experiment with $a = 7$ and times $0.5\ t_\infty < t < t_\infty$. The lower exponential part remains constant in form and thickness (approximately 8 to 10 particle diameters), whereas the thickness of the linear part decreases with decreasing thickness of the flowing layer. Collapsed velocity profiles similar to that presented in figure 12 for $a = 7$ are obtained for all values of a. We can

characterise these profiles by expressing a shear rate γ as the inverse slope of a best linear fit through the linear part of the velocity field. By dimensional arguments this shear rate can be written as

$$\gamma = \left(g / \widetilde{h}_i\right)^{1/2} F\left[a = h_i / d_i, \phi / h_i\right], \tag{6}$$

where ϕ is the particle diameter. We here introduce the modified initial height, $\widetilde{h}_i$, defined by

$$\widetilde{h}_i = h_i - d_i \tan(60°)/2$$

as a length scale that describes the fraction of the granular column actually involved in the flowing region. When we plot the experimentally determined shear rates for all values of h_i and d_i against the shear rate scale $\left(g / \widetilde{h}_i\right)^{1/2}$ (figure 13), the data collapse onto the linear function

$$\gamma = 6.1\left(g / \widetilde{h}_i\right)^{1/2}. \tag{7}$$

We note that, if instead of $\widetilde{h}_i$ the initial height h_i is used in the term for the shear rate scale, the data collapse onto a linear function that gives physically unrealistic negative values for large values of h_i. Since the ratio ϕ / h_i is very small in comparison to the aspect ratio, we may define a non-dimensional shear rate

$$\gamma\left(\widetilde{h}_i / g\right)^{1/2} = F(a). \tag{8}$$

Figure 14 shows that $F(a)$ is effectively constant.
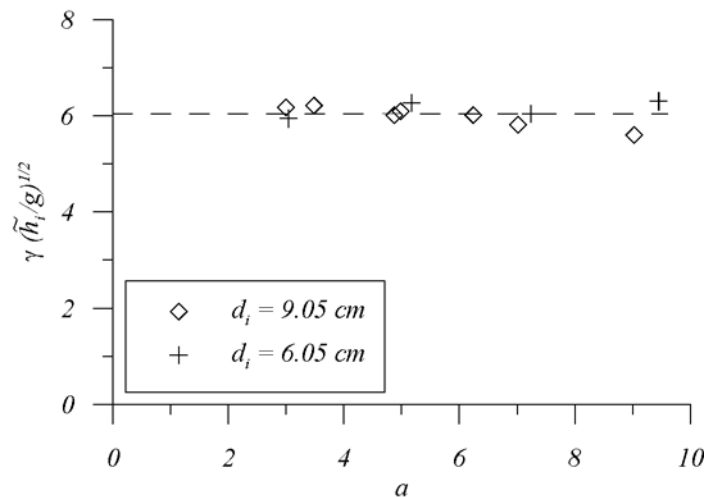
Figure 14. The non-dimensional shear rate $\gamma\left(\widetilde{h}_i / g\right)^{1/2}$ plotted against the aspect ratio.

In contrast to the clear dependence of the shear rate on the aspect ratio (or on $\widetilde{h}_i$) that we have demonstrated here, a different behaviour is claimed in Lajeunesse et al. (2005). These authors follow a similar scaling approach as proposed for steady uniform flows observed in heap flow

and rotating drum geometries (e.g. Bonamy et al. 2002, G.D.R. Midi 2004). They suggest that velocity profiles obtained for different values of a, at different times and for different particle diameters, ϕ, collapse onto a universal curve by normalising velocity by $(g\phi)^{1/2}$ and depth by ϕ. With a linear fit through the linear part of all the normalised profiles, the authors of (Lajeunesse et al. 2005) claim the relationship $\gamma = 0.3(g/\phi)^{1/2}$. We think that their interpretation of the data is misleading and substantiate our view by the following arguments. First, in their presented data, the systematic variation of the velocity profiles as a function of time is not shown. Instead particular profiles for experiments with different a and ϕ were depicted. Second, the presented velocity profiles nearly exclusively correspond to the late stages of the experiment (i.e. when the thickness of the flowing layer is less than 7-8 particle diameters). Thus, a dominant part of the considered profiles corresponds to the lower exponential region, and the linear part of the presented profiles has a depth of hardly five particle diameters. Finally, the presented data show a large scatter around the proposed linear function $\gamma = 0.3(g/\phi)^{1/2}$. This large scatter (particularly that in the exponential region), however, give reason to assume that the form and/ or depth of the lower exponential region is dependent upon particle characteristics. This view and suggestions for further investigations of this problem are amplified in the last section.

5. SUMMARY AND DISCUSSION

This paper presents experimental results of the dynamics of static and moving regions of granular material that characterise inertial granular flows initiated by column collapse. During collapse, the upper, flowing region continuously deposits material from its base. Thus, the area of static material grows with time, and the internal interface separating upper, flowing and lower, static material propagates towards the free surface.

The discrete nature of the internal interface allowed us to quantify its temporal and spatial variation as a function of the initial aspect ratio. The resulting data were analysed by two different approaches. First by integrating under the entire interface we determined global deposition rates, dA_D/dt. Second we measured the thickness variation of the flowing and static regions at fixed horizontal distances, x, and were able to calculate local deposition rates, $\partial h_D (x, t)/\partial dt$. At a fixed position, scaled to the final maximum runout, we also analysed the form and temporal variation of the velocity profile with depth in the flowing layer.

Experimental observations in previous studies (referenced in section 1) have shown qualitatively that inertial granular column collapses involve two transient stages: an initial free-fall phase and a subsequent lateral spreading phase. These two phases are also evident in the contrasting behaviour of the motion of the interface, and consequently in the rate of deposition which occurs from the base of the flowing layer.

In the free-fall phase, the rate of growth of the static area with time is independent of the initial height and scales as $gd_i t$. This finding is in good agreement with previous results which show that, in this initial phase, also the shape of the free surface below the critical height $h_c \sim$ 2.8 d_i (including the horizontal position of the flow front) does not change with h_i (Lube et al. 2005, Staron & Hinch 2005).

In the lateral spreading phase, the static area increases linearly with time dependent on the aspect ratio. Granular columns with higher aspect ratios show higher deposition rates, which scale as $f(a)(gd_i^3)^{1/2}$, where $f(a)$ is a linear function. The local vertical growth of the interface is independent of the local flow depth and velocity. Data show that, for the major part of the flow length, the derivative $\partial^2 h_D / \partial t \partial x$ is a constant dependent on the aspect ratio, but experimental runs with two connected high-resolution, high-speed cameras are needed to explore this relationship in detail. This is planned in future investigations.

Our data of the vertical velocity profiles with depth show: (a) a time-invariant form comprising a lower exponential and an upper linear region; and (b) a scaling relationship for the shear rate as $\gamma = c\left(g / \tilde{h}_i \right)^{1/2}$. The shear rate is, however, independent of the local flow depth and velocity, but decreases by increasing the area involved in the flow (i.e. increasing a). Beside column collapses, granular flows in heap flow and rotating drum geometries comprise linear vertical velocity profiles. However, no physical explanation for this has yet been offered. This behaviour is in contrast with steady uniform flows on inclines close to the (static) angle of repose. In this situation, the shear rate varies as the square root of depth resulting in the so-called Bagnold scaling. The widely accepted reason for this scaling relationship is the constant ratio of shear stress and normal stress (Pouliquen 2005).

Here we interpret the characteristics of the velocity profiles in a qualitative way and suggest some directions for future investigations. One possible way of looking at the problem is by a simple rheological analogue. Viscous fluids produce a classic parabolic profile with shear rate increasing linearly with depth. If one could describe inertial granular flows by a rheological

law then this would have to involve a linear dependence of "effective" viscosity with depth. This law implies the effects of viscosity are zero (or very small) near the free surface and increases linearly with depth.

Whereas the velocity of the interface and the major (linear) part of the velocity profile are time-invariant, the lower exponential region seems to have the key role in describing how particles at the base of the flowing layer come to rest. We here propose that within this region, the flow velocity decreases below a critical threshold, which causes a rapid decline in granular temperature and an increase in inter-particle friction. Taking a typical speed of 10 cm/s and thickness of 0.5 cm for the exponential region gives a time-scale of 0.05 s. It might be worthwhile testing through molecular dynamics simulation, for example, whether this time-scale is relevant in describing how an agitated particulate system becomes motionless when external forcing is removed. The data presented in Lajeunesse et al. (2005) for different grain diameters give reason to assume that form and/ or depth of the exponential region may vary with the particle characteristics. Detailed investigations making use of a high resolution, high-speed camera of the exponential region for flows where the grain diameter is varied by at least an order of magnitude will provide further insight. Moreover, it will be most interesting to investigate the dynamics of the interface for collapses in inclined channels, in particular approaching the static angle of repose (AOR). When the basal inclination is equal to the AOR, the interface may coincide with the rigid base. To further stress this idea, at inclination sufficiently above the AOR, even downward motion of the interface into loose bed material could be expected, giving a framework to describe both sedimentation and erosion from granular flows.

REFERENCES

Anderson, K.G. & Jackson, R. 1992 A comparison of the solutions of some proposed equations of motion of granular materials for fully developed flow down inclined planes, J. Fluid Mech. **92**, 145.

Balmforth, N.J. & Kerswell, R.R. 2005 Granular collapse in two dimensions. J. Fluid Mech. **538**, 399-428.

Bonamy, D., Daviaud, F. & Laurent, L. 2002 Experimental study of granular surface flows via a fast camera: a continuous description. Phys. Fluids, **14**, 1666-1673.

Dalziel, S.B. 2005 DigiFlow User Guide, http://www.damtp.cam.ac.uk/lab/digiflow/.

G.D.R. Midi 2004 On dense granular flows. Eur. Phys. J. E **14**, 341.

Huppert, H.E., Hallworth, M.A., Lube, G. & Sparks, R.S.J. 2003 Granular column collapses Bull. Am. Phys. Soc. **48**, 68.

Iverson, R. M. & Denlinger, R. P. 2001 Flow of variably fluidized granular masses across three-dimensional terrain. Part I: Coulomb mixture theory. J. Geophys. Res. **106**, 537–552.

Kerswell, R. R. 2005 Dam break with Coulomb friction: A model for granular slumping? Phys. Fluids **17**, 057101, 1–16.

Lajeunesse, E., Mangeney-Castelnau, A. & Vilotte, J. P. 2004 Spreading of a granular mass on a horizontal plane. Phys. Fluids **16**, 2371–2381.

Lajeunesse, E., Monnier, J.B. & Homsy, G.M. 2005 Granular slumping on a horizontal surface. Phys. Fluids **17**, 103302.

Lube, G., Huppert, H. E., Sparks, R. S. J & Hallworth, M. A. 2004 Axisymmetric collapses of granular columns. J. Fluid Mech. **508**, 175–199.

Lube, G., Huppert, H.E., Sparks, R.S.J. & Freundt, A. 2005 Collapses of two-dimensional granular columns. Phys. Rev. E **72**, 041301.

Margreth, S., Stoffel, L. & Wilhelm, C. 2003 Winter opening of high alpine pass roads - analysis and case studies from the Swiss Alps. Cold Reg. Sci. Technol. **37**: 467-482.

Pouliquen, O. 1999 Scaling laws in granular flows down rough inclined planes. Phys. Fluids **11**, 542-548.

Pouliquen, O., Cassar, C., Forterre, Y., Jop, P. & Nicolas, M. 2005 How do grains flow: towards a simple rheology of dense granular flows. Proceedings Powders & Grains.

Savage, S. B. & Hutter, K. 1989 The motion of a finite mass of granular material down a rough incline. J. Fluid Mech. **199**, 177–215.

Savage, S. B. 1998 Analyses for slow quasi-static, high concentration flows of granular materials. J. Fluid Mech. **377**, 1–26.

Sparks, R.S.J. & Aspinall, W.P. 2004 Volcanic Activity: Frontiers and Challenges in Forecasting, Prediction, and Risk Assessment. AGU Geophysical Monograph "State of the Planet" 150, IUGG Monograph 19, 359-374.

Staron, L. & Hinch, E.J. 2005 Study of the collapse of granular columns using DEM numerical simulation. J. Fluid Mech., **545**, 1-27.

Zenit, R. 2005 Computer simulations of the collapse of a granular column. Phys. Fluids **17**, 031703, 1–4.

Chapter VII

Granular column collapses down rough, inclined channels

Abstract

We present experimental results for the collapse of rectangular columns of sand down rough, inclined channels. The basal inclination α was varied from 4.2° to 25°, and the results are compared with previous results for horizontal channels. Two different forms of flow behaviour occur dependent on the value of the initial aspect ratio $a = h_i/d_i$ (where h_i and d_i are the initial height and basal length of the column, respectively). For small aspect ratios only a marginal part of the column participates in the motion, whereas for large aspect ratios the entire upper free surface collapses. For $\alpha \leq 20°$ and $a > 2.8$, the deposit geometry satisfies a self-similar form with respect to their maximum vertical and horizontal extent. The maximum runout distance, the maximum deposit height and the time to reach the maximum runout can be expressed by dimensional analysis as functions comprising separate terms for a and α. The inertial flows are characterised by a moving internal interface separating flowing and static regions of material. For $a > 2.8$, there are two flow regimes. In the first, free-fall phase, the deposited area A_D below the internal interface varies with the square root of time independent of the initial height and the basal inclination. In the subsequent lateral spreading phase, the deposition rate decreases with increasing basal inclination and increases with the initial height. The local deposition rate at fixed longitudinal distances is a constant dependent on the initial aspect ratio, the basal inclination and the longitudinal position, but invariant with flow velocity and depth. The local deposition rate decreases with increasing basal inclination. In the lateral spreading phase, there is a universal velocity profile in the flowing layer for each value of a and α comprising a lower exponential and an upper linear region. The velocity profiles are independent of flow depth and the velocity and can be characterised by a shear rate as $\gamma(\alpha, \tilde{h}_i) = c_S(\alpha)\left(g / \tilde{h}_i\right)^{1/2}$, where $\tilde{h}_i$ is a length-scale describing the fraction of the column involved in flow, and c_S is an increasing function of the basal inclination.

1. Introduction

The physical behaviour of granular media is a relatively young but already extensively studied research discipline. Its ubiquitous applications in industrial processes, engineering problems, and agriculture and its prominence in geological processes have resulted in interdisciplinary investigations from a wide range of research fields. Of particular interest for the hazard assessment of geophysical mass flows is the flow and deposition behaviour in granular free-surface flows driven by gravity.

Currently, there are two major problems in understanding natural particulate flows, such as avalanches of debris and snow, and pyroclastic flows formed in explosive volcanic eruptions. First, measurements on active flows are sparse. Except for some recent field studies on snow avalanches (Gauer *et al.* 2006), measurements are restricted to approximations of their flow front velocity. Most of our current knowledge on flow and deposition mechanisms stems from interpretations of their final deposits. However, as the detailed mechanisms of deposition remain hitherto unknown, these interpretations currently are rather loose and qualitative. The second problem is that, although a variety of theories and governing equations for particular aspects of granular flow have been established, these mostly describe flows of mono-disperse particles in steady, uniform motion. Possibly the most-investigated situation of gravitational free-surface flows is the motion of thin frictional sheets of particles at inclinations close to the static angle of repose (e.g. Savage & Hutter 1989, Pouliquen 1999, Pouliquen & Forterre 2002). A review of the models for chute and heap flows as well as flows in rotating drums was recently published by G.D.R. Midi (2004). Geophysical mass flows, however, are characterised by their unsteady form of motion, a high mobility as they propagate over terrain well below the angle of repose (AOR), and time- and space-dependent processes of erosion and deposition.

Recently, a number of studies started investigating thick, inertial granular flows formed by the sudden release of vertical columns of particles. So far, investigations have focussed on the flow behaviour above a horizontal base and have considered unhindered axisymmetric collapses from cylinders (Huppert *et al.* 2003, Lajeunesse *et al.* 2004, Lube *et al.* 2004a, b) and wall-bounded collapses from rectangular columns into channels (Huppert *et al.* 2003, Mangeney-Castelnau *et al.* 2004, Balmforth & Kerswell 2005, Kerswell, 2005, Lajeunesse *et al.* 2005, Lube *et al.* 2005, Siavoshi & Kudrolli 2005, Staron & Hinch. 2005, Zenit *et al.*

2005, Larrieu *et al.* 2006, Lube *et al.* 2006, and Thompson & Huppert 2006). Granular collapse flows are characterised by their unsteady form of motion, large time-dependent changes of the free surface and the creation of final deposits through the continuous upward propagation of an internal interface separating already deposited from still moving material. As a consequence of the internal interface motion, the flow propagates on a layer of deposited material (for most of its length), and hence the flow behaviour is independent of the roughness of the rigid base. Furthermore, inertial forces largely dominate frictional (inter particle) forces except for the very last stage of surface avalanching, which insignificantly alters the overall shape of the deposits. Thus, most aspects of flow are also largely independent of the grain type, and the shape of the deposits, including their maximum vertical and horizontal extension, and the time to reach the final maximum runout can be described solely in terms of the initial geometry of the granular column and the gravitational constant.

Whereas inertial granular collapse flows show a number of similarities with natural particulate flows, such as the ability to propagate at slopes below the AOR, time- and space-dependent deposition processes, and the relatively immaterial effect of inter-particle friction, they differ largely from uniform frictional sheet flows e.g. down rough chutes at inclinations close to the static AOR. This study presents experimental results for granular collapse flows into rough, inclined channels. The major aims of this investigation are to elucidate:
- which additional processes occur when the base of the channel is systematically steepened?
- up to which inclinations do the mathematical relationships obtained for the horizontal case describe flow behaviour on inclined planes?
- how does the behaviour of the internal interface and the form of velocity profiles in the flowing layer change with the basal inclination?

The paper is organised as follows. In section 2, we give a description of the experimental set-up and the measurement techniques. Section 2 briefly summarises the observed flow behaviour. An analysis of the shape of the final deposits including its maximum horizontal and vertical extension is presented in section 3. In section 4, we present an analysis of the time t_∞ to reach the maximum runout distance as a function of the initial geometry of the column and the basal inclination. This section also describes the position of the flow front as a function of time. Section 5 elucidates the effect of the basal inclination on the behaviour of the internal interface and the velocity profiles. Finally, we summarise and discuss the results obtained in section 6.

2. The experiments

2.1. Experimental set-ups

The experiments investigate two-dimensional granular flows formed by the collapse of rectangular columns of sand into a wide, inclined channel. The channel had a constant width of 20 cm whose rear panel was constructed of wood and covered with a thin sheet of paper, whereas its frontal panel was transparent Plexiglas. The basal panel was roughened by gluing sheets of sandpaper to it. The basal inclination of the tank, α, was varied from 4.2° to 25°. A container accommodated the granular material at one end of the tank (Figure 1). A rectangular box of the same width, 20 cm, as the channel and variable initial basal length d_i comprised a frontal gate to release the granular material. A release mechanism was constructed to allow for very fast and reproducible lifting velocities of the gate. It consisted of releasing a large weight connected to the gate via a pulley construction at the ceiling. The weight fell freely for the first 0.75 m to reach a high velocity (approximately 4 m s^{-1}) before it lifted the gate extremely rapidly. The time for the gate release in any experiment was very much less than the typical time scale of the resultant motion.
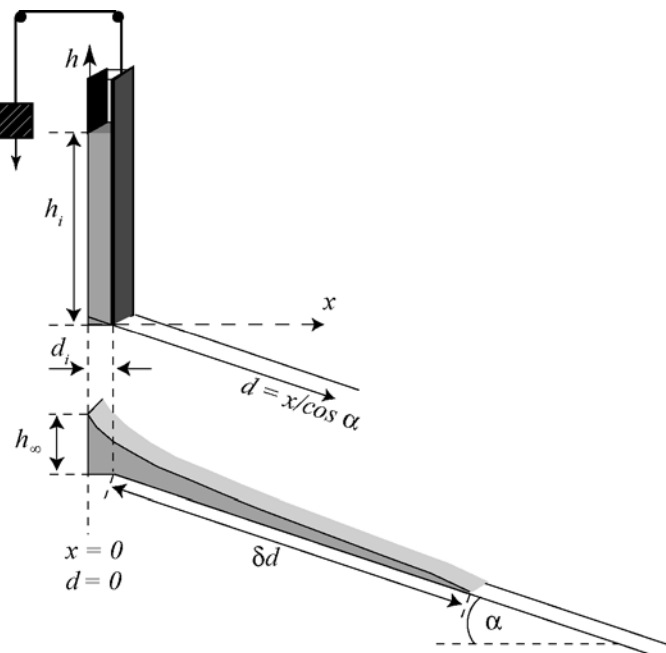
Figure 1. The experiments set-up with a sketch of the initial column of particles (top), the final deposit (bottom) and the definition of the coordinate system used.

We employed a mixture of industrial black and light grey coloured Quartz sands of grain-size 1.4 ± 0.4 mm with a (static) angle of repose of 31°. This was found to give the best contrast results for the digital image analysis described below. The initial aspect ratio a, defined by the ratio of initial height, h_i, to initial basal length, d_i, was varied systematically over roughly two

orders of magnitude. The initial basal lengths and range of aspect ratios for the different values of basal inclination are presented in Table I.

Basal inclination	Initial basal length d_i (cm)	Range in $a = h_i/d_i$
4.2°	6.3	0.8–14.1
10°	6.3	0.8-7.9
15°	6.05	0.5-14.3
	9.05	3.0-7.0
20°	6.05	3.2–11.7
	9.05	0.2-2.4
25°	6.05	0.4-9.0

TABLE 1. Initial basal length and range of initial aspect ratio for each inclination.

2.2. Measurement methods

After each experiment the maximum runout distance δd, the distance from the gate to the final front, was measured along the inclined plane (Figure 1). Height profiles $h(x)$ of the final deposits were obtained by measuring the vertical height difference between the upper free surface and the inclined base at horizontal spacing of 2 cm. In the following, the subscript $h(x)$ is used as the vertical coordinate; x is the horizontal coordinate with $x = 0$ starting at the rear of the reservoir; and $d = x/cos\alpha$ is the longitudinal coordinate along the inclined plane.

Experiments were recorded by a fast camera at 120 frames per second (fps) to investigate the behaviour of the collapses through the vertical Plexiglas plane. From these movies we measured the instantaneous position of the flow front as a function of time, $d(t)$, and the time t_∞ when the motion of the flow front ceased.

Experiments with $a = 5$, 7 and 9 at inclinations of 4.2°, 15°, 20° and 25° were repeated and recorded by two cameras to investigate the time-dependent form of the internal interface and velocity profiles with depth. Before preparing the initial columns of sand, a 5 mm grid was tied to the inner side of the frontal pane to give a reference frame. With the fast digital camera at 120 fps the entire flow was filmed through the transparent frontal pane. To obtain curves of the interface between static and flowing particles, $h_D (x, t)$, we first analyzed every fifth and sixth frame using the Pattern Match algorithm of Dalziel (2005). Finally, we carefully corrected, were necessary, these curves to match exactly the interface between the uppermost static and the lowermost flowing particle. A digital high-resolution, high-speed camera operating at 1000 fps was positioned as close as possible and perpendicular to the inclined plane at a distance $\delta d/3$ from the gate (Figure 1). Detailed velocity profiles with depth in the

flowing layer were obtained using the particle image velocimetry (PIV) algorithm written by Dalziel (2005).

3. Experimental observations

Much of the flow behaviour of granular collapse flows into rough, inclined channels is very similar to that previously reported for collapses into horizontal channels (Huppert *et al.* 2003, Lube *et al.* 2005, Balmforth & Kerswell 2005 and Lajeunesse *et al.* 2005). We will thus give a brief description of these collapses and elucidate the major differences between the two cases.

Upon suddenly lifting the gate, an initial discontinuity develops within the granular column separating a lower static from an upper moving region in each experiment. In cross-section it is observed as a straight line intersecting at a zero height at $x = d_i$, where x is the horizontal distance from the origin. This initial line is inclined at approximately 60° to the horizontal independent of a and α. Lajeunesse et al. (2005) have reported that for spherical glass beads (and $\alpha = 0°$) this inclination is slightly lower but also independent of a. This discontinuity represents the initial shape of the internal interface, which propagates towards the upper free surface as the grains run out.

Two main kinds of flow behaviour occur depending on the value of the initial aspect ratio. For aspect ratios smaller than 1.7, only an outer marginal part of the column is involved in the motion. This flowing region propagates down the inclined plane. Contrasting behaviour of the motion of the internal interface is observed for the outer part of the flow in contrast to the region close to the origin. In the outer part, the interface propagates upwards, effectively depositing material. Close to the origin, the interface moves slightly downwards before its position equilibrates towards the end of the experiment. As material flows downwards, the interface eventually reaches the upper free surface along the entire flow length. As for the horizontal case, there is some final stage of thin avalanching across the upper free surface before the motion stops. The erosive behaviour causes two different forms of deposit shapes for the low aspect ratio regime. At $a < 1$, some part of the initial upper surface of the column remains undisturbed at a final height $h_\infty = h_i$, and the final deposit has a truncated wedge form. For $1 < a < 1.7$, the entire upper free surface becomes mobilised in the late stage of the experiment resulting in wedge shaped deposits. For larger aspect ratios, the entire upper free

surface flows from the beginning. For $a > 2.8$, we observe to stages of motion. There is an initial free-fall phase, during which the upper part of the column above a critical height of approximately 2.8 d_i is in purely vertical motion. In this phase, the internal interface propagates upwards, except for the region within the reservoir, where some slight downward motion is observed. Once the upper free surface of the column has reached the critical height of 2.8 d_i, particles in the entire flowing region spread outwards, and the interface propagates upwards throughout the flow. This second stage of motion is referred to as the lateral spreading phase.

With increasing basal inclination a different form of flow behaviour than for the horizontal case occurs. For aspect ratios larger than ten and within a region 1/3 to 1/2 of the final maximum runout distance, the generally continuous upward motion of the internal interface is interrupted. In this region, the flowing layer does not comprise a unique velocity profile as discussed later in section 6.2. The flow first divides into two vertical regions within each shows a velocity profile (normal to the plane) with a lower exponential and an upper linear part. A short time after the development of these regions, the lower region stops quite abruptly and the internal interface jumps upwards from its current position to the base of the upper horizontal region. In this region, the upper free surface develops a pronounced bump-like disturbance that also remains preserved in the final deposit. This behaviour becomes particularly strong for large aspect ratio experiments at inclinations of 15° and 20°. In addition, for inclinations up to 20° the internal interface reaches the upper free surface along the entire flow length approximately simultaneously and terminates motion. At the steepest studied inclination of 25°, however, the internal interface reaches the upper free surface of the rear region first, after which the still moving frontal region decouples and propagates further as a mobile flow that thins out to a thickness of a few grain diameters.

4. Final geometry

4.1. Final height profiles

The contours of the final deposits vary with both the initial aspect ratio and the basal inclination. To allow a comparison between all the profiles, we here consider data of the vertical depth between the upper free surface and the inclined plane at horizontal spacing. Thus, in the non-inclined reservoir the deposit depths were reduced by *(d_i - x)tan α*. The influence of the basal inclination is illustrated in figure 2. This graph, which shows profiles of five experiments where *a* was kept constant at *a* = 7 and α was varied from 4.2° to 25°, gives
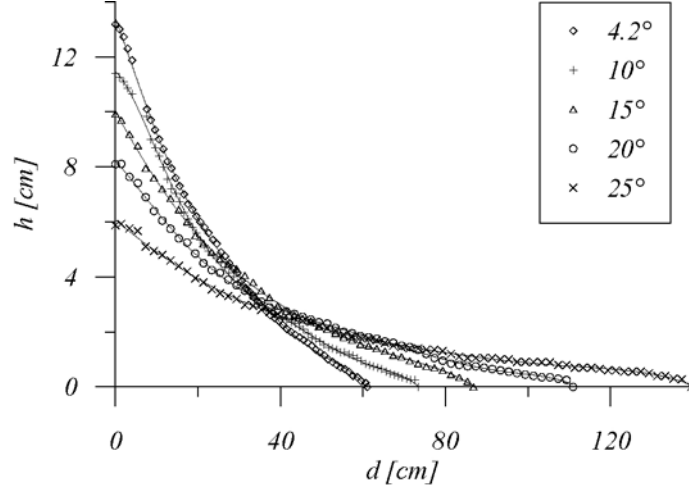
Figure 2. Shape of final deposits for five experiments with constant initial height h_i (~ 44 cm) and basal length d_i (6.05 cm) at inclinations from 4.2° to 25°.

an impression how the deposits become progressively thinner and elongated with increasing inclination. The final profiles for experiments with varying aspect ratio while α is kept constant is shown in figure 3a-e. At inclinations of 4.2°, 10° and 25°, the profiles are relatively smooth curves. At α = 15° and α = 20°, the profiles comprise a pronounced bump-like disturbance, whose amplitude and distance from the origin increase with the aspect ratio.

The contours of the final deposits can be written in non-dimensional form as

$$h(x)/\tilde{h}_\infty = \eta(x/d_\infty, a, \alpha) \tag{1}$$

where $\tilde{h}_\infty = h_\infty - d_i \cos\alpha$ and $d_\infty = \delta d + d_i / \cos\alpha$. We will now test whether the function η can be split into two dimensionless functions $\tilde{\eta}$ and F_P as $h(x)/\tilde{h}_\infty = \tilde{\eta}(x/d_\infty, a)F_P(\alpha)$ to allow a separate analysis of the effect of the aspect ratio and the basal inclination. For the function $\tilde{\eta}$ of a and x/d_∞ we know by definition that

$$\tilde{\eta}(0,a) = 1 \text{ and } \tilde{\eta}(1,a) = 0. \tag{2}$$

Lube et al. (2005) have shown that for α = 0° in the second flow regime ($a>2.8$), the height profiles obey a self-similarity of the form

$$h(x)/\tilde{h}_\infty = \tilde{\eta}(x/d_\infty), \tag{3}$$

where the non-dimensional profiles are independent of the aspect ratio. In figure 3f-j the height profiles are presented in non-dimensional form for each inclination respectively. It is seen that there is a very good collapse for α = 4.2° and α = 10° (as there is for α = 0°, Lube *et al.* 2005). There is some minor scatter for the non-dimensional, collapsed profiles at α = 15° and α = 20°, which, however, can be attributed to the bump-like disturbances mentioned
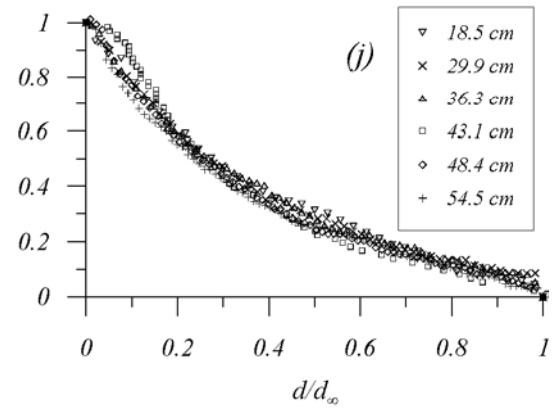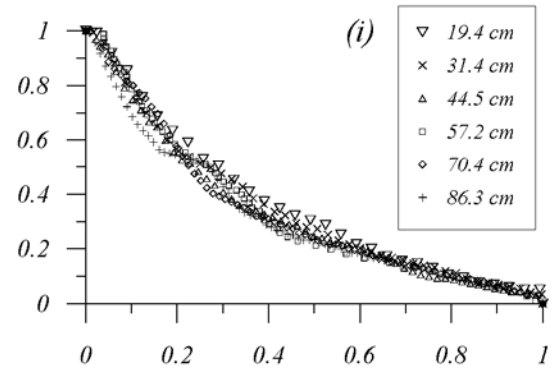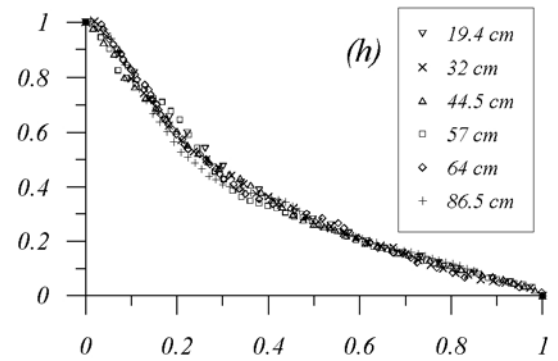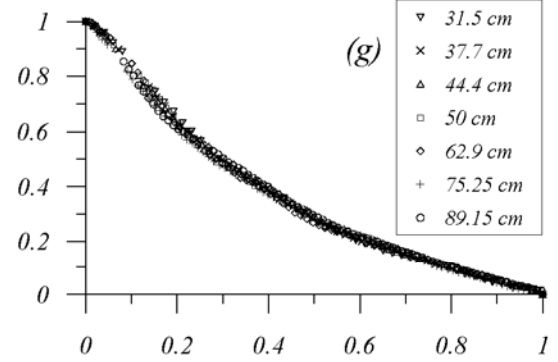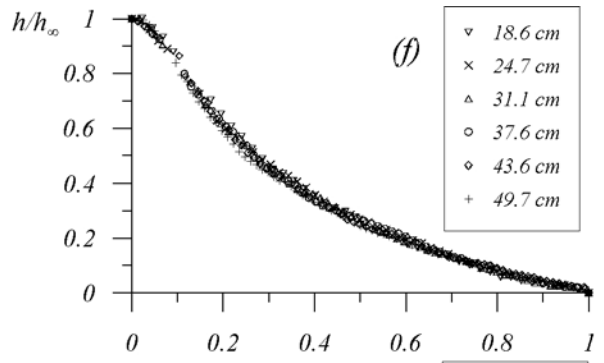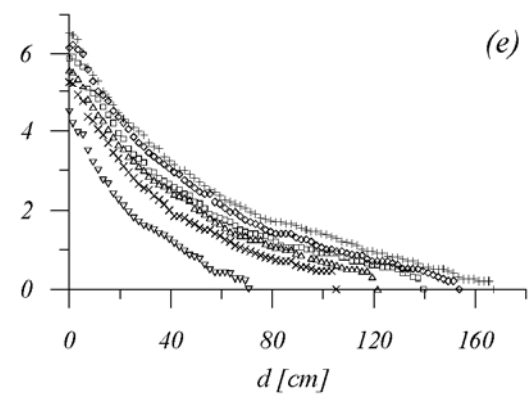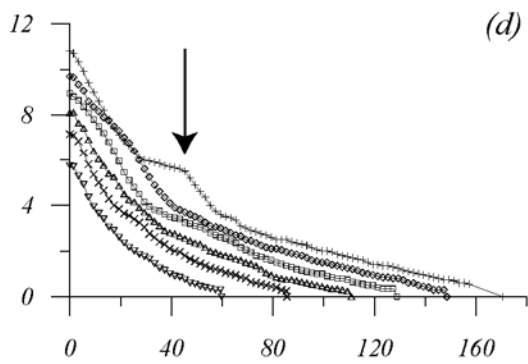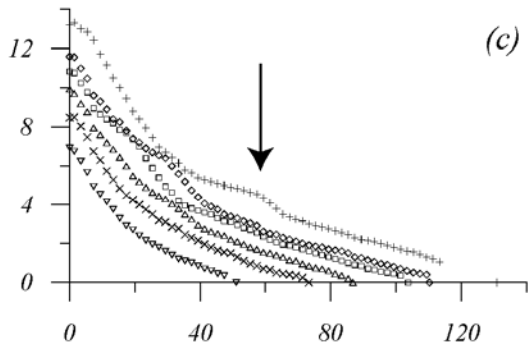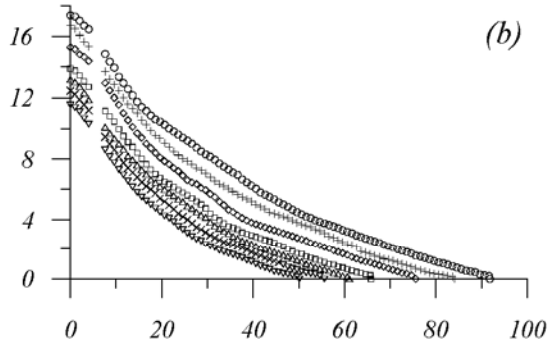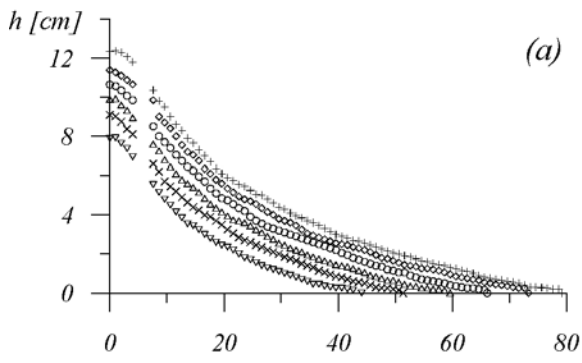
Figure 3 (previous page). Shape of final deposits for experiments with aspect ratios ranging from 3 to 14.3 in non-normalised and normalised form for (a, f) 4.2°, (b, g) 10°, (c, h) 15°, (d, i) 20° and (e, j) 25°. Arrows mark examples of the bump-like disturbance.

previously. No satisfactory collapse occurs for $\alpha = 25°$, where the height profiles do not include such a disturbance, but still vary with a in non-dimensional form. Plotting the height profile data of figure 2 for $a = 7$ in non-dimensional form (Figure 4), shows that a dependence on the basal inclination exists. To understand the function F_P better, we will now analyse the dependence of d_∞ and h_∞ on a and α.
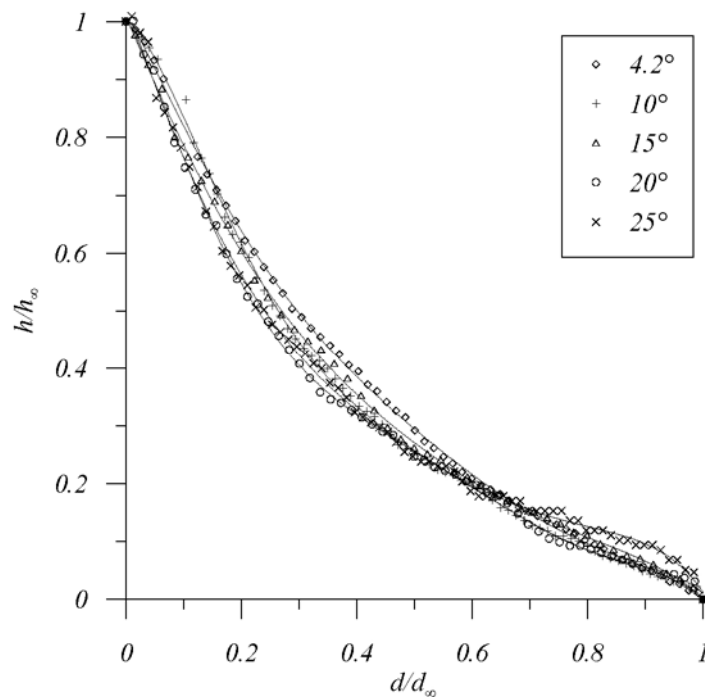
Figure 4. Shape of final deposits for the data shown in figure 2 in non-dimensional form.

4.2. Scaling arguments for the maximum runout distance

Experimental observations that the form of collapse differs with both the aspect ratio and the basal inclination, immediately suggest using a and α as the fundamental parameters for the analysis of the maximum runout distance. For $\alpha = 0°$, it was shown that a is the only parameter and, because inertial effects dominate frictional effects, the collapses are independent of the particle characteristics (Huppert *et al.* 2003; Lajeunesse *et al.* 2004, 2005; Lube *et al.* 2004a-b, 2005). Also, because most of the flow propagates on a layer of already deposited material the flow behaviour is also independent of basal friction (Lajeunesse *et al.* 2005; Lube *et al.* 2005, 2006). This is in contrast to steady, frictional flows on inclines close to the static angle of repose that reveal a strong dependence on the basal roughness. The
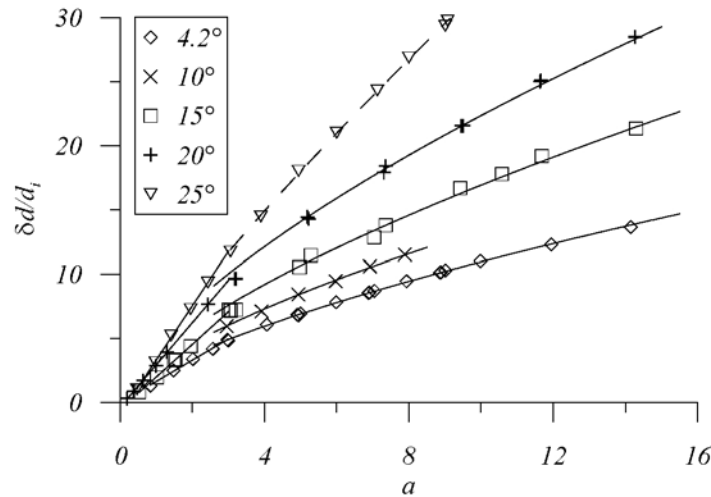
Figure 5. The normalised maximum runout distance against the aspect ratio for basal inclination ranging from 4.2° to 25°. Linear best-fits are drawn to the data with a < 2.8. The solid lines for the experiments with a > 2.8 represent powerlaw functions of the form $\delta d / d_i = k_H(\alpha)a^{2/3}$. The dashed line for the experiments at 25° represents the best-fit powerlaw through the data a > 2.8.

basal roughness is not varied in our experiments. Further, we assume that the maximum runout distance can be expressed by dimensional arguments as a function of two separate non-dimensional terms for a and α

$$\delta d = d_i \zeta(a) F_D(\alpha) \ . \tag{4}$$

For small values of a, where only the outer margin of the column takes part in the flow, the collapse is independent of d_i and (4) simplifies to

$$\delta d = k_L(\alpha)h_i, \tag{5}$$

where k_L is a constant dependent on the basal inclination. At large aspect ratio ζ depends on both h_i and d_i. For the case of $\alpha = 0°$, it was shown experimentally that $\zeta \propto a^{2/3}$ (Lajeunesse *et al.* 2005; Lube *et al.* 2005). An analytical explanation for this scaling was provided by Lajeunesse *et al.* (2005).

In figure 5 we plot the data of the maximum runout distance normalised by d_i for the different values of a and α. For all values of α and $a < 2.8$, δd varies linearly according to (5). At $a > 2.8$ and for $\alpha \leq 20°$, the data are well represented by powerlaws of the form

$$\delta d / d_i = k_H(\alpha)a^{2/3}. \tag{6}$$

At $\alpha \leq 25°$ the runout data are not well described by a two-thirds powerlaw. A best-fit through the data gives $\delta d / d_i = 4.6a^{0.84}$. This deviation demonstrates the different flow behaviour that
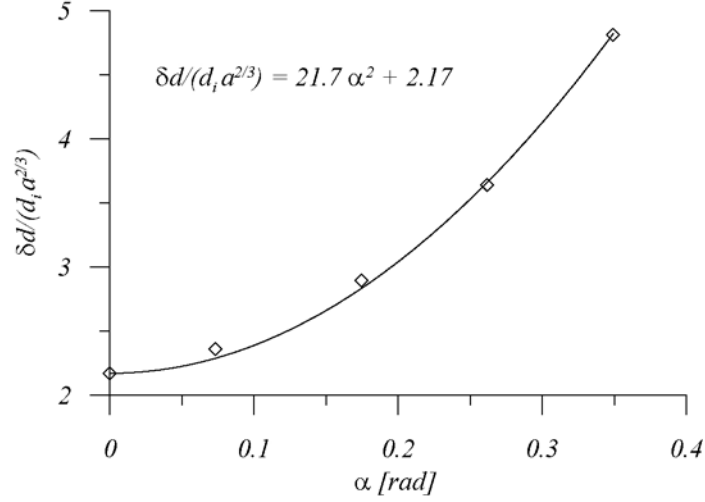
Figure 6. The maximum runout distance normalised by $d_i a^{2/3}$ plotted against the basal inclination.

occurs when the basal inclination becomes close to the angle of repose. In order to specify the functional form of F_D, we plot $\delta d /(d_i a^{2/3})$ against α (Figure 6). Data can be approximated by the semi-empirical functions

$$\delta d /(d_i a^{2/3}) = k_H(0) + 21.7\alpha^2 \text{ (for } a>2.8),\tag{7}$$

where $k_H(0) = 2.17$ for different grain forms and sizes (Lube *et al.* 2005).

4.3. Scaling arguments for the maximum height

The maximum deposit height at $x = 0$ also depends on a and α, and we assume the mathematical description can be expressed as a function of two separate terms for a and α as

$$h_\infty = d_i \varphi(a) F_H(\alpha),\tag{8}$$

where φ and F_H are dimensionless functions of the aspect ratio and the basal inclination, respectively. The functions can be determined for small values of a, where $h_\infty = h_i$, and thus $\varphi(a) = a$ and $F_H = 1$ as demonstrated for the data $a \leq 1$ (Figure 7). For $a > 1$, best-fits of the data h_∞/d_i against the aspect ratio indicate a powerlaw form ma^n, where both m and n vary with a and α. However, when instead of h_∞ the modified final height $\tilde{h}_\infty = h_\infty - d_i \tan\alpha$ is plotted as $\tilde{h}_\infty / d_i$ against a (Figure 8), the data for α ≤ 20° are nicely represented in the form

$$\tilde{h}_\infty / d_i = c_H(\alpha) a^{2/5}.\tag{9}$$

The variation of c_H with the basal inclination is presented in figure 9 showing the ratio $\tilde{h}_\infty /(d_i a^{2/5})$ plotted against α. The data are well represented by the semi-empirical fit

$$\tilde{h}_\infty /(d_i a^{2/5}) = c_H(0) - 1.58\alpha^{4/3},\tag{10}$$
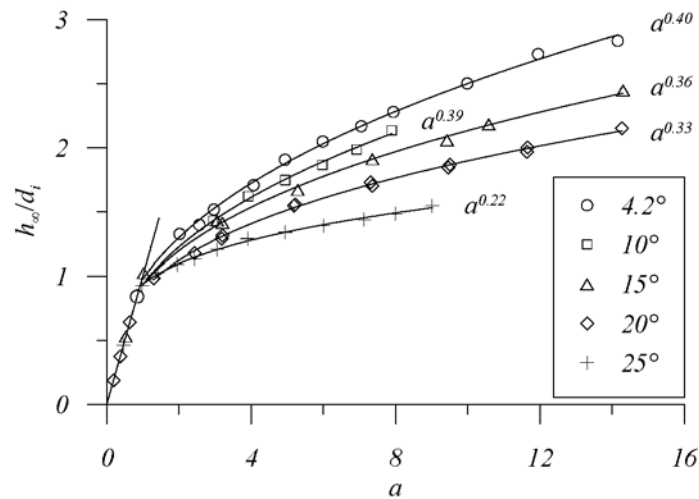
Figure 7. The normalised maximum deposit height plotted against the aspect ratio.
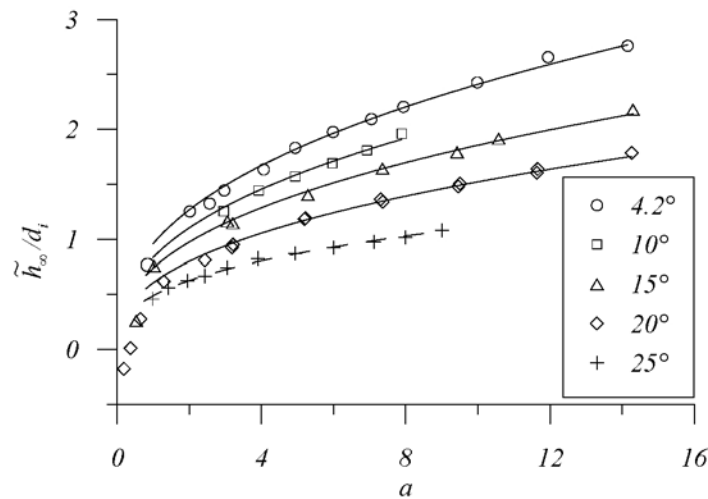

Figure 8. The modified maximum deposit height plotted against the aspect ratio. The solid lines represent functions of the form $\tilde{h}_\infty / d_i = c_H(\alpha) a^{2/5}$. The dashed line shows the best-fit powerlaw through the data for $\alpha = 25°$.
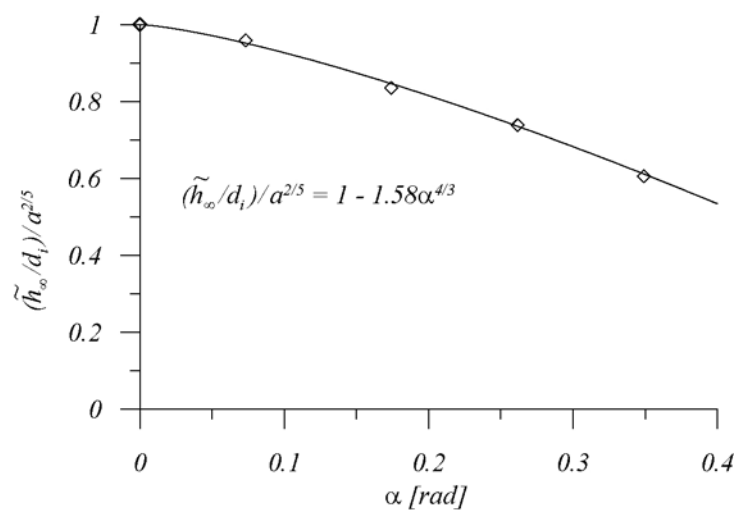

Figure 9. The experimentally determined values for $c_H(\alpha) = \tilde{h}_\infty /(d_i a^{2/5})$ against the basal inclination.

149

where $c_H(0) = 1$ for different grain types and basal roughness (Lube *et al.* 2005). As for the maximum runout distance, the final height data for $\alpha = 25°$ at $a > 1$ cannot be described in the same function as all the other data. A best-fit powerlaw through the data reveals $\tilde{h}_\infty / d_i = 0.49 a^{0.36}$.

5. Flow front kinematics

From the time-dependent data of the instantaneous flow front position we can obtain the time, t_∞, at which the motion at the flow front ceases. For $\alpha = 0°$ this time depends only on the initial height h_i and g as $t_\infty \propto (h_i / g)^{1/2}$ (Lajeunesse *et al.* 2005, Lube *et al.* 2005). In analogy to the maximum runout and maximum height, we can express t_∞ as

$$t_\infty = (h_i / g)^{1/2} F_T(\alpha). \tag{11}$$

In figure 10 we plot data of t_∞ against the time-scale $(h_i/g)^{1/2}$. Data is nicely represented by linear functions of the form

$$t_\infty = F_T(\alpha)(h_i / g)^{1/2}. \tag{12}$$

The variation of F_T with the basal inclination is shown in figure 11. As for δd and h_∞, a powerlaw function describes the data as $t_\infty /(h_i / g)^{1/2} = F_T(0) + 9.84\alpha^2$, where $F_T(0°)$ equals 3.27 for different types of grains and basal roughness (Lube *et al.* 2005). The data for $\alpha = 25°$ is a slightly too scattered to analysed with confidence.
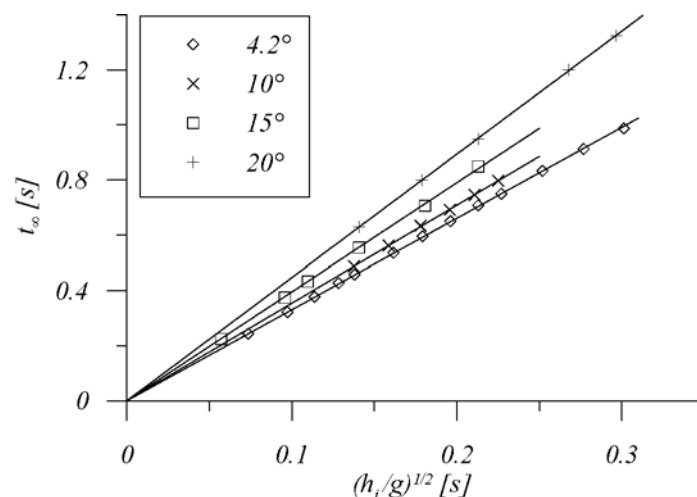

Figure 10. The final time t_∞ plotted against the time-scale $(h_i/g)^{1/2}$ for experiment with different aspect ratios and basal inclinations.

Figure 12 shows the position of the flow front as a function of time for several experiments where α was kept constant and the aspect ratio was varied from 3 to 14.3. There is an initial
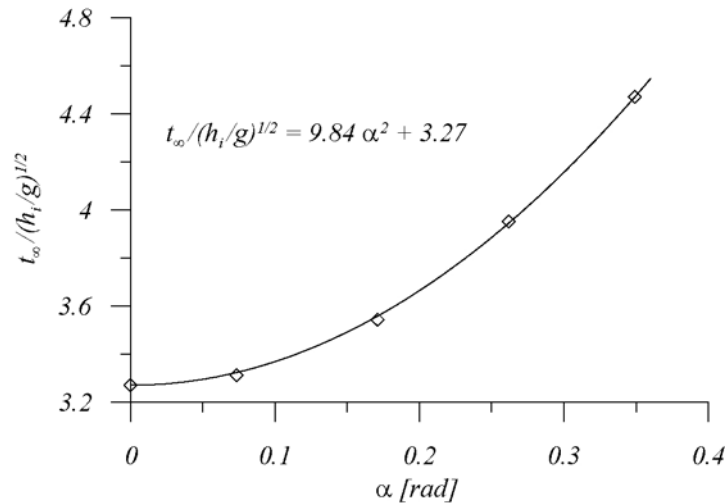
Figure 11. The normalised final time $t_\infty/(h_i/g)^{1/2}$ plotted against the basal inclination.

acceleration phase followed by a phase of approximately constant velocity before the flow fronts decelerate to come to an abrupt halt. The plots also show that the flow front propagation in the first two phases is independent of the value of h_i. The value of the constant velocity increases with the basal inclination.

6. Static and moving regions

6.1. Motion of the internal interface

The motion of the internal interface between static and moving particles was analysed by two different approaches. First, by integrating under the entire internal interface we obtained data for the static area, A_D, as a function of time for different a and basal inclinations of 15°, 20° and 25°. Second, in order to characterise vertical deposition rates, we measured the thickness of the static region, $h_D(d, t)$, at fixed distances, d.

The typical form of the A_D against time curves are shown in figure 13 for four experiments at 15° and aspect ratios varying from 5.3 to 14.3. The data are plotted as A_D - A_W against time in figure 13a, where $A_W = 0.5d_i^2 tan60°$ is the area of the initial static wedge, and hence the initial value of A_D. The two phases of collapse, the initial free-fall phase and the subsequent lateral spreading phase, are evident in this graph. In the free-fall phase the static area increases with time independent of the initial height. The collapsed data follows the relationship $A_D - A_W \propto t^2$. At a time depending on a, the data departs from this universal curve and the static area increases at a lower rate. For the two large aspect ratio experiments with $a = 10.6$ and $a = 14.3$, A_D varies approximately linear with time in this lateral spreading phase. Thus, for these cases the deposition rate dA_D/dt is effectively constant. For the two experiments with $a = 5.3$
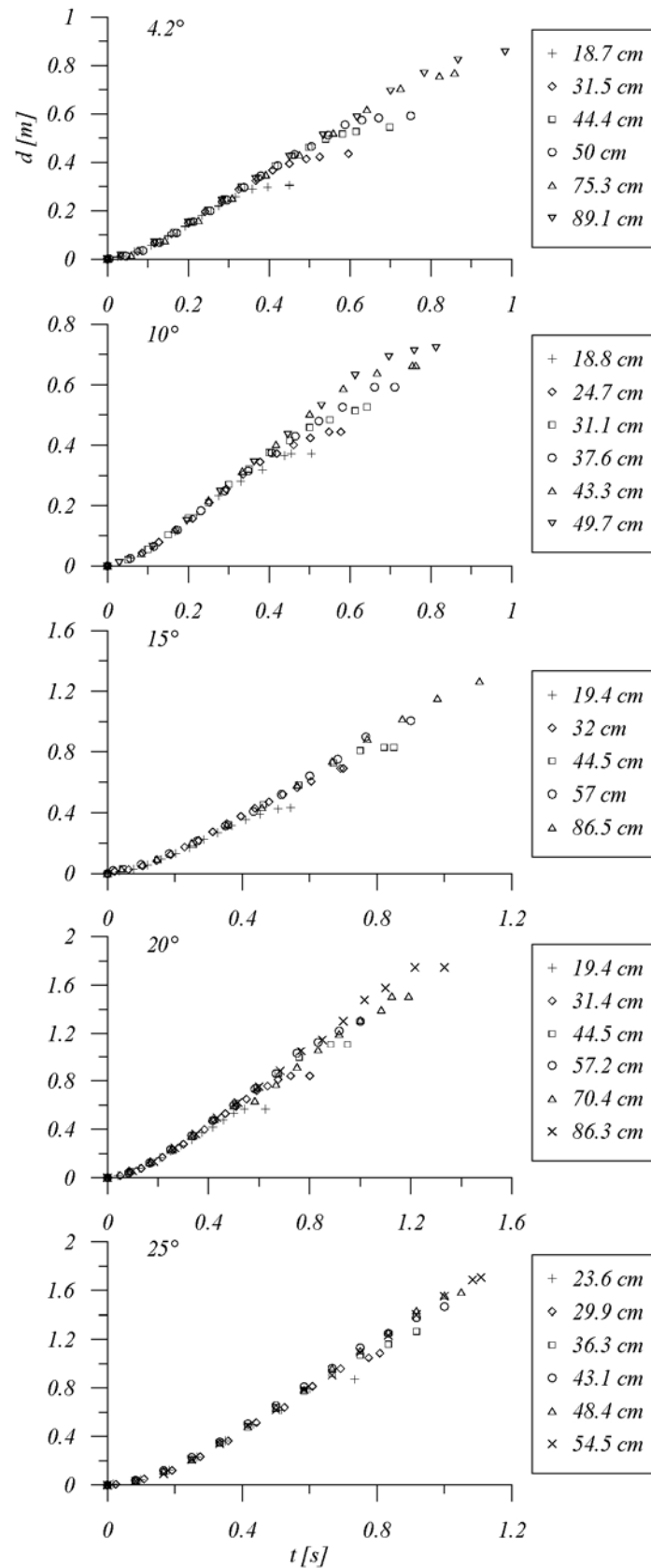
Figure 12. The position of the flow front as a function of time for 4.2°, 10°, 15°, 20° and 25°.

and $a = 7.3$, however, the deposition rate in the second phase is not constant but increases with time.
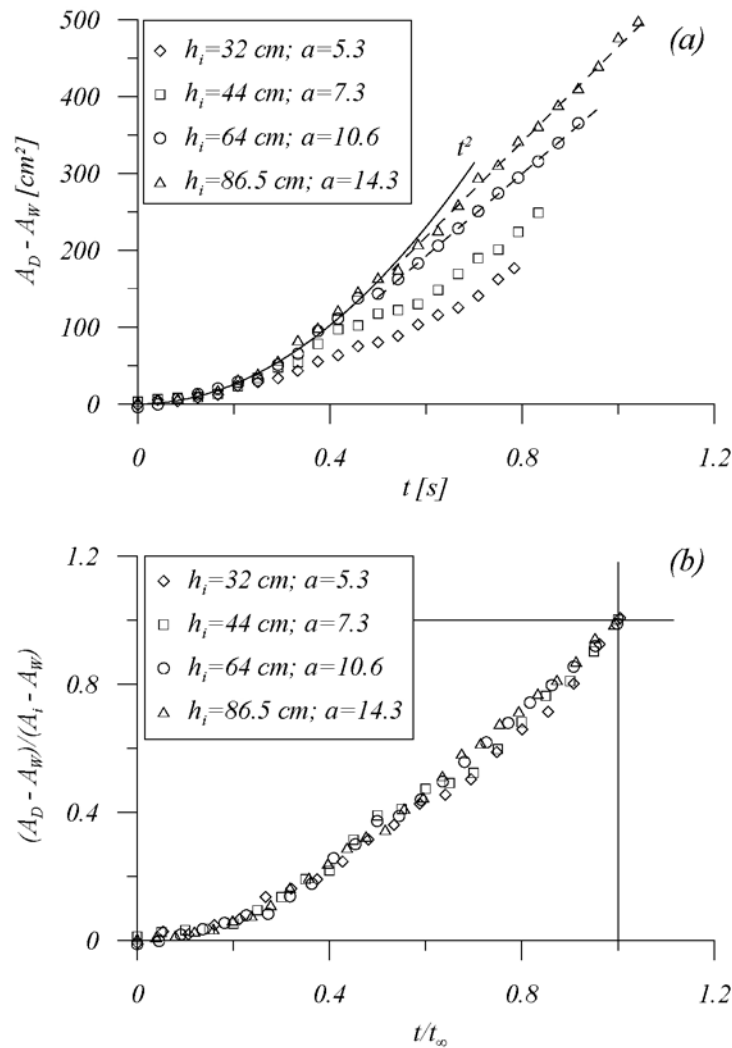
Figure 13. The deposited area below the internal interface as a function of time for four experiments at 15° in (a) non-normalised and (b) normalised form.

In figure 13b the same data is shown in non-dimensional form, where $(A_D - A_W)$ is normalised by $(A_i - A_W)$ and time by the final emplacement time t_∞, and $A_i = h_i d_i$. As shown by Lube et al. (2006) for $\alpha = 0°$, this scaling collapses the data onto a universal curve. The collapse, however, is not perfect in the lateral spreading phase. Whereas the data for $a = 10.6$ and $a = 14.3$ (for which the deposition rate is constant with time) merge quite well, a slight departure is seen for the two experiments at lower aspect ratios.

Unfortunately, the data for $\alpha = 20°$ and $25°$ is slightly too scattered to be analysed with confidence in a similar way. Anyhow, the principal effect of the basal inclination on the deposition behaviour is demonstrated in figure 14. Here the data $A_D - A_W$ against time are shown for three experiments at 15°, 20° and 25°, where h_i (~ 44 cm) and d_i (6.05 cm) were kept constant. As for the case of constant inclination reported above, deposition in the first
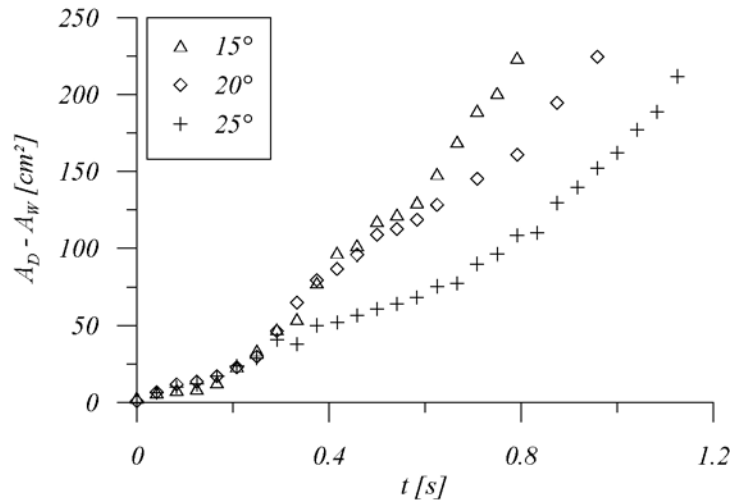
Figure 14. The deposited area as a function of time for three different basal inclinations and constant h_i (~ 44 cm) and d_i (6.05 cm).

phase is independent of the basal inclination and $A_D - A_W \propto t^2$. In the second phase, data varies with the basal inclination, and the deposition rate at equal times strongly decreases with increasing α.
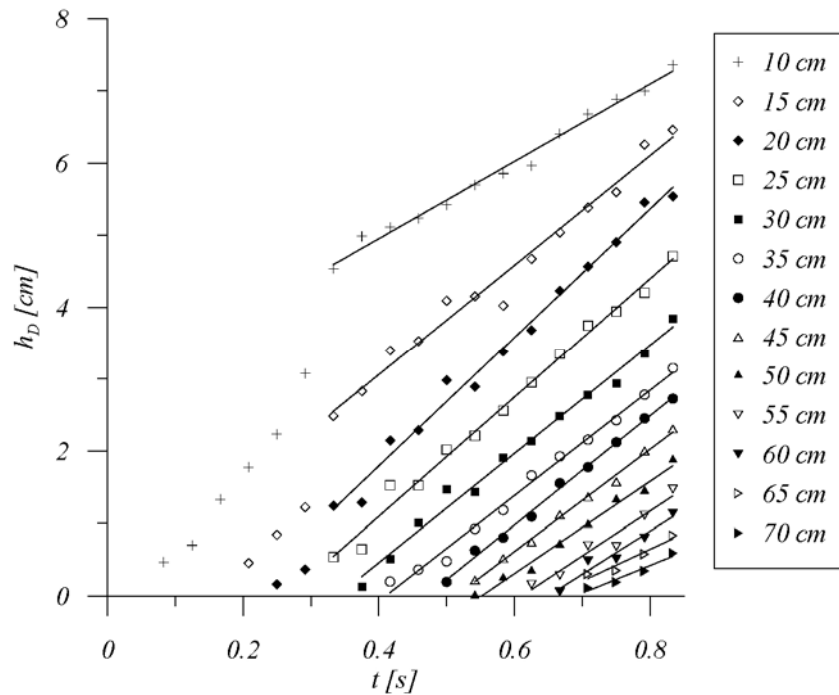

Figure 15. Thickness variation of the static region as a function of time at fixed longitudinal spacing of 5 cm for an experiment at 15° basal inclination where a = 7.3 and d_i = 6.05 cm. Solid lines represent linear best-fits through the data in the lateral spreading phase.

Further insight is gained from analysing the thickness variation of the static region over time at fixed distances *d*. Figure 15 shows the data h_D *(d = const.)* against time at regular spacing

154

of 5 cm for an experiment with $a = 7.3$ and $\alpha = 15°$. At $d = 10$ cm, 15 cm and 20 cm, the data h_D against time show an initial nonlinear increase followed by approximately linear segments. The initial part is observed during the free-fall phase, whereas the final linear segment occurs during the lateral spreading phase. At the outer positions ($d > 20$ cm), there is only one behaviour corresponding to linear growth of the layer during the lateral spreading phase. The data show that during the lateral spreading phase there is a linear growth with time of the static layer along the flow length. Thus, local deposition rates $\partial h_D / \partial t$ can be calculated from linear best-fits. In figure 16 the data $\partial h_D(d, t)/\partial t$ for inclinations of 15°, 20° and 25° at constant h_i and d_i are presented. For comparison the corresponding data for $\alpha = 0°$ is also shown. It is seen that the local deposition rate varies along the flow length. There is an increasing region close to the gate followed by a slightly decreasing or approximately constant region. Although the data at high values of α is slightly scattered, the general tendency that the local deposition rate strongly decreases with increasing inclinations becomes clear.
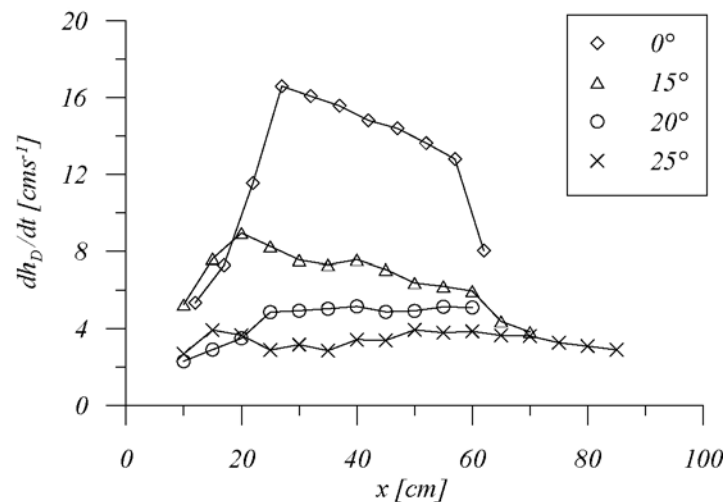

Figure 16. The local deposition rate $\partial h_D/\partial t$ against the longitudinal distance from the gate for experiments with different basal inclinations and constant h_i (~ 44 cm) and d_i (6.05 cm).

6.2. Velocity profiles

Velocity profiles in the flowing layer have been analysed normal to the inclined plane at the fixed position $\delta d/3$ from the gate. The flow front approaches this distance in the lateral spreading phase. Two different kinds of behaviour can be seen. Upon by-passing of the frontal region with direct contact to the base, the velocity profile is typically S-shaped with a high slip velocity at the base and lower shear rate close to the upper free surface. A little time later, when the interface front approaches the observation point, the velocity profiles show a clear exponential region above the interface followed a linear region. Figure 17 illustrates the

velocity profiles in this second stage for inclination of 4.2°, 15°, 20° and 25° and constant h_i (~ 44 cm). The slope of the linear region decreases with increasing α. Thus, the shear rate increases with increasing inclination.
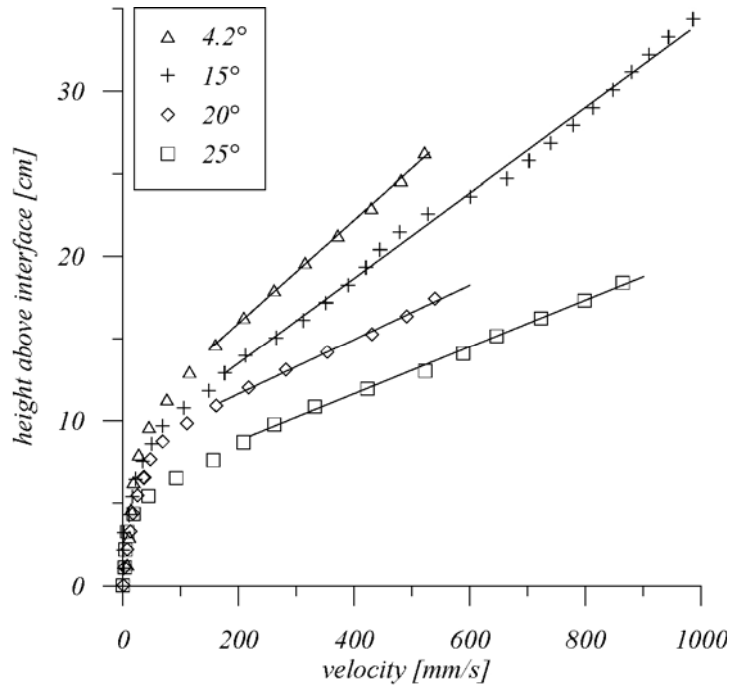

Figure 17. Typical form of velocity profiles during the lateral spreading phase for four experiments with different basal inclinations and constant h_i (~ 44 cm).

Furthermore, at each inclination and for each aspect ratio a universal velocity profile exists in this second stage when the interface front has approached the observation point. This is shown in figure 18 for α = 4.2° and h_i = 42.25 cm. Here the height in the flowing layer above the interface is plotted against velocity. Thus, for each inclination and each aspect ratio a shear rate can be calculated as the inverse slope of the linear part of the collapsed profiles. Lube *et al.* (2006) have shown that for α = 0° this shear rate follows the relationship

$$\gamma_0 = 6.1\left(g / \tilde{h}_i\right)^{1/2},$$
(13)

where $\tilde{h}_i$, defined by

$$\tilde{h}_i = h_i - d_i \tan(60°)/2,$$
(14)

is a length scale that describes the fraction of the granular column actually involved in the flowing region. In figure 19 we show the experimentally determined shear rates against the shear rate scale $\left(g / \tilde{h}_i\right)^{1/2}$ for the different inclinations. Except for 0° and 15°, only experiments for a = 5, 7 and 9 were analysed. Anyhow, the data can be approximated by

linear functions of the form $\gamma(\alpha, \tilde{h}_i) = c_S(\alpha)\left(g/\tilde{h}_i\right)^{1/2}$. The general tendency of increasing c_S with the basal inclination is evident.
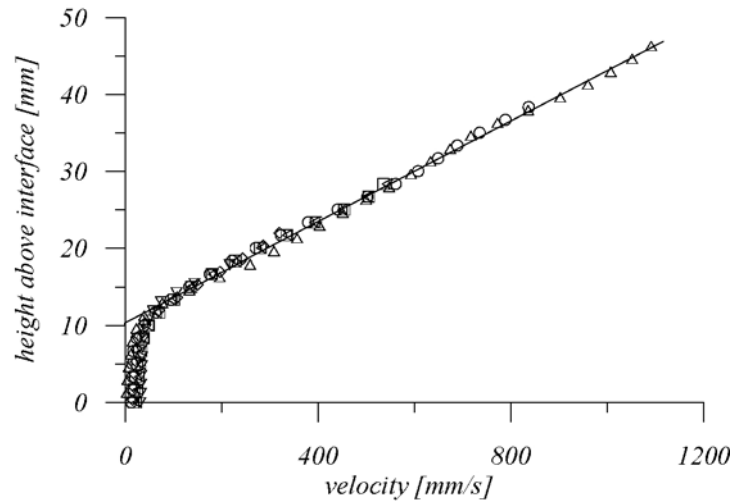

Figure 18. Collapse of velocity profiles in the lateral spreading phase for an experiment at α = 4.2° and a = 6.7. Different symbols represent velocity profiles at different times.
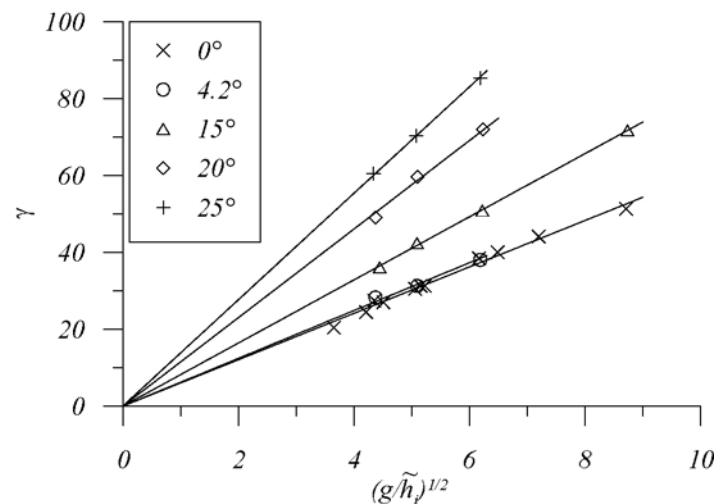
Figure 19. Experimentally determined shear rates against the shear rate scale $\left(g/\tilde{h}_i\right)^{1/2}$ for basal inclinations varying from 0° to 25°.

7. Summary and conclusions

Experimental results for the collapse of rectangular columns of sand into rough, inclined channels are presented. Both, the shape of final deposits and the kinematic behaviour was analysed as a function of the initial aspect ratio and the basal inclination of the channel.

The main results from the analysis of the resulting deposits are:

- As for collapses into horizontal channels, two different flow regimes at low and large aspect ratios exist.

- In the range of tested basal inclinations, the final deposits for $a > 2.8$ and $\alpha \leq 20°$ satisfy a self-similar form with respect to their maximum horizontal and longitudinal extent.

- For $\alpha \leq 20°$, the final runout distance and the maximum deposit height can be expressed by dimensional analysis as functions with two separate terms for the aspect ratio and basal inclination respectively.

- For $\alpha = 25°$, the flow separates into horizontal (as for $\alpha \leq 20°$) *and* longitudinal regions of static and moving material. This different behaviour in comparison to lower basal inclinations is evident in the shape of final deposits, including δd and h_∞. For example, the final runout distance for $a > 2.8$ follows a powerlaw of the form $\delta d / d_i = 4.6 a^{0.84}$ instead of $\delta d / d_i = a^{2/3}(k_H(0) + 21.7\alpha^2)$ which is the case for $\alpha \leq 20°$. Under the assumption that all potential energy of the initial columns is dissipated by frictional forces (e.g. $\mu M_i g \delta d = M_i g h_i$, where M_i is the mass of the initial column), the maximum runout distance should follow the relationship $\delta d / d_i \propto a^1$. The convergence of the powerlaw exponent at high basal inclinations to 1 could thus be interpreted by a flow transition from inertial to more frictional flow when the frontal region (at $\alpha = 25°$) decouples from the parent flow and travels further as thin sheet flow of a few particle diameters thickness. Experimental investigations for which the basal roughness is changed systematically and experiments testing a range of materials with different static angles of repose could provide further insight.

The analysis of the kinematic behaviour revealed the following results:

- For $\alpha \leq 20°$, the overall time to reach the maximum runout distance can be expressed as a function of the initial height, the basal inclination and g. As for δd and h_∞, this function comprises separate terms for the variation of the aspect ratio (or initial height as t_∞ is independent of d_i) and for α. The term for the basal inclination shows a similar mathematical form as that for the description of the maximum runout as $F_T(\alpha) = c_T(0) + 9.84\alpha^2$. Again, the relationship does not describe the final time of collapses for experiments at the 25° inclination.

- As recently shown for $\alpha = 0°$ (Lube *et al.* 2006), the two phases of collapse (the free-fall phase and the lateral spreading phase) are evident in different deposition behaviour from the base of the internal interface. In the free-fall phase, the deposition rate at constant α is independent of the initial height and α and scales as $dA_D/dt \propto t$. In the lateral spreading phase,

the deposition rate increases with the initial height and decreases with increasing the basal inclination.

- The general tendency of the decreasing deposition rate with increasing basal inclination is also evident in the data of the thickness of the internal interface (normal to the inclined plane) at fixed longitudinal positions.

- In parallel with decreasing deposition rates at higher inclinations, the shear rate measured in the lateral spreading phase at the fixed longitudinal distance *δd/3* from the gate increases with the basal inclination. The shear rate can be expressed as $\gamma(\alpha, \tilde{h}_i) = c_S(\alpha)\left(g / \tilde{h}_i\right)^{1/2}$, where c_S is an increasing function of the basal inclination.

It will be interesting to explore how the kinematical behaviour changes when the basal inclination is equal or larger than the static angle of repose. An immediate assumption from these experimental findings is that for flows at the AOR, where a flow regime of steady, uniform motion develops, the internal interface coincides with the rigid base. A continuative investigation could also be the study of granular collapse flows down inclined channels at the AOR over a bed of loose particles. These experiments might show that the interface then tends to propagate downwards effectively causing erosion.

ACKNOWLEDGEMENTS

REFERENCES

Balmforth, N. J. & Kerswell, R. R. 2005 Granular collapses in two dimensions. J. Fluid Mech. **538**, 399–428.

Dalziel, S.B. 2005 DigiFlow User Guide, http://www.damtp.cam.ac.uk/lab/digiflow/.

G.D.R. Midi 2004 On dense granular flows. Eur. Phys. J. E **14**, 341.

Gauer, P., Rammer, L, Kern, M., Lied, K., Kristensen, K. & Schreiber, H. 2006 On pulsed Doppler radar measurements of avalanches and their implication to avalanche dynamics. Geophysical Research Abstracts, Vol. 8, 04683.

Huppert, H.E., Hallworth, M.A., Lube, G. & Sparks, R.S.J. 2003 Granular column collapses Bull. Am. Phys. Soc. **48**, 68.

Huppert, H.E., Lube, G., Sparks, R.S.J. & Hallworth, M.A. 2004 Granular Column Collapse. ICTAM Proceedings, Kluwer Academic Publishers.

Hutter, K., Koch, T., Pluss, C. & Savage, S.B. 1995 The dynamic of avalanches of granular materials from initiation to runout. Part. II experiments. Acta Mech. **109**, 127.

Kerswell, R. R. 2005 Dam break with Coulomb friction: A model for granular slumping? Phys. Fluids **17**, 057101, 1–16.

Lajeunesse, E., Mangeney-Castelnau, A. & Vilotte, J. P. 2004 Spreading of a granular mass on a horizontal plane. Phys. Fluids **16**, 2371–2381.

Lajeunesse, E., Monnier, J.B. & Homsy, G.M. 2005 Granular slumping on a horizontal surface. Phys. Fluids **17**, 103302.

Larrieu, E., Staron, L. & Hinch, E. J. 2006 Raining into shallow water as a description of the collapse of a column of grains. J. Fluid Mech. **554**, 259–270.

Lube, G., Huppert, H. E., Sparks, R. S. J & Hallworth, M. A. 2004 Axisymmetric collapses of granular columns. J. Fluid Mech. **508**, 175–199.

Lube, G., Huppert, H. E., Sparks, R. S. J. & Freundt, A. 2005 Collapses of two-dimensional granular columns. Phys. Rev. E **72**, 041301.

Lube, G., Huppert, H. E., Sparks, R. S. J. & Freundt, A. 2006 Static and flowing regions in granular column collapses down channels. Phys. Fluids (sub judice).

Pouliquen, O. 1999 Scaling laws in granular flows down rough inclined planes," Phys. Fluids **11**, 542.

Pouliquen, O. & Forterre, Y. 2002 Friction law for dense granular flows: application to the motion of a mass down a rough inclined plane. J. Fluid Mech. **453**, 131.

Staron, L. & Hinch, E. J. 2005 Study of the collapse of granular columns using 2D discrete grains simulation. J. Fluid Mech., **545**, 1-27.

Savage, S.B. & Hutter, K. 1989 The motion of a finite mass of granular material down a rough incline. J. Fluid Mech. **199**, 177.

Siavoshi, S. & Kudrolli, A. 2005 Failure of a granular step. Phys. Rev. E., **71**, 051302,1-6.

Thompson, E. L. & Huppert, H. E. 2006 Granular column collapses: further experimental results. Phys. Fluids (sub judice).

Zenit, R. 2005 Computer simulations of the collapse of a granular column. Phys. Fluids **17**, 031703, 1–4.

Lebenslauf

Gert Lube

Research Division "Dynamics of the Ocean Floor", Leibniz-Institut fuer Meereswissenschaften, IFM-GEOMAR, Gebäude Ostufer, Wischhofstr. 1-3, D-24148 Kiel, Germany,
Phone: +49 431 600 2140   Fax: +49 431 600 2924   Email: glube@ifm-geomar.de

PERSÖNLICHE DATEN		AKADEMISCHE QUALIFIKATION
Geboren	6. Januar 1977 in Magdeburg	Diplomgeologe, EMA Greifswald
Nationalität	deutsch	
Familienstand	ledig	

AKADEMISCHE ANSTELLUNGEN UND LEHRTÄTIGKEIT

2003-heute	**Leibniz-Institut IFM-Geomar, Kiel** Wissenschaftlicher Angestellter im DFG-Projekt FR 928.
2004-2005	**Institute of Natural Resources, Massey University, New Zealand** Betreuung von einem Master Studenten bei Feldarbeiten mit Laser-Distance-Meters.
1996-1998	**Institut fuer Geowissenschaften, EMA Universität, Greifswald** Wissenschaftlicher Hilfskraft für K/Ar Isotopenmessungen sowie XRF and ICPMS Analysen.

AUSBILDUNG

2003-07. 2006	**Leibniz-Institut IFM-Geomar, Kiel** Doktorarbeit: *The flow and depositional mechanisms of granular matter: Experimental and field studies with implications for pyroclastic flows.* Doktorvater: Dr. Armin Freundt.
8-9. & 11-12.2005	**DAMTP, University of Cambridge, Großbritannien** Forschungsaufenthalt im Rahmen eines David-Crighton Fellowships
2002	**DAMTP, University of Cambridge, Großbritannien** Summerschool *Geophysical and Environmental Fluid Dynamics.*
2002	**Department of Earth Sciences, University of Bristol, Großbritannien** Pre-doctorial als *Young Scientist* im EC Fifth Framework Program *"Volcano dynamics in relation to monitoring, hazards mitigation and volcano crisis response"* zur theoretischen und experimentellen Analyse granularer Ströme.
2001-2002	**Montserrat Vulkan Observatorium, Montserrat, Westindische Inseln** Trainingsprogramm als Vulkanologe durch ein EC Fifth Framework Fellowship.
1999-2000	**Department of Earth Sciences, University of Bristol, Großbritannien** DAAD Jahresstipendiat zur Spezialisierung in Fluidmechanik, Geophysik, Physikalischer Vulkanologie und zur Bearbeitung eines Forschungsprojekts an granularen Strömen unter Betreuung von Prof. R. Stephen J. Sparks FRS.
1996-2001	**Institut fuer Geowissenschaften, EMA Universität, Greifswald** Diplom in Geologie mit Spezialisierung auf Physikalische Vulkanologie, Petrologie. Bewertung: sehr gut
1985-1995	**Werner-von-Siemens Gymnasium für Naturwissenschaften, Magdeburg** Abitur: Bewertung 1.2

AUSZEICHNUNGEN UND STIPENDIEN

▪ Gordon-Research Young Scholar's Award of the Queen's College Oxford 2006
▪ David-Crighton Fellowship of the University of Cambridge 2005
▪ Young Scientist's Travel Award of the European Geophysical Union Meeting Vienna 2005
▪ Marie-Curie EC Fifth Framework Fellowship 2001-2002
▪ DAAD Jahresstipendium 1999-2000

AUSGEWÄHLTE FELD- UND LABORERFAHRUNG

Mt. Ngauruhoe, Neuseeland (2004/ 2005): Laser-Distance-Meter und RTK-GPS Vermessungen, sowie Sedimentologische Analyse der 1975 Pyroklastischen Stromablagerungen. Erstellung einer detaillierten Datenbasis für den Vergleich von numerischen Modellen/ analogen Experimenten mit natürlichen Ablagerungen.

Montserrat, Westindische Inseln (2001/ 2002): Unter Betreuung des Montserrat Vulkan Observatoriums. Gefahrenzonen-Kartierung der 1997-99 Pyroklastischen Stromablagerungen, COSPEC und open-path FTIR Spectroskopie, GPS und Telemetrische Deformationsmessung, Vulkanologische Feldbeobachtung während Eruptionen, Seismische Datenanalyse.

Gran Canaria,, Spanien (2000): Geologische Kartierung, rheologische und geochemische Analyse des Hochtemperatur Ignimbrites VI und von Fallout Aschesequenzen.

Experimentelle und theoretische Arbeiten an granularen Strömen und Dichteströmungen mit Hilfe von Hochgeschwindigkeits-Kameras und Digitaler Bildanalyse.

Planung und Aufbau von Experimentaltanks und diverser elektronischer und mechanischer Messinstrumente.

Geochemische Analyseverfahren mit XRF und ICPMS.

WISSENSCHAFTLICHES INTERESSE

▪ Physik vulkanischer Eruptionen
▪ Transport und Sedimentationsprozesse in Geophysikalischen Massenströmen
▪ Anwendung von Fluid Mechanik zum Verständnis von Fließprozessen in Natur und Umwelt
▪ Physik granularer Ströme mit und ohne Fluidphase und von Dichteströmungen
▪ Gefahrenforschung

SPRACHKENNTNIS UND WEITERE AUSBILDUNG

▪ Englisch und Russisch (flüssig in Wort und Bild), Spanisch (Grundkenntisse).
▪ MS DOS, MS Windows, Turbo Pascal Programmierung, Erfahrung mit MS Office, ArcView, Coral and Adobe Anwendungen, MatLab, GS Surfer and Grapher.
▪ Zivildienst am Kreiskrankenhaus Güstrow (1995-96).
▪ Klassische Musikausbildung (Klarinette).

BESONDERE AUSSERBERUFLICHE INTERESSEN

▪ Photographie, Windsurfen, Berg- und Radwandertouren.